University of California, San Diego
Division of Structural Engineering
Structural Systems Research Project

Report No. SSRP- 99/09

SUBSTATION EQUIPMENT INTERACTION – RIGID AND FLEXIBLE CONDUCTOR STUDIES

by

André Filiatrault
Professor of Structural Engineering

Spyridon Kremmidas
Assistant Development Engineer

Ahmed Elgamal
Professor of Structural Engineering

Frieder Seible
Professor of Structural Engineering

Division of Structural Engineering
University of California, San Diego
La Jolla, California 92093-0085

September 24, 1999

DISCLAIMER

Opinions, findings, conclusions and recommendations expressed in this report are those of the authors and do not necessarily reflect views of the Pacific Gas and Electric Company (PG&E) and the Pacific Earthquake Engineering Research Center (PEER).

ACKNOWLEDGEMENTS

The research project described in this report was funded by the PEER/PG&E Directed Studies under the PG&E Agreement No. 09566 (Prime Agreement CEC 500-97-010) "Electric System Seismic Safety and Reliability" – SA2115-59652.

We greatly appreciated the input and coordination provided by Professor Gregory Fenves from the University of California at Berkeley and Mr. Eric Fujisaki and Dr. William Savage from PG&E during the development of this research project. The support of Dr. Leon Kempner from Bonneville Power Administration is also gratefully acknowledged.

The authors extend their sincere appreciation to Mr. Constantin Christopoulos, Doctorate student at UC-San Diego, for his assistance in conducting the shake table tests.

LIST OF SYMBOLS

A1	First double amplitude for damping evaluation
A2	Second double amplitude for damping evaluation
c_A	Viscous damping coefficient of generic equipment A
$E_{D\delta}$	Energy dissipated per cycle at displacement amplitude δ
F_δ	Force at the displacement amplitude δ
F_s	Slip force of bus slider
F_y	Yield force
k_A	Lateral stiffness of generic equipment A
K_e	Elastic restoring stiffness of bus slider
K_o	Elastic stiffness
m_A	Mass of generic equipment A
n_j	Number of cycles to be performed in load step j
p	Number of intermediate cycles between double amplitudes
Q_y	Yield force
$x_{rA}(t)$	Relative displacement at the top of generic equipment A
$\dot{x}_{rA}(t)$	Relative velocity at the top of generic equipment A
$\ddot{x}_{aA}(t)$	Absolute acceleration at the top of generic equipment A
β	Strain-hardening ratio
βK_o	Post-yield stiffness
δ	Displacement
δ^*	Displacement at 75% of yield force
δ_y	Yield displacement
δ_j	Peak displacement in load step j
Δ	Increment in peak displacement between two consecutive steps
μ	Displacement ductility factor
ζ	Equivalent viscous damping ratio

TABLE OF CONTENTS

1. INTRODUCTION

Both rigid and flexible conductors interconnect electrical substation equipment. During earthquakes, significant interaction and equipment damage due to forces transferred through the connectors have been observed. Flexible bus ("cables") exert relatively little force, provided that they remain slack. Rigid bus (typically aluminum tubular sections) may utilize connectors with small gaps for thermal displacement, thus accommodating some seismic displacement before transferring forces between the connected equipment. Some utilities have implemented slack or loops in flexible and rigid bus to provide flexibility between interconnected pieces of equipment.

1.1 Scope of Research

The primary objective of this research project was to investigate experimentally, through quasi-static and shake table testing, the interactions between components of substation equipment connected by both flexible and rigid bus. The intention was to generate experimental data that would provide guidance in the seismic design of conductor assemblies. Another objective was to provide experimental validation data for a current PEER-PG&E project in which analytical methods are being used to study substation equipment connected by flexible and rigid bus. Specific tests conducted in this project were:

(i) Full-scale quasi-static cyclic tests of three different types of rigid bus with spring connectors.

(ii) Full-scale quasi-static cyclic tests of one rigid bus-slider.

(iii) Full-scale quasi-static tests of two different types of flexible bus.

(iv) Full-scale shake table tests of five different pairs of generic substation equipment connected with three different rigid bus assemblies.

1.2 Report Layout

Following an introduction to the project, and scope of the current study in this chapter, **Chapter 2** describes the quasi-static tests performed on rigid bus assemblies with spring connectors. **Chapter 3** presents the quasi-static tests performed on a rigid bus slider. **Chapter 4** describes the quasi-static tests performed on flexible bus specimens. **Chapter 5** presents the shake table tests performed on five pairs of generic substation equipment connected with three different rigid bus assemblies. Finally, the report concludes with specific recommendations for the seismic design of interconnected equipment.

2. QUASI-STATIC TESTS OF RIGID BUS WITH SPRING CONNECTORS

This chapter describes the full-scale quasi-static tests performed on three different types of rigid bus with spring connectors. These tests were performed in the longitudinal directions of the bus assemblies under prescribed displacement history.

2.1 Description of Test Specimens

Three different rigid bus-spring connector assemblies were supplied by PG&E and were tested under quasi-static loading. Two specimens of each spring type were provided; one specimen was tested under quasi-static loading and the other was used for the shake table tests. Figure 2.1 presents a general view of the three specimens. Drawings of the specimens are included in Appendix A.

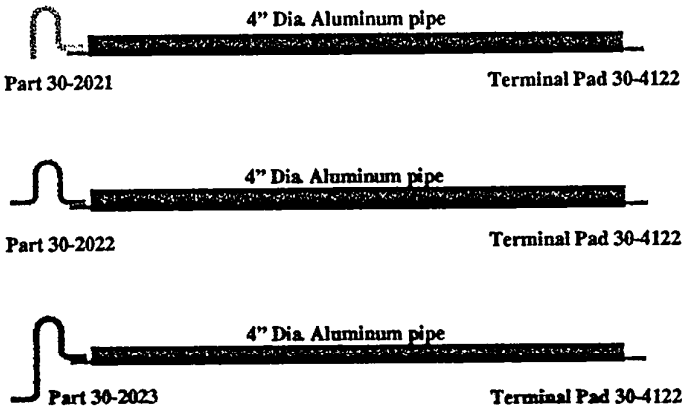

Figure 2.1 Rigid Bus Assemblies with Spring Connectors.

Each rigid bus was made of a 10-ft long SPS aluminum pipe (4.5 in outside diameter and 4.026 in inside diameter) with offset terminal pads welded at each end. Each bus incorporated a different spring connector. The first spring connector (Part 30-2021) is non-symmetrical with one horizontal and one vertical terminal pad. The second spring connector (Part 30-2022) is symmetrical with two horizontal terminal pads. Finally, the third spring connector is non-symmetrical with two horizontal terminal pads at different elevations. Figure 2.2 presents the dimensions of the three spring connectors tested.

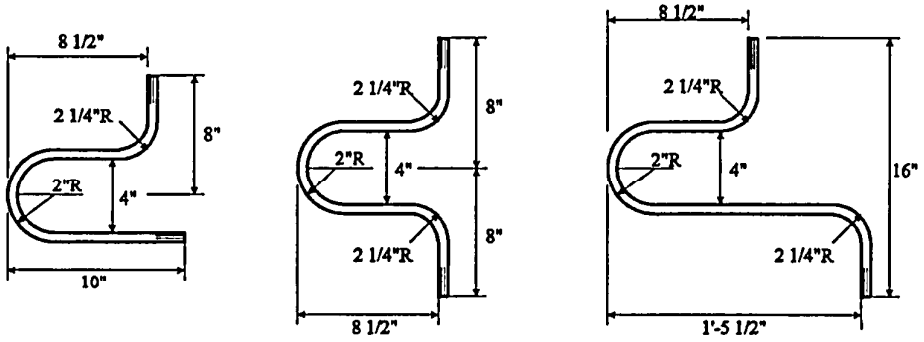

PG&E Code No 30-2021 PG&E Code No 30-2022 PG&E Code No 30-2023

Figure 2.2 Dimensions of Spring Connectors.

Each spring was made up of three pairs of copper alloy straps (1/8" thick by 3" wide) separated by two ¼" gaps. Shim plates were inserted in the gaps only at the ends of the springs to provide continuous connections to the terminal pads.

2.2 Preliminary Tensile Tests

Preliminary monotonic tensile tests were performed on three different coupons taken from one of the spring connector (Part 30-2023) in order to evaluate the properties of the copper alloy. Three different coupons were tested according to the ASTM E8-98 standard (American Society for Testing Materials, 1999). Figure 2.3 presents the tensile stress-strain curve obtained from one of the test. It can be seen that the copper alloy exhibits almost a perfect elastic-plastic behavior that can be characterized by Young's modulus and yield strength. Table 3.1 presents these material properties based on the mean values of the three tests performed. The yield strain of the material is also indicated in this table.

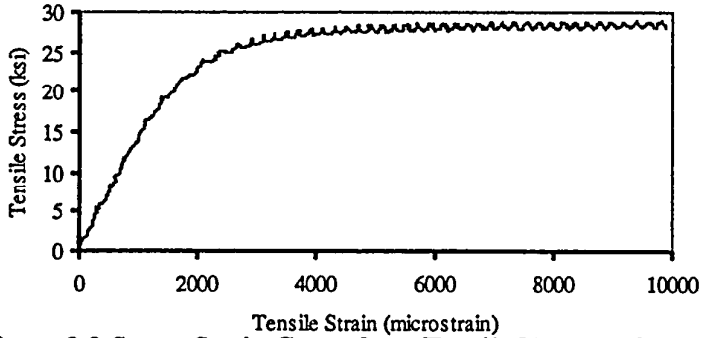

Figure 2.3 Stress-Strain Curve from Tensile Tests on Copper Alloy.

Table 2.1 Material Properties for Copper Alloy.

Young's Modulus	14 100 ksi
Yield Strength	27 ksi
Yield Strain	1915 $\mu\varepsilon$

2.3 Experimental Set-Up for Quasi-Static Cyclic Tests

Figure 2.4 illustrates the experimental set-up used to perform the quasi-static cyclic tests on the three rigid bus-spring connector assemblies. A 220-kip actuator with a 24-in stroke was attached to the strong wall of the laboratory and applied horizontal loading in the longitudinal direction of the bus assembly. The head of the actuator was prevented from moving in perpendicular directions of the loading by a supporting chain system. Also, locking the swivel near the bus assembly prevented rotation of the head of the actuator. The bus assembly was inserted between the head of the actuator and a vertical steel column anchored to the strong floor of the laboratory. The terminal pad of the spring connector was attached to the column by a transfer plate and the other end of the bus was connected to the head of the actuator by a similar transfer plate. A 10-kip capacity axial load-cell was inserted between the head of the actuator and the terminal pad of the pipe to measure accurately the applied load during the test. Figure 2.5 presents photographs of the connection details at each end of the rigid bus assembly.

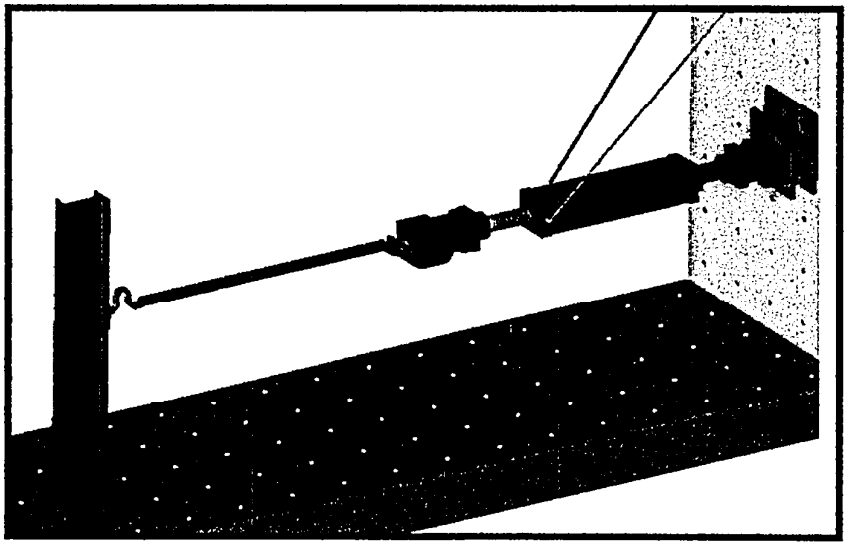

Figure 2.4 Experimental Set-Up for Quasi-Static Tests on Rigid Bus Assemblies.

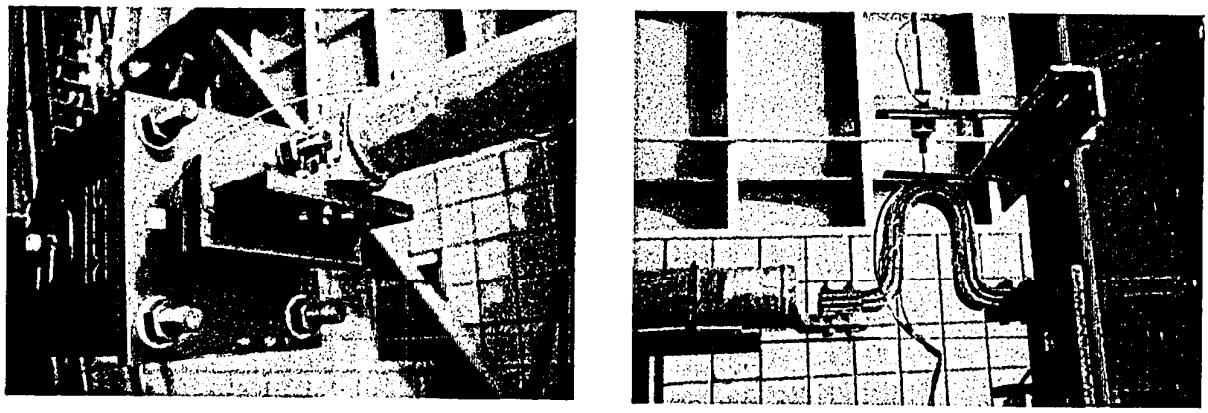

Figure 2.5 Details of Connections at Ends of Rigid Bus Assemblies.

2.4 Instrumentation

Figure 2.6 illustrates the instrumentation used for the quasi-static tests on the rigid bus assemblies. The force-displacement hysteresis loops were obtained by measuring the load across the 10-kip load cell and the displacement across the spring connector. Also, six strain gauges were installed on the top and bottom surface of each pair of straps at the position of maximum bending moment. The strain gauge readings were used at the beginning of each test to define the yield displacement of the specimen, as described in the next section.

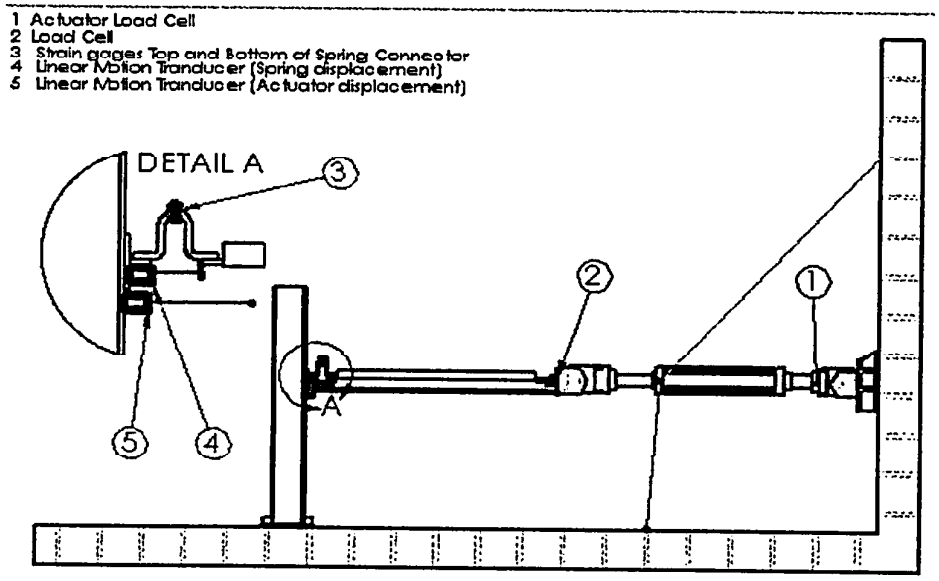

Figure 2.6 Instrumentation for Quasi-Static Tests on Rigid Bus Assemblies.

2.5 Test Protocol

The ATC-24 loading protocol (Applied Technology Council, 1992) was used to perform the quasi-static tests on the rigid bus assemblies. This protocol has been developed for the cyclic seismic testing of components of steel structures. The protocol consists of stepwise increasing displacement cycles as illustrated in Fig.2.7.

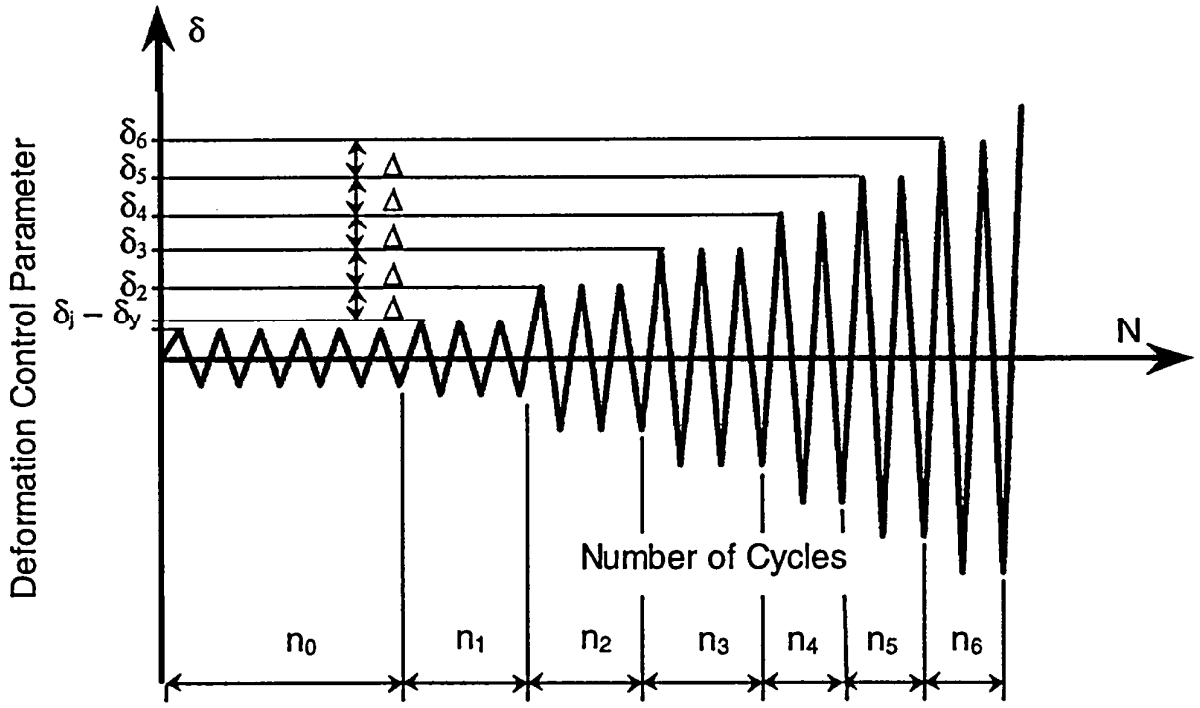

Figure 2.7 ATC-24 Test Protocol Used for Quasi-Static Tests of Rigid Bus Assemblies.

The loading history is defined by the following parameters:

δ_y	the yield displacement across the spring connector;
$\delta_j = \delta_y + (j-1)\Delta$	the peak displacement across the spring connector in load step j;
n_j	the number of cycles to be performed in load step j;
Δ	the increment in peak displacement between two consecutive steps.

The displacement is expressed in terms of the displacement ductility factor, μ, defined as:

$$\mu = \frac{\delta}{\delta_y} \tag{1.1}$$

The following parameters were used during the tests:

$$\begin{aligned} &\Delta = \delta_y \\ &n_0 = 6; \quad n_1 = n_2 = n_3 = 3; \quad n_j = 2 \; for \; j > 3 \end{aligned} \tag{1.2}$$

The yield displacement, δ_y, was obtained from the strain gauge readings during the first cycle in each loading direction. The specimen was displaced until a strain-gauge reading of $1500\mu\varepsilon$ was obtained at the location of maximum bending moment on the spring connector. It was then assumed that this displacement, δ^*, corresponded to 75% of the yield force of the specimen, $0.75Q_y$. The yield force, Q_y, and the yield displacement, δ_y, were obtained by linear extrapolation from these 75% yield values, as illustrated in Fig. 2.8. The procedure was then repeated in the other loading direction and the mean values were taken as the final yield displacement and yield force.

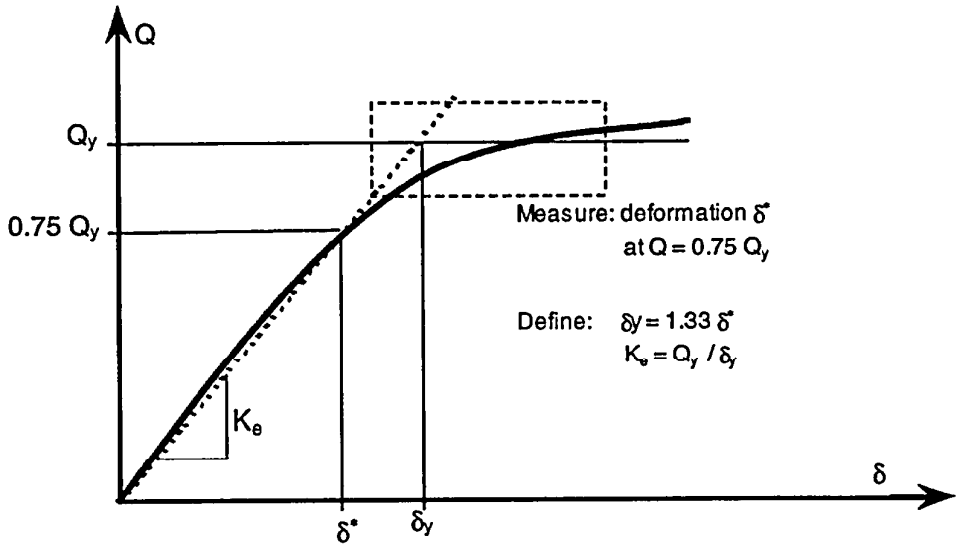

Figure 2.8 Determination of Yield Displacement and Yield Force of Rigid-Bus Assemblies.

Table 2.2 presents the experimental values of yield displacements and yield forces obtained for the three rigid bus assemblies tested. The 30-2021 and 30-2022 spring connectors have similar yield displacements and yield forces. The 30-2023 spring connector, being significantly more flexible, exhibits higher yield displacement and lower yield force than the other two springs.

Table 2.2 Experimental Yield Displacements and Yield Forces for Rigid Bus Assemblies

Spring Part No.	Yield Displacement, δ_y (in)	Yield Force, F_y (lbs)
30-2021	1.3	401
30-2022	1.3	347
30-2023	3.0	188

2.6 Static Linear Elastic Analysis of Spring Connectors

In order to predict the yield force, yield displacement, and location of maximum stress of each spring connector before the quasi-static tests, static linear analyses were performed. The commercial computer program SAP2000 (Computers and Structures, 1998) was used for this purpose. Each spring connector was modeled by straight linear-elastic frame elements capable of flexural and axial deformations. Each pair of straps was modeled as superimposed frame elements. The gaps between pairs of strap were also incorporated in the model. It was assumed that the terminal pads acted as fixed supports by constraining the rotation of the three end nodes at each end of the spring. Note that because of symmetry, only half of the 30-2022 spring was modeled. The elastic modulus shown in Table 2.1 was used in the models.

Figure 2.9 illustrates the displaced shape of the spring 30-2022 model under a horizontal concentrated force applied at one end of the spring and causing a maximum axial strain of 1915 $\mu\varepsilon$, corresponding to the yield strain of the material (see Table 2.1). From these analyses, the initial stiffness, the yield force and the yield displacement of each spring connector could be estimated and are indicated on each deformed shape.

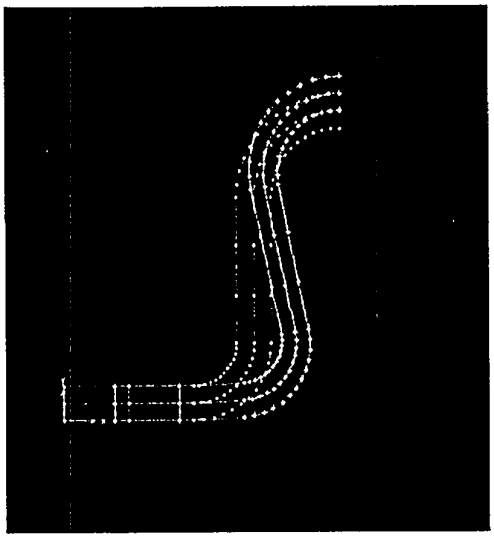

Figure 2.9 Static Linear Elastic Analysis of 30-2022 Spring Connectors.

2.7 Experimental Results

Figure 2.10 to 2.12 presents photographs of each specimen at the maximum displacement ductility factors achieved during each test. In the positive direction, the ductility factor was increased until the gap of the connector closed and contact occurred. The photographs clearly indicate the ductile characters of the spring connectors. Note also the significant vertical motion at the end of the rigid bus caused by the bending flexibility of the aluminum pipe.

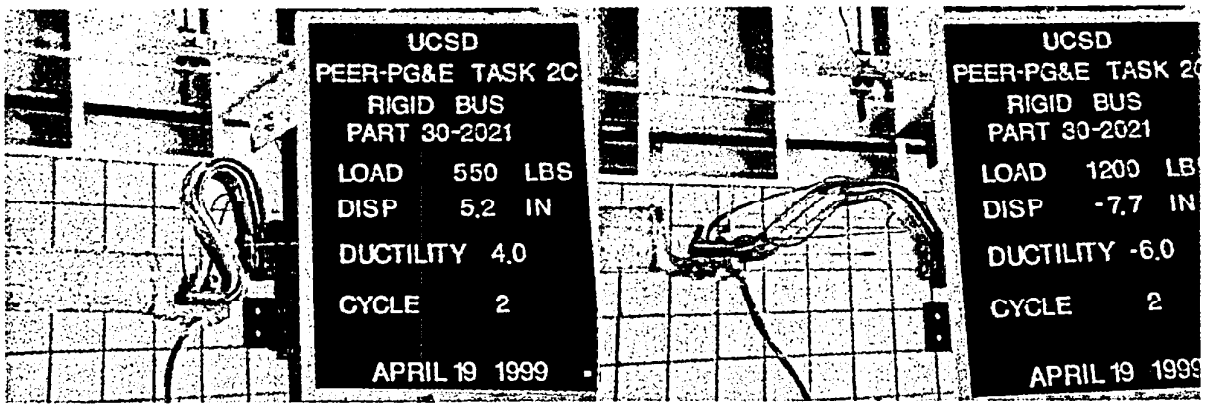

Figure 2.10 Rigid Bus with 30-2021 Spring Connector at Maximum Ductility.

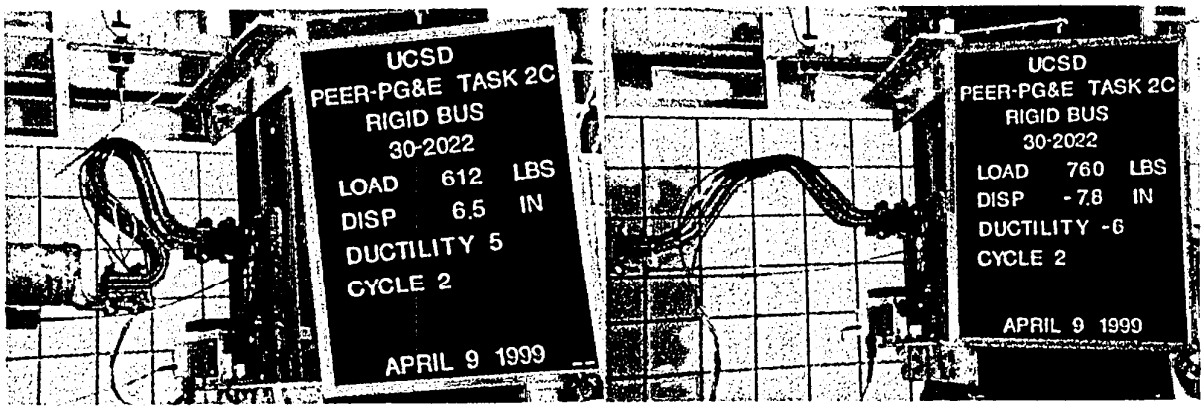

Figure 2.11 Rigid Bus with 30-2022 Spring Connector at Maximum Ductility.

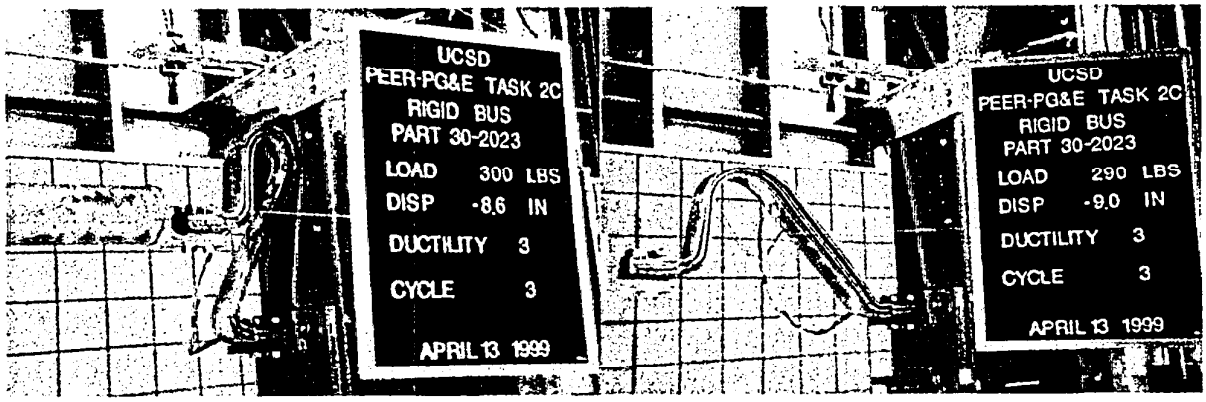

Figure 2.12 Rigid Bus with 30-2023 Spring Connector at Maximum Ductility.

Figure 2.13 presents the load-displacement response of each spring connector obtained at ductility levels less than unity. Also shown on the figures are the load-displacement responses predicted by the SAP-2000 analyses described in the previous section. For the 30-2021 spring, the numerical model slightly underestimates the elastic stiffness of the unit. This can be explained by the fact that the vertical terminal pad induces a rotation constraint on a longer length than assumed in the model. For the 30-2022 spring, the situation is reversed; the numerical model overestimates the elastic stiffness of the unit. This can be attributed to the vertical motion of the end of the pipe (see Fig. 2.11) that introduces a rotational flexibility at one end of the spring. Finally, for the 30-2023 spring, the predictions of the numerical model agree well with the test results.

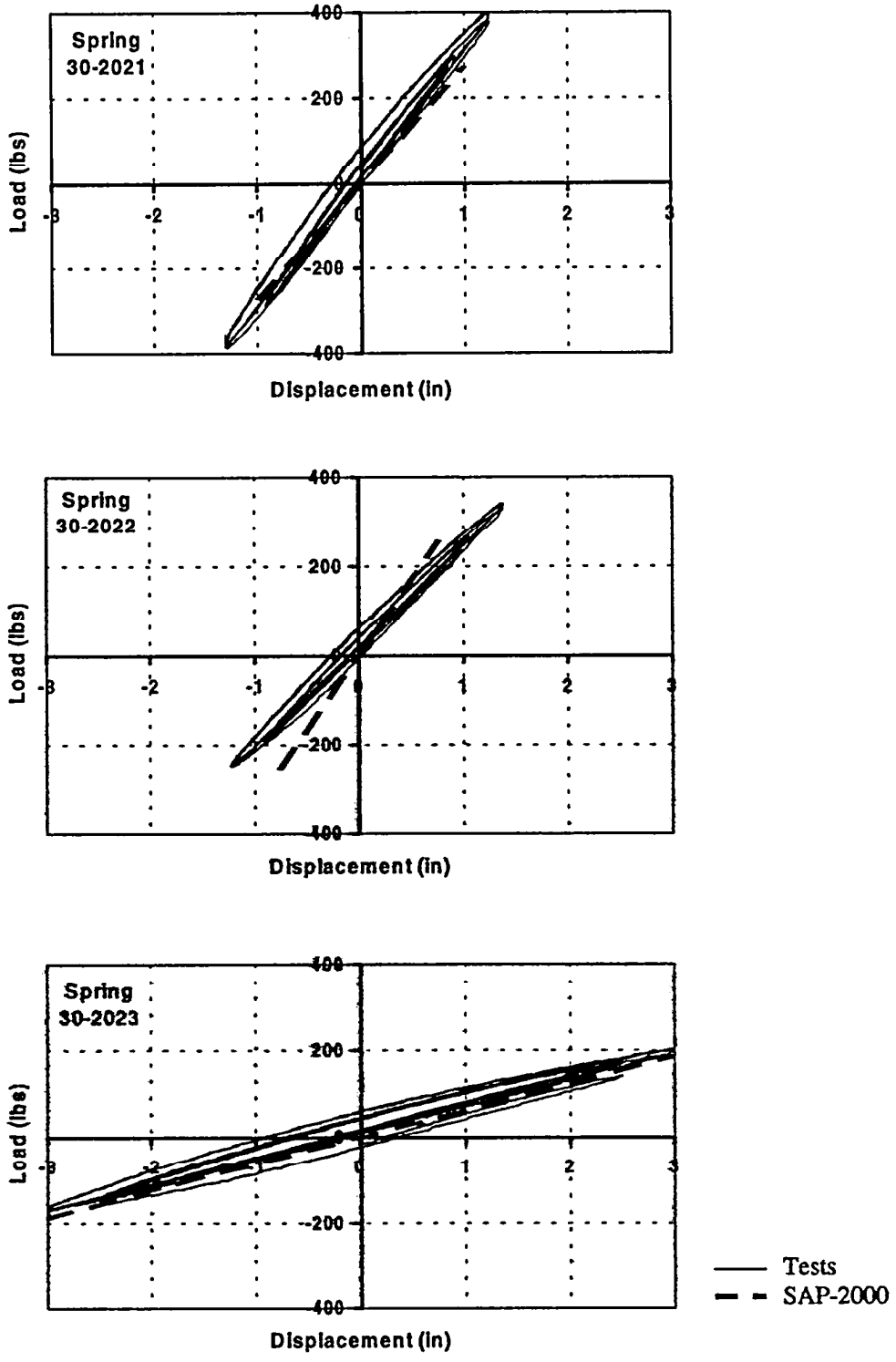

Figure 2.13 Load-Displacement Responses of Spring Connectors for Ductility Less than Unity.

Figure 2.14 presents the load-displacement response of each spring connector obtained for the complete range of ductility levels considered in the tests. The three spring connectors tested exhibit large and stable hysteresis loops with good energy dissipation capabilities. For ductility levels less than four, the hysteresis loops are nearly symmetric about the load axis. For larger ductility levels, the stiffness of springs 30-2021 and 30-2022 increases for negative loading and deformation (opening of the spring conductor) because of the tension stiffening effect. This effect is more predominant for spring 30-2021 than for spring 30-2022. Because of its lower stiffness, this tension stiffening effect is not observable for spring 30-2023. Also the load level developed by

Spring 30-2023 is significantly lower than the loads induced in the other two springs.

Two of the spring connectors (30-2022 and 30-2023) were tested to failure. During the last cycle of each test, the specimen was pulled monotonically until failure occurred. Figure 2.15 presents photographs of the failure region of each of the spring connectors. For both specimens, failure occurred across the net area of the cast-aluminum terminal pad connection that is welded to the aluminum tubing. Although failures occurred for large ductility levels in the spring connector of about 10, they were extremely brittle. The recorded failure loads were 8.3 kips and 9.0 kips for springs 30-2022 and 30-2023, respectively. These correspond to a very low failure tensile stress of less than 4 ksi across the net area.

2.8 Bilinear Modeling

The load-displacement hysteretic behavior of the three spring connectors can be simply modeled by a bi-linear solid with elastic stiffness K_o, post-yield stiffness βK_o, and yield force F_y, as illustrated in Fig. 2.16. Table 2.3 presents numerical values K_o, βK_o, and F_y, based on linear-regressions of the envelope curves of each of the loops (backbone curves). Figure 2.17 compares the predictions of the bi-linear models to the experimental data for the same displacement histories used in the quasi-static tests.

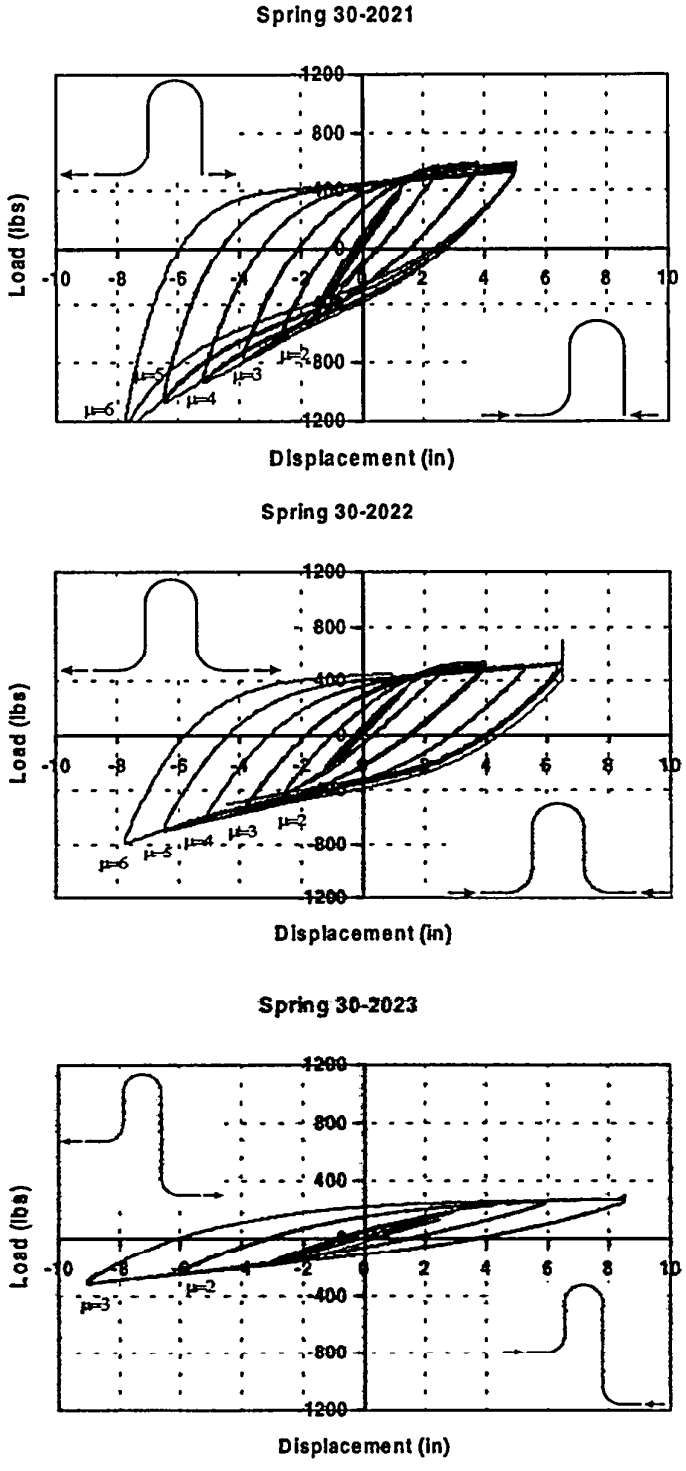

Figure 2.14 Load-Displacement Responses of Spring Connectors for all Ductility Levels.

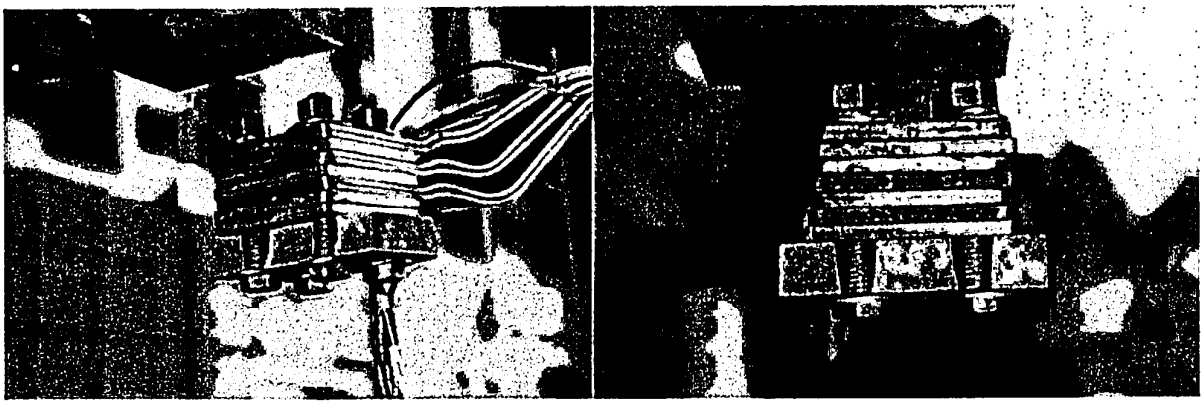

Spring 30-2022 **Spring 30-2023**

Figure 2.15 Failure Surfaces for Springs 30-2022 and 30-2023.

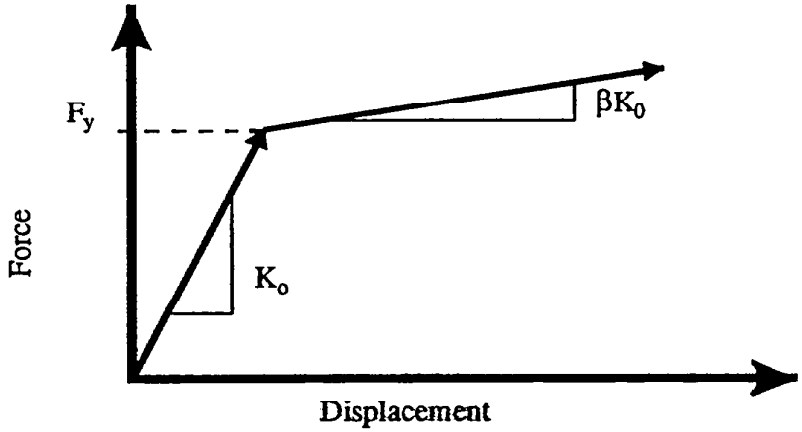

Figure 2.16 Bi-Linear Modeling of Spring Connectors.

Table 2.3 Numerical Values of Parameters for Bi-Linear Modeling of Spring Connectors.

Spring	Initial Stiffness K_o (lbs/in)	Post-Yield Stiffness βK_o (lbs/in)	Strain-Hardening Ratio, β	Yield Force F_y (lbs)
30-2021	308	79	0.26	401
30-2022	233	61	0.26	347
30-2023	63	21	0.33	188

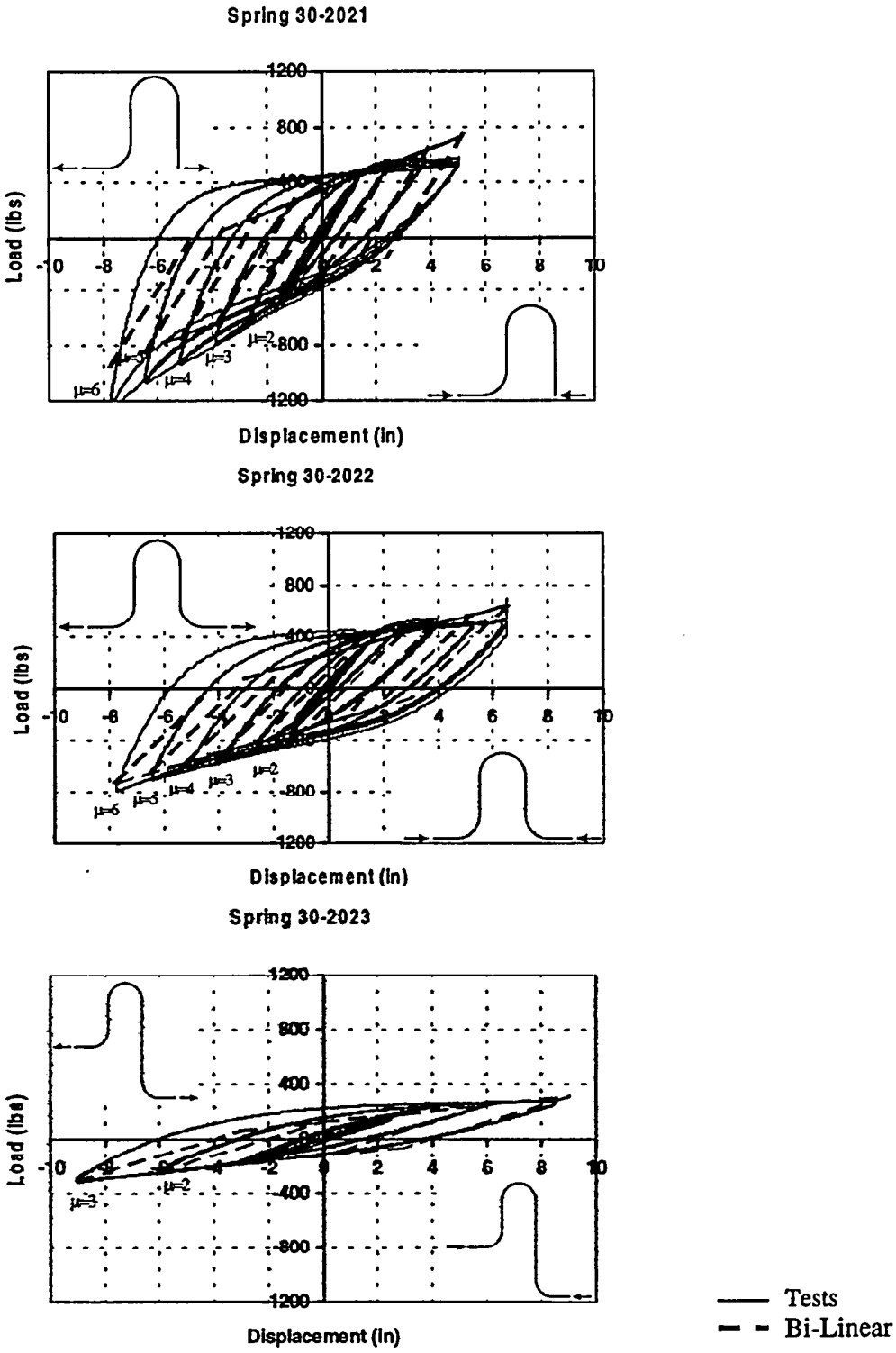

Figure 2.16 Bi-Linear Modeling of Spring Connectors.

2.9 Equivalent Viscous Damping Ratios

The energy dissipation capacity of each spring connector, for different displacement amplitudes, can be characterized by an equivalent viscous damping ratio, ζ. This equivalent damping ratio corresponds, for a given displacement amplitude, to a purely viscous dashpot that will dissipate the same amount of energy per cycle as the real spring connector. Based on the hysteresis loops shown in Fig. 2.14, the equivalent viscous damping ratio of a spring connector, ζ, at a given displacement amplitude, δ, is given by (Clough and Penzien, 1993):

$$\zeta = \frac{E_{D\delta}}{2\pi F_\delta \delta} \tag{1.3}$$

where $E_{D\delta}$ is the energy dissipated per cycle at a displacement amplitude δ and F_δ is the force at the displacement amplitude δ.

Table 2.4 presents the equivalent damping ratios for the three spring connectors tested at different displacement amplitudes corresponding to ductility levels greater or equal than one. The values presented correspond to the mean values of the different cycles for a given displacement amplitude. Only the symmetric cycles, before contact occurred, are presented. Figure 2.18 compares graphically these same results.

For the three specimens tested, the equivalent damping ratios increase with displacement amplitude, indicating higher energy dissipation capacity of the spring connectors at large inelastic displacements. Spring 30-2021 and spring 30-2022 exhibit damping ratios significantly higher than the more flexible spring 30-2023 for the complete range of displacement amplitudes.

Table 2.4 Equivalent Viscous Damping Ratios for Spring Connectors.

Spring 30-2021		Spring 30-2022		Spring 30-2023	
Displacement Amplitude (in)	Equivalent Damping Ratio (%)	Displacement Amplitude (in)	Equivalent Damping Ratio (%)	Displacement Amplitude (in)	Equivalent Damping Ratio (%)
1.0	2.84	1.0	2.00	2.3	4.52
1.3	4.75	1.3	3.00	3.0	5.56
2.6	13.1	2.6	10.1	6.0	17.6
3.9	18.0	3.9	20.8	6.0	23.0
5.2	20.1	5.2	29.9		
6.5	---	6.5	31.3		

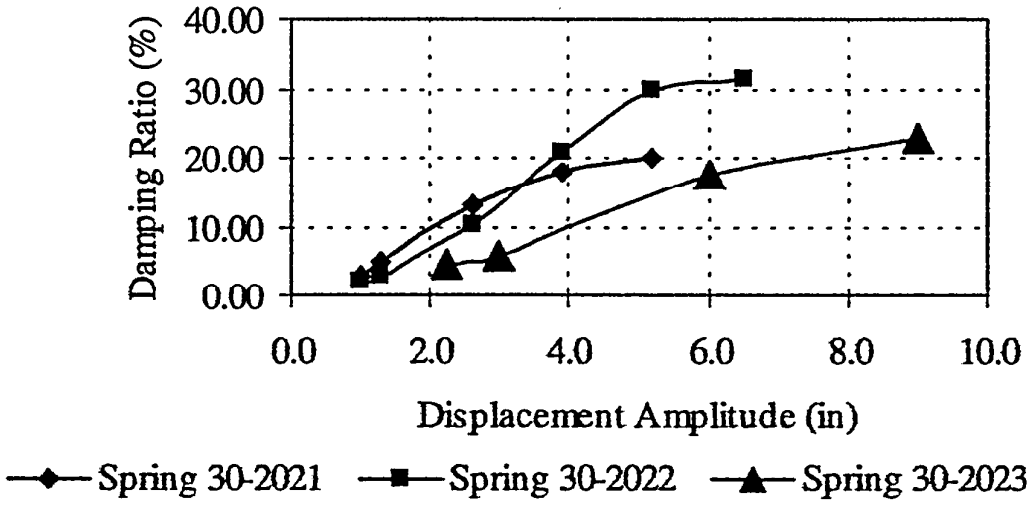

Figure 2.18 Comparison of Equivalent Viscous Damping Ratios for Spring Connectors.

3. QUASI-STATIC TEST OF RIGID BUS SLIDER

This chapter describes the quasi-static test performed on the rigid bus slider specimen provided by PG&E. This test was performed in the longitudinal direction of the bus assembly under prescribed displacement history.

3.1 Description of Test Specimen

Two identical rigid bus slider assemblies were supplied by PG&E. One was used for the quasi-static test and the other for the shake table tests. Figure 3.1 presents a general view of the specimen. Drawings of the specimen are also included in Appendix A.

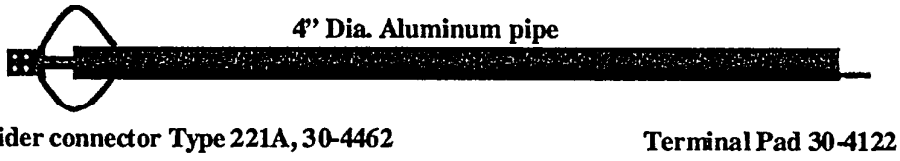

Figure 3.1 Rigid Bus Slider.

The specimen was made of a 10-ft long SPS aluminum pipe (4.5 in outside diameter and 4.026 in inside diameter) with a slider connection at one end, and an offset terminal pad at the other end.

The details of the slider connector are shown in Fig. 3.2. A shaft sliding against the inside surface of the pipe generates the friction force. A restoring force is also provided by two looped aluminum cables, welded on the pipe and on a terminal pad that is attached to the end of the shaft.

3.2 Experimental Set-Up for Quasi-Static Test

The experimental set-up used for the quasi-static test on the rigid bus slider assembly was similar as the one used for the quasi-static tests on the rigid bus-spring connector assemblies described in Chapter 2 (see section 2.3). Figure 3.3 presents a photograph of the connection detail at the end of the slider connector.

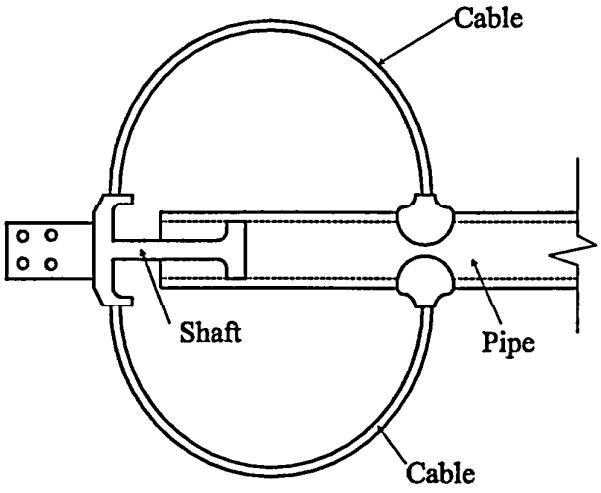

Figure 3.2 Slider Connector.

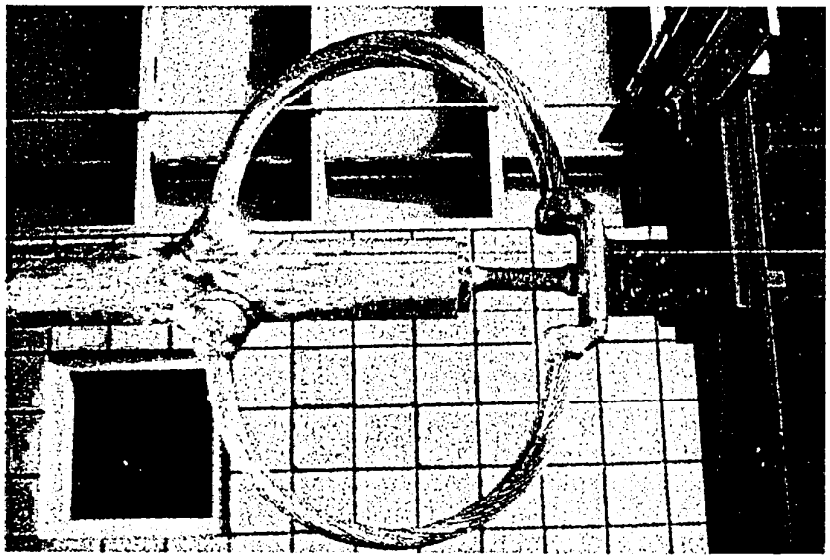

Figure 3.3 Connection at End of Slider Connector.

3.3 Instrumentation

Only the instrumentation required to measure the force displacement hysteresis loops in the longitudinal direction of the rigid bus slider assembly was installed. The force was measured across the 10-kip load cell that was inserted between the head of the actuator and the aluminum pipe (see section 2.3), and the displacement was measured across the full length of the specimen.

3.4 Test Protocol

The ATC-24 loading protocol (Applied Technology Council, 1992), used for the quasi-static tests of the rigid bus assemblies (see section 2.5), was used once again to perform the quasi-static test on the rigid bus slider assembly. In the case of the slider, however, the yield displacement must be defined differently since Coulomb-type friction is responsible for the nonlinear behavior of the specimen. An arbitrary value of 1 in was taken as the yield displacement, δ_y, across the slider connector.

3.5 Experimental Results

Figure 3.4 presents photographs of the specimen at the maximum displacements achieved during the test. In the positive direction, the displacement was increased until contact occurred between the aluminum pipe and the terminal pad. In the negative direction, the displacement was increased until the shaft slid out of the aluminum pipe.

δ = + 3.5 in **δ = - 3.5 in**

Figure 3.4 Rigid Bus Slider at Maximum Displacements.

Figure 3.5 presents the load-displacement response of the rigid bus slider obtained for the complete range of displacements considered in the test. The specimen exhibits a behavior that is typical of a Coulomb-type friction system coupled with an elastic restoring force mechanism. Before the slider can move, the static friction between the shaft and the interior surface of the pipe must be overcome. For the specimen tested, this slip force can be estimated at 53 lbs. After slipping has started, the force increment is obtained by the elastic flexural deformation of the two cable loops. For the specimen tested, this elastic post-slip stiffness can be estimated at 83 lbs/in.

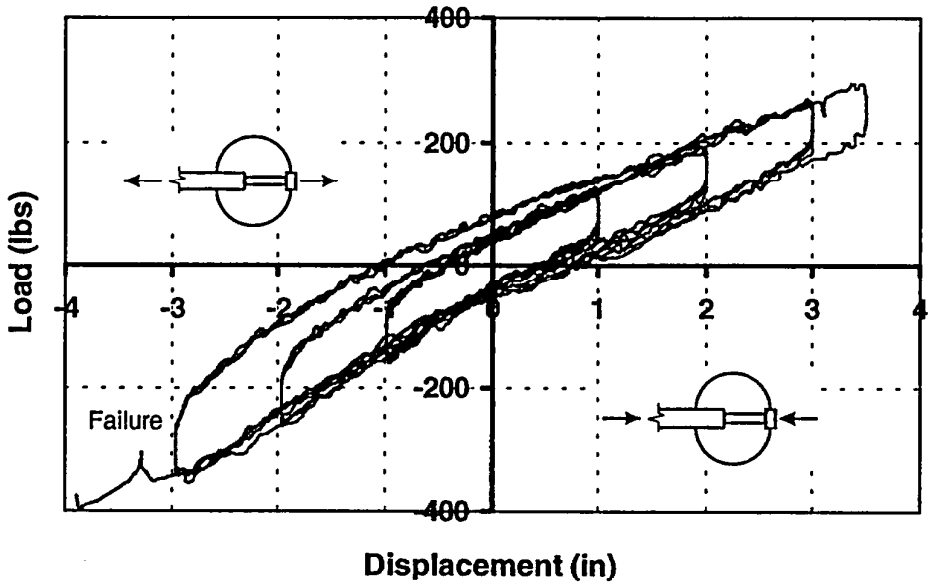

Figure 3.5 Load-Displacement Response of Rigid-Bus Slider.

Therefore, the overall behavior of the rigid bus slider tested can be simply modeled as a rigid-plastic behavior with a slip force of 53 lbs, and a post-slip stiffness of 83 lbs/in. Figure 3.6 compares the predictions of this simple model to the experimental data for the same displacement history used in the quasi-static-test.

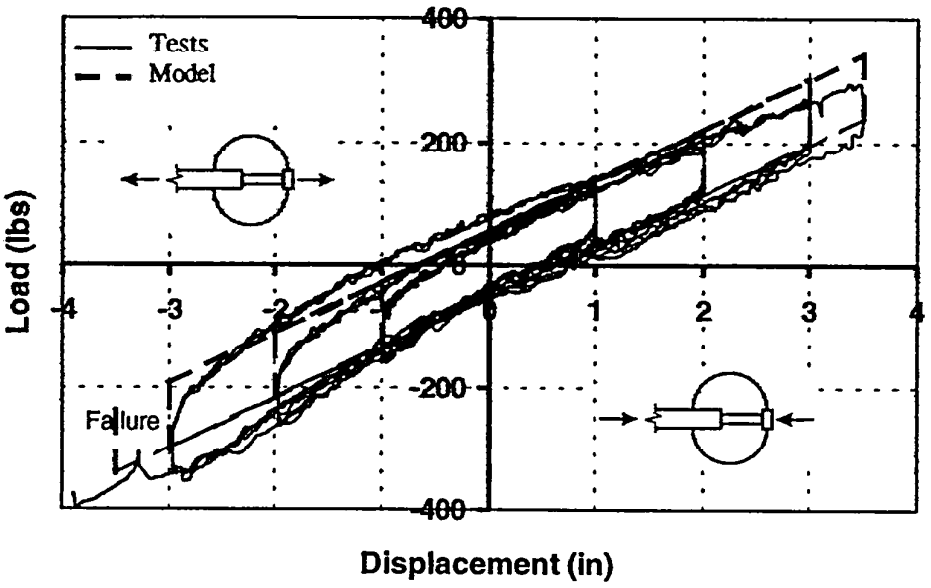

Figure 3.6 Rigid-Plastic Modeling of Rigid Bus Slider.

3.6 Equivalent Viscous Damping Ratios

The procedure described in section 2.9 was applied again on the hysteresis loops of Fig. 3.5 to evaluate the equivalent viscous damping ratio, ζ, of the bus slider for various displacement amplitudes. The resulting damping ratios are presented in Table 3.4 and are graphically shown in Fig. 3.7. For comparison purposes, the damping ratios computed for the three spring connectors tested and discussed in Chapter 2 are also shown in this figure.

Contrary to the spring connectors, the equivalent damping ratio of the bus slider decreases slightly with increasing displacement amplitude. The energy dissipated per cycle, $E_{D\delta}$, at a displacement amplitude δ can be written as:

$$E_{D\delta} = 4F_s\delta \tag{3.1}$$

where F_s is the slip force of the bus slider. The force, F_δ, at a displacement δ is given by:

$$F_\delta = F_s + K_e\delta \tag{3.2}$$

where K_e is the elastic restoring stiffness. Substituting equations (3.1) and (3.2) into equation (1.3) leads to a theoretical expression for the damping ratio, ζ, for the bus slider:

$$\zeta = \frac{2F_s}{\pi(F_s + K_e\delta)} \tag{3.3}$$

Equation (3.3) shows that the damping ratio of the bus slider decreases with increasing displacement amplitudes. For a slip force $F_s = 53\,lbs$, and a restoring stiffness $K_e = 83\,lbs/in$, equation (3.3) yields damping ratios of 0.25, 0.15, and 0.11 for displacement amplitudes $\delta = 1, 2, and\ 3\,in$, respectively. These predicted values agree reasonably well with the experimental values shown in Fig. 3.7.

For the range of displacements allowed by the slider, however, the equivalent viscous damping ratios provided by the bus slider are higher that the ones exhibited by the three

spring connectors. This result indicates the superior energy dissipation capacity of the bus slider at small displacement amplitudes.

Table 3.4 Equivalent Viscous Damping Ratios for Bus Slider.

Displacement Amplitude (in)	Equivalent Damping Ratio (%)
1.0	19.1
2.0	17.5
3.0	15.6

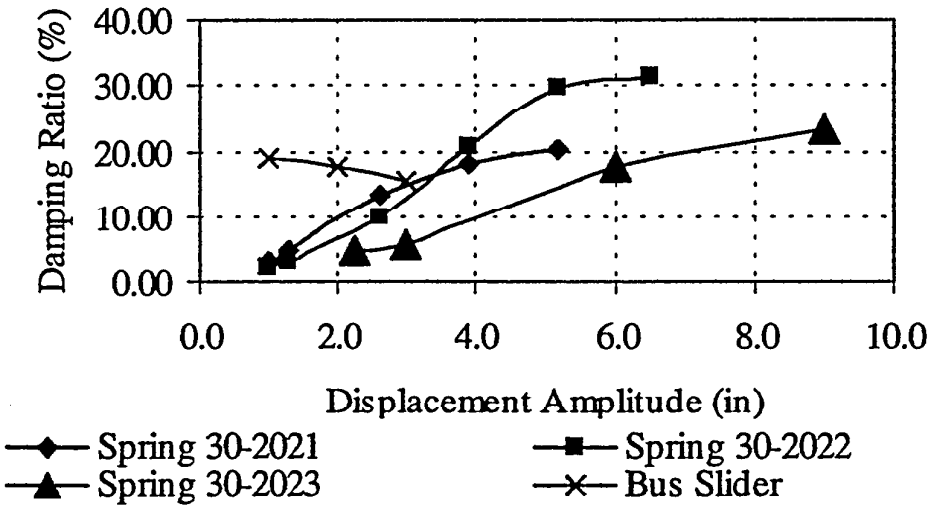

Figure 3.7 Comparison of Equivalent Viscous Damping Ratios for Bus Slider and Spring Connectors.

4. QUASI-STATIC TESTS OF FLEXIBLE BUS ASSEMBLIES

This chapter describes the full-scale quasi-static tests performed on two different types of flexible bus assemblies (cables). These tests were performed in the longitudinal direction of the assemblies under prescribed initial slackness and displacement history.

4.1 Description of Test Specimens

Three different flexible bus assemblies were supplied by PG&E for the quasi-static and shake table tests. Figure 4.1 presents a general view of the three specimens. Drawings of the specimens are included in Appendix A.

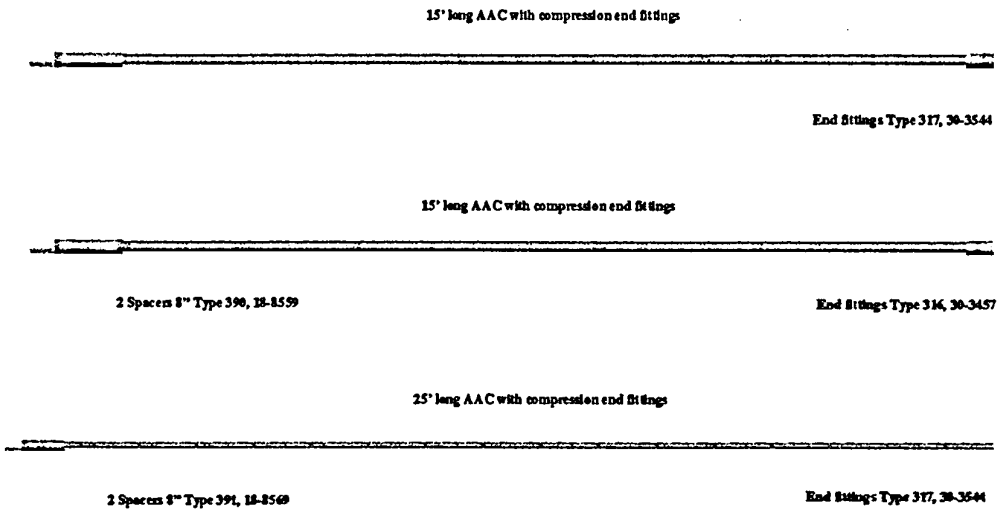

Figure 4.1 Flexible Bus Assemblies.

The first specimen consisted of a 2300 MCM single conductor, 15 ft long, with two compression end fittings. The 2300-type all aluminum cable (AAC) has a nominal diameter of 3.000 in and is composed of 49 wires. Its rated tensile strength is 34 300 lbs. The second specimen consisted of 1113 MCM bundled conductors, 15 ft long, with two spacers and two compression end fittings. The 1133-type all aluminum cable (AAC) has a nominal diameter of 1.095 in and is composed of 31 wires. Its rated tensile strength is 18 500 lbs. Finally, the third specimen consisted of a 2300 MCM bundled conductors, 25 ft long, with two spacers and two compression end fittings.

During unpacking of the specimens, it was observed that the cables were damaged at several locations. As shown in Fig. 4.2, individual strands were pulled apart permanently presumably because of the very tight loops used for shipping the cables. This local damage induced zones of unequal flexural flexibility in the cables, and caused problems in setting the initial geometry of the test specimens.

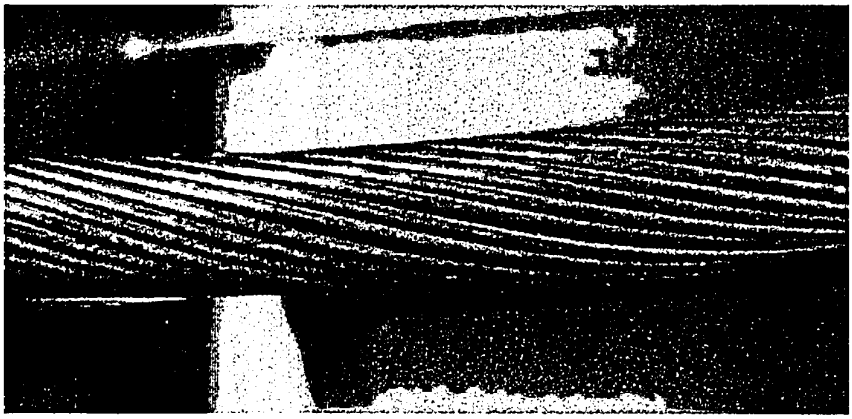

Figure 4.2 Local Damage to Flexible Conductor.

4.2 Experimental Set-Up for Quasi-Static Tests

The experimental set-up for the quasi-static tests on the flexible bus assemblies was similar as the one used for the quasi-static tests on the rigid bus-spring connector assemblies in Chapter 2 (see section 2.3).

The amount of initial slackness introduced in the cables was based on a single vertical loop having a maximum vertical displacement approximately equal to 10% of the length of each specimen. Because of the very low flexural rigidity of the specimens and the local damage experienced by the cables, it became very difficult to shape the specimens in this initial geometry. Figure 4.3 shows photograph of the first specimen (a 2300 MCM single conductor) supported in its initial geometry by a crane. When the crane support was removed just before the start of the test, the cable sagged laterally. For the 1113 MCM bundled conductors, it was easier to maintain the initial geometry of the specimen, as shown in Fig. 4.4.

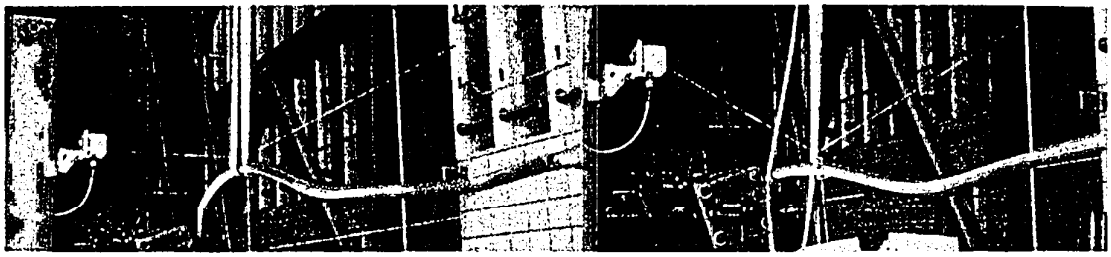

With Crane Support **Without Crane Support**

Figure 4.3 Initial Geometry of 2300 MCM Single Conductor.

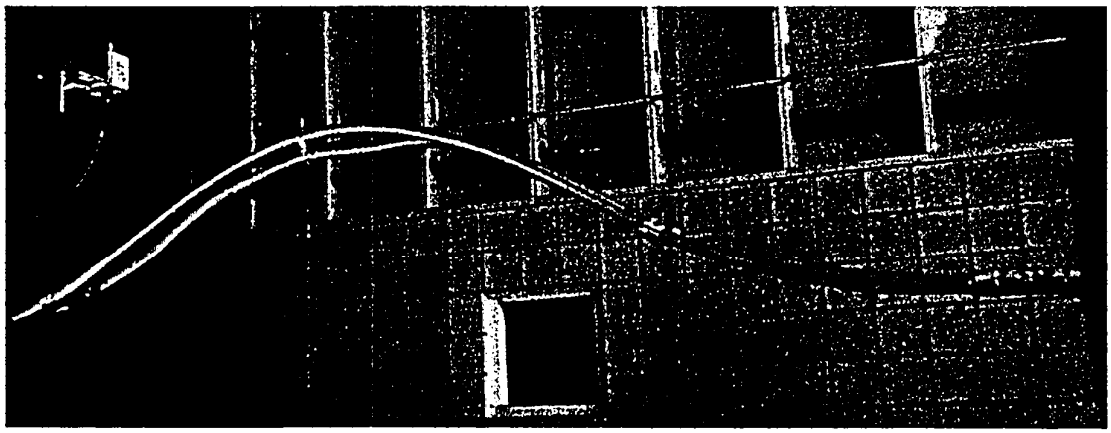

Figure 4.4 Initial Geometry of 1113 MCM Bundled Conductors.

4.3 Instrumentation

Only the instrumentation required to measure the force displacement hysteresis loops in the longitudinal direction of the flexible bus assemblies was installed. The force was measured across the 10-kip load cell that was inserted between the head of the actuator and the aluminum pipe (see section 2.3), and the displacement was measured across the full length of the specimens.

4.4 Test Protocol

The ATC-24 loading protocol (Applied Technology Council, 1992), used for the quasi-static tests of the rigid bus assemblies (see section 2.5), was used once again to perform the quasi-static tests on the flexible bus assemblies. As for the case of the rigid bus slider, an arbitrary value of 1 in was taken as the yield displacement, δ_y, across each of the specimen.

4.5 Experimental Results

Figures 4.5 and 4.6 present the load-displacement responses of the 2300 MCM single conductor and of the 1113 MCM bundled conductors, respectively. The behavior is similar for both specimens with virtually zero stiffness in compression and elastic tensile stiffness when the initial slack is overcome. The maximum compressive load measured during the two tests was less than 50 lbs. For the specimen incorporating 1113 MCM bundled conductors, the cable dropped from its initial geometry at a tensile displacement of 2.5 in. This reduced the compressive resistance of the cables to approximately 20 lbs for the subsequent cycles. Also for the 1113 MCM bundled conductors, the two cables were manufactured with different lengths, as seen in Fig. 4.7. This caused one cable to be taut much more than the other one.

Based on these results, it became clear that for the length of conductors tested the flexural stiffness of the cables played an insignificant role in the load-displacement responses. Therefore, it was decided not to test the third specimen that incorporated even longer cables (25 ft).

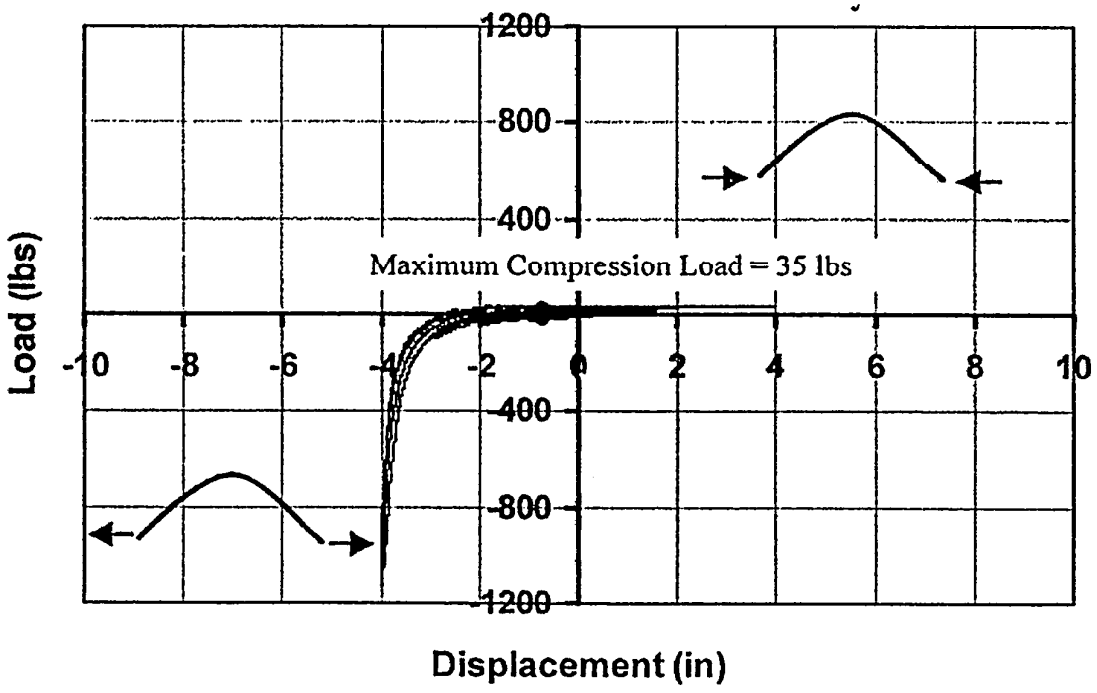

Figure 4.5 Load-Displacement Response of 2300 MCM Single Conductor.

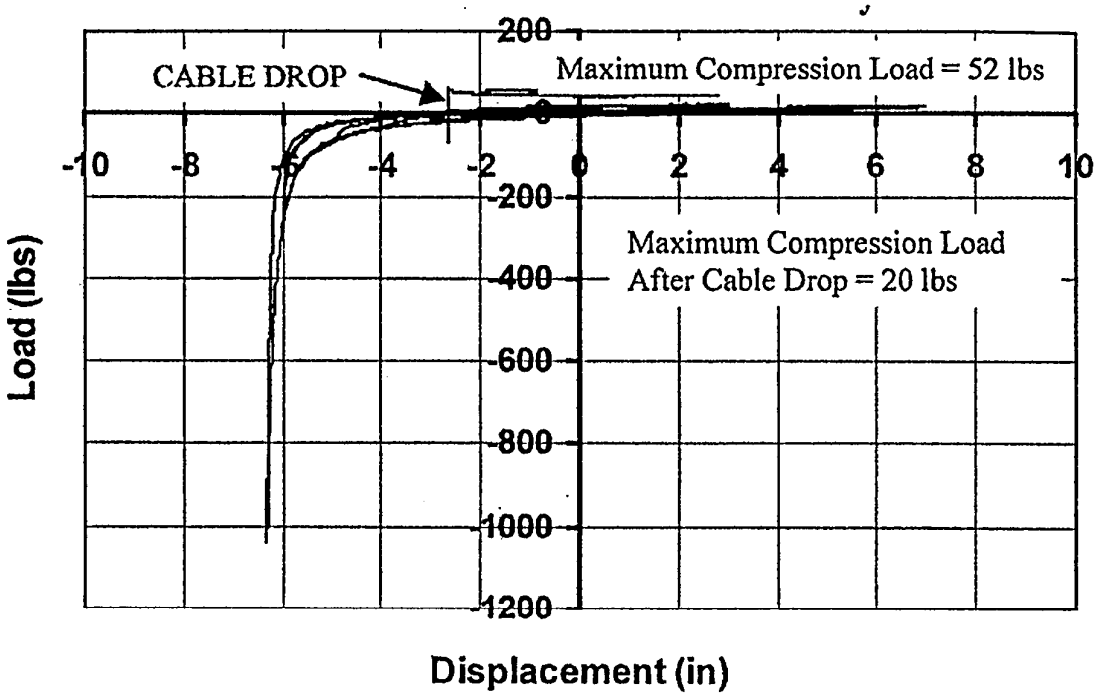

Figure 4.6 Load-Displacement Response of 1113 MCM Bundled Conductors.

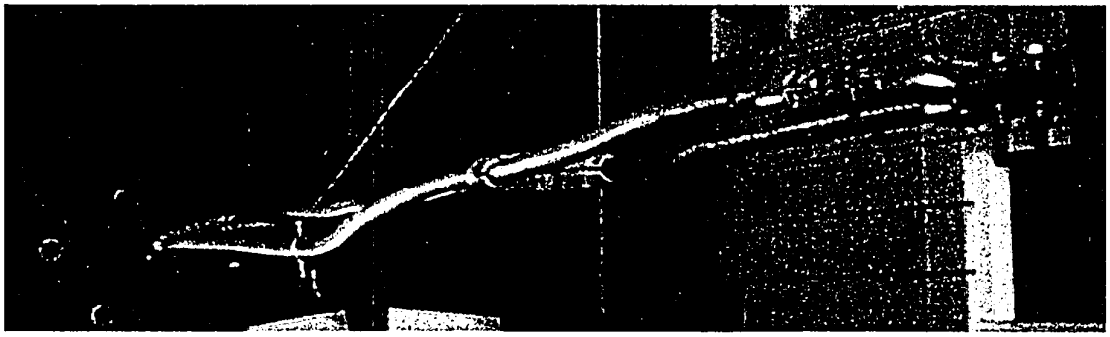

Figure 4.7 Unequal Cable Lengths for 1113 MCM Bundled Conductors.

5 SHAKE TABLE TESTS OF PAIRS OF GENERIC SUBSTATION EQUIPMENT CONNECTED WITH RIGID BUS ASSEMBLIES

This chapter describes the shake table tests performed on five pairs of generic substation equipment connected with three different rigid bus assemblies. Simulated horizontal ground motions were applied in the longitudinal direction of the bus assemblies by the uniaxial earthquake simulation facility at UC-San Diego. The variables considered in the tests were:

- the dynamic characteristics of the generic equipment
- the types of rigid bus assemblies
- the simulated ground motions
- the intensities of the simulated ground motions

5.1 Description of UC-San Diego Uniaxial Earthquake Simulation Facility

The uniaxial earthquake simulation system at UC-San Diego features a 4.8 tons shake table made of an all-welded steel construction, as shown in Figure 5.1. The shake table has plan dimensions of 10 ft x 16 ft with a specimen payload capacity of 40 tons. A 90-kips fatigue-rated actuator drives the system. The bearing system consists of eight 5-in Garlock DU cylinders sliding on two stationary shafts. The usable peak-to-peak stroke is 12 in. The flow rate of the hydraulic system allows a peak sinusoidal velocity of 40 in/s. The actuator can induce peak accelerations of 9.0 g for the bare table and 1.0 g for the fully loaded table. The workable frequency range of the simulator spans from 0 to 50 Hz.

The control system of the shake table includes an advanced, second generation, digital controller incorporating a Three-Variable-Control (TVC), together with Adaptive Inverse Control (AIC), On-Line Iteration (OLI) techniques and Resonance Canceling Notch Filters. This advanced control system allows the reproduction of earthquake ground motions with high fidelity (Filiatrault et al., 1996, 2000).

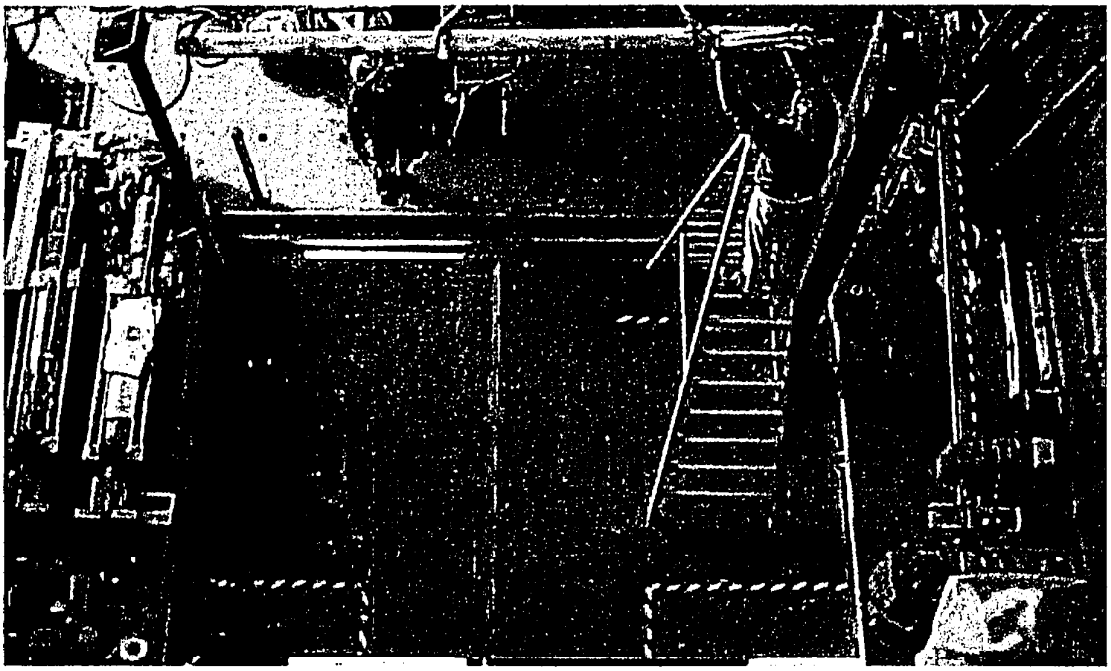

Figure 5.1 Shake Table of the UC-San Diego Uniaxial Earthquake Simulation System.

5.2 Description of Generic Substation Equipment

Initially, four different pairs of generic substation equipment were considered for the shake table tests. Each pair of generic equipment was designed to be representative of the dynamic properties of actual interconnected substation electrical equipment. Table 5.1 presents the target dynamic characteristics of the four pairs of generic equipment.

Table 5.1 Target Dynamic Characteristics of Pairs of Generic Equipment.

Pair	Equipment A			Equipment B		
	Equipment No.	Seismic Weight (lbs)	Natural Frequency (Hz)	Equipment No.	Seismic Weight (lbs)	Natural Frequency (Hz)
1	1	800	2	3	150	6
2	1	800	2	4	150	12
3	2	90	2	3	150	6
4	2	90	2	4	150	12

From table 5.1, four different generic equipment specimens are required to satisfy the test schedule. For each specimen, the seismic weight and the natural frequency are fixed.

Therefore, the design variables are the lateral stiffness of each specimen and the appropriate strength to assure an elastic dynamic response. For simplicity, it was decided to anchor steel cantilevered columns of appropriate stiffness and strength to the shake table. Figure 5.2 illustrates the test set-up for the shake table tests. In order to mobilize sufficient strength for a given lateral stiffness, the height of all cantilevers was fixed at 14 ft. Table 5.2 presents the tubular steel sections used to fabricate each column. Appendix B presents the shop drawings used to fabricate the specimens.

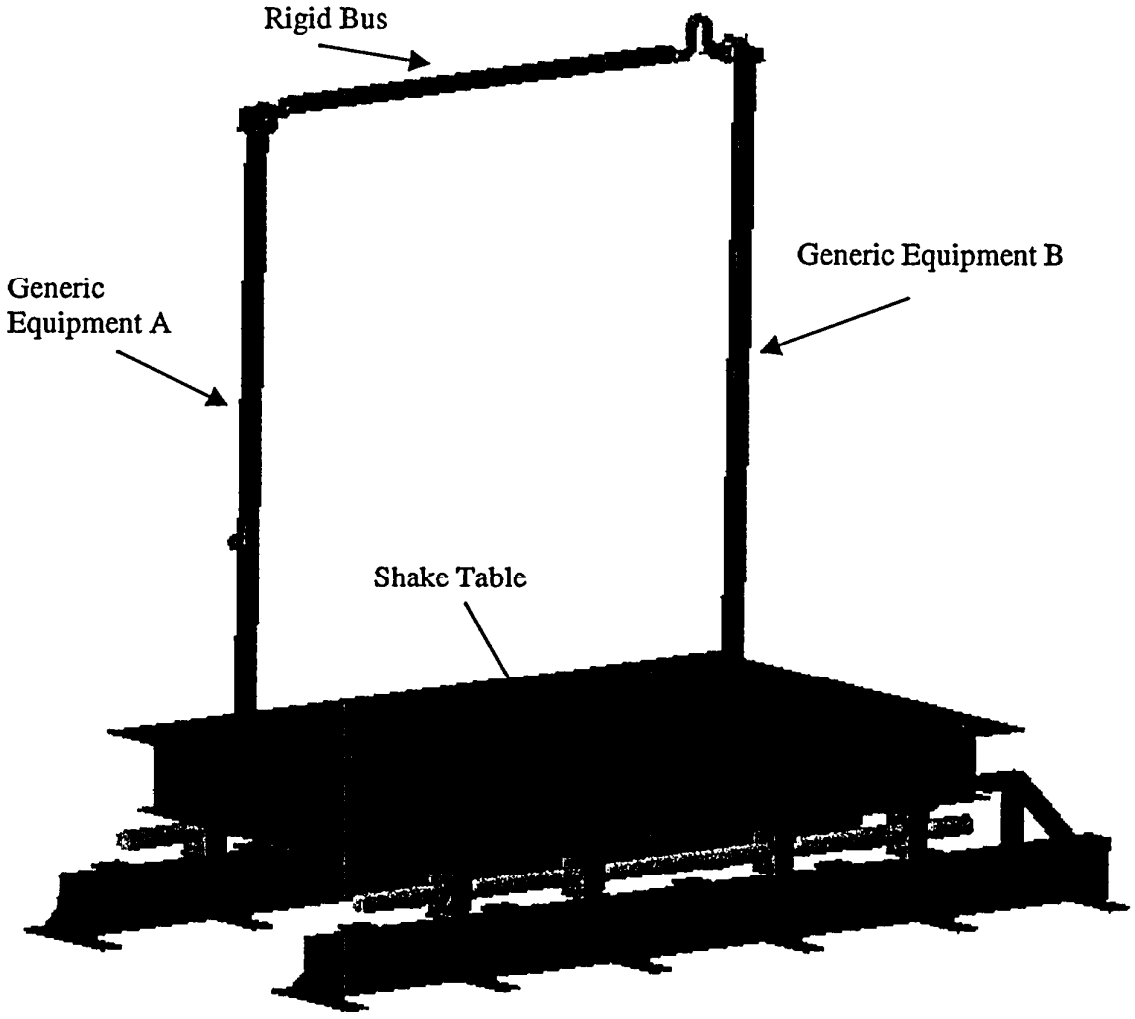

Figure 5.2 Test Set-Up for Shake Table Tests.

Table 5.2 Tubular Steel Sections Used for Generic Equipment Specimens.

Equipment	Seismic Weight (lbs)	Natural Frequency (Hz)	Tubular Section
1	800	2	7x5x3/16 in
2	90	2	3-1/2x2-1/2x1/4 in
3	150	6	8x6x3/16 in
4	150	12	12x8x5/16 in

In order to adjust the natural frequency of each equipment specimen, supplemental steel weights were added at the top of the columns, as illustrated in Fig. 5.3. Table 5.3 indicates the final lumped weight added at the top of each equipment specimen along with the total weight of each specimen.

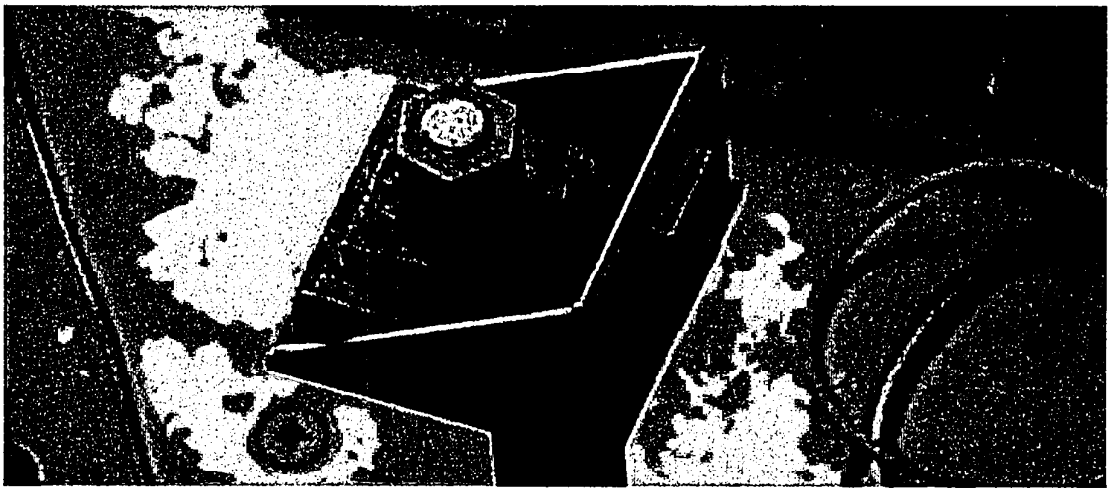

Figure 5.3 Supplemental Steel Weights at Top of Generic Equipment Specimen.

Table 5.3 Values of Steel Weights at Lumped Top of Generic Equipment Specimen.

Equipment	Target Seismic Weight (lbs)	Target Natural Frequency (Hz)	Lumped Top Weight (lbs)	Total Weight (lbs)
1	800	2	747	951
2	90	2	76	200
3	150	6	94	334
4	150	12	30	595

5.3 Instrumentation

The instrumentation used during the shake table tests of the generic interconnected equipment included the following measurements:

- Absolute displacement, velocity and acceleration of the shake table;
- Absolute displacement, velocity and acceleration at the top of each equipment
- Relative displacement between equipment
- Axial strain at the location of maximum moment in the spring connector

The velocity measurements were obtained directly with special string potentiometers calibrated with velocity.

5.4 Earthquake Ground Motions and Shake Table Fidelity

Two recorded components of near-field earthquake ground motions were used for the seismic tests on the shake table: Tabas (1978 Iran earthquake) and Newhall (1994 Northridge, California, earthquake). These two records are representative of earthquakes known to have a high potential for damaging structures and equipment. Figure 5.4 presents the acceleration time-histories for both full-scale records (100% span).

The Tabas record was modified using a nonstationary response-spectrum matching technique developed by Abrahamson (1997) to match the IEEE 693 (1997) target response spectrum for testing, and it was further high-pass filtered using a cut-off frequency of 1.5 Hz so as not to exceed the displacement limit of 6 in of the shake table.

Preliminary nonlinear dynamic time-history analyses were performed to estimate the response of the interconnected equipment. Based on the results of these preliminary analyses, different intensities were retained for each ground motion record. Table 5.4 presents these intensities for the two ground motions considered. Significant inelastic response of the rigid bus conductors was anticipated at the largest intensities. Note also that certain tests were conducted at intermediate intensity levels.

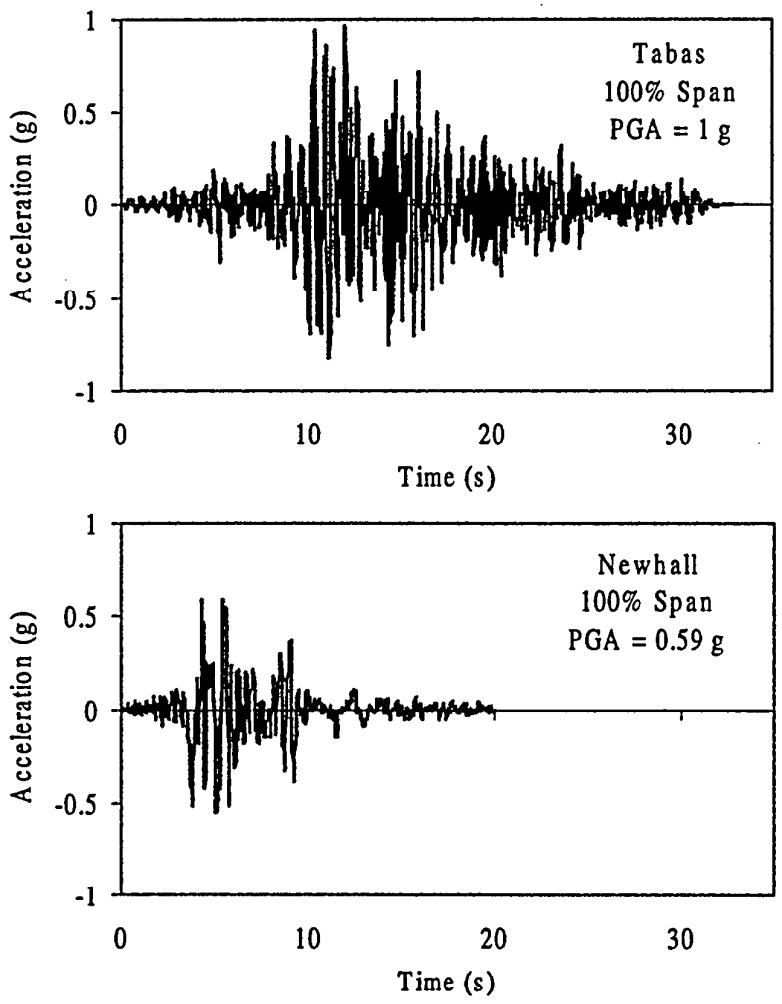

Figure 5.4 Acceleration Time-Histories of Earthquake Ground Motions.

Table 5.4 Intensities of Earthquake Ground Motions Retained for the Shake Table Tests

Record	Intensity 1 (% Span)	Intensity 2 (% Span)	Intensity 3 (% Span)
Tabas	25	50	200
Newhall	30	100	---

The performance of the shake table was optimized for each record and intensity using the On-Line Iteration (OLI) technique of the electronic controller. Figure 5.5 compares the absolute acceleration response spectra, at 5% damping, of the accelerograms of Fig. 5.4 scaled at the different intensities listed in Table 5.4 (desired signals) with the response spectra of the acceleration time-histories recorded on the shake table (feedback signals). The feedback signals shown represent the mean values of three different tests on the shake table.

As discussed earlier, the target natural frequencies of the generic equipment varied between 2 and 12 Hz. The mean differences (in %) between the desired and the feedback spectral values in the 2-12 Hz frequency range are also indicated in Fig. 5.5. The maximum difference for all records is less than 6%. Based on this result, the performance of the shake table was considered adequate. For comparison purposes, each graph in Fig. 5.6 shows also the IEEE 693 (IEEE, 1997) required response spectrum for 2% damping and for high performance level amplified by a factor of two to account for the amplification of earthquake motion at the base of the generic equipment.

5.5 Shake Table Test Program

Three different types of shake table tests were conducted on the rigid bus conductors:

1) Frequency Evaluation Tests
2) Damping Evaluation Tests
3) Seismic Tests

These tests are briefly described below.

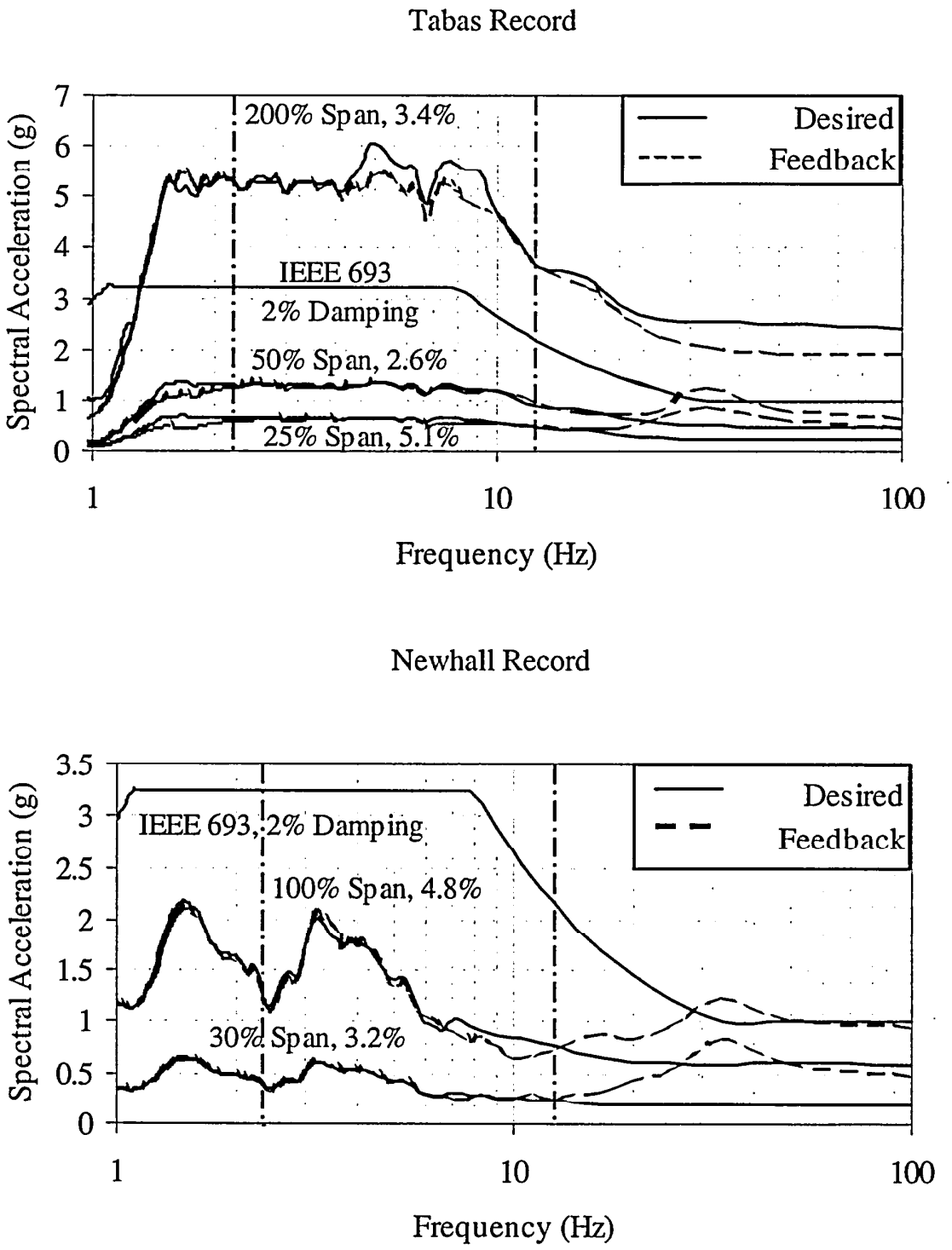

Figure 5.5 Absolute Acceleration Response Spectra, 5% Damping, Bare Shake Table.

5.5.1 Frequency Evaluation Tests

The purpose of the frequency evaluation tests was to identify the natural frequencies and mode shapes of the various pairs of interconnected generic substation equipment. For this purpose, a low-amplitude 0-40 Hz, clipped-band, and flat white noise excited each configuration. A dedicated ambient vibration analysis software (Experimental Dynamic Investigations, 1993) was used to determine the natural frequencies from power spectral density plots of the absolute acceleration records at the top of each equipment. The structural mode shapes were obtained from the amplitudes of the spectral peaks and by the phase and coherence between the measured acceleration time-histories. For all frequency evaluation tests, the following test protocol was followed:

- Nyquist frequency = 40 Hz
- Sampling rate = 80 Hz
- Number of points per sampling windows = 2048
- Duration of each sampling window = 25.6 s
- Frequency resolution = 0.0391 Hz
- Number of sampling windows = 8
- Total duration = 204.8 s

5.5.2 Damping Evaluation Tests

The purpose of the damping evaluation tests was to estimate the first modal equivalent viscous damping of each equipment configuration. In these tests, each pair of generic equipment was excited by a low-amplitude base sinusoidal input at its previously identified fundamental frequency. When a steady-state response was obtained, the input was suddenly stopped and the absolute accelerations at the top of the equipment were recorded. The first modal damping ratio of the structural configuration was then established by the logarithmic decrement method (Clough and Penzien, 1993).

5.5.3 Seismic Tests

In the seismic tests, the ground motions defined in section 5.4 excited the pairs of interconnected equipment. All seismic test data were acquired at a sampling rate of 200 Hz to capture potential impacts between the rigid bus and the top of the Equipment.

5.6 Rigid Bus Specimens

Three different rigid bus connector assemblies were tested with each of the four pairs of interconnected equipment defined in Table 5.1. These rigid bus assemblies were:

1) The bus assembly with the spring connector 30-2022 described in Section 2.2.
2) The rigid bus slider described in Section 3.1.
3) A seismic connector with a 4 in diameter rigid bus developed by Bonneville Power Administration (BPA).

The first two rigid bus specimens were tested previously under quasi-static loading, as described in Chapters 2 and 3. The third rigid bus specimen was provided by PG&E only for the shake table tests and was not tested under quasi-static loading.

Figure 5.6 presents photographs of the BPA seismic connector tested on the shake table. The connector includes three vertically parallel 6061-T6 aluminum alloy, 1.3 in diameter, cables (Hood conductor, AAC/TW). These cables are welded to 6061-T6-aluminum alloy T-shape plates that are mounted to the rigid conductor. This seismic connector was similar to the specimen tested in a previous investigation at Portland State University (Starkel et al., 1998). Drawings of the BPA seismic connector are included in Appendix A of this report.

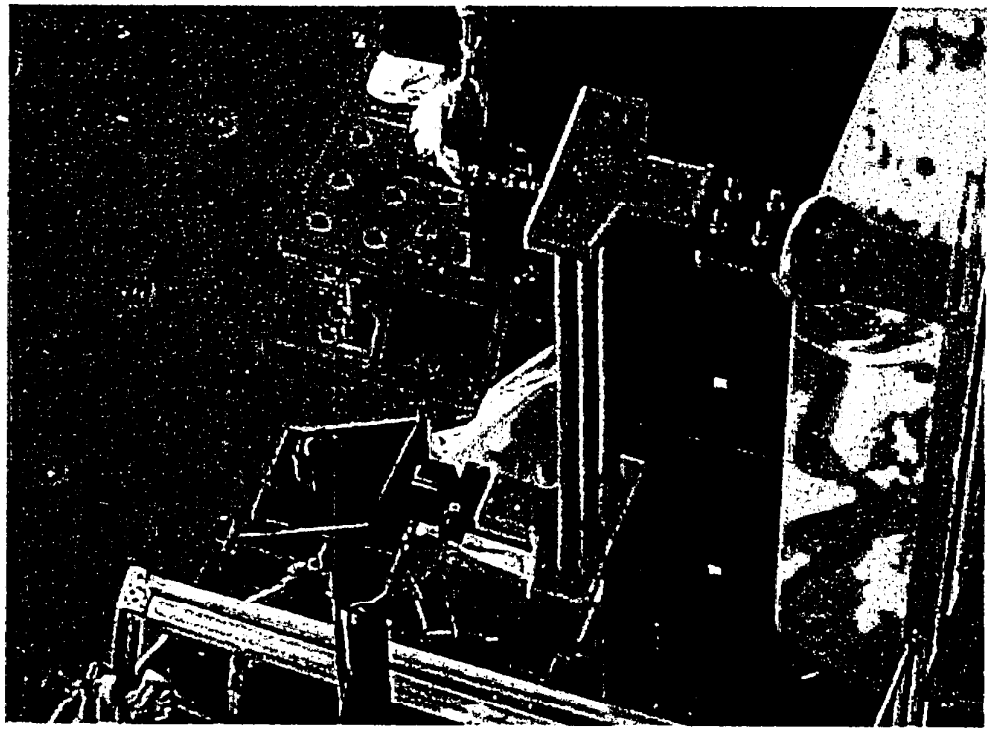

Detail of Seismic Connector

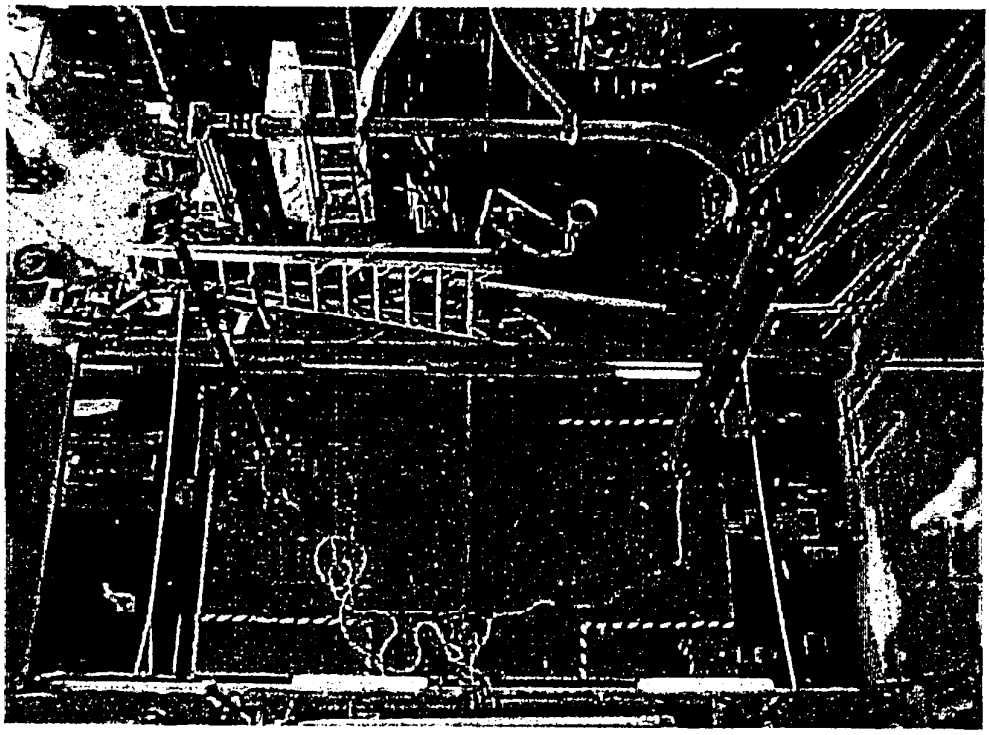

General Arrangement on Shake Table

Figure 5.6 BPA Seismic Connector.

5.7 Test Sequence

Table 5.4 presents the test sequence that was adopted for the shake table tests. Included are the frequency and damping evaluation tests, as well as the seismic tests under the various earthquake ground motion records. This sequence was developed in order to optimize the use of the rigid bus conductor specimens provided by PG&E. Note that some test numbers are missing from Table 5.4. These are tests that were originally scheduled but later cancelled in order to maintain the integrity of the equipment configurations until the end of the test sequence. Finally, tests listed with Pair No. 5 in Table 5.4 refers to Pair No. 2 with Equipment 4 modified with a lateral bracing member, as described in section 5.6.3.

Table 5.4 Shake Table Test Sequence

Test RB-#	Pair No.	Conductor	Test Description	Input Signal	Span (%)
1	4	None	Frequencies of Uncoupled Equipment	White Noise	---
2	4	None	Damping - A	Sinusoidal	---
3	4	None	Damping - B	Sinusoidal	---
4	4	Spring 30-2022	Frequencies of Coupled Equipment	White Noise	---
5	4	Spring 30-2022	Damping - A & B	Sinusoidal	---
6	4	Spring 30-2022	Seismic	Newhall	30
7	4	Spring 30-2022	Seismic	Newhall	100
8	4	Spring 30-2022	Seismic	Tabas	25
9	4	Spring 30-2022	Seismic	Tabas	50
10	4	None	Frequencies of Uncoupled Equipment	White Noise	---
11	4	None	Damping - A	Sinusoidal	---
12	4	None	Damping - B	Sinusoidal	---
13	4	Bus Slider	Frequencies of Coupled Equipment	White Noise	---
14	4	Bus Slider	Damping - A & B	Sinusoidal	---
15	4	Bus Slider	Seismic	Newhall	100
17	4	Bus Slider	Seismic	Tabas	50
18	4	Bus Slider	Seismic	Tabas	200
22	4	BPA Isolator	Frequencies of Coupled Equipment	White Noise	---
23	4	BPA Isolator	Damping – A & B	Sinusoidal	---
24	4	BPA Isolator	Seismic	Newhall	30
26	4	BPA Isolator	Seismic	Tabas	25
28	4	None	Seismic	Newhall	30
29	4	None	Seismic,	Newhall	100
30	4	None	Seismic	Tabas	25
31	4	None	Seismic	Tabas	50
33	3	None	Frequencies of Uncoupled Equipment	White Noise	100
35	3	None	Damping - B	Sinusoidal	100

Test RB-#	Pair No.	Conductor	Test Description	Input Signal	Span (%)
36	3	Spring 30-2022	Frequencies of Coupled Equipment	White Noise	---
37	3	Spring 30-2022	Damping – A & B	Sinusoidal	---
38	3	Spring 30-2022	Seismic	Newhall	30
39	3	Spring 30-2022	Seismic	Newhall	100
40	3	Spring 30-2022	Seismic	Tabas	25
41	3	Spring 30-2022	Seismic	Tabas	50
45	3	Bus Slider	Frequencies of Coupled Equipment	White Noise	---
46	3	Bus Slider	Damping – A & B	Sinusoidal	---
47	3	Bus Slider	Seismic	Newhall	100
49	3	Bus Slider	Seismic	Tabas	50
54	3	BPA Isolator	Frequencies of Coupled Equipment	White Noise	---
55	3	BPA Isolator	Damping – A & B	Sinusoidal	---
56	3	BPA Isolator	Seismic	Newhall	30
58	3	BPA Isolator	Seismic	Tabas	25
60	3	None	Seismic	Newhall	30
61	3	None	Seismic	Newhall	100
62	3	None	Seismic	Tabas	25
63	3	None	Seismic	Tabas	50
66	1	None	Frequencies	White Noise	---
67	1	None	Damping - A	Sinusoidal	---
68	1	None	Damping - B	Sinusoidal	100
69	1	Spring 30-2022	Frequencies of Coupled Equipment	White Noise	---
70	1	Spring 30-2022	Damping – A & B	Sinusoidal	---
71	1	Spring 30-2022	Seismic	Newhall	30
72	1	Spring 30-2022	Seismic	Tabas	25
76	1	Bus Slider	Frequencies of Coupled Equipment	White Noise	---
77	1	Bus Slider	Damping – A & B	Sinusoidal	---
78	1	Bus Slider	Seismic	Newhall	100
79	1	Bus Slider	Seismic	Tabas	50
83	1	BPA Isolator	Frequencies of Coupled Equipment	White Noise	---
84	1	BPA Isolator	Damping – A & B	Sinusoidal	---
85	1	BPA Isolator	Seismic	Newhall	30
87	1	BPA Isolator	Seismic	Tabas	25
96	2	Spring 30-2022	Frequencies of Coupled Equipment	White Noise	---
97	2	Spring 30-2022	Damping – A & B	Sinusoidal	---
98	2	Spring 30-2022	Seismic	Newhall	30
99	2	Spring 30-2022	Seismic	Tabas	25
100	2	Spring 30-2022	Seismic	Tabas	50
101	2	Spring 30-2022	Seismic	Newhall	100
102	2	Spring 30-2022	Seismic	Tabas	100
103	2	Spring 30-2022	Seismic	Tabas	150
107	2	Bus Slider	Frequencies of Coupled Equipment	White Noise	---
108	2	Bus Slider	Damping – A & B	Sinusoidal	---
109	2	Bus Slider	Seismic	Newhall	30
110	2	Bus Slider	Seismic	Tabas	25
111	2	Bus Slider	Seismic	Tabas	50
112	2	Bus Slider	Seismic	Newhall	100
116	2	BPA Isolator	Frequencies of Coupled Equipment	White Noise	---
117	2	BPA Isolator	Damping - A & B	Sinusoidal	---
118	2	BPA Isolator	Seismic	Newhall	30

Test RB-#	Pair No.	Conductor	Test Description	Input Signal	Span (%)
119	2	BPA Isolator	Seismic	Tabas	25
120	2	BPA Isolator	Seismic	Tabas	50
121	2	BPA Isolator	Seismic	Newhall	100
122	2	BPA Isolator	Seismic	Tabas	75
123	2	BPA Isolator	Seismic	Tabas	100
124	2	None	Seismic	Newhall	30
125	2	None	Seismic	Tabas	25
126	2	None	Seismic	Tabas	50
127	2	None	Seismic	Newhall	100
130	5	None	Frequencies	White Noise	---
131	5	None	Damping - A	Sinusoidal	---
132	5	None	Damping - B	Sinusoidal	---
133	5	Spring 30-2022	Frequencies	White Noise	---
134	5	Spring 30-2022	Damping A-B, First Mode	Sinusoidal	---
135	5	Spring 30-2022	Damping A-B, Second Mode	Sinusoidal	---
136	5	Spring 30-2022	Seismic	Newhall	30
137	5	Spring 30-2022	Seismic	Tabas	25
138	5	Spring 30-2022	Seismic	Tabas	50
139	5	Spring 30-2022	Seismic	Newhall	100
140	5	Spring 30-2022	Seismic	Tabas	100
141	5	Spring 30-2022	Seismic	Tabas	150
142	5	Bus Slider	Frequencies	White Noise	---
143	5	Bus Slider	Damping A-B	Sinusoidal	---
144	5	Bus Slider	Seismic	Newhall	30
145	5	Bus Slider	Seismic	Tabas	25
146	5	Bus Slider	Seismic	Tabas	50
147	5	Bus Slider	Seismic	Newhall	100
148	5	Bus Slider	Seismic	Tabas	100
149	5	BPA Isolator	Frequencies	White Noise	---
150	5	BPA Isolator	Damping – First Mode	Sinusoidal	---
151	5	BPA Isolator	Damping – Second Mode	Sinusoidal	
152	5	BPA Isolator	Seismic	Newhall	30
153	5	BPA Isolator	Seismic	Tabas	25
154	5	BPA Isolator	Seismic	Tabas	50
155	5	BPA Isolator	Seismic	Newhall	100
156	5	BPA Isolator	Seismic	Tabas	100
157	5	None	Seismic	Newhall	30
158	5	None	Seismic	Tabas	25
159	5	None	Seismic	Tabas	50
160	5	None	Seismic	Newhall	100

5.8 Results of Frequency and Damping Evaluation Tests

The detailed results of all frequency evaluation tests conducted on all generic equipment combinations are presented in Appendix C. Included are power spectral density, phase, and coherence plots obtained from the absolute acceleration records at the top of each equipment. The results of the damping evaluation tests are presented in Appendix D. For each damping evaluation test, the detailed calculations of the first modal damping ratios by the logarithmic decrement method are included.

Table 5.5 summarizes the results of the frequency and damping evaluation tests on the stand alone (unconnected) generic equipment specimens. The fundamental frequencies of equipment 3 and 4 are substantially lower than the target frequencies shown in Table 5.3. For these stiffer equipment specimens, it was not possible to completely prevent rotation at the base. Rocking of the base caused the fundamental frequencies to be lower than anticipated. Therefore, it was decided to repeat the tests on Pair No. 2 with Equipment 4 equipped with a lateral bracing member (2 angles 3x3x3/8 back-to-back) to increase its natural frequency to 12 Hz. This new pair of equipment is referred to as Pair No. 5. Figure 5.7 presents a photograph of the modified Equipment 4. The shop drawings of the brace assembly are included in Appendix B.

Table 5.5 Measured Natural Frequencies and Damping of Generic Equipment Specimens.

Equipment	Natural Frequency (± 0.04 Hz)			First Modal Damping Ratio (%)
	Mode 1	Mode 2	Mode 3	
1	1.99	19.84	23.75	0.42
2	1.88	16.88	29.22	0.52
3	4.10	Not Measured	Not Measured	0.41
4	5.47	28.30	Not Measured	0.39
4 with Brace	12.23	Not Measured	Not Measured	0.29

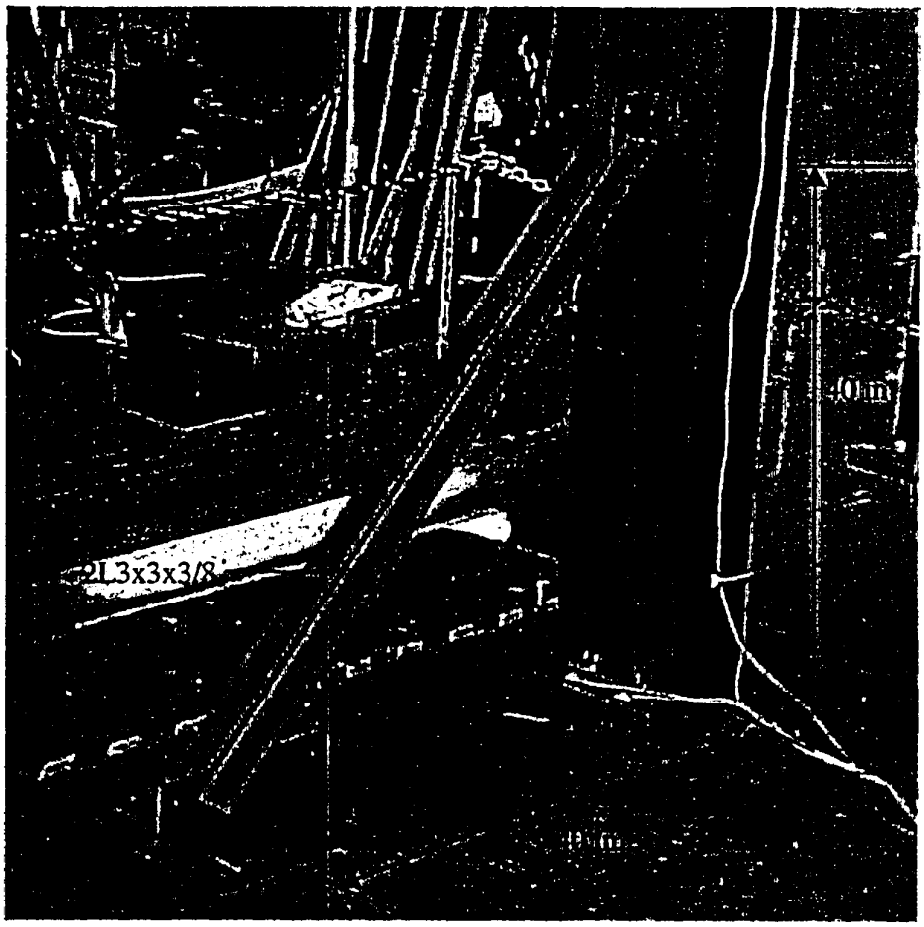

Figure 5.7 Equipment 4 Retrofitted with Bracing Element.

Tables 5.6 to 5.8 summarize the results of the frequency and damping evaluation tests on the five pairs of generic equipment specimens interconnected by the three different rigid bus assemblies. The mode shapes are represented by the relative motions at the top of the equipment specimens. For the tests involving the bus slider, a mechanical locking device was introduced at the sliding interface to prevent slippage. This locking device was removed for the seismic tests.

The natural frequencies measured on the generic equipment specimens interconnected by the bus assemblies fall between the natural frequencies obtained for the stand alone generic equipment specimens (see Table 5.5). The lowest natural frequencies were

obtained with the flexible BPA seismic connector, while the highest natural frequencies correspond to the pairs of equipment interconnected with the rigid bus slider. With the bus slider, the vibrations of at the top the equipment specimens are in phase for all frequencies since the bus slider is rigid.

Table 5.6 Results of Frequency and Damping Evaluation tests on Equipment Interconnected by Bus Assembly with Spring Connector.

Pair	Mode 1				Mode 2			Mode 3		
	Natural Frequency (± 0.04 Hz)	Mode Shape		Damping Ratio (%)	Natural Frequency (± 0.04 Hz)	Mode Shape		Natural Frequency (± 0.04 Hz)	Mode Shape	
		A	B			A	B		A	B
1	2.38	1	0.64	1.10	5.15	1	-3.71	20.08	1	0.70
2	2.58	1	0.49	0.63	5.82	1	-4.52	20.08	1	0.60
3	3.01	1	0.83	1.00	6.60	1	-0.78	17.31	1	-0.16
4	3.79	1	0.54	0.90	6.72	1	-0.98	17.31	1	-0.05
5	2.96	1	0.14	1.85	11.37	1	-15.3	Not Measured	-	---

Table 5.7 Results of Frequency and Damping Evaluation Tests on Equipment Interconnected by Bus Slider.

Pair	Mode 1				Mode 2			Mode 3		
	Natural Frequency (± 0.04 Hz)	Mode Shape		Damping Ratio (%)	Natural Frequency (± 0.04 Hz)	Mode Shape		Natural Frequency (± 0.04 Hz)	Mode Shape	
		A	B			A	B		A	B
1	2.54	1	0.99	1.08	19.81	1	0.66	28.20	1	0.40
2	3.05	1	1.00	1.16	19.81	1	0.47	26.02	1	1.11
3	3.16	1	1.06	1.86	15.43	1	0.88	20.04	1	0.72
4	4.30	1	1.00	1.57	14.92	1	0.66	20.08	1	0.56
5	5.78	1	0.96	0.47	Not Measured	-	---	Not Measured	-	---
Note: These tests were performed with the slider mechanically locked to prevent slippage										

Table 5.8 Results of Frequency and Damping Evaluation Tests on Equipment Interconnected by Rigid Bus with BPA Seismic Connector.

Pair	Mode 1				Mode 2			Mode 3		
	Natural Frequency (± 0.04 Hz)	Mode Shape		Damping Ratio (%)	Natural Frequency (± 0.04 Hz)	Mode Shape		Natural Frequency (± 0.04 Hz)	Mode Shape	
		A	B			A	B		A	B
1	2.07	1	0.16	1.84	3.39	1	---	20.08	1	0.86
2	2.07	1	0.10	1.60	4.22	1	-17.8	20.08	1	0.63
3	2.34	1	0.24	1.65	3.40	1	-1.75	15.66	1	-0.63
4	2.38	1	0.10	1.85	4.34	1	-4.47	15.39	1	-0.62
5	2.11	1	0.01	0.36	8.42	-	---	15.43	-	---

5.9 Results of Seismic Tests

The results of all seismic tests conducted on the five pairs of generic equipment specimens interconnected by the three different rigid bus assemblies are presented in Appendix E. Included for each seismic test are time-history plots of:

- Absolute acceleration of the shake table
- Relative horizontal displacement at the top of Equipment A
- Relative horizontal displacement at the top of Equipment B
- Absolute horizontal acceleration at the top of Equipment A
- Absolute horizontal acceleration at the top of Equipment B
- Relative displacement between Equipment A and Equipment B
- Longitudinal force in the connector
- Force-displacement hysteresis loops across the connector
- Axial strain at the apex of the spring connector

The longitudinal force in the connector, $F_c(t)$, was obtained by considering the dynamic equilibrium at the top of equipment specimen A, adjacent to the connector:

$$F_c(t) = m_A \ddot{x}_{aA}(t) + c_A \dot{x}_{rA}(t) + k_A x_{rA}(t) \qquad (5.1)$$

where $m_A, c_A, and\ k_A$ are the mass, viscous damping coefficient and lateral stiffness of equipment specimen A, respectively, and $x_{rA}(t), \dot{x}_{rA}(t), and\ \ddot{x}_{aA}(t)$ are the relative displacement, relative velocity, and absolute acceleration at the top of equipment specimen A, respectively.

The test series with Equipment Pairs No. 4, 3, and 1 were performed for low intensity ground motions so that no damage occurred in the connectors. For the tests with Equipment Pairs No. 2 and No. 5, higher intensity ground motions were used to evaluate the behavior of the various connectors for their full range of performance.

The spring connector 30-2022 exhibited slight inelastic behavior in Tests RB-7, RB-100, RB-101, RB-138, and RB-139 (pages E3, E35, E36, E55, and E56) and severe yielding in Tests RB-102, RB-103, RB-140, and RB141 (pages E37, E38, E57, and E58). In these latter tests, maximum axial strains in excess of 10 000 $\mu\varepsilon$ were recorded in the spring connector.

Figure 5.8 shows photographs of the spring connector at the completion of Test RB-103. The yielding regions are clearly visible along with the significant permanent vertical deformation between the two ends of the connector.

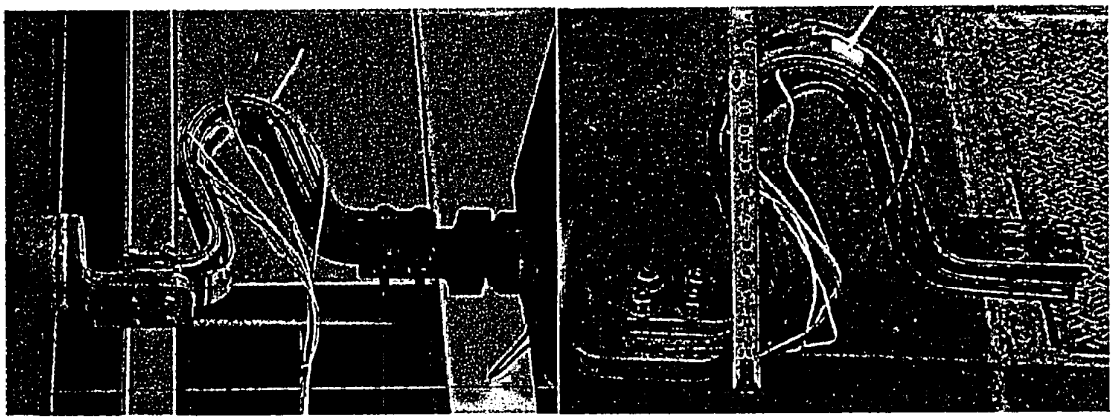

Figure 5.8 Spring 30-2022 After Shake Table Test No. RB-103.

The bus slider performed well except for Tests RB-18 and RB-148 where the shaft came out of the aluminum pipe during the shaking. This induced sever impact loading between the shaft and the pipe as shown by the very large forces and accelerations recorded at the top of the generic equipment specimens. After Test RB-18, the looped cables had yielded permanently and it was not possible to re-insert the shaft inside the pipe. The unit had to be replaced for the following tests. Figure 5.9 presents a photograph of the bus slider at the end of Test RB-18. This damage could be avoided by increasing the available travel distance of the shaft inside the aluminum pipe.

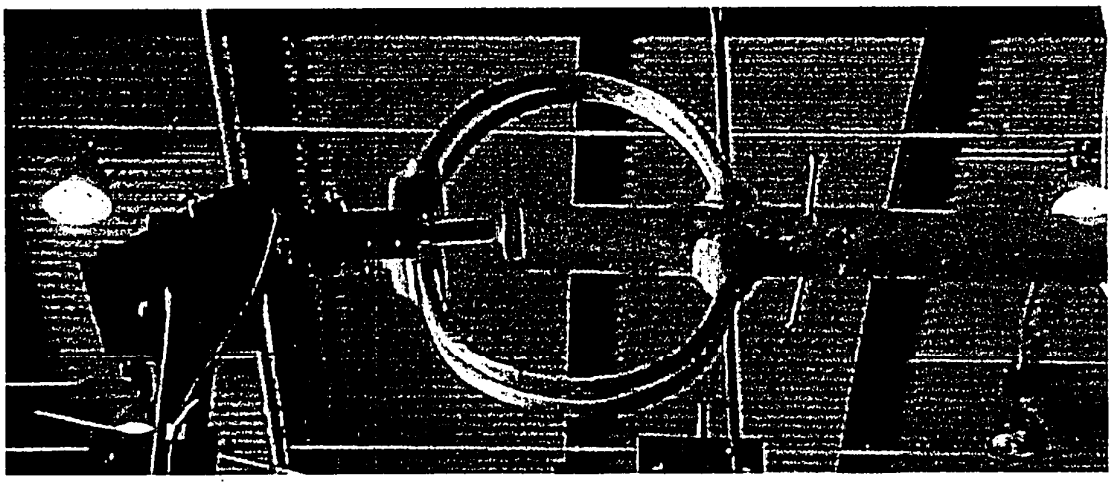

Figure 5.9 Bus Slider After Shake Table Test RB-18.

The BPA isolator did not suffer any visible damage during the shake table testing. For the largest intensity tests (Tests RB-121, RB-122, RB-123, and RB-156), significant second-order vertical deflections were observed between the top and bottom ends of the isolator. These deflections introduced significant bending strains in the two load cells.

The physical arrangement of the rigid bus along with its significant mass caused a rigid-body rotation of the whole specimen during some of the tests, since no torsional stiffness was provided by the load-cell connections. This observation suggests that a rigid bus equipped with a BPA isolator could induce significant torsional couples at the top of the equipment under transverse seismic loading.

The maximum experimental values recorded for all seismic tests are summarized presented in Table 5.9. Included in this table for each seismic test are: the maximum relative displacement and maximum absolute acceleration at the top of both equipment specimens, and the maximum force induced in the connector. Note that, although no yielding occurred in the equipment specimens, the behavior of the stand alone equipment specimens is not perfectly linear (e.g. the maximum displacement and acceleration values more than double when the ground motion intensity is increased by a factor of two). This non-linearity is particularly important for equipment specimens A (1 and 2 in Table 5.5), and is believed to be the results of the rocking of the base.

The maximum forces induced in the various connectors during the seismic shake table tests are presented in Figs. 5.10 and 5.11. The results are presented for each ground motion, equipment pair, and intensity level. The BPA connector, being more flexible than the other two connectors, consistently induces the smaller forces. The spring connector consistently induces the largest forces.

Table 5.9. Maximum Experimental Values from Seismic Tests.

Pair	Ground Motion-Span (%)	Peak Relative Displacement Equipment A (in)				Peak Relative Displacement Equipment B (in)				Peak Absolute Acceleration Equipment A (g)				Peak Absolute Acceleration Equipment B (g)				Peak Connector Force (lbs)		
		Spring	Slider	BPA	Stand Alone	Spring	Slider	BPA	Stand Alone	Spring	Slider	BPA	Stand Alone	Spring	Slider	BPA	Stand Alone	Spring	Slider	BPA
1	Newhall-30	0.98	---	2.07	1.50	0.70	---	0.71	0.63	0.55	---	0.91	0.59	0.76	---	0.78	1.14	218	---	71
	Newhall-100	---	3.65	---	5.08	---	1.51	---	2.06	---	1.84	---	1.92	---	1.56	---	3.59	---	334	---
	Tabas-25	1.69	---	2.22	2.06	1.17	---	0.85	1.13	1.01	---	1.00	0.81	1.13	---	0.84	1.97	293	---	99
	Tabas-50	---	3.04	---	4.94	---	1.15	---	2.00	---	1.51	---	1.90	---	1.45	---	3.54	---	301	---
2	Newhall-30	1.40	0.63	1.88	1.50	0.67	0.29	0.45	0.40	0.96	0.40	0.81	0.59	0.61	0.47	0.73	0.80	313	120	77
	Newhall-100	2.89	3.16	6.25	5.08	1.30	0.93	1.55	1.07	1.97	1.75	2.55	1.92	1.23	1.51	2.79	2.56	642	380	195
	Tabas-25	1.56	1.00	1.94	2.06	0.71	0.29	0.74	0.46	1.07	0.56	0.87	0.81	0.85	0.53	1.24	1.19	373	137	96
	Tabas-50	3.09	2.91	4.59	4.94	1.27	0.61	1.39	0.98	2.08	1.49	1.95	1.90	1.69	1.28	2.34	2.32	652	284	150
3	Newhall-30	1.03	---	1.53	1.73	0.79	---	0.87	0.63	0.96	---	0.88	0.87	0.78	---	0.84	1.14	47	---	30
	Newhall-100	3.15	2.95	---	5.67	2.51	1.29	---	2.06	3.15	2.55	---	2.24	2.36	1.53	---	3.59	153	118	---
	Tabas-25	1.68	---	2.41	3.04	1.33	---	0.83	1.13	2.00	---	1.55	1.17	1.28	---	0.79	1.97	110	---	52
	Tabas-50	3.61	2.04	---	7.82	2.72	1.09	---	2.00	3.92	2.19	---	3.04	2.76	1.44	---	3.54	205	123	---
4	Newhall-30	1.05	---	1.10	1.77	0.55	---	0.43	0.36	1.60	---	0.71	0.70	0.80	---	0.74	0.93	94	---	28
	Newhall-100	2.80	2.36	---	5.71	1.49	0.78	---	1.11	3.88	2.82	---	2.43	2.07	1.48	---	2.73	224	164	---
	Tabas-25	0.92	---	1.94	2.94	0.47	---	0.71	0.49	1.54	---	1.21	1.11	0.75	---	1.22	1.20	93	---	41
	Tabas-50	1.97	1.25	---	7.75	0.95	0.45	---	0.96	3.52	1.73	---	2.84	1.73	1.08	---	2.36	217	97	---
	Tabas-200	---	8.17	---	---	---	4.49	---	---	---	31.8	---	---	---	9.4	---	---	---	2433	---
5	Newhall-30	0.71	0.66	1.50	1.91	0.20	0.18	0.17	0.18	0.65	0.41	0.67	0.79	0.61	0.44	0.51	0.49	273	207	106
	Newhall-100	2.00	2.56	5.91	5.19	0.33	0.31	0.25	0.20	1.66	1.65	2.40	1.90	1.35	2.25	1.01	1.22	698	511	121
	Tabas-25	1.05	0.81	1.88	3.23	0.25	0.17	0.28	0.20	1.02	0.47	0.84	0.73	0.98	0.60	0.91	1.71	478	168	93
	Tabas-50	1.93	2.42	3.91	4.42	0.36	0.34	0.31	0.34	1.75	1.34	1.63	1.73	1.75	1.38	1.59	3.13	748	323	137

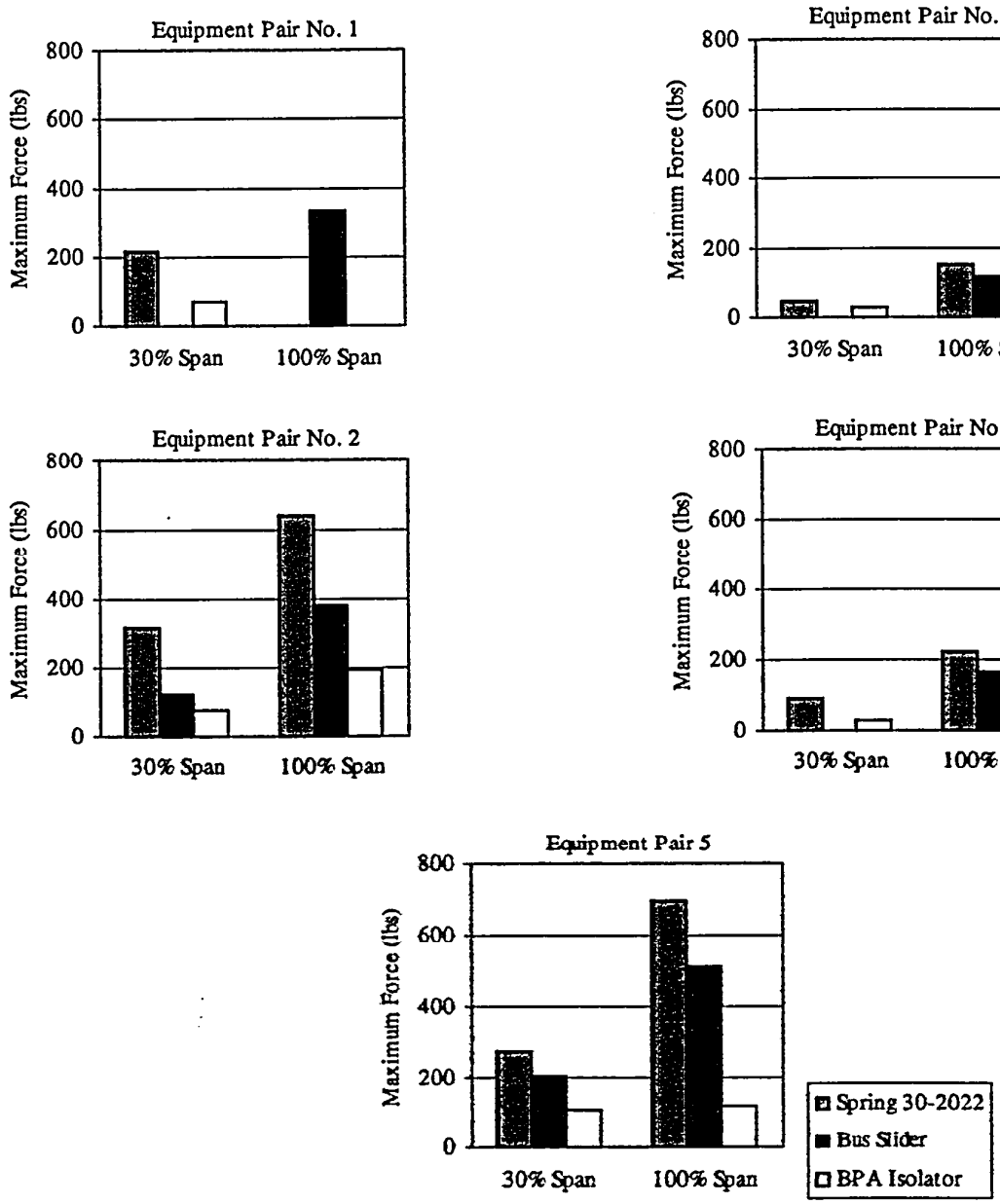

Figure 5.10 Maximum Forces in Connectors, Newhall Ground Motion.

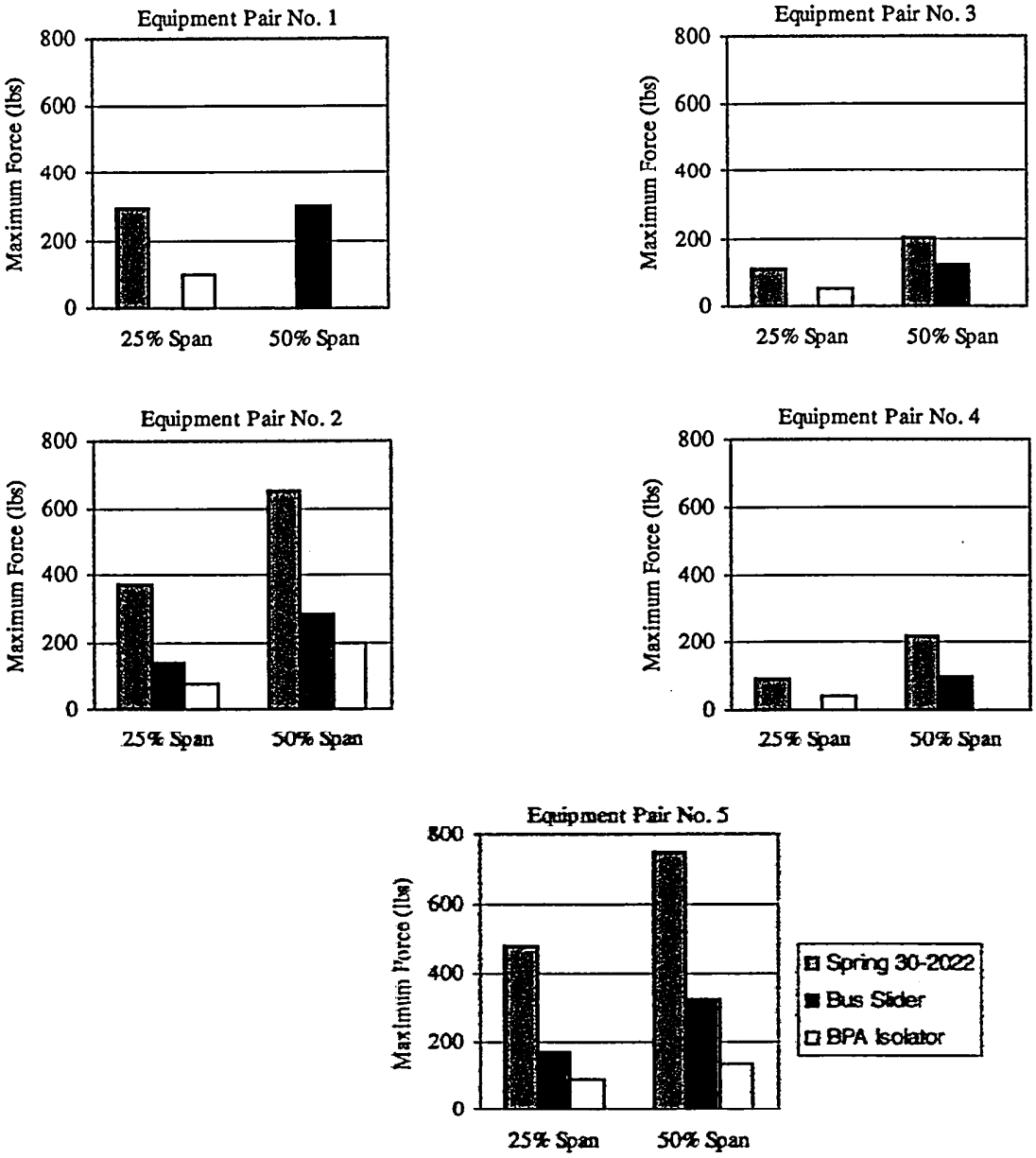

Figure 5.11 Maximum Forces in Connectors, Tabas Ground Motion.

The effect of the various connectors on the dynamic response of the generic equipment specimens can be evaluated by defining a Displacement Amplification Factor (DAF) and an Acceleration Amplification Factor (AAF) as:

$$DAF = \frac{\text{Maximum Relative Displacement of Interconnected Equipment}}{\text{Maximum Relative Displacement of Stand Alone Equipment}} \qquad (5.2)$$

$$AAF = \frac{\text{Maximum Absolute Acceleration of Interconnected Equipment}}{\text{Maximum Absolute Acceleration of Stand Alone Equipment}} \qquad (5.3)$$

The DAF and AAF values computed at the top of Equipment A and Equipment B during the seismic tests are presented in Figs.5.12 to 5.19. The results are presented for each ground motion, equipment pair, and intensity level.

The presence of rigid bus connectors can amplify or reduce the dynamic response of equipment components depending on their dynamic characteristics and the frequency content and intensity of the earthquake ground motion input. In general, the displacement at the top of the lighter and stiffer equipment B is more amplified than the displacement at the top of the heavier and more flexible equipment A.

Among the three connectors investigated, the bus slider consistently reduces the response at the top of both equipment specimens. The only case where the bus slider amplifies the response is for equipment B of Pair No. 5 under the 100% Newhall ground motion.

This response reduction occurs despite that the bus slider induces larger forces than the BPA connector does (see Figs. 5.110 and 5.11). The energy dissipation capacity of the bus slider is larger than of the BPA connector and causes an increase of the equivalent damping of the coupled system.

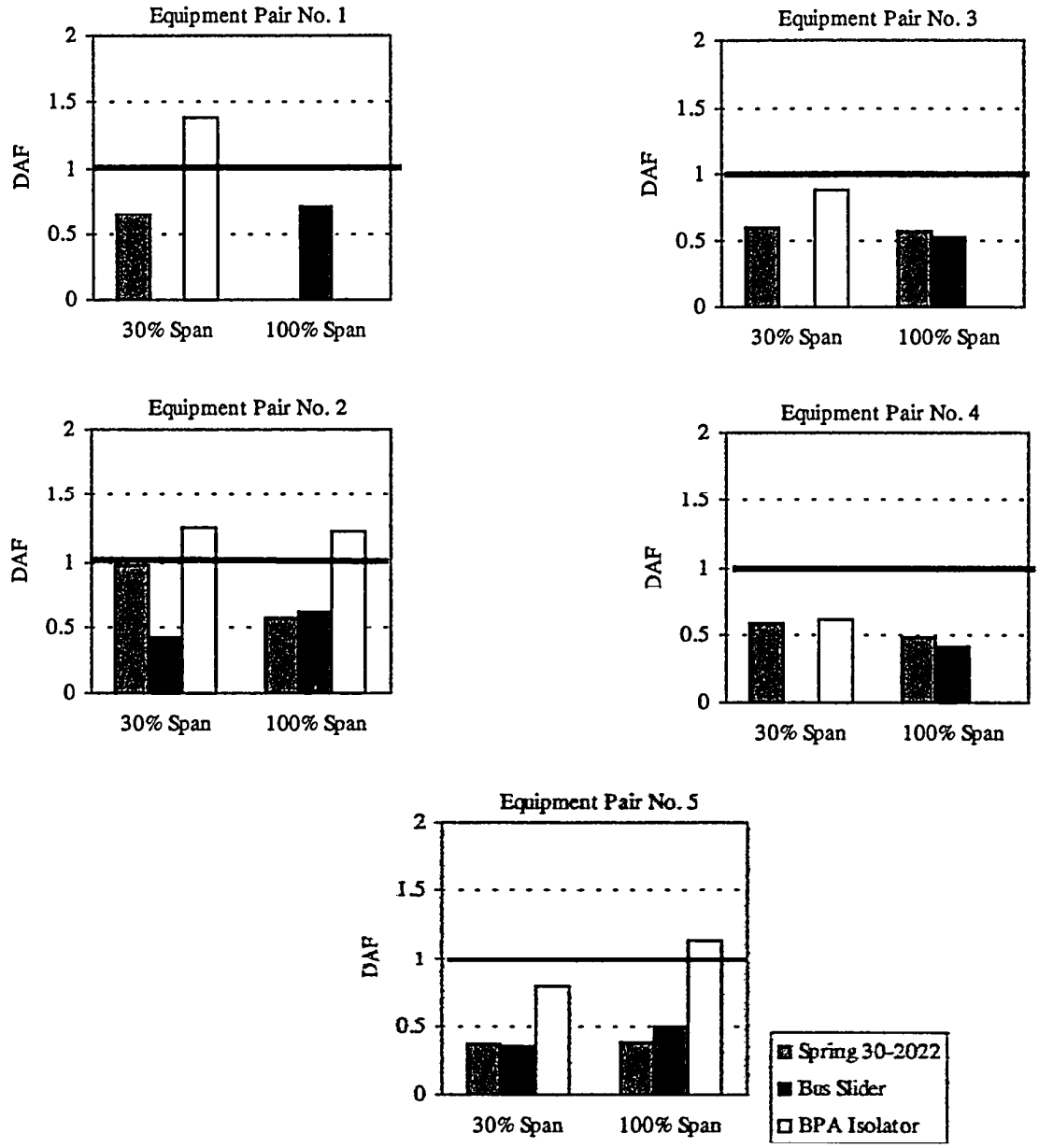

Figure 5.12 Displacement Amplification Factor (DAF),
Equipment A, Newhall Ground Motion.

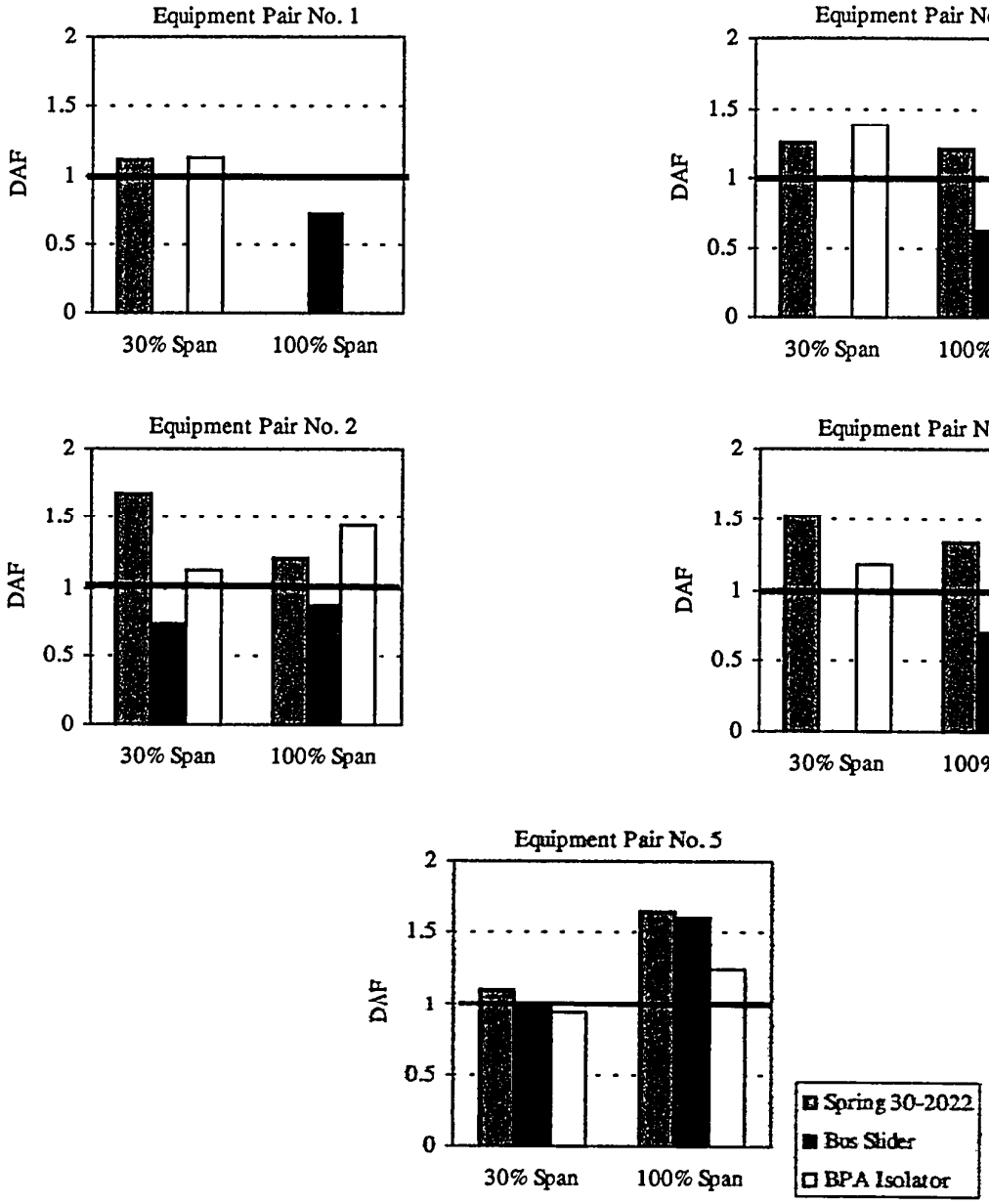

Figure 5.13 Displacement Amplification Factor (DAF),
Equipment B, Newhall Ground Motion.

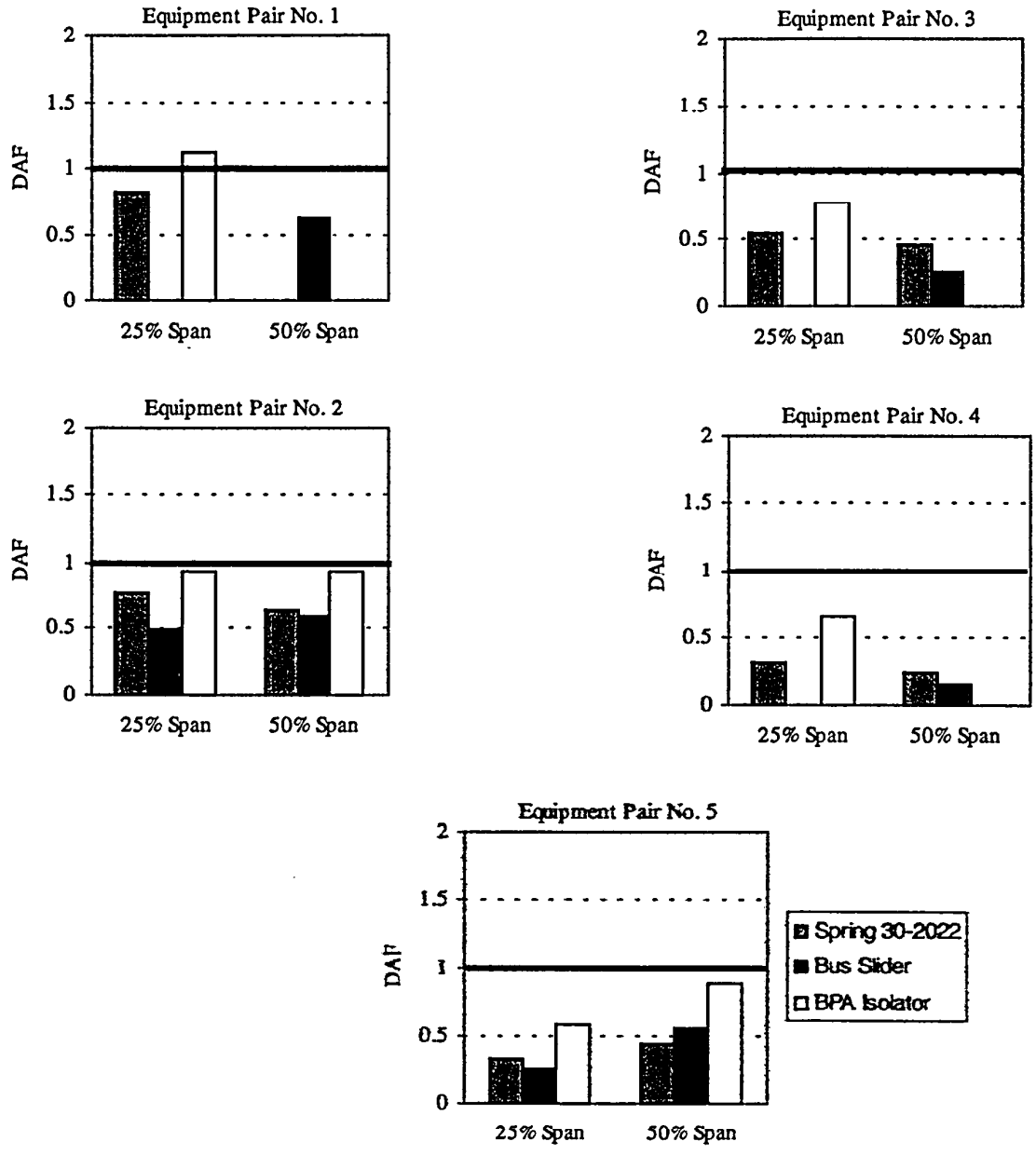

Figure 5.14 Displacement Amplification Factor (DAF),
Equipment A, Tabas Ground Motion.

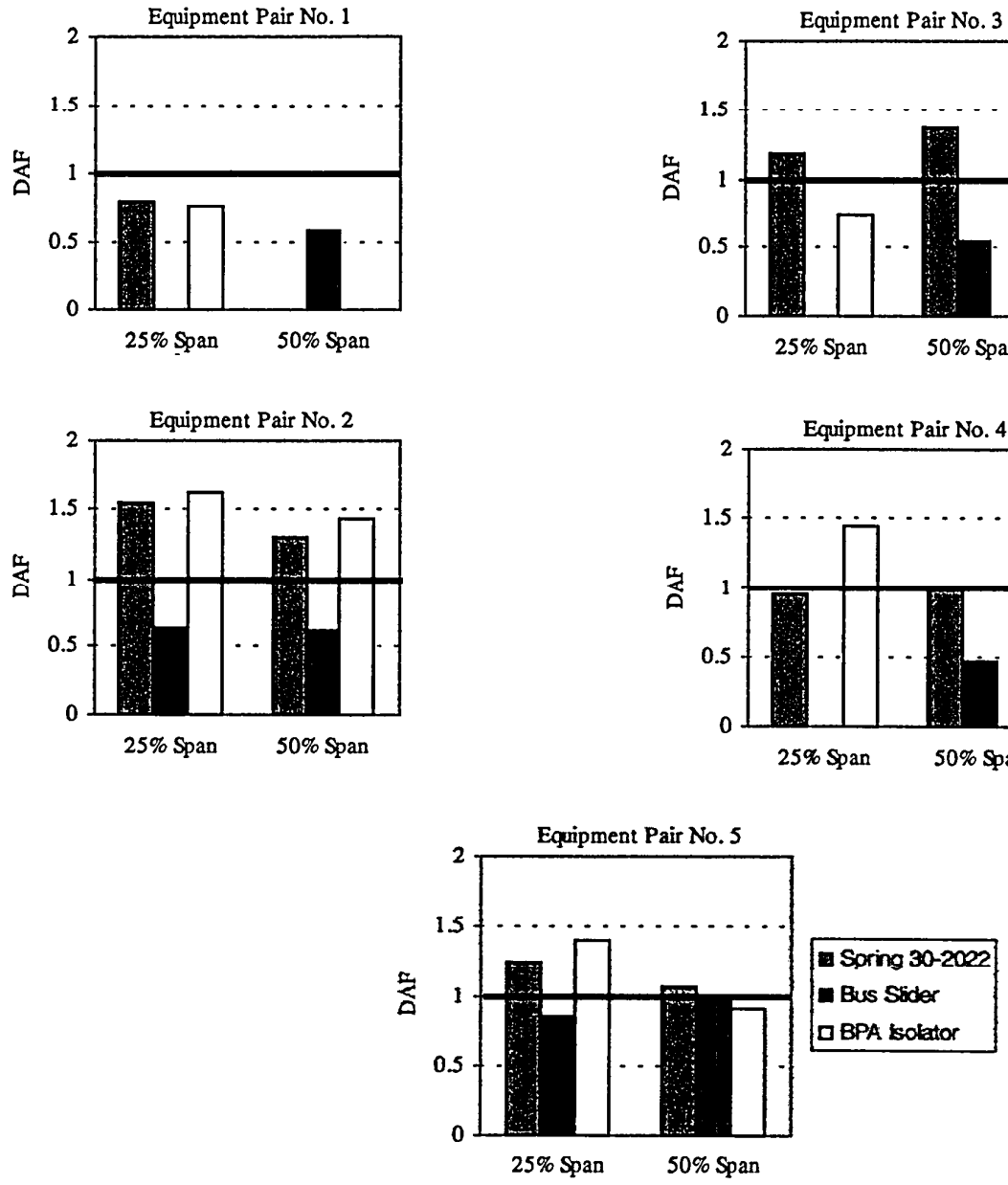

Figure 5.15 Displacement Amplification Factor (DAF),
Equipment B, Tabas Ground Motion.

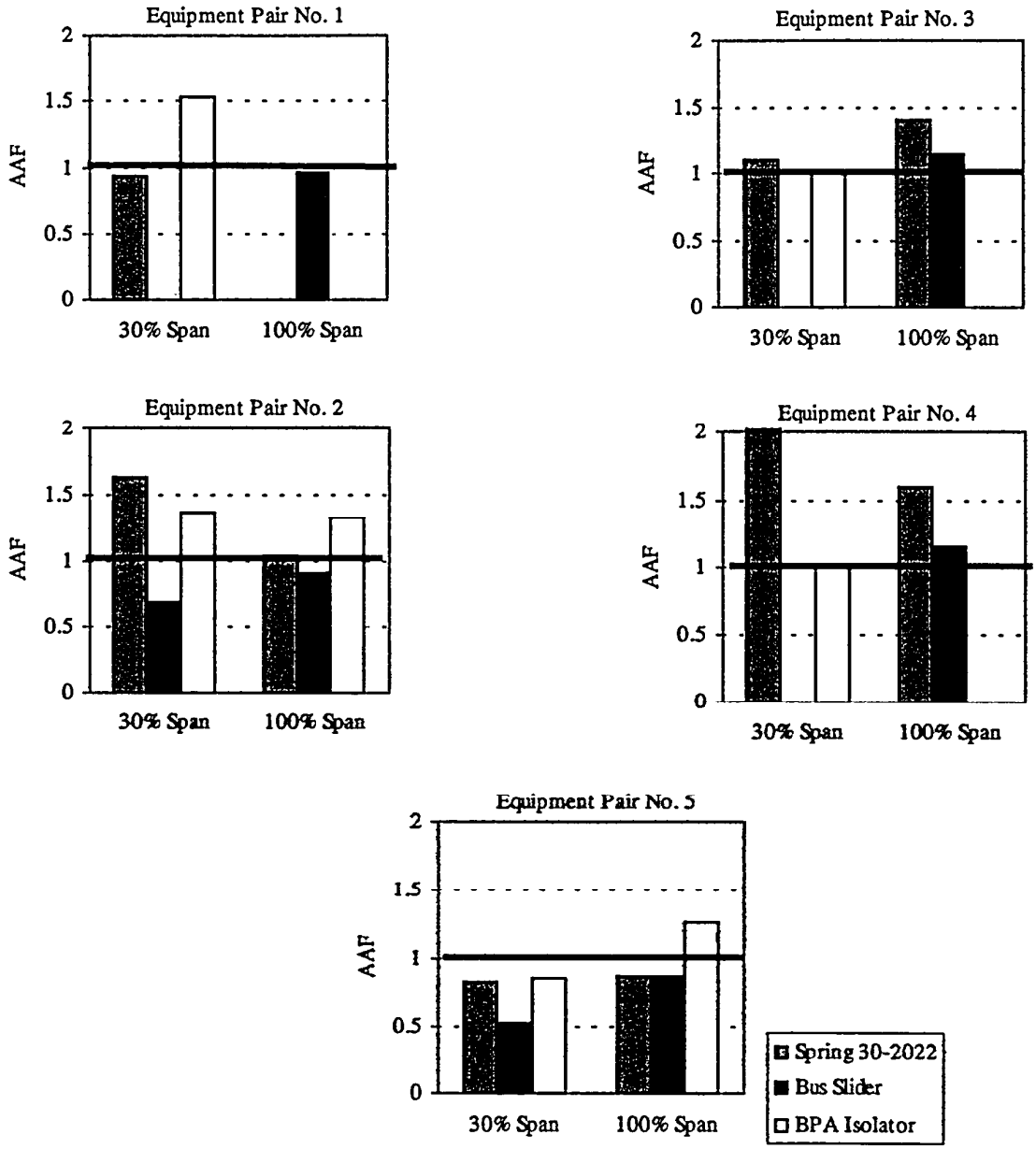

Figure 5.16 Acceleration Amplification Factor (AAF), Equipment A, Newhall Ground Motion.

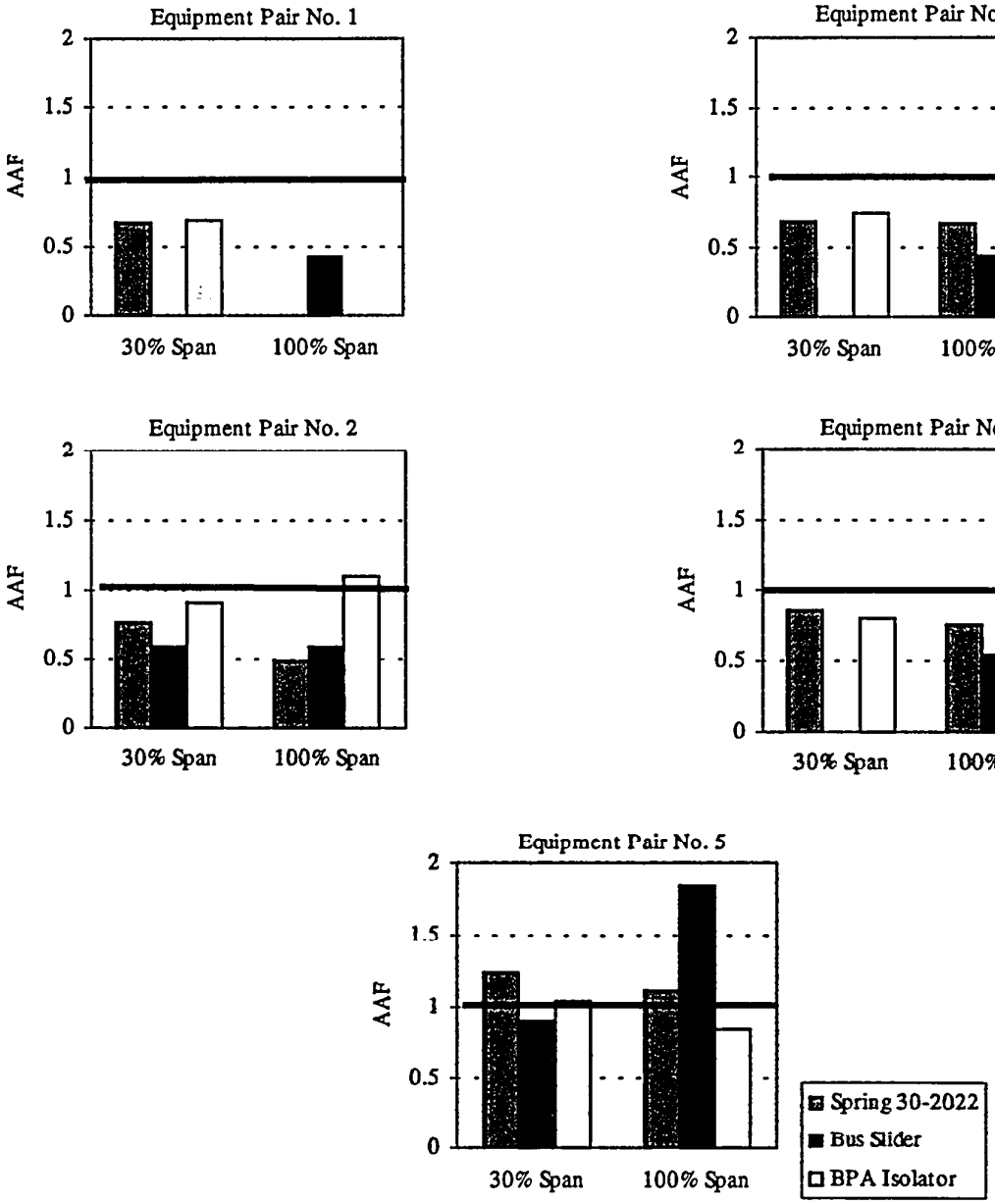

Figure 5.17 Acceleration Amplification Factor (AAF), Equipment B, Newhall Ground Motion.

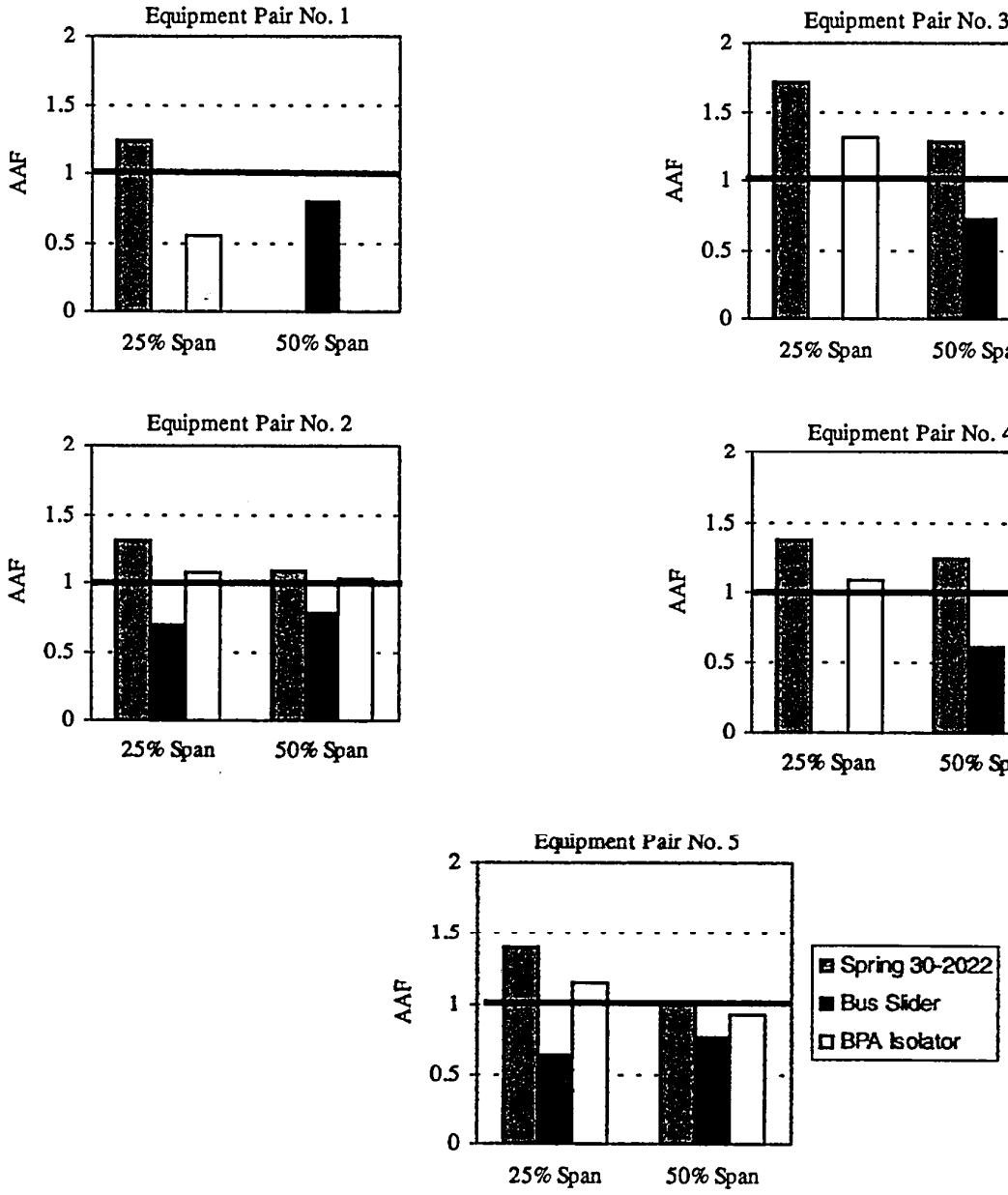

Figure 5.18 Acceleration Amplification Factor (AAF),
Equipment A, Tabas Ground Motion.

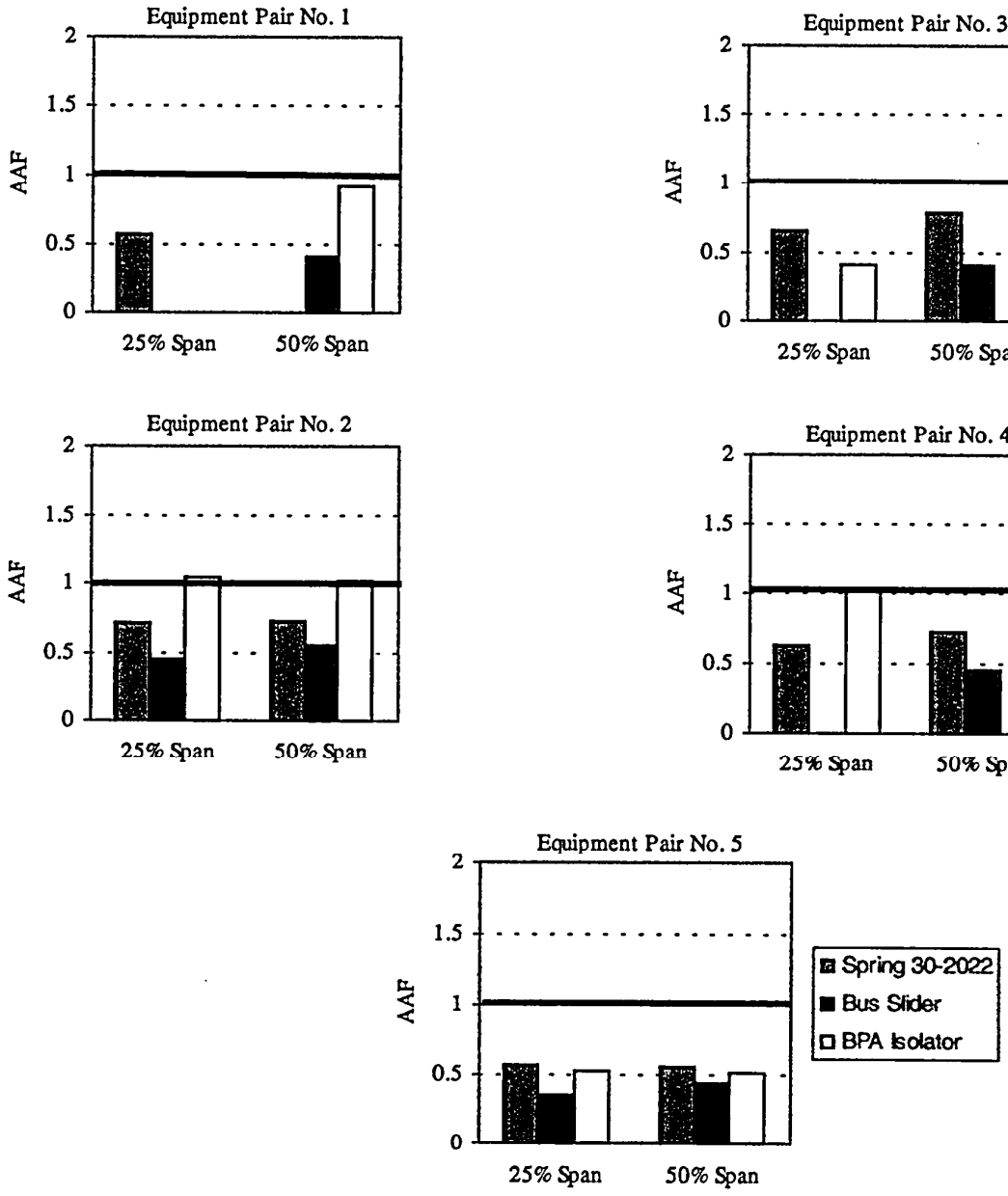

Figure 5.15 Displacement Amplification Factor (DAF), Equipment B, Tabas Ground Motion.

6 CONCLUSIONS

The quasi-static and shake table tests performed in this project has provided an opportunity to evaluate the interactions between components of substation equipment connected by both flexible and rigid bus. The tests have provided also validation data for a current PEER-PG&E analytical project.

Based on the results of the quasi-static tests performed on flexible and rigid bus connectors, the following conclusions can be drawn:

- The copper alloy used to manufacture the three spring connectors tested (Parts 30-2021, 30-2022, and 30-2023) exhibits almost a perfect elastic-plastic bchavior that can be characterized by an elastic modulus of 14 100 ksi and yield strength of 27 ksi.
- The modcling of spring connectors by straight linear-elastic frame elements with a commercial structural analysis package is reasonably accurate to estimate the elastic stiffness, yield force and yield displacement of the connectors.
- The three spring connectors tested exhibited large and stable hysteresis loops with good energy dissipation capabilities. For ductility levels less than four, the hysteresis loops were nearly symmetric in tension and compression. For larger deformations, tension-stiffening effects were observed. These effects were more predominant for spring 30-2021. Finally, the load level developed by spring 30-2023 was significantly lower than the loads induced in the other two spring connectors.
- For the two spring connectors tested to failure (30-2022 and 30-2023), a brittle fracture occurred across the net area of the cast-aluminum terminal pad connection that is welded to the aluminum tubing. Failure stresses less than 4 ksi were recorded.
- The load-displacement hysteretic behavior of the three spring connectors tested can be simply modeled by a bi-linear solid.
- The equivalent damping ratios of the three spring connectors increase with displacement amplitude, indicating higher energy dissipation capacity at large inelastic displacements. Spring 30-2021 and spring 30-2022 exhibit damping ratios

significantly higher than the more flexible spring 30-2023 for the complete range of displacement amplitudes considered in the tests.

- The rigid bus slider tested exhibited a behavior that is typical of a Coulomb-type friction system coupled with an elastic restoring force mechanism. The hysteretic behavior of the bus slider tested can be simply modeled by a rigid-plastic solid with a slip force of 53 lbs and a post-slip stiffness of 83 lbs/in.
- Contrary to the spring connectors, the equivalent damping ratio of the bus slider decreases slightly with displacement amplitude. For the range of displacements allowed by the slider, however, the equivalent viscous damping ratios provided by the bus slider were higher than the ones exhibited by the three spring connectors. This result indicates the superior energy dissipation capacity of the bus slider at small displacement amplitudes.
- For the lengths of the two flexible bus specimens tested (15 ft), the flexural stiffness of the cables played an insignificant role in the load-displacement responses. The specimens can be simply modeled by an elastic gap element.
- For the 1113 MSM bundled conductors tested, the two cables were manufactured with different lengths causing one cable to be taut much more than the other one.

Based on the results of the shake table tests performed on four different pairs of generic equipment connected by three different types of rigid bus connectors, the following conclusions can be drawn:

- The natural frequencies measured on the generic equipment specimens interconnected by the bus assemblies were always between the natural frequencies obtained for the uncoupled equipment specimens. The lowest natural frequencies were obtained with the BPA isolator, while the highest natural frequencies corresponded to the pairs of equipment connected by the rigid bus slider.
- The spring connector (30-2022) tested performed similarly as the quasi-static tests. Yielding occurred under the highest intensity ground motions along with significant vertical deformation at the end of the aluminum pipe.

- The bus slider performed well except for two high intensity tests where the shaft came out of the aluminum pipe during shaking. This induced sever impact loading between the shaft and the pipe as shown by the very large accelerations recorded at the top of the generic equipment. This damage could be avoided by increasing the available travel distance of the shaft inside the aluminum pipe and by increasing the length of the looped cables to avoid an undesirable increase of the elastic restoring stiffness.
- The BPA isolator did not suffer any visible damage during the shake table testing
- The physical arrangement of the rigid bus and BPA assembly along with its significant mass caused a rigid-body rotation of the whole specimen during some of the tests. This observation suggests that a rigid bus equipped with a BPA isolator could induce significant torsional couples at the top of the equipments under transverse seismic loading.
- The BPA connector, being more flexible than the other two connectors, consistently induces the smaller forces. The spring connector consistently induces the largest forces.
- Among the three connectors investigated, the bus slider consistently reduces the response at the top of both equipment specimens. This response reduction occurs despite that the bus slider induces larger forces than the BPA connector does. The energy dissipation capacity of the bus slider is larger than of the BPA connector and causes an increase of the effective damping of the coupled system.

7 REFERENCES

Abrahamson, M. 1997. Private Communication

American Society for Testing Materials, 1999. "E8-99 Standard Test Methods for Tension Testing of Metallic Materials", ASTM E8-99 Standard, West Conshohocken, PA.

Applied Technology Council, 1992. "Guidelines for Cyclic Seismic Testing of Components of Steel Structures", ATC-24, Redwood City, CA .

Clough, R.W., and Penzien, J., 1993. "Dynamics of Structures", Second Edition, McGraw-Hill, New York.

Computers and Structures, 1998. "SAP 2000 Three Dimensional Static and Dynamic Finite Element Analysis of Structures", Computers and Structures Inc., Berkeley, CA.

Experimental Dynamic Investigations, 1993. "U2 & V2 Manual", Vancouver, Canada

Filiatrault, A., Tremblay, R., Thoen, B.K. and Rood, J., **1996**."A Second Generation Earthquake Simulation System in Canada: Description and Performance Evaluation", 11th World Conference on Earthquake Engineering, Acapulco, Mexico, Paper # 1204 on CD-ROM.

Filiatrault, A., Kremmidas, S., Seible, F., Clark, A.J., Nowak, R., and Thoen, B.K. **2000**. "Upgrade of First Generation Uniaxial Seismic Simulation System with Second Generation Real-Time Three-Variable Digital Control System", 12th World Conference on Earthquake Engineering, Auckland, New Zealand (in press).

IEEE. 1997. "Recommended practices for Seismic Design of Substations, Draft No. 6", Piscataway, NJ.: IEEE Standards department.

Starkel, D.L., Mueller III, W., and Kempner, L., 1998." Seismic Evaluation Seismic Connection with Rigid Bus Conductor", Portland State University, Bonneville Power Administration.

APPENDIX A

DRAWINGS OF RIGID AND FLEXIBLE BUS SPECIMENS

To: Andre Filiatrault/Ahmed Elgamal, UCSD, Fax 619/822-2260
From: Eric Fujisaki, PG&E 415/973-9857, Fax 415 973-9209

PEER-PG&E Task 2C
Substation Equipment Interaction

The attached figures outline the hardware associated with the suggested experiments for Task 2C. These are described as follows:

1. Rigid bus with spring connectors (dwg. 417440 Figures 1, 2, and 3). A 3" dia. aluminum pipe with welded end fittings, rigidly connected at one end, and having spring connector at other end. 3" standard NEMA terminal pads to be used. Three different springs proposed (Figures 1, 2, and 3).

2. Rigid bus with slider connector (dwg. 0462267 Type 221A). A 3" dia. aluminum pipe with welded end fitting on one end, slider connector on other end. 4" standard NEMA pad on slider end, 3" pad on other. Bolt hole pattern for 3" and 4" pads are the same; bolt hole edge distances different (see figures).

3. Various cable connectors with either 3" or 4" standard NEMA terminal pads at their ends. The exact cables to be used are not yet determined.

4. "BPA" type connector with 4" dia. rigid bus. This experiment will be similar to the tests done by BPA at Portland State University, except that the boundary conditions used will be different. A BPA flexible connector will be attached at one end of a 4" dia. rigid bus (aluminum tube) at one end. The other end of the 4" rigid bus will have two 45 degree bends, ending in a vertically oriented terminal pad. All terminal pads will be 5" non-standard (needs further discussion with BPA).

Adaptability of Support Hardware: The support hardware in the experiment that represents the two pieces of substation equipment should be designed to accommodate the different types of terminal pads described above. These differences include terminal pad size, bolt hole size and spacing, and orientation of the pad (horizontal and vertical). It would be beneficial to design the bus support points to be able to accept a bolt-on adapter such that the appropriate type of terminal pad could be installed and changed easily. Since terminal pad strength is not the focus of this project, the pads on the equipment ends could be made as stiff and strong as needed.

Support Spacing on the Shake Table: This needs further discussion. The spacing is probably not critical for rigid bus, but some provisions for testing different lengths for flexible bus is desirable.

Instrumentation for Shake Table Tests: In addition to displacements and accelerations at the terminal pads, there should be some way to measure forces applied to the terminals, since this is an important parameter for the equipment that is actually attached to the terminals in the field. The axial force in the bus is probably the most important, but maybe there are other components of force that should also be measured (e.g., for eccentrically loaded connectors); needs some thought.

PG&E-PEER Project Task 2C

The following summarizes the required parts and assemblies to be provided by PG&E.

Item	Description	PG&E Ident./Code	Number Req'd	Sketch
Spring connector	Flexible connector, 2000A, 3" NEMA pad	Dwg. 417440, Grp. 3, Figure 1, code 30-2021	2	1
Spring connector	Flexible connector, 2000A, 3" NEMA pad	Dwg. 417440, Grp. 3, Figure 2, code 30-2022	2	1
Spring connector	Flexible connector, 2000A, 3" NEMA pad	Dwg. 417440, Grp. 3, Figure 3, code 30-2023	2	1
Rigid bus assy., straight	4" dia. SPS, aluminum rigid bus, make from 10'-0" long pipe, with offset terminal pads attached.	Terminal pads: Dwg 046267 Type 174, code 30-4122 at each end. Alternate: Dwg. 046267 Type 608, code 30-0233.	1 assy.	1
Rigid bus-slider assy	4" dia. SPS, aluminum rigid bus, make from 10'-0" long pipe, with slider connection on one end, offset terminal pad on other end, attached.	Slider connector: Dwg 046267 Type 221A, code 30-4462. Alternate: Dwg. 046267, Type 685, code 30-0381. Terminal pad: Dwg. 046267 Type 174, code 30-4462. Alternate: Dwg. 046267 Type 608, code 30-0233.	2 assy.	2
Rigid bus with (2)-45 deg. bends.	4" dia. SPS, aluminum rigid bus, make from 10'-0" long pipe, 2'-0" drop, offset terminal pads attached at each end.	Terminal pads: Dwg. 064116 Figure 14, code 30-4404 at each end. Alternate: Dwg. 046267 Type 608, code 30-0233 at each end.	1 assy.	4
Flexible jumper, 2300 MCM single conductor	15'-0" long, AAC, with compression end fittings.	End fittings: Dwg 046267 Type 317, code 30-3544.	1	3
Flexible jumper, (2)-1113 MCM bundled conductors	15'-0" long, AAC, with compression end fittings, 2 spacers.	End fittings: Dwg 046267 Type 316, code 30-3457. Spacers: Dwg 046267 Type 390, code 18-8559.	1	3
Flexible jumper, (2)-2300 MCM bundled conductors	25'-0" long, AAC, with compression end fittings, 2 spacers.	End fittings: Dwg 046267 Type 317, code 30-3544. Spacers: Dwg 046267 Type 391, code 18-8569.	1	3
Spare rigid bus	4" dia. SPS aluminum rigid bus	Spares for expanding length of specimens if needed	4	NA
Welded splice connectors	Splice connectors for 4" SPS aluminum rigid bus	Dwg 046267 type 203, code 30-7139.	8	NA

Design Drafting
62-3690

PACIFIC GAS AND ELECTRIC COMPANY

GENERAL COMPUTATION SHEET

SHEET NO. ____ OF ____ SHEETS
JOB FILE NO. ____
LOCATION ____

SUBJECT PEER TASK 2C

MADE BY ____ DATE ____ CHECKED BY ____ APPROVED BY ____

LENGTHS, SLOPE OF WORK

(1)

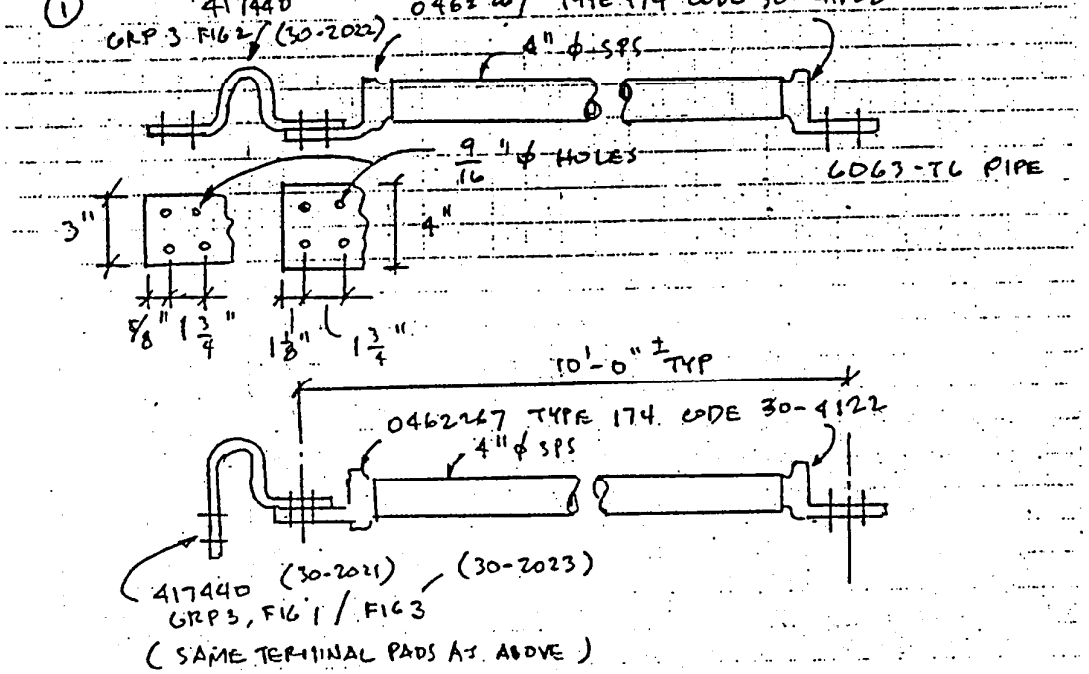

(2)

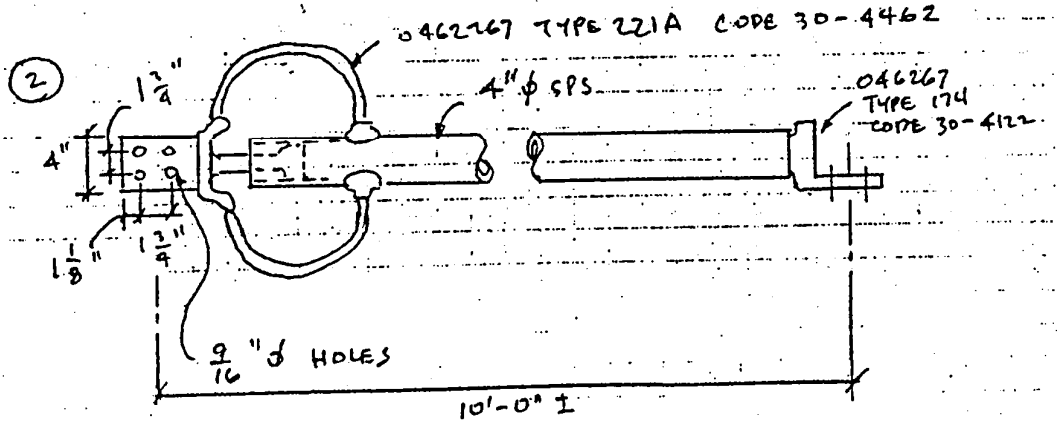

Design Drafting
62-3690

PACIFIC GAS AND ELECTRIC COMPANY

GENERAL COMPUTATION SHEET

SHEET NO. ____ OF ____ SHEETS
JOB FILE NO. ____
LOCATION ____

SUBJECT TASK 2C

MADE BY ____ DATE ____ CHECKED BY ____ APPROVED BY ____

(3) VARIOUS CABLE CONFIGURATIONS

TYP. TERMINAL PAD FOR CABLE CONNECTOR
(MAY BE WELDED, BOLTED OR CRIMPED TO CABLE

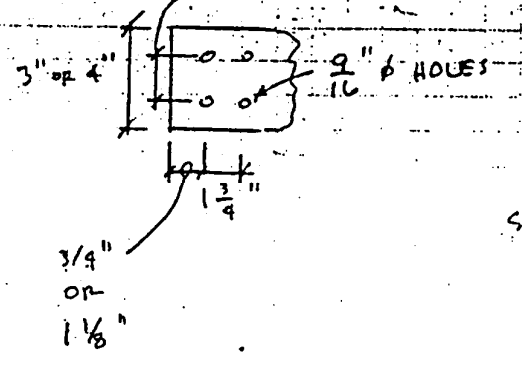

2300 MCM - 1 & 2 BUNDLED
1113 MCM - 2 BUNDLED
x 25' SPAN MAX
x 15' SPAN FOR 1113 & SINGLE 2300

SPACERS - 2 REQD IN EACH BUNDLED ASSY, 6" SP.

(4) "BPA" TYPE CONNECTOR (CODE 30-4404) TYP. BOTH ENDS

064116 FIG 14

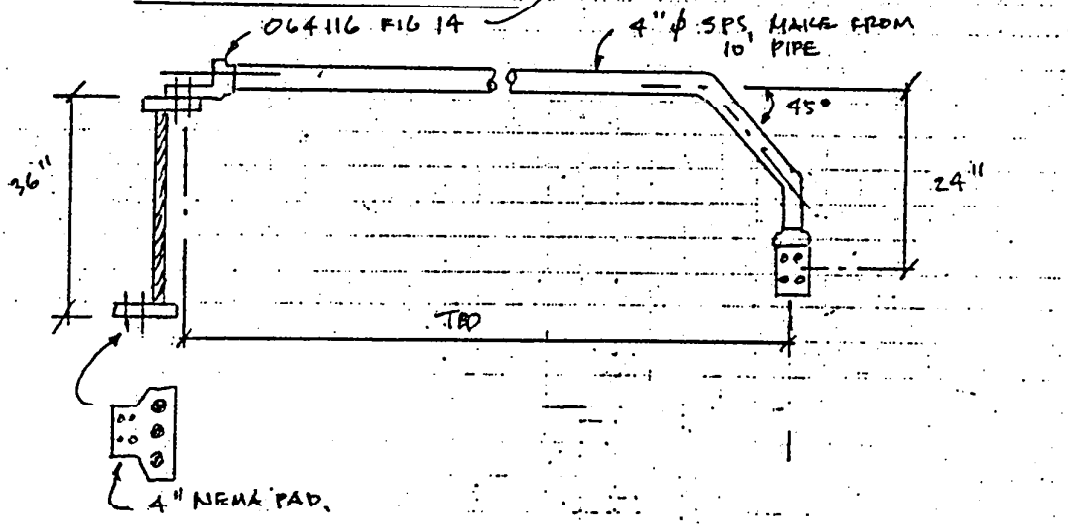

Design Drafting
62-3690

PACIFIC GAS AND ELECTRIC COMPANY

GENERAL COMPUTATION SHEET

SHEET NO. ____ OF ____ SHEETS
JOB FILE NO. ____
LOCATION ____

SUBJECT ____

MADE BY ____ DATE ____ CHECKED BY ____ APPROVED BY ____

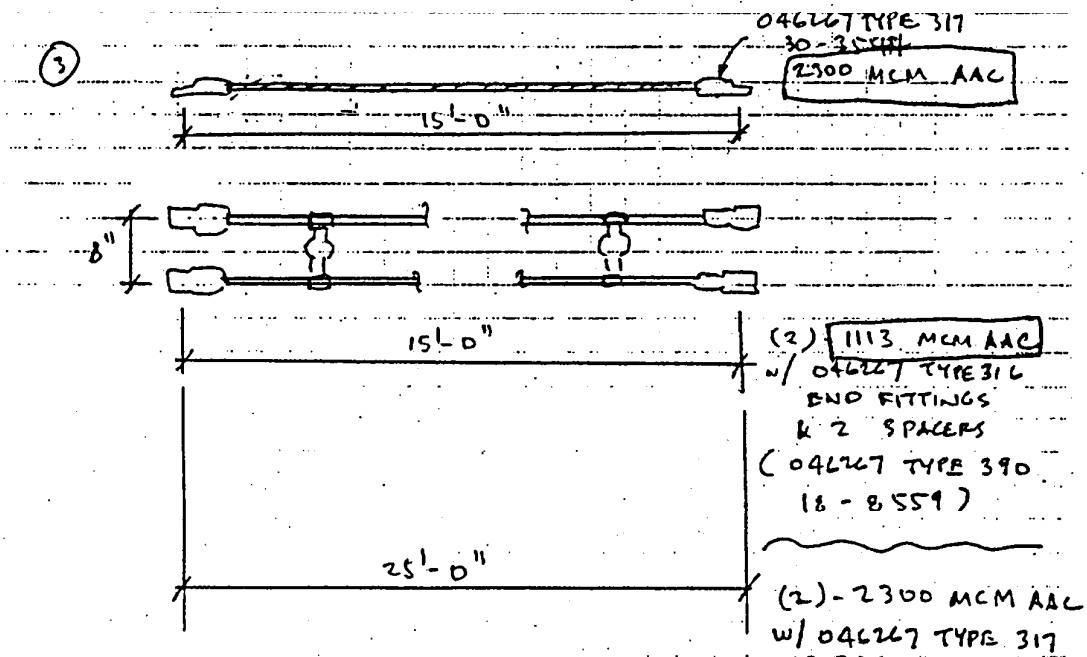

(2) 1113 MCM AAC w/ 046267 TYPE 316 END FITTINGS & 2 SPACERS (046267 TYPE 390 18-8559)

(2)-2300 MCM AAC w/ 046267 TYPE 317 END FITTINGS & 2 SPACERS (046267 TYPE 391 18-8569)

APPENDIX B

SHOP DRAWINGS OF GENERIC EQUIPMENT SPECIMENS

EQUIPMENT 1 : 2 Hz 800lbs

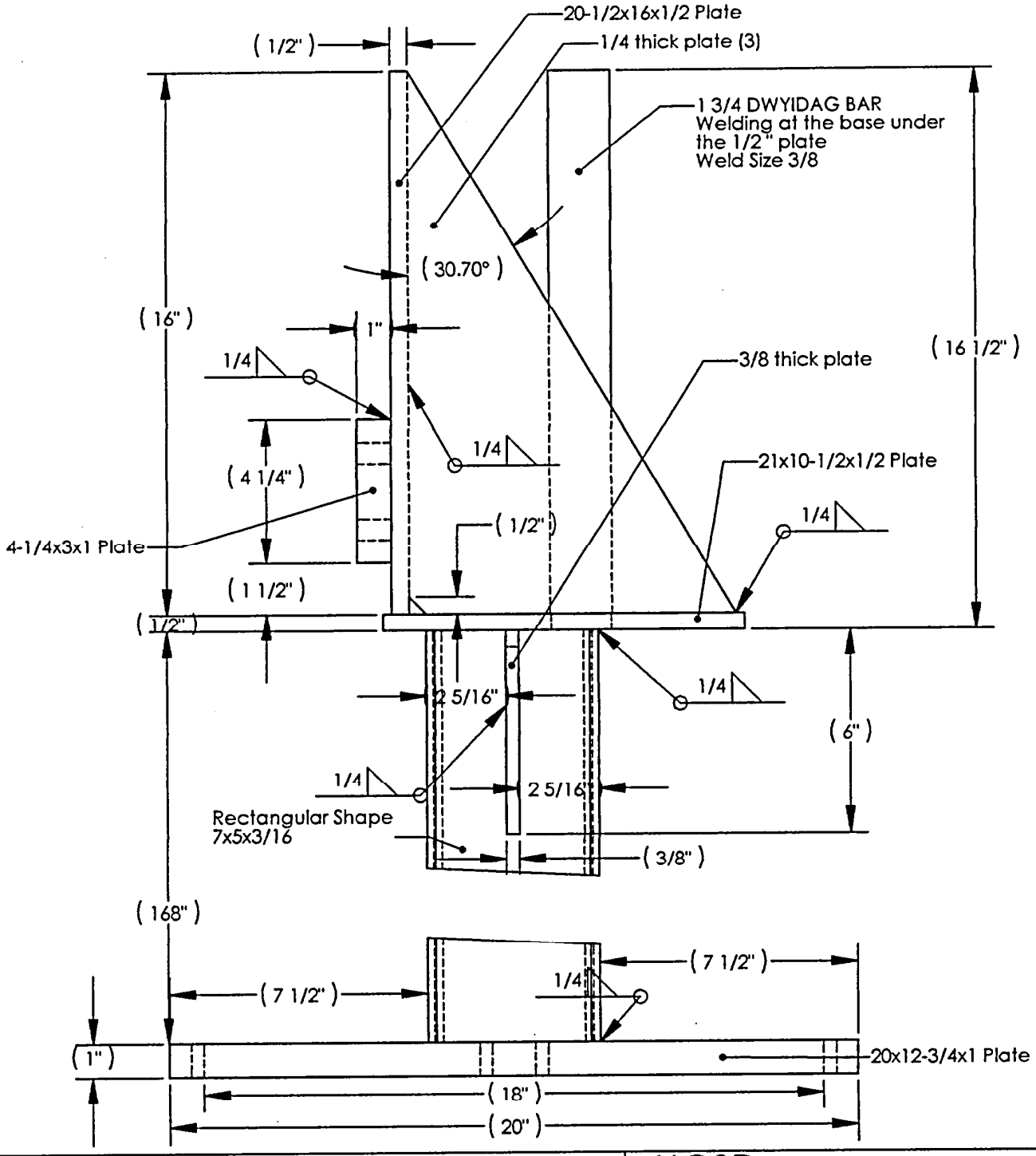

UNLESS OTHERWISE SPECIFIED DIMENSIONS ARE IN INCHES. TOLERANCES ARE: FRACTIONS ±X/X DECIMALS .XX ±.XX .XXX ±.XXX ANGLES ±X°	CONTRACT NO.		UCSD University of California, San Diego
	APPROVALS	DATE	HSS 7x5x3/16 BEAM Side View
	DRAWN Spiro Kremmidas	5/20/1999	
	CHECKED Andre Filiatrault	5/20/1999	
MATERIAL	ENGR.		SIZE A / DWG. NO. / REV. 1
FINISH	ISSUED		
DO NOT SCALE DRAWING			SCALE 1:4 / CAD FILE: / SHEET 1 OF 4

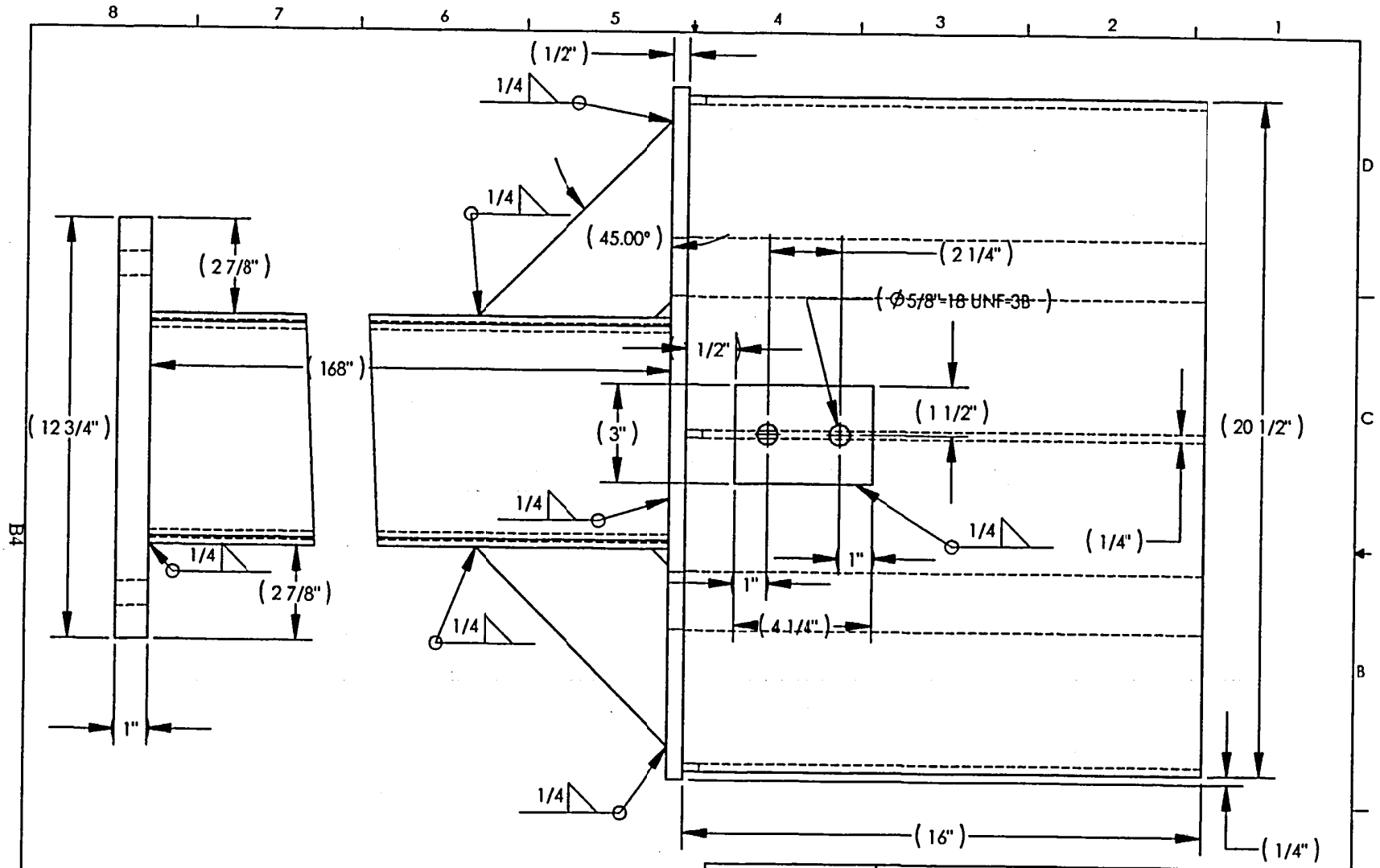

Plates A-36	Quantity
20x12-3/4x1	1
21x10-1/2x1/2	1
20-1/2x16x1/2	1
4-1/4x3x1	1
1/4 thick plate	3
3/8 thick plate	2

UNLESS OTHERWISE SPECIFIED DIMENSIONS ARE IN INCHES
TOLERANCES ARE:
FRACTIONS DECIMALS ANGLES
+ .XX+ .XX + 1
.XXX+.XXX

MATERIAL --

FINISH --

DO NOT SCALE DRAWING

CAD GENERATED DRAWING, DO NOT MANUALLY UPDATE

APPROVALS	DATE
DRAWN Spiro Kiremidjian	5/20/1999
CHECKED Andre Filiatrault	5/20/1999
RESP ENG	
MFG ENG	
QUAL ENG	

UCSD
University of California, San Diego

HSS 7x5x3/16 BEAM
Front View

SIZE A | DWG. NO. | REV. 1
SCALE 1:4 | CAD FILE: | SHEET 2 OF 4

NOTE:
Same Base Plate as
the one in HSS 3-1/2x2-1/2x1/4 BEAM

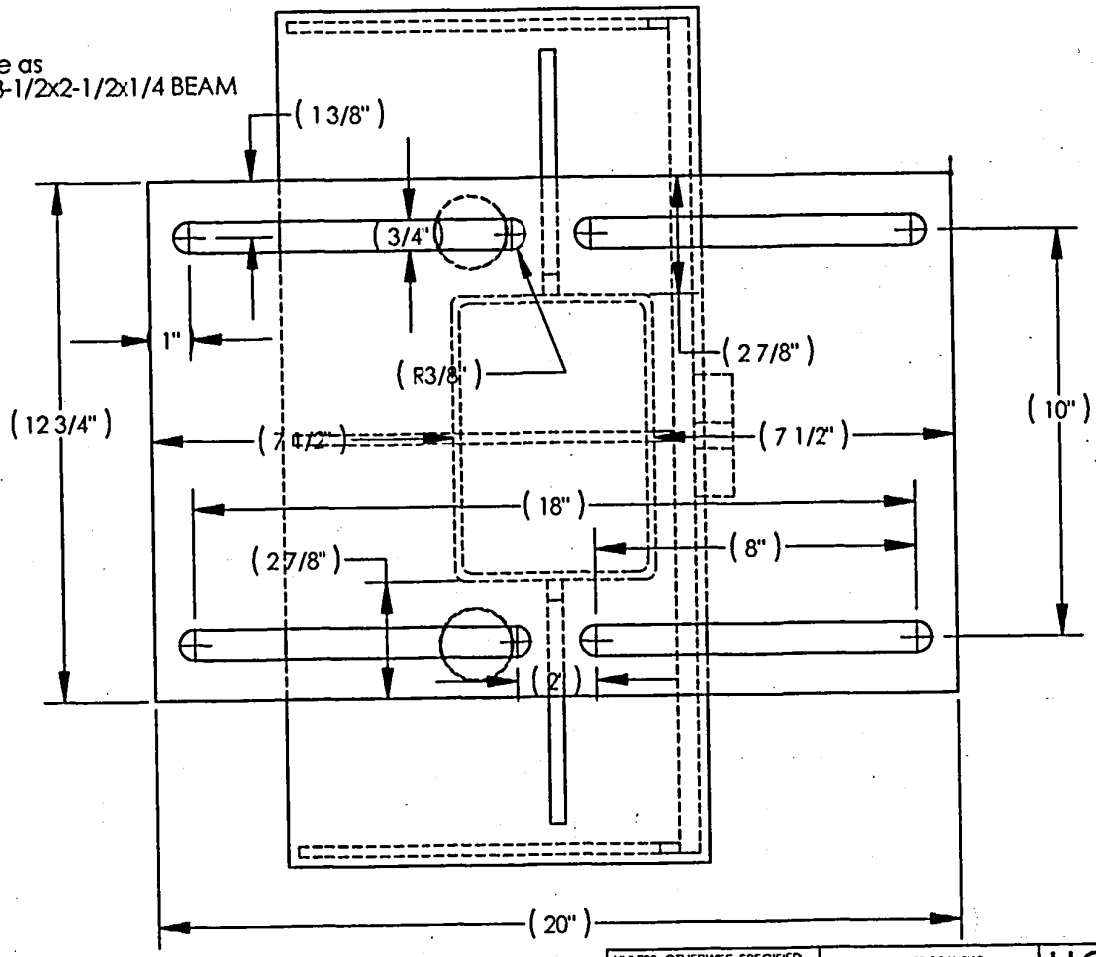

UNLESS OTHERWISE SPECIFIED DIMENSIONS ARE IN INCHES TOLERANCES ARE: FRACTIONS DECIMALS ANGLES ± .XX± .XX ± 1 .XXX±.XXX	CAD GENERATED DRAWING, DO NOT MANUALLY UPDATE	UCSD University of California, San Diego
	APPROVALS / DATE	HSS 7x5x3/16 BEAM Bottom View
	DRAWN Spiro Kiremidjian 5/20/1999	
	CHECKED Andre Filiatrault 5/20/1999	
MATERIAL --	RESP ENG	
FINISH --	MFG ENG	SIZE A · DWG. NO. · REV. 1
DO NOT SCALE DRAWING	QUAL ENG	SCALE 1:4 · CAD FILE: · SHEET 3 OF 4

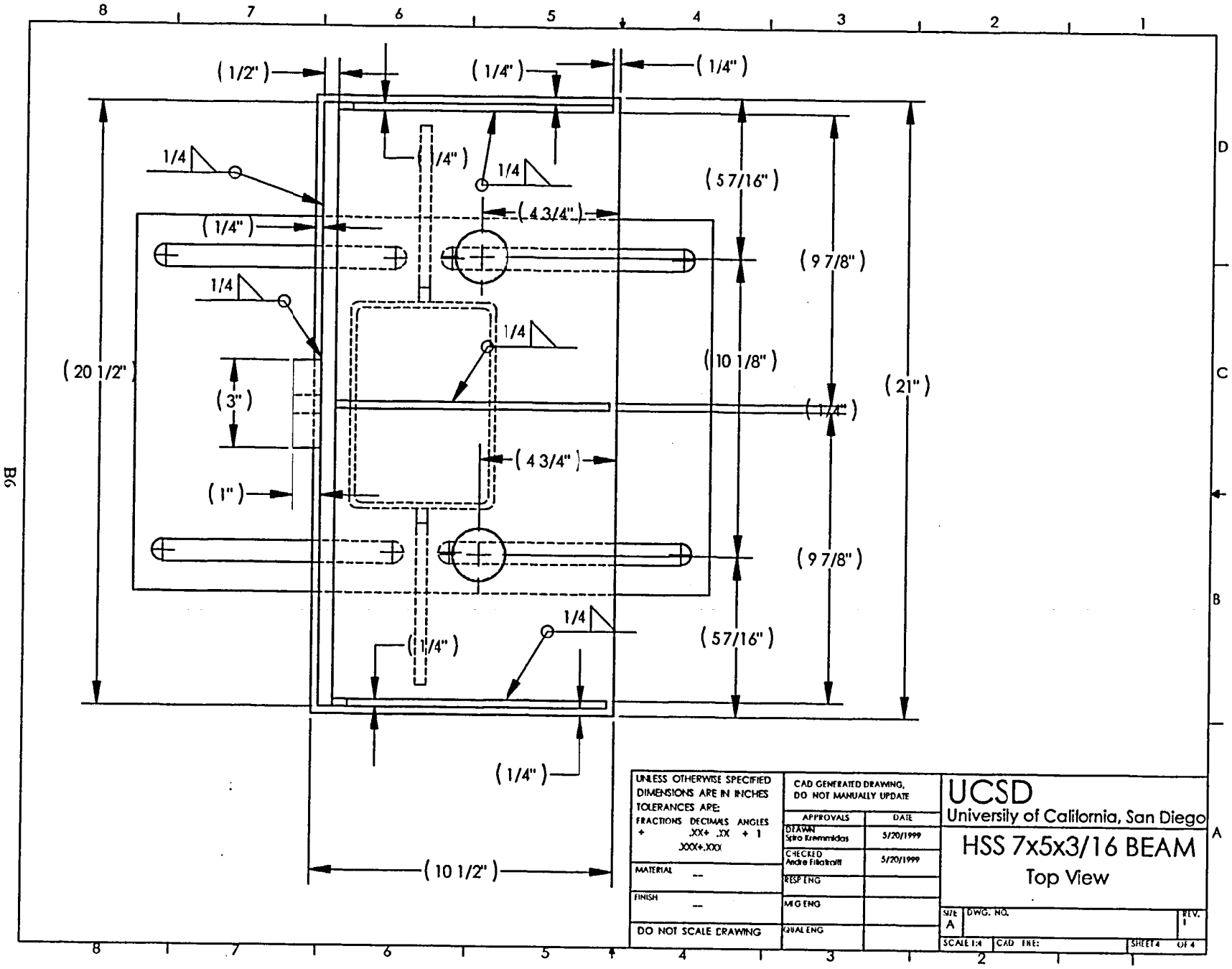

UNLESS OTHERWISE SPECIFIED DIMENSIONS ARE IN INCHES TOLERANCES ARE: FRACTIONS DECIMALS ANGLES + .XX+ .XX + 1 .XXX+.XXX	CAD GENERATED DRAWING, DO NOT MANUALLY UPDATE	UCSD University of California, San Diego
	APPROVALS / DATE	HSS 7x5x3/16 BEAM Top View
MATERIAL --	DRAWN Spiro Kremmidas 5/20/1999	
FINISH --	CHECKED Andre Filiatrault 5/20/1999	
DO NOT SCALE DRAWING	RESP ENG	
	M G ENG	
	QUAL ENG	
	SIZE A / DWG. NO. / REV. 1	
	SCALE 1:4 / CAD FILE: / SHEET 4 OF 4	

EQUIPMENT 2: 2 Hz 90lbs

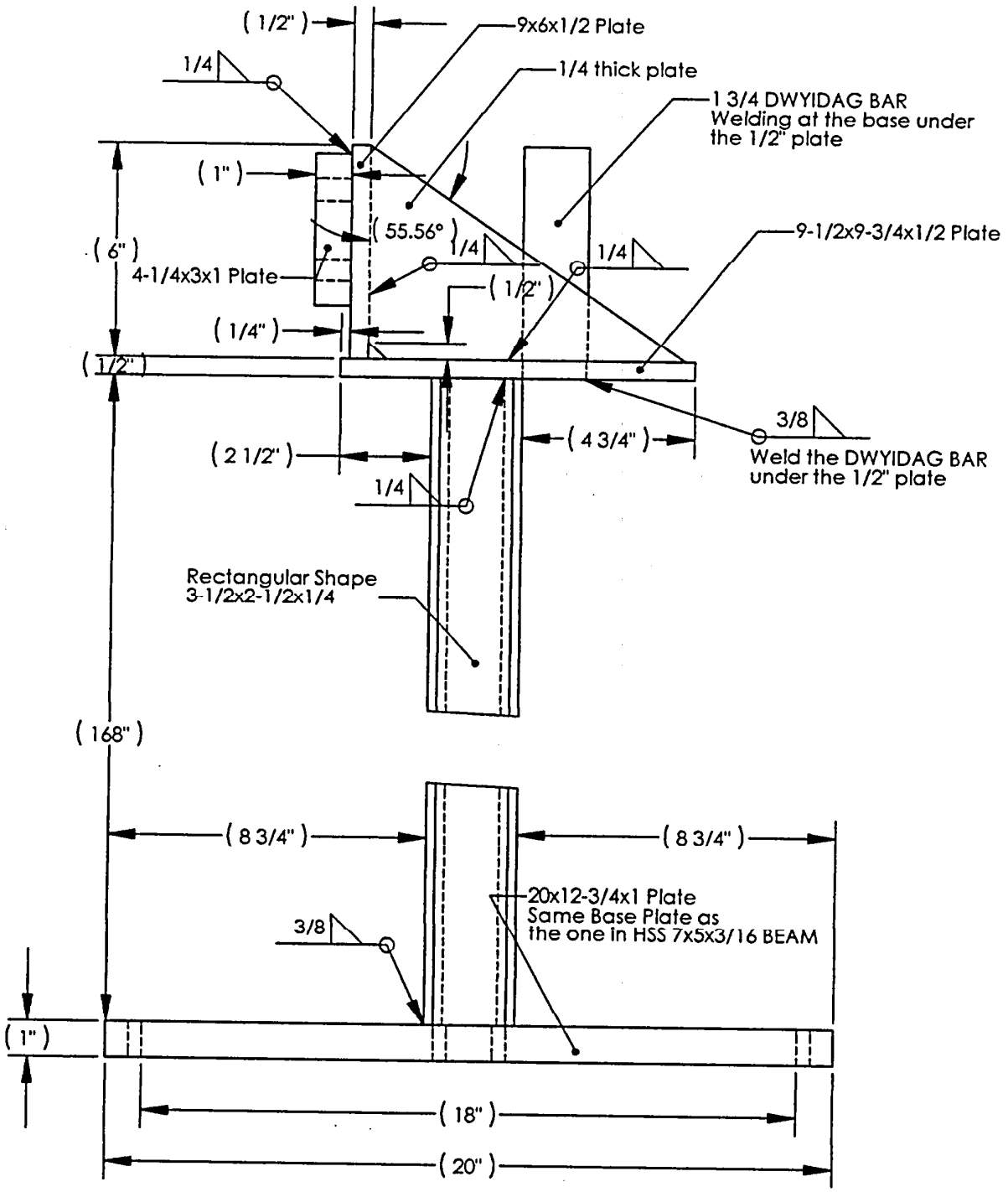

UNLESS OTHERWISE SPECIFIED DIMENSIONS ARE IN INCHES. TOLERANCES ARE:	CONTRACT NO.		UCSD University of California, San Diego
FRACTIONS ±X/X DECIMALS .XX ±.XX .XXX ±.XXX ANGLES ±X°	APPROVALS	DATE	HSS 3-1/2x2-1/2x1/4 BEAM Side View
	DRAWN Spiro Kremmidas	5/20/1999	
	CHECKED Andre Filiatrault	5/20/1999	
MATERIAL	ENGR.		SIZE A | DWG. NO. | REV. 1
FINISH	ISSUED		
DO NOT SCALE DRAWING			SCALE 1:4 | CAD FILE: | SHEET 1 OF 4

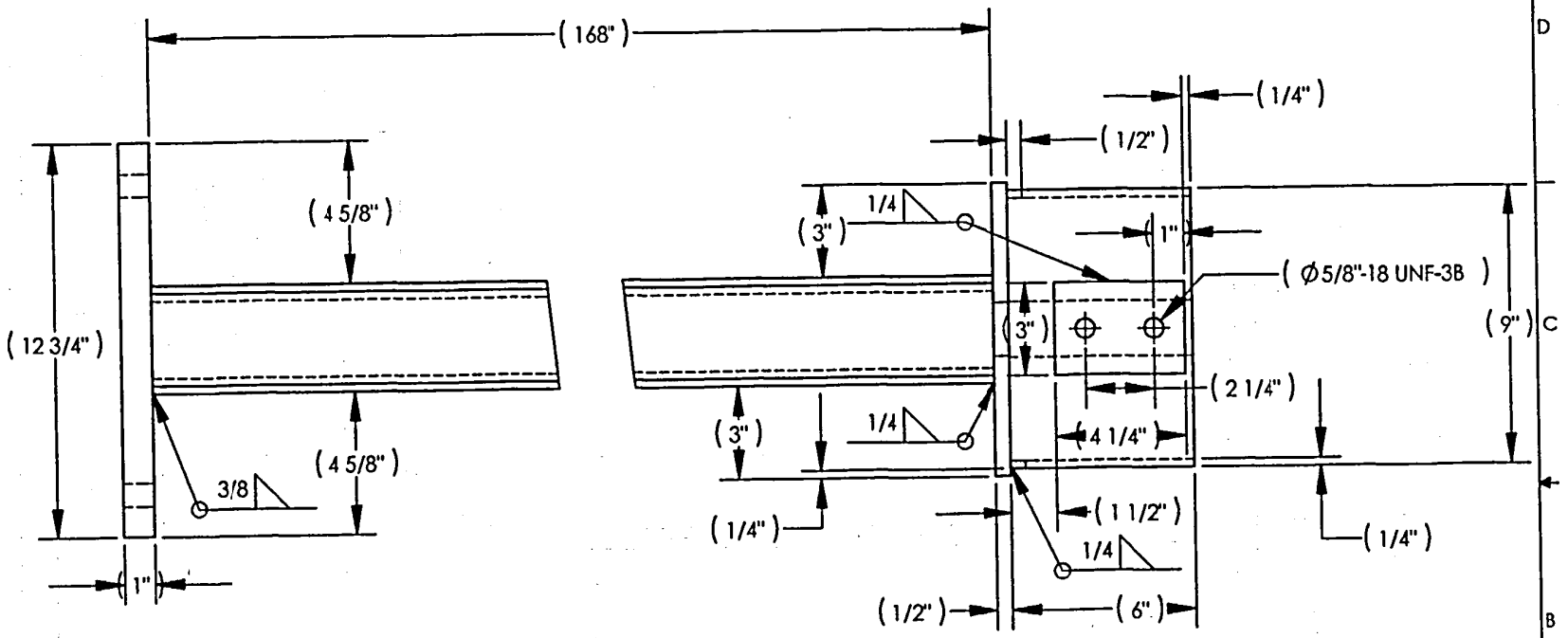

Plates A-36	Quantity
20x12-3/4x1	1
9-1/2x9-3/4x1/2	1
9x6x1/2	1
4-1/4x3x1	1
1/4 thick plates	2

UNLESS OTHERWISE SPECIFIED DIMENSIONS ARE IN INCHES TOLERANCES ARE: FRACTIONS DECIMALS ANGLES ± .XX± .XX ± 1 .XXX±.XXX	CAD GENERATED DRAWING, DO NOT MANUALLY UPDATE	
	APPROVALS	DATE
	DRAWN Spiro Kremmidas	5/20/1999
	CHECKED Andre Filiatrault	5/20/1999
MATERIAL --	RESP ENG	
FINISH --	MFG ENG	
DO NOT SCALE DRAWING	QUAL ENG	

UCSD
University of California, San Diego

HSS 3-1/2x2-1/2x1/4 BEAM

Front View

SIZE	DWG. NO.	REV.
A		1
SCALE 1:4	CAD FILE:	SHEET 2 OF 4

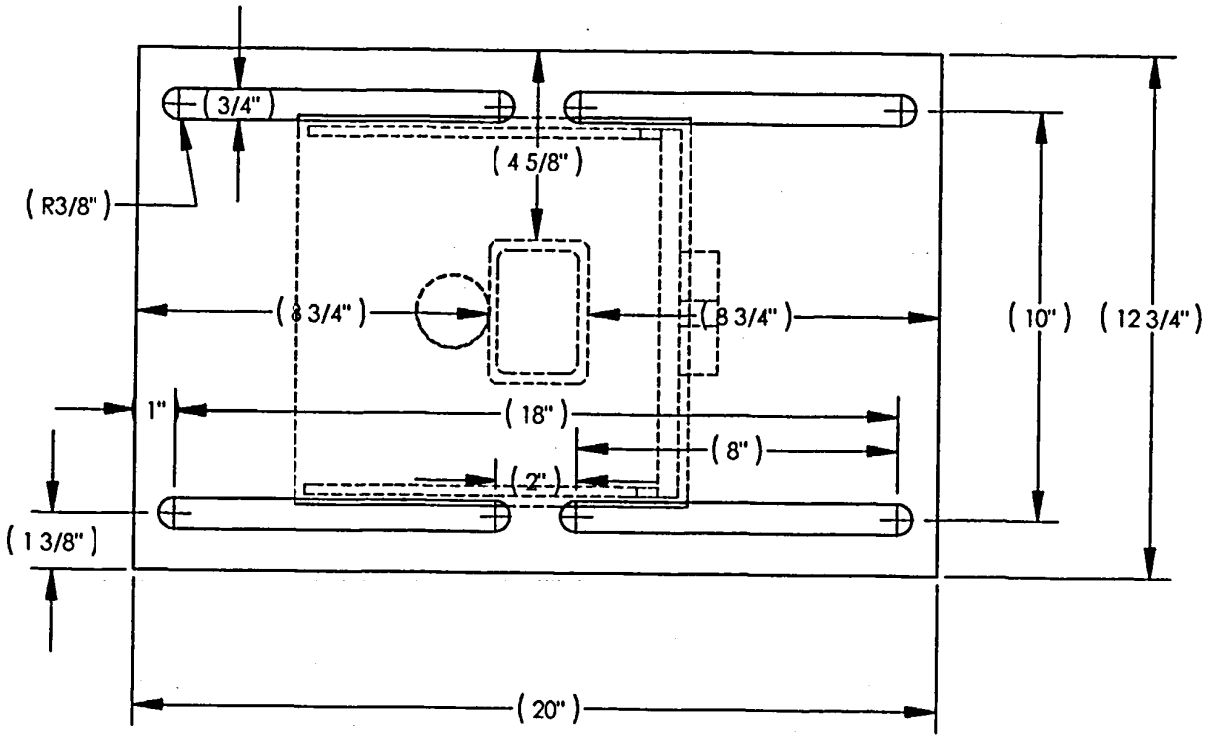

UNLESS OTHERWISE SPECIFIED DIMENSIONS ARE IN INCHES TOLERANCES ARE: FRACTIONS DECIMALS ANGLES + .XX+ .XX + 1 .XXX+.XXX	CAD GENERATED DRAWING, DO NOT MANUALLY UPDATE	UCSD University of California, San Diego
MATERIAL —	APPROVALS / DATE	HSS 3-1/2x2-1/2-1/4 BEAM
FINISH —	DRAWN Spiro Kremmidas 5/20/1999	Bottom View
DO NOT SCALE DRAWING	CHECKED Andre Filiatrault 5/20/1999	SIZE A · DWG. NO. · REV. 1
	RESP ENG	SCALE 1:4 · CAD FILE: · SHEET 3 OF 4
	MFG ENG	
	QUAL ENG	

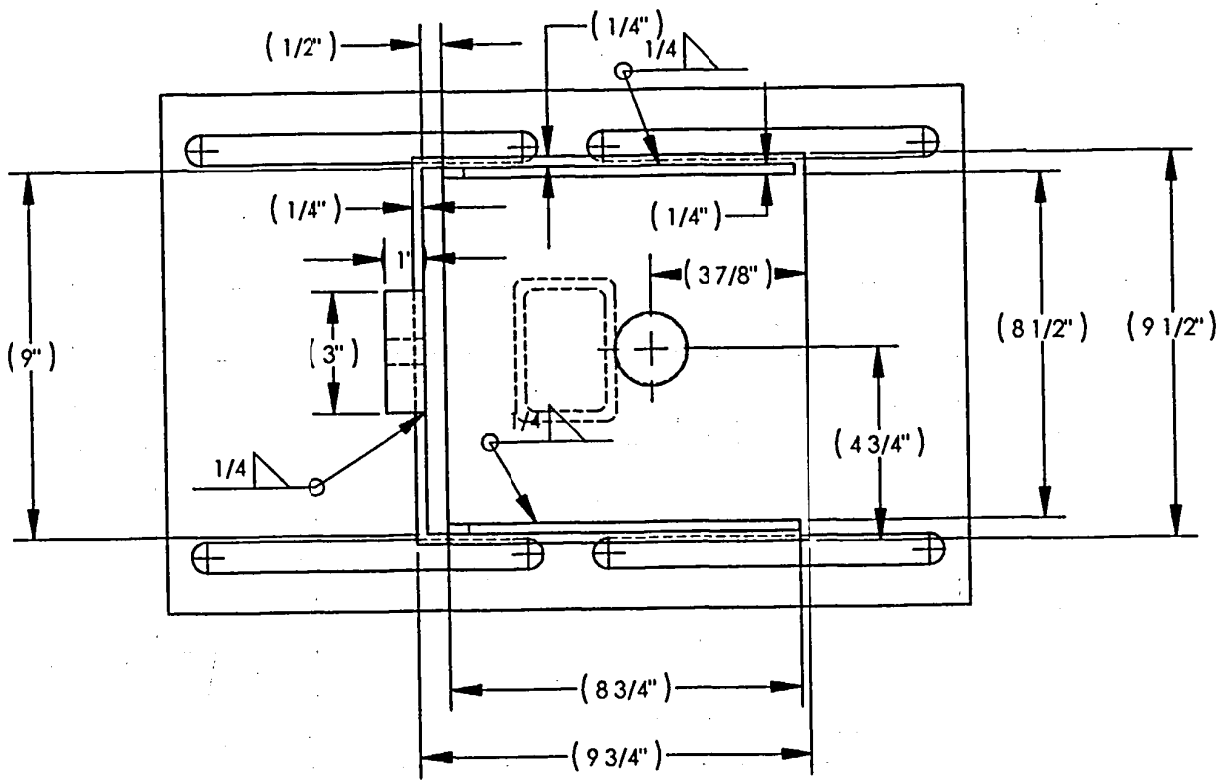

UNLESS OTHERWISE SPECIFIED DIMENSIONS ARE IN INCHES TOLERANCES ARE: FRACTIONS DECIMALS ANGLES + .XX+ .XX + 1 .XXX+.XXX	CAD GENERATED DRAWING, DO NOT MANUALLY UPDATE	UCSD University of California, San Diego
	APPROVALS / DATE	HSS 3-1/2x2-1/2x1/4 BEAM Top View
MATERIAL --	DRAWN Spiro Kremmidas 5/20/1999	
FINISH --	CHECKED Andre Filiatrault 5/20/1999	
DO NOT SCALE DRAWING	RESP ENG	
	MFG ENG	SIZE A / DWG. NO. / REV. 1
	QUAL ENG	SCALE 1:4 / CAD FILE: / SHEET 4 OF 4

EQUIPMENT 3 : 6 Hz 150lbs

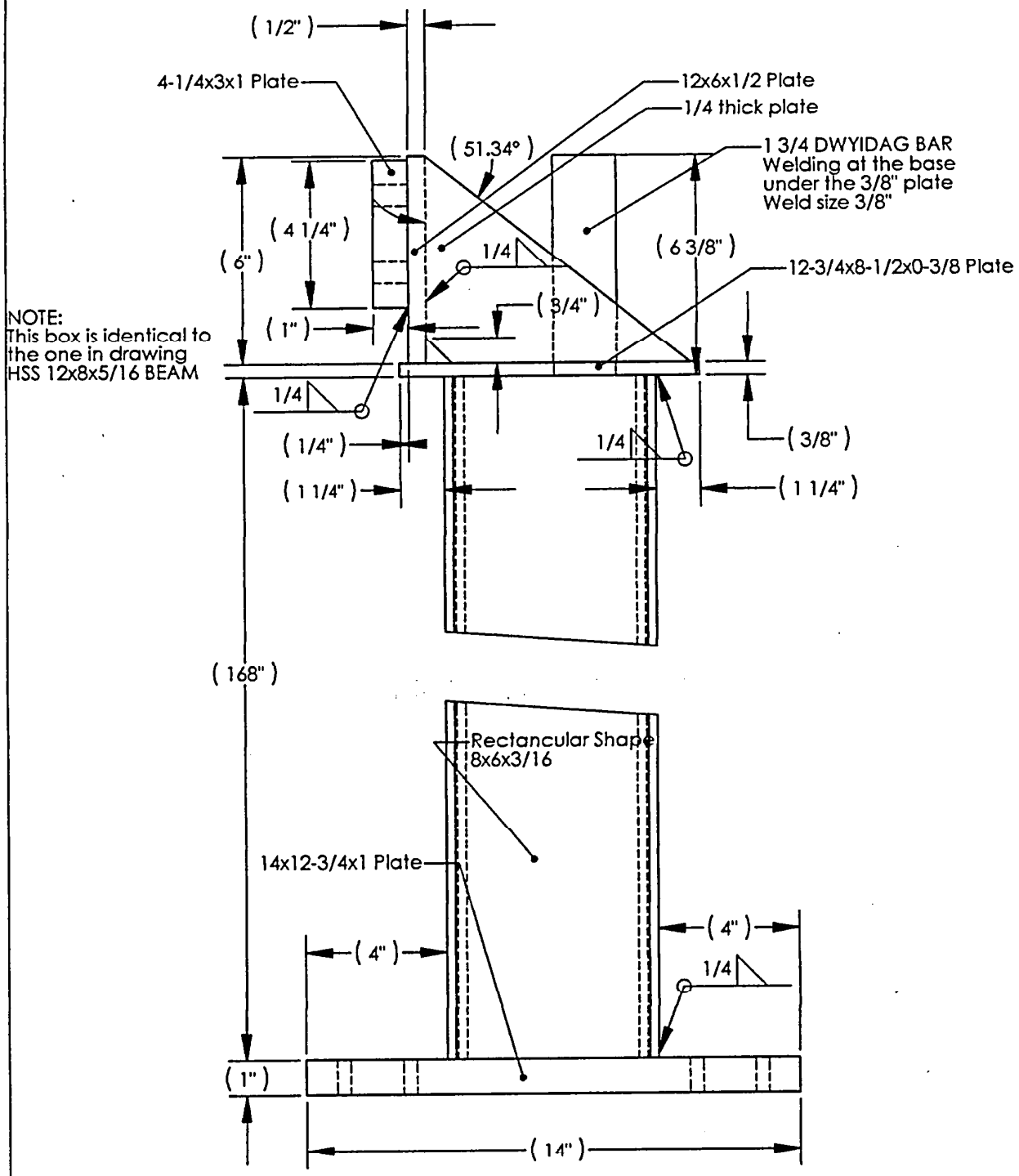

UNLESS OTHERWISE SPECIFIED DIMENSIONS ARE IN INCHES. TOLERANCES ARE:	CONTRACT NO.		UCSD University of California, San Diego
FRACTIONS ±X/X DECIMALS .XX ±.XX .XXX±.XXX ANGLES ±X°	APPROVALS	DATE	HSS 8x6x3/16 BEAM Side View
	DRAWN Spiro Kremmidas	5/20/1999	
	CHECKED Andre Filiatrault	5/20/1999	
MATERIAL	ENGR.		SIZE A | DWG. NO. | REV. 1
FINISH	ISSUED		
DO NOT SCALE DRAWING			SCALE 1:4 | CAD FILE: | SHEET 1 OF 3

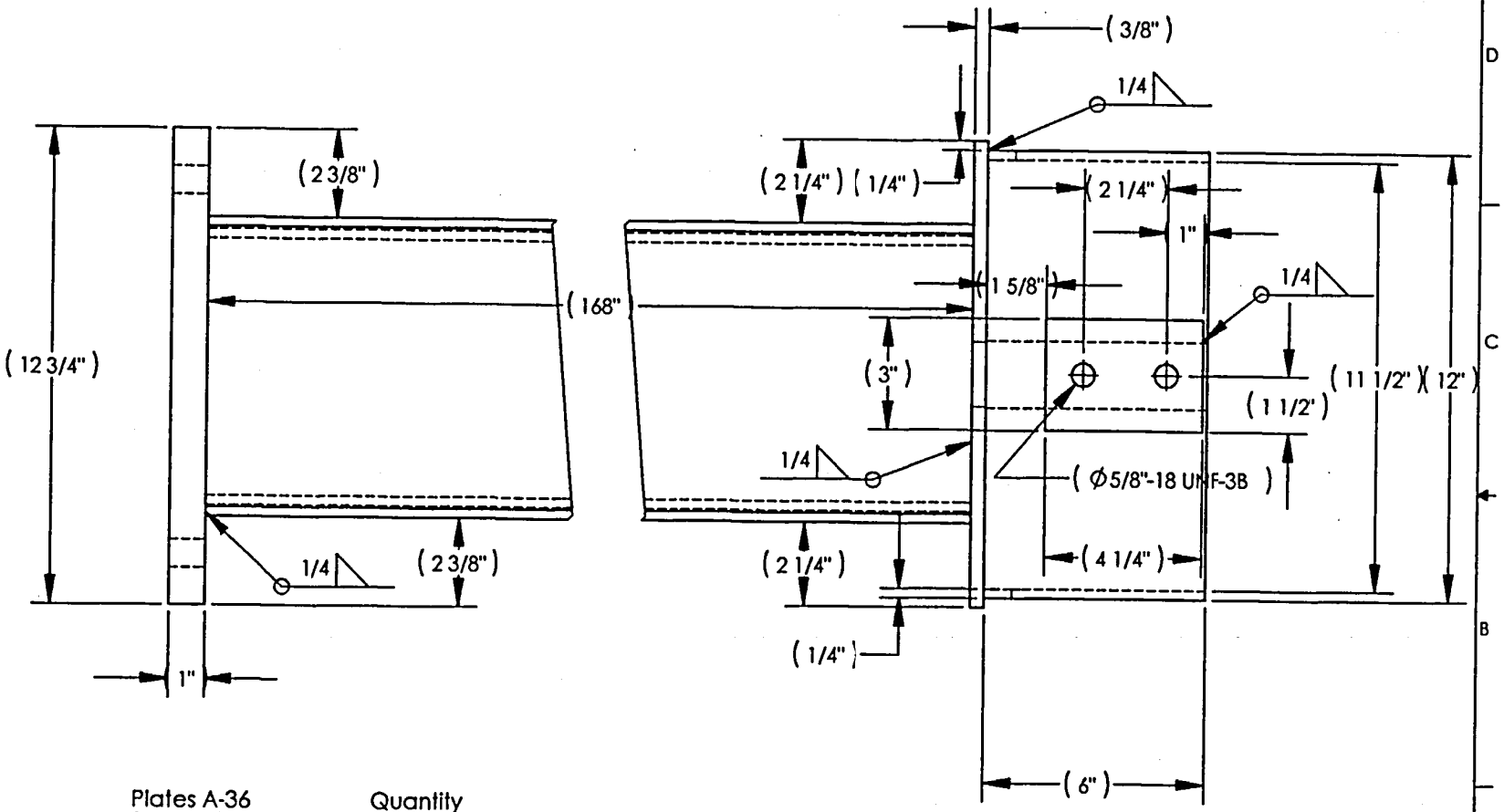

Plates A-36	Quantity
14x12-3/4x1	1
12-3/4x8-1/2x3/8	1
12x6x1/2	1
4-1/4x3x1	1
1/4 thick plate	2

UNLESS OTHERWISE SPECIFIED DIMENSIONS ARE IN INCHES
TOLERANCES ARE:
FRACTIONS ± DECIMALS .XX± .XXX ANGLES ± 1
MATERIAL --
FINISH --
DO NOT SCALE DRAWING

CAD GENERATED DRAWING, DO NOT MANUALLY UPDATE

APPROVALS	DATE
DRAWN Spiro Kremmidas	5/20/1999
CHECKED Andre Filiatrault	5/20/1999
RESP ENG	
MFG ENG	
QUAL ENG	

UCSD
University of California, San Diego

HSS 8x6x3/16 BEAM
Front View

SIZE A | DWG. NO. | REV. 1
SCALE 1:4 | CAD FILE: | SHEET 2 OF 3

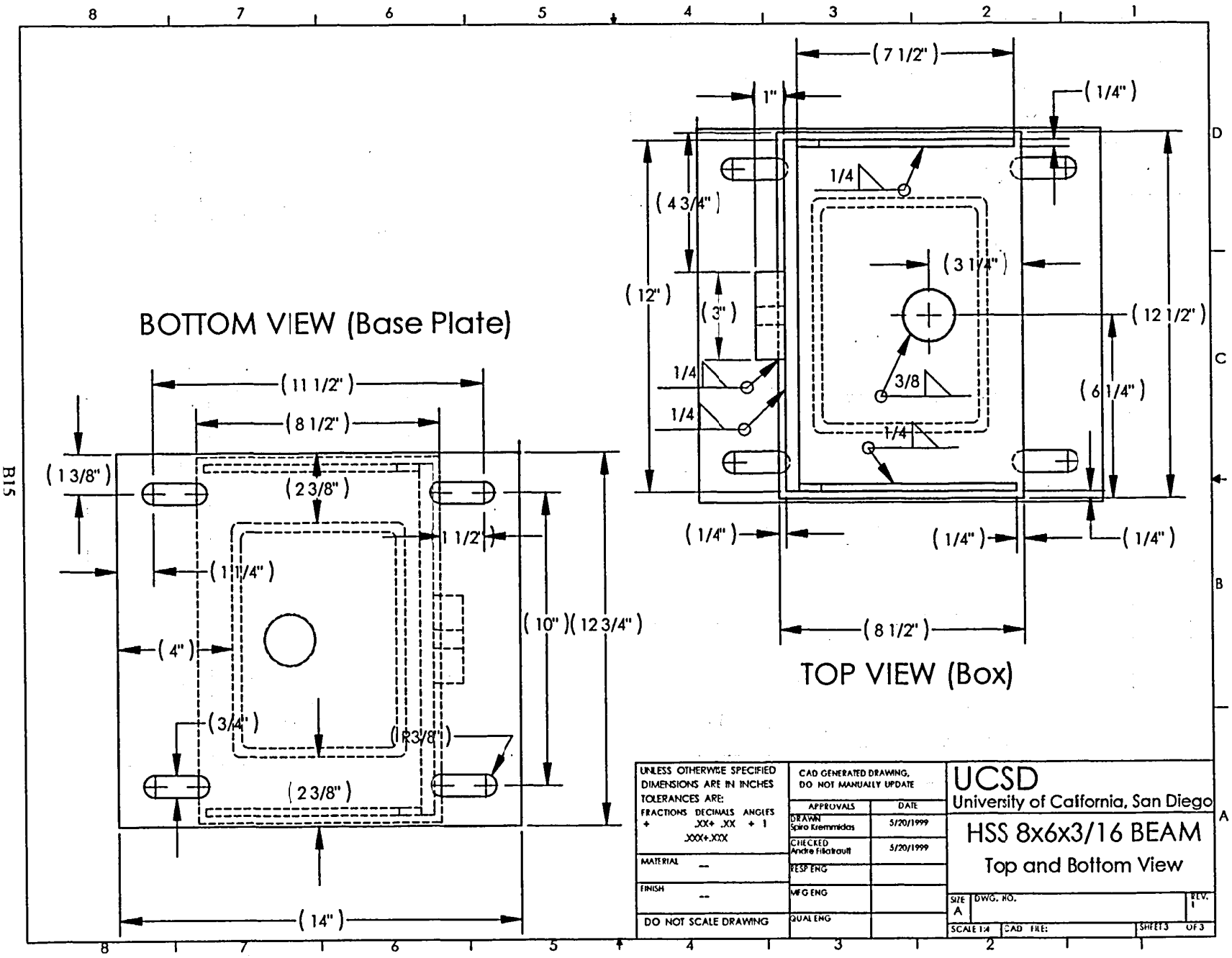

UNLESS OTHERWISE SPECIFIED DIMENSIONS ARE IN INCHES TOLERANCES ARE: FRACTIONS DECIMALS ANGLES ± .XX± .XX ± 1 .XXX±.XXX	CAD GENERATED DRAWING, DO NOT MANUALLY UPDATE	UCSD University of California, San Diego
	APPROVALS / DATE	HSS 8x6x3/16 BEAM
MATERIAL --	DRAWN Spiro Kremmidas 5/20/1999	Top and Bottom View
FINISH --	CHECKED Andre Filiatrault 5/20/1999	
DO NOT SCALE DRAWING	RESP ENG	
	MFG ENG	SIZE A DWG. NO. REV. 1
	QUAL ENG	SCALE 1:4 CAD FILE: SHEET 3 OF 3

EQUIPMENT 4 : 12 Hz 150lbs

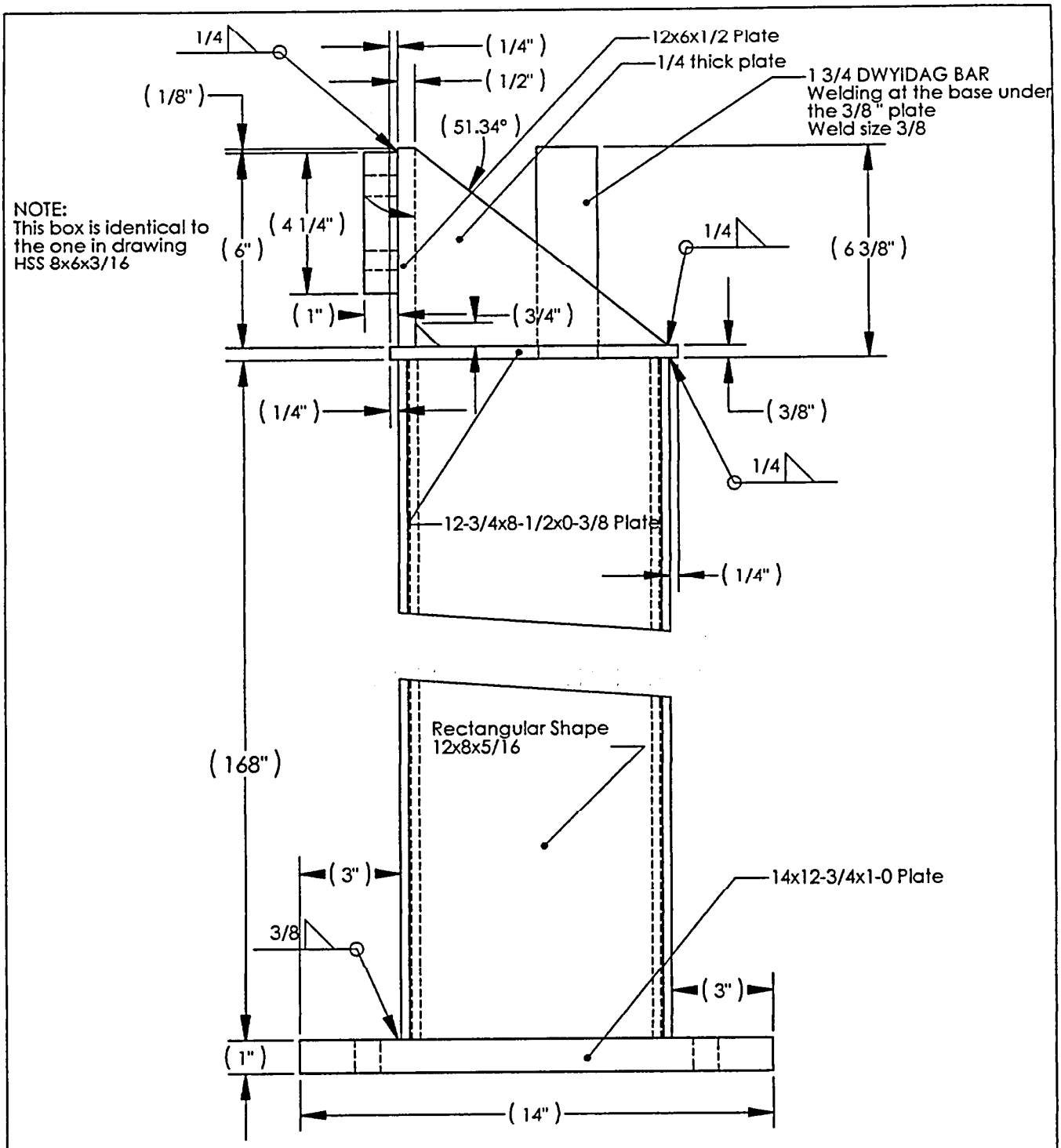

UNLESS OTHERWISE SPECIFIED DIMENSIONS ARE IN INCHES. TOLERANCES ARE:	CONTRACT NO.		UCSD University of California, San Diego
FRACTIONS ±X/X DECIMALS .XX ±.XX .XXX ±.XXX ANGLES ±X°	APPROVALS	DATE	HSS 12x8x5/16 BEAM Side View
	DRAWN Spiro Kremmidas	5/19/1999	
	CHECKED Andre Filiatrault	5/19/1999	
MATERIAL	ENGR.		SIZE A / DWG. NO. / REV. 1
FINISH	ISSUED		
DO NOT SCALE DRAWING			SCALE 1:4 / CAD FILE: / SHEET 1 OF 3

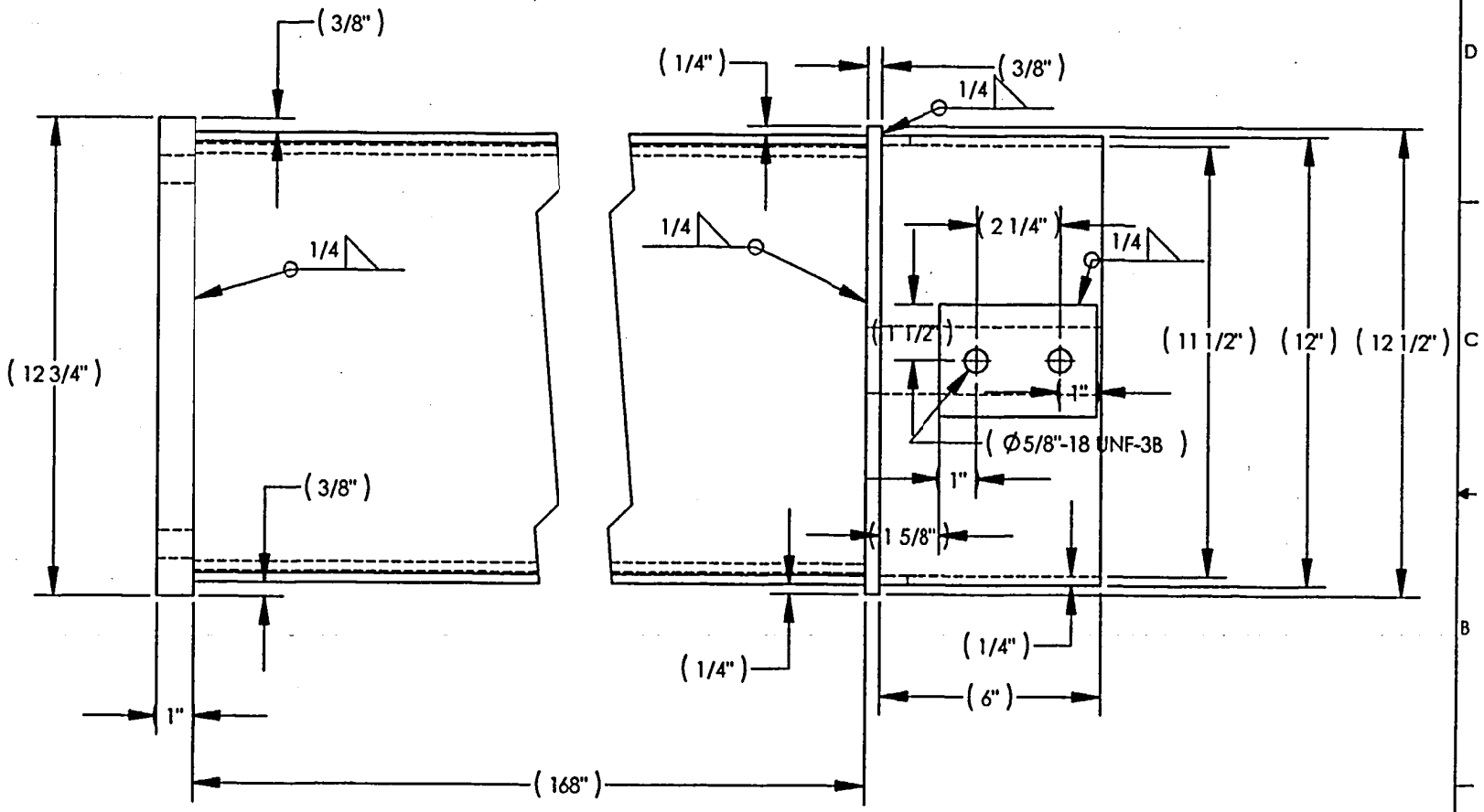

Plates A-36	Quantity
14x12-3/4x1	1
12-3/4x8-1/2x3/8	1
12x6x1/2	1
4-1/4x3x1	1
1/4 thick plates	2

UNLESS OTHERWISE SPECIFIED
DIMENSIONS ARE IN INCHES
TOLERANCES ARE:
FRACTIONS DECIMALS ANGLES
+ .XX+ .XX + 1
.XXX+.XXX

MATERIAL --

FINISH --

DO NOT SCALE DRAWING

CAD GENERATED DRAWING.
DO NOT MANUALLY UPDATE

APPROVALS	DATE
DRAWN Saira Rammidos	5/20/1999
CHECKED Andre Filiatrault	5/20/1999
RESP ENG	
M/G ENG	
QUAL ENG	

UCSD
University of California, San Diego

HSS 12x8x5/16 BEAM
Front View

SIZE A | DWG. NO. | REV. 1

SCALE 1:4 | CAD FILE: | SHEET 2 OF 3

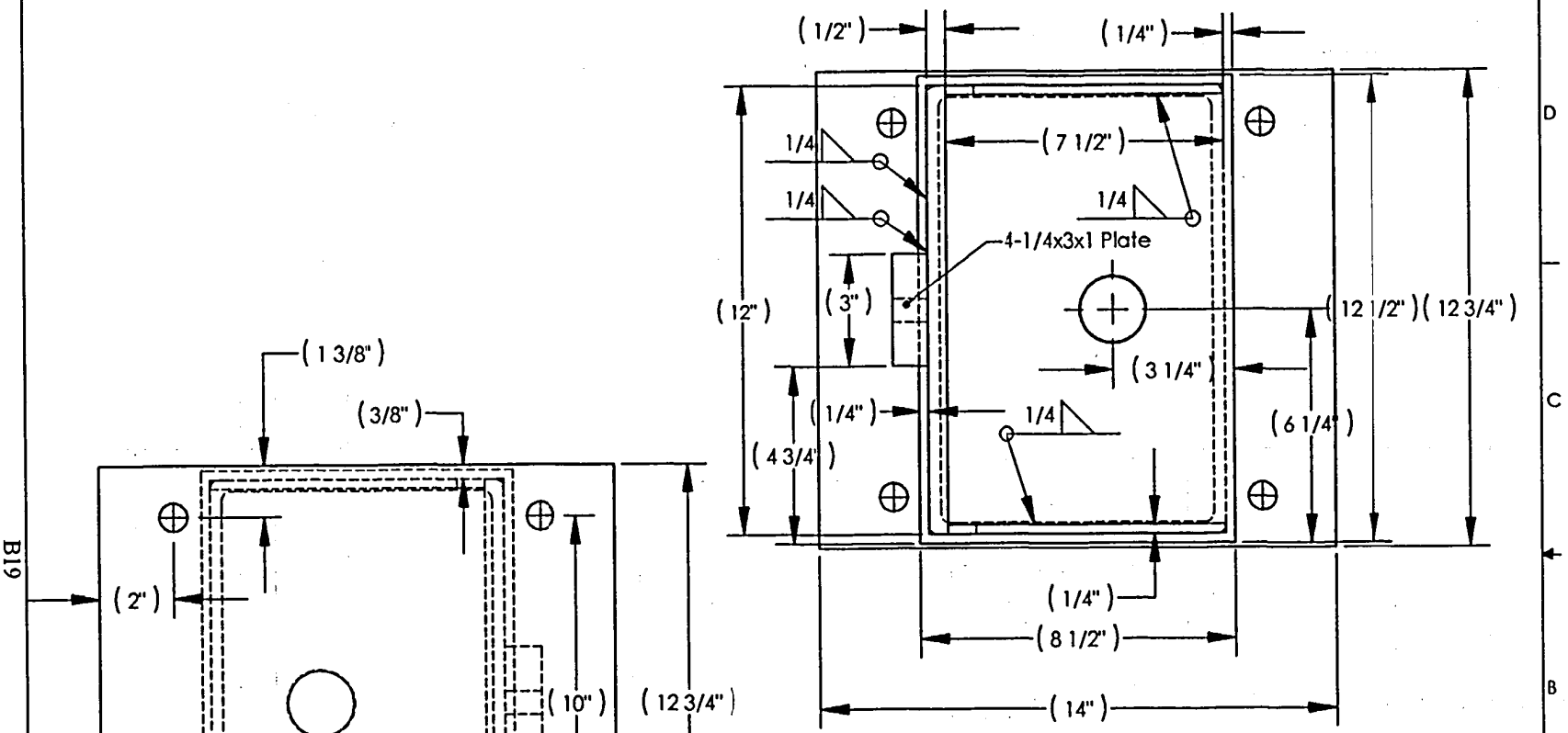

UNLESS OTHERWISE SPECIFIED DIMENSIONS ARE IN INCHES TOLERANCES ARE: FRACTIONS DECIMALS ANGLES + .XX+ .XX + 1 .XXX+.XXX	CAD GENERATED DRAWING, DO NOT MANUALLY UPDATE	UCSD University of California, San Diego
	APPROVALS / DATE	
	DRAWN Spiro Kremmidas 5/20/1999	HSS 12x8x5/16 BEAM
	CHECKED Andre Filiatrault 5/20/1999	Top and Bottom View
MATERIAL --	RESP ENG	
FINISH --	MFG ENG	SIZE A / DWG. NO. / REV. 1
DO NOT SCALE DRAWING	QUALENG	SCALE 1:4 / CAD FILE: / SHEET 3 OF 3

BRACING ELEMENT FOR EQUIPMENT 4

L3x3x3/8
STEEL GRADE A36
Quantity = 2

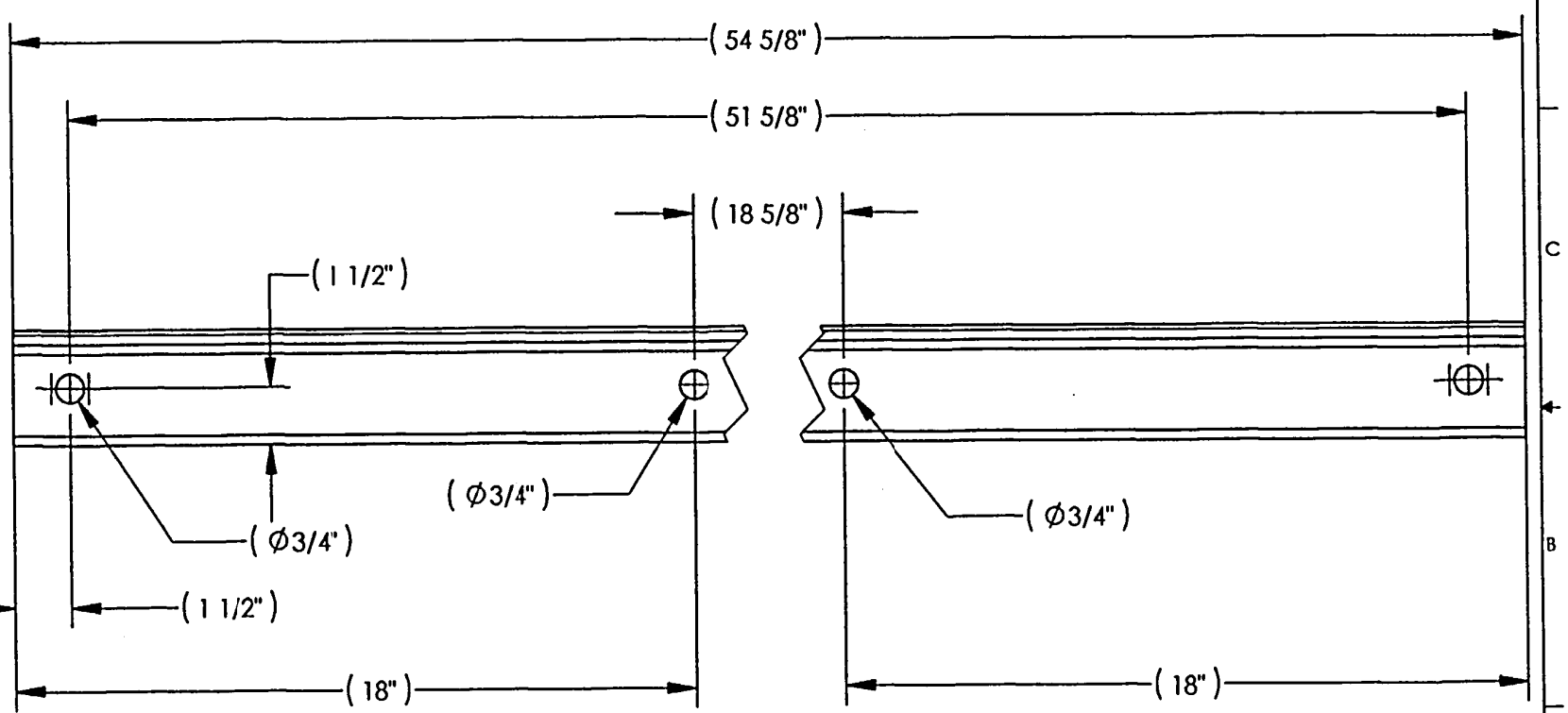

UNLESS OTHERWISE SPECIFIED DIMENSIONS ARE IN INCHES TOLERANCES ARE: FRACTIONS DECIMALS ANGLES + .XX+ .XX + 1 .XXX+.XXX	CAD GENERATED DRAWING, DO NOT MANUALLY UPDATE	UCSD University of California, San Diego
	APPROVALS / DATE	
	DRAWN Spiro Kremmidas 7-27-1999	Brace PEER/PG&E
	CHECKED	
MATERIAL --	RESP ENG	
FINISH --	MFG ENG	SIZE A DWG. NO. REV. 1
DO NOT SCALE DRAWING	QUAL ENG	SCALE 1:4 CAD FILE: SHEET 1 OF 1

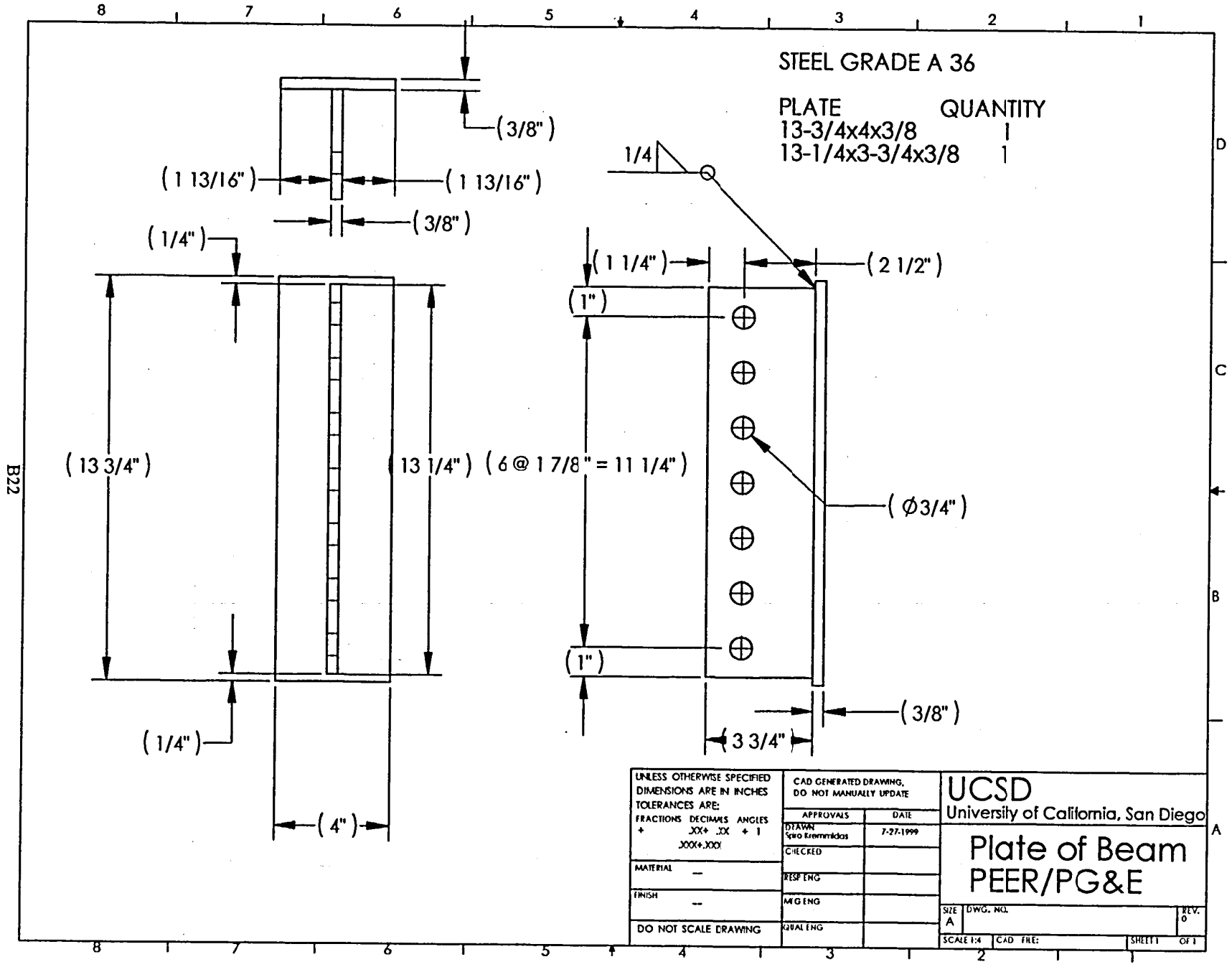
STEEL GRADE A 36
PLATE QUANTITY
13-3/4x4x3/8 1
13-1/4x3-3/4x3/8 1
(3/8")
(1 13/16")
(1 13/16")
(3/8")
(1/4")
(13 3/4")
(13 1/4")
(1/4")
(4")
1/4
(1 1/4")
(2 1/2")
(1")
(6 @ 1 7/8" = 11 1/4")
(Ø3/4")
(1")
(3/8")
(3 3/4")
B22
D
C
B
A
UNLESS OTHERWISE SPECIFIED DIMENSIONS ARE IN INCHES
TOLERANCES ARE:
FRACTIONS DECIMALS ANGLES
+ .XX+ .XX + 1
.XXX+.XXX
MATERIAL —
FINISH —
DO NOT SCALE DRAWING
CAD GENERATED DRAWING, DO NOT MANUALLY UPDATE
APPROVALS DATE
DRAWN Spiro Kremmidas 7-27-1999
CHECKED
RESP ENG
MFG ENG
QUAL ENG
UCSD
University of California, San Diego
Plate of Beam
PEER/PG&E
SIZE A
DWG. NO.
REV. 0
SCALE 1:4
CAD FILE:
SHEET 1 OF 1

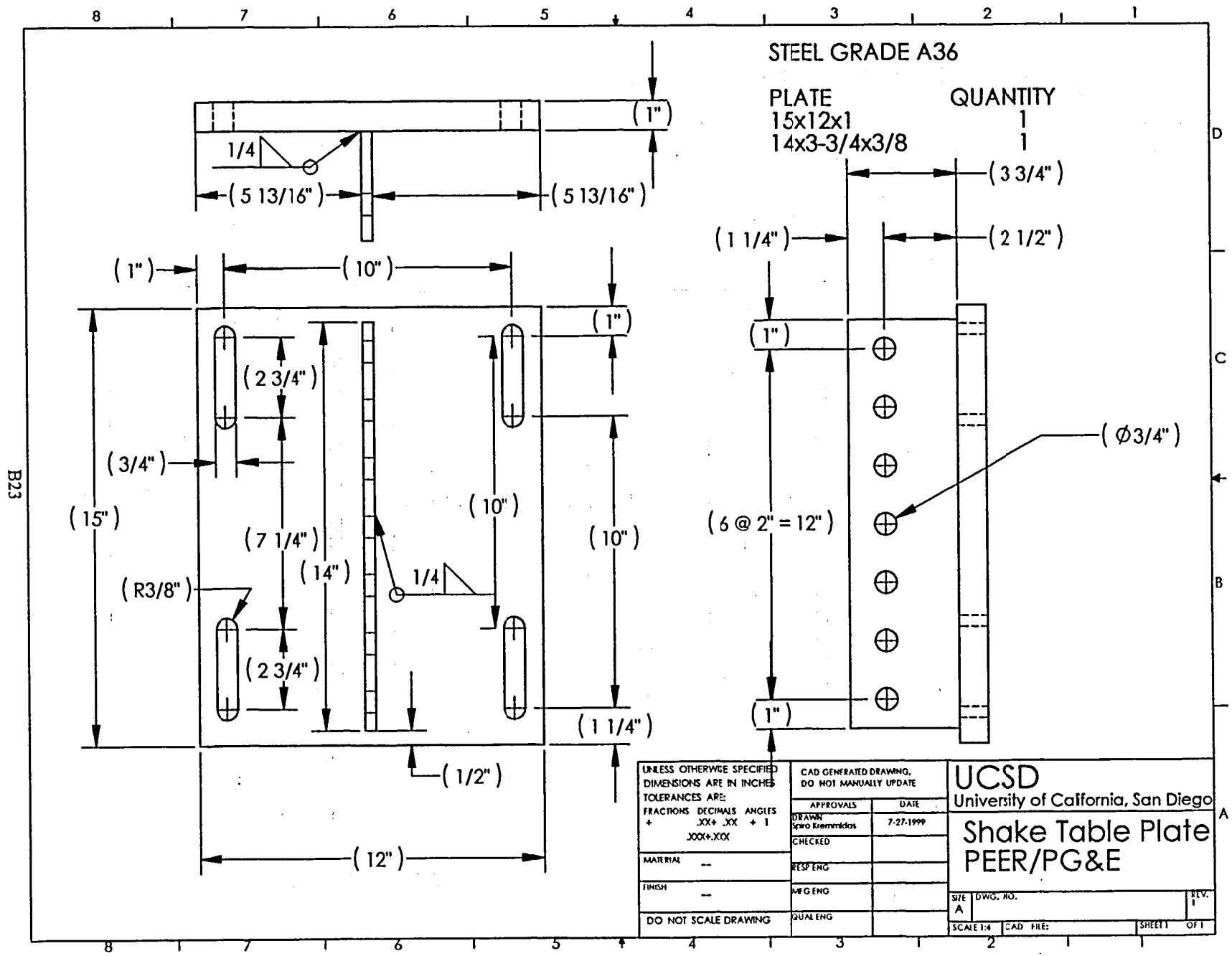
STEEL GRADE A36
PLATE
15x12x1
14x3-3/4x3/8
QUANTITY
1
1
(1")
1/4
(5 13/16")
(5 13/16")
(1")
(10")
(1")
(2 3/4")
(3/4")
(15")
(7 1/4")
(14")
(R3/8")
(2 3/4")
(10")
1/4
(10")
(1 1/4")
(1/2")
(12")
(3 3/4")
(1 1/4")
(2 1/2")
(1")
(Ø3/4")
(6 @ 2" = 12")
(1")
UNLESS OTHERWISE SPECIFIED DIMENSIONS ARE IN INCHES
TOLERANCES ARE:
FRACTIONS DECIMALS ANGLES
+ .XX+ .XX + 1
.XXX+.XX
MATERIAL --
FINISH --
DO NOT SCALE DRAWING
CAD GENERATED DRAWING, DO NOT MANUALLY UPDATE
APPROVALS DATE
DRAWN Spiro Kiremidjian 7-27-1999
CHECKED
RESP ENG
MFG ENG
QUAL ENG
UCSD
University of California, San Diego
Shake Table Plate
PEER/PG&E
SIZE A
DWG. NO.
REV. 1
SCALE 1:4
CAD FILE:
SHEET 1 OF 1
B23

APPENDIX C

RESULTS OF FREQUENCY EVALUATION TESTS

TEST RB-1
EQUIPMENT COMBINATION 4
INDIVIDUAL EQUIPMENT

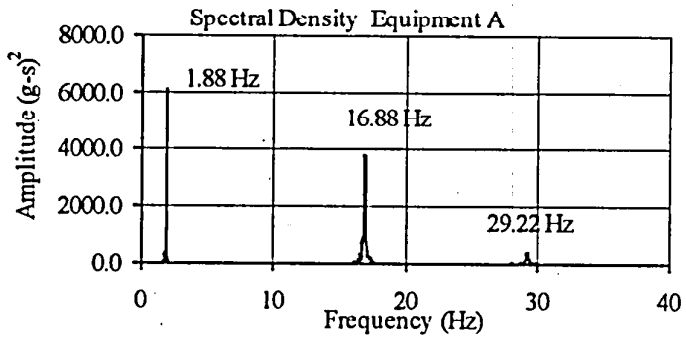

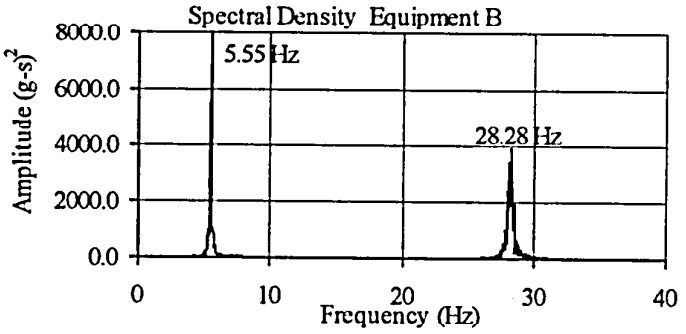

TEST RB-4
EQUIPMENT COMBINATION 4
SPRING 30-2022 CONNECTOR

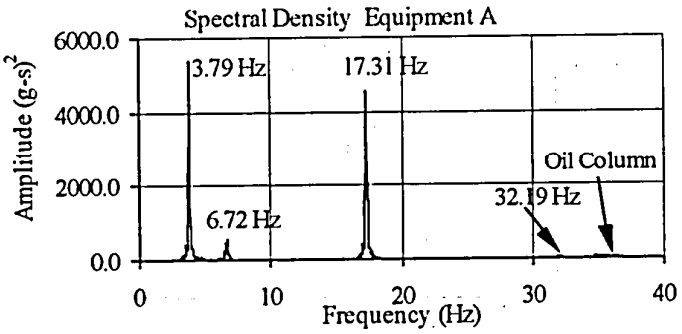

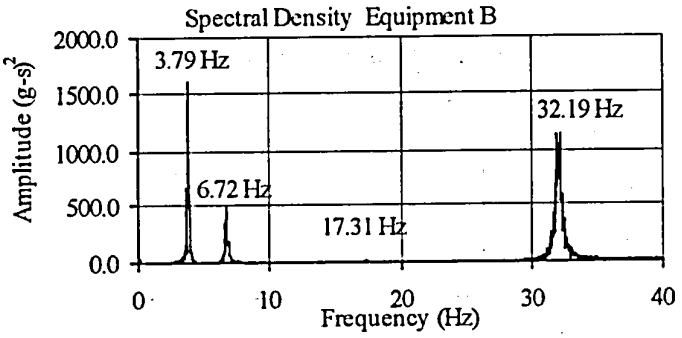

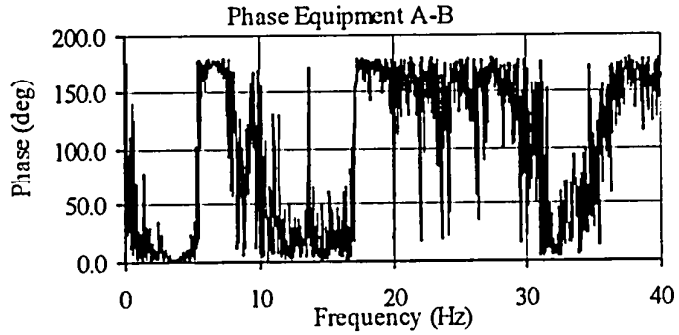

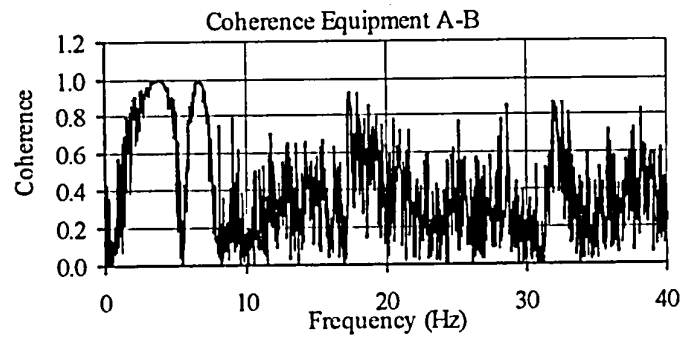

TEST RB-10
EQUIPMENT COMBINATION 4
INDIVIDUAL EQUIPMENT

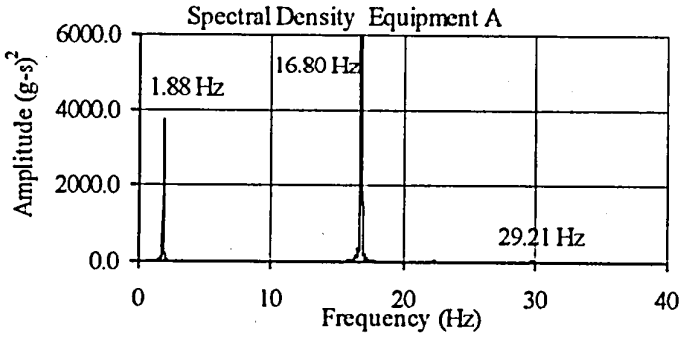

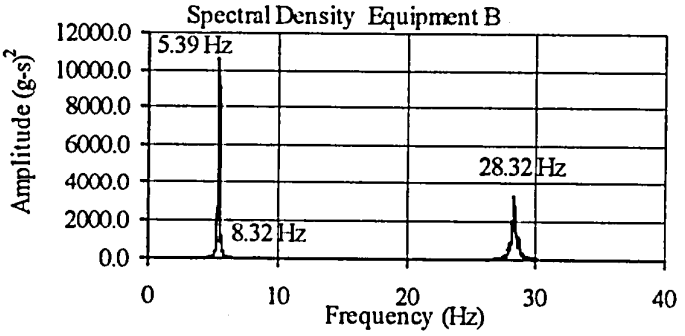

TEST RB-13
EQUIPMENT COMBINATION 4
BUS SLIDER CONNECTOR

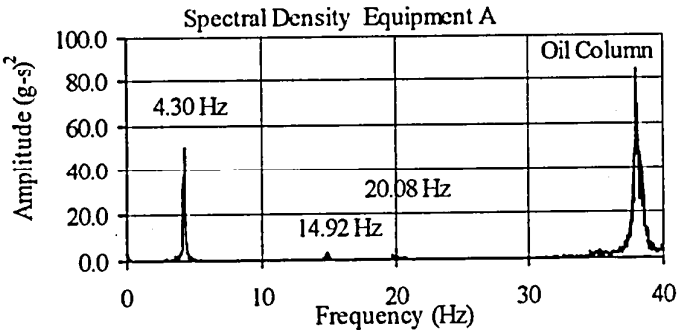

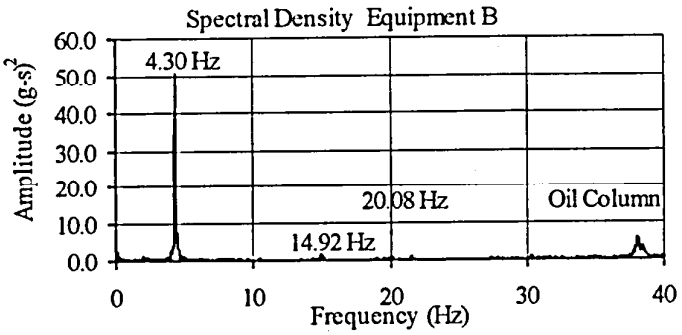

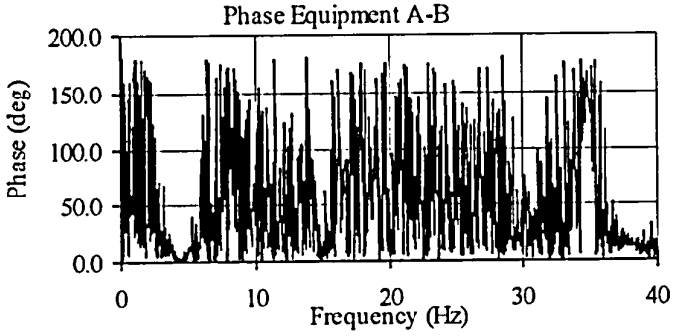

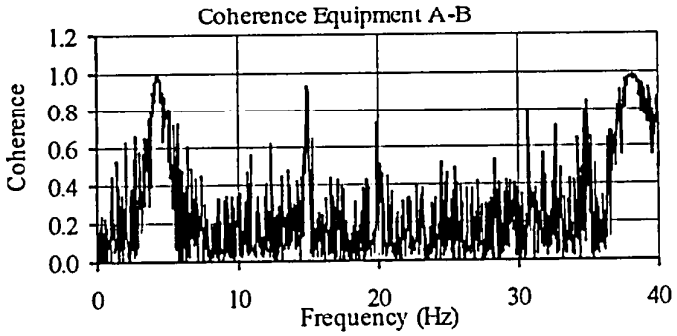

TEST RB-22
EQUIPMENT COMBINATION 4
BPA ISOLATOR CONNECTOR

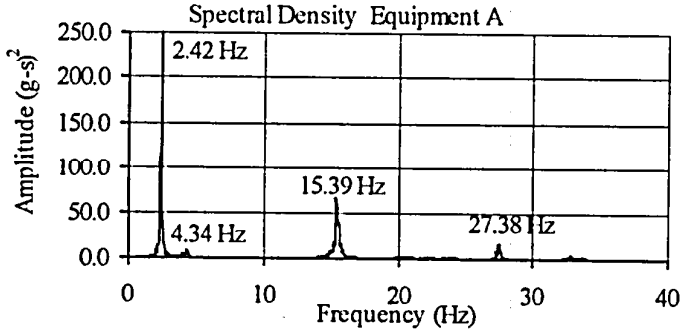

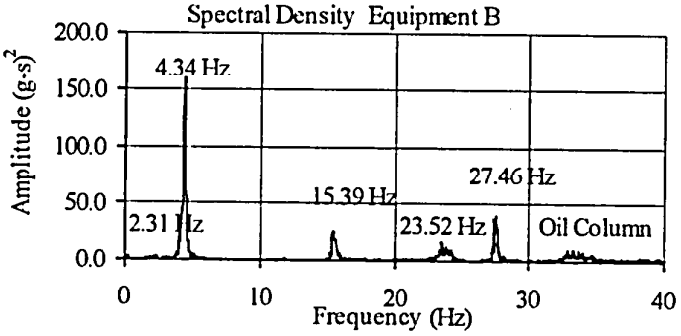

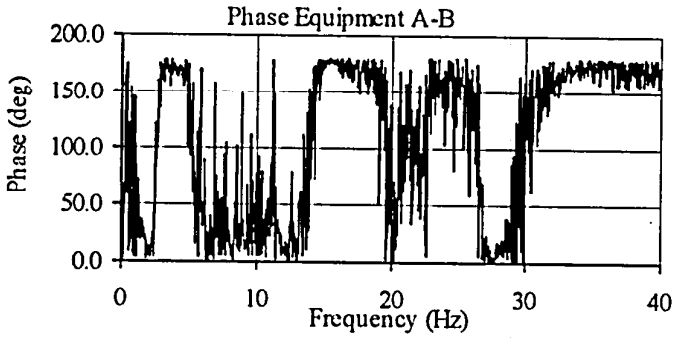

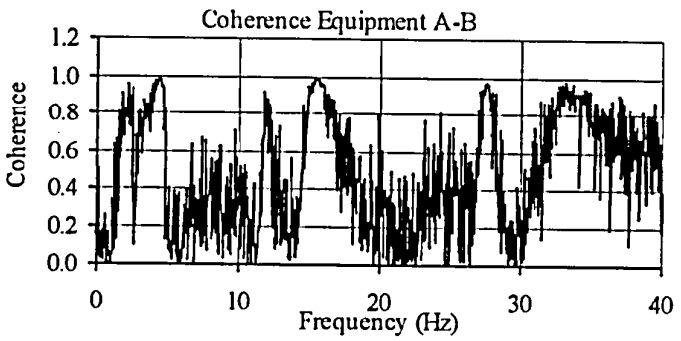

TEST RB-33
EQUIPMENT COMBINATION 3
INDIVIDUAL EQUIPMENT

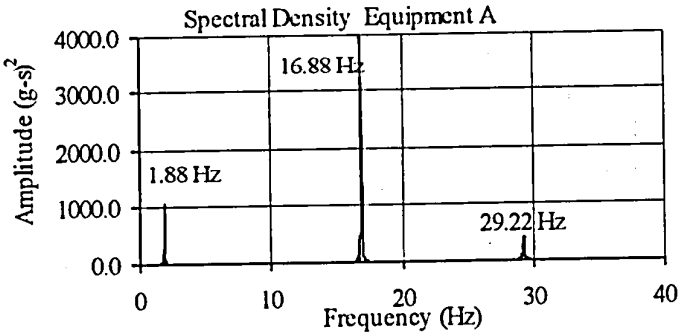

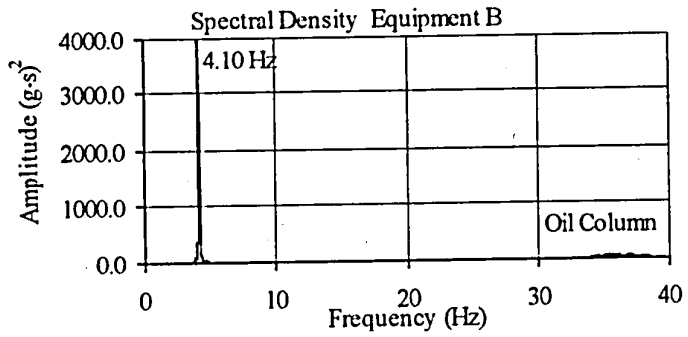

TEST RB-36
EQUIPMENT COMBINATION 3
SPRING 30-2022 CONNECTOR

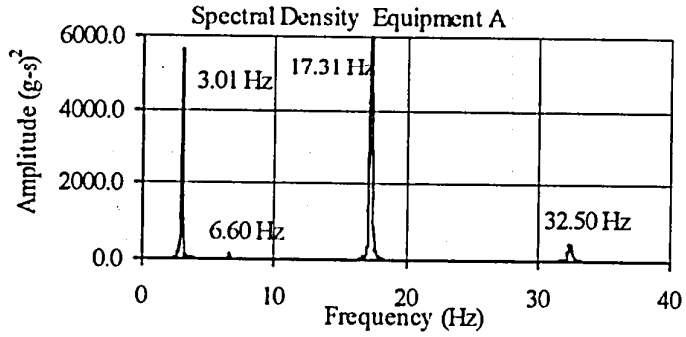

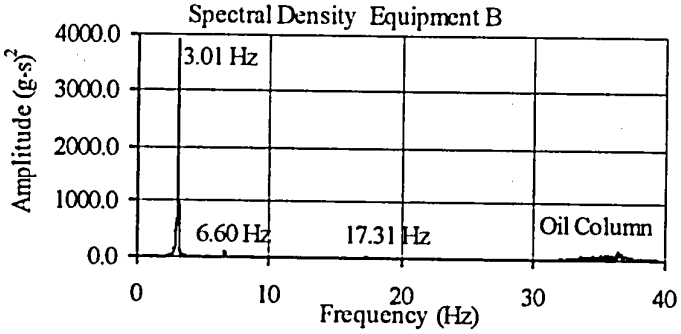

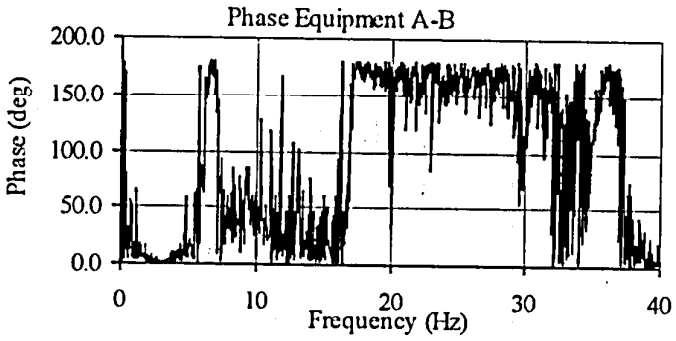

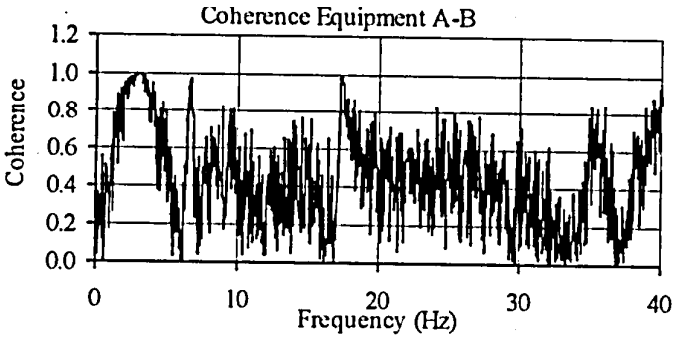

TEST RB-45
EQUIPMENT COMBINATION 3
BUS SLIDER CONNECTOR

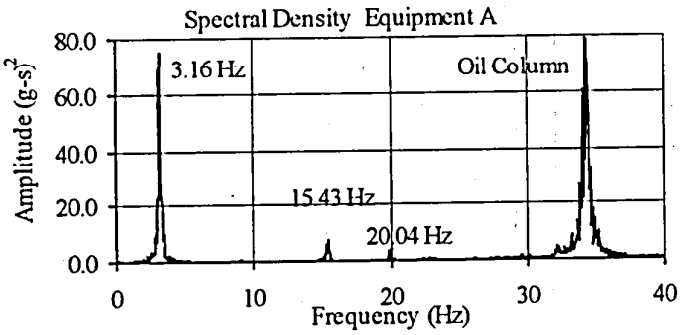

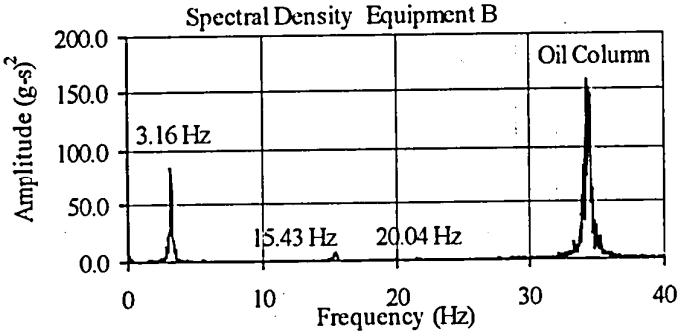

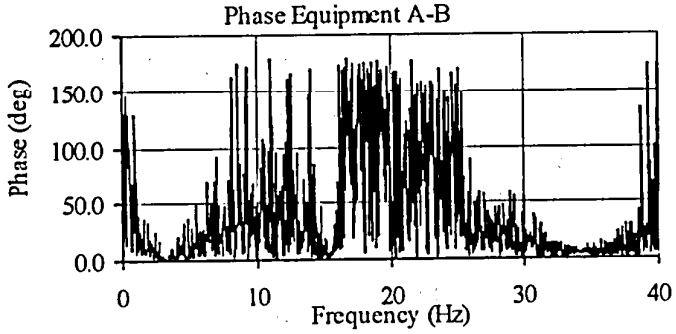

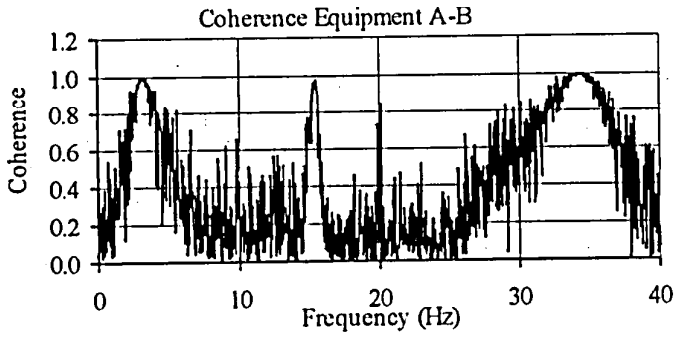

TEST RB-54
EQUIPMENT COMBINATION 3
BPA ISOLATOR CONNECTOR

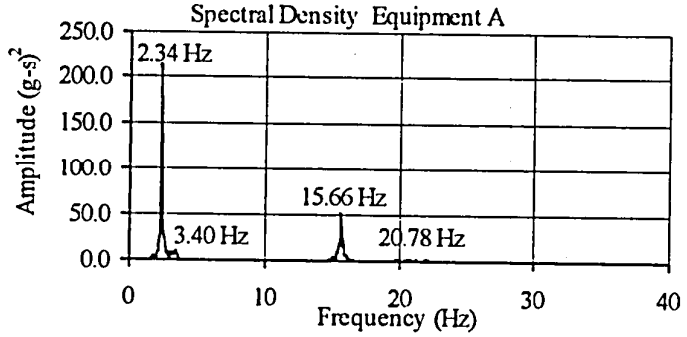

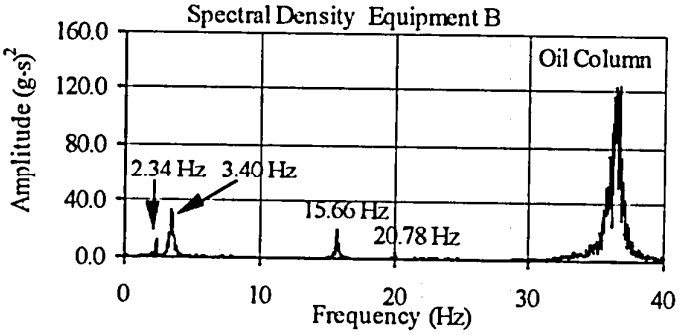

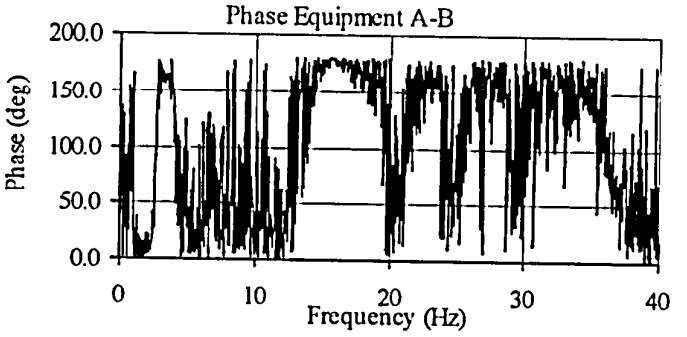

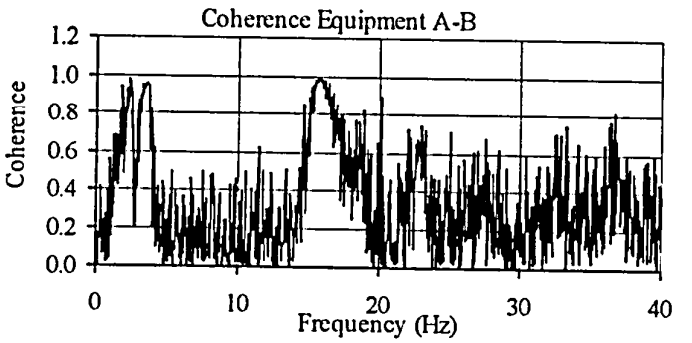

TEST RB-66
EQUIPMENT COMBINATION 1
INDIVIDUAL EQUIPMENT

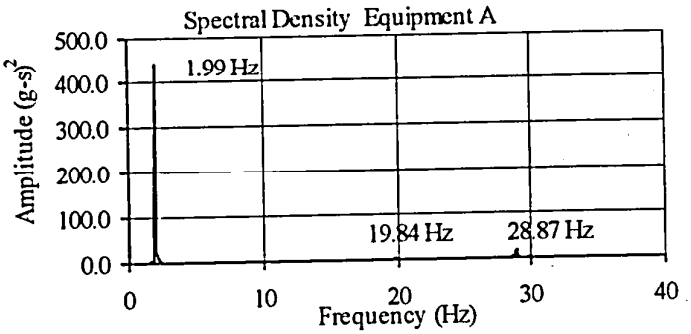

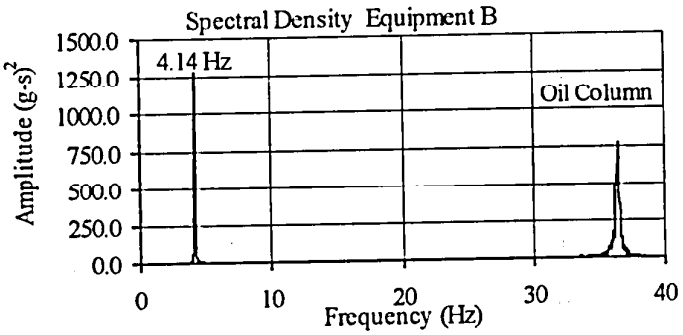

TEST RB-69
EQUIPMENT COMBINATION 1
SPRING 30-2022 CONNECTOR

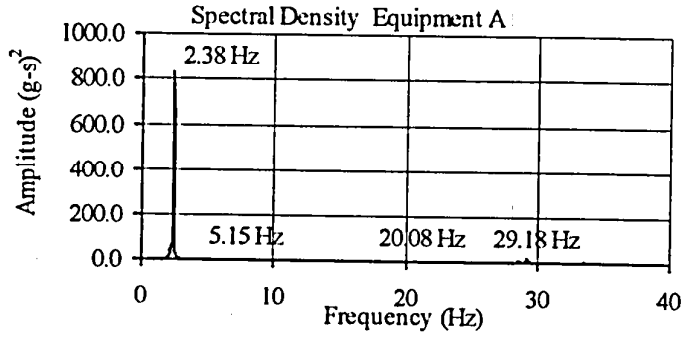

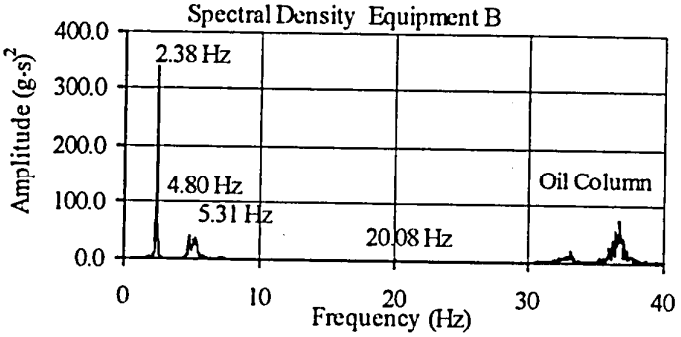

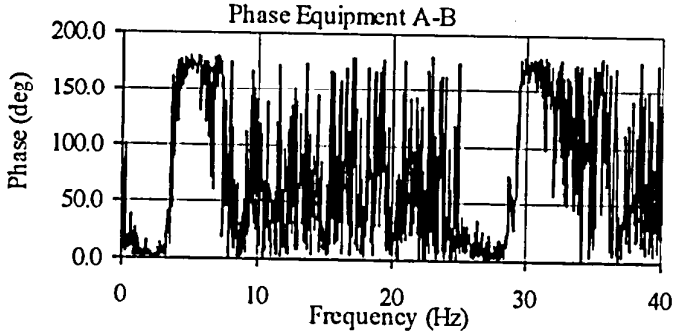

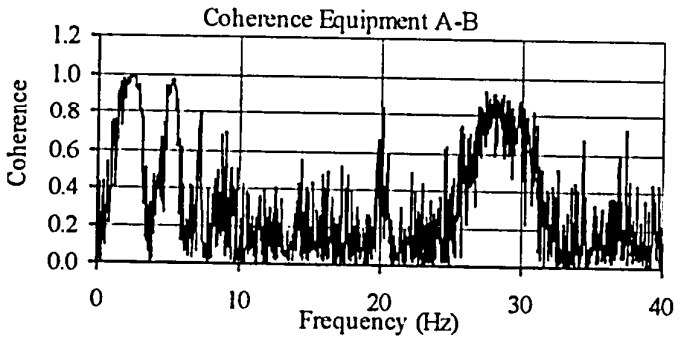

TEST RB-76
EQUIPMENT COMBINATION 1
BUS SLIDER CONNECTOR

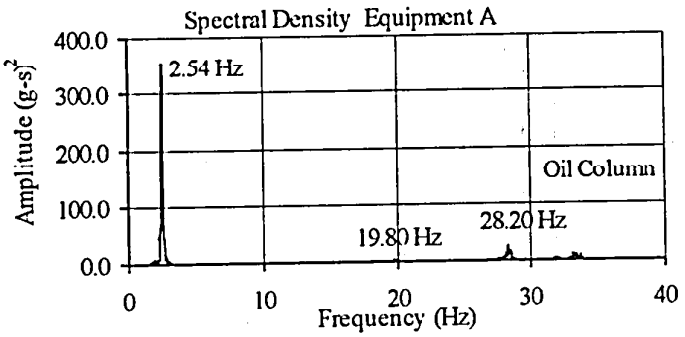

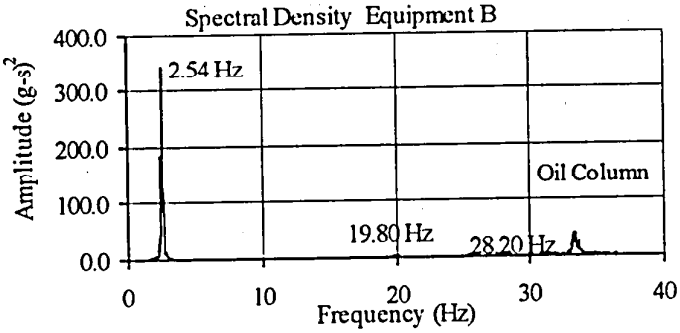

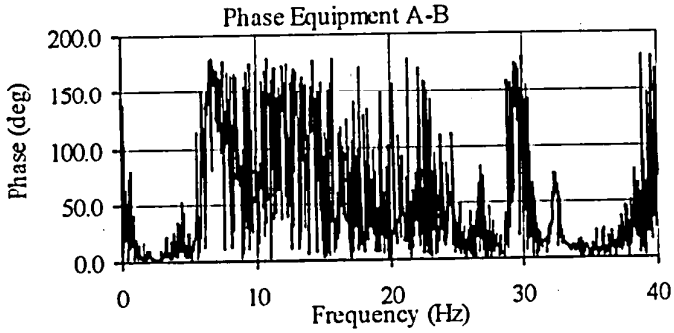

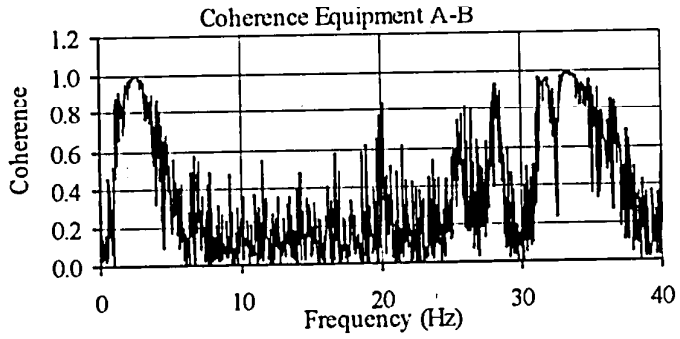

TEST RB-83
EQUIPMENT COMBINATION 1
BPA ISOLATOR CONNECTOR

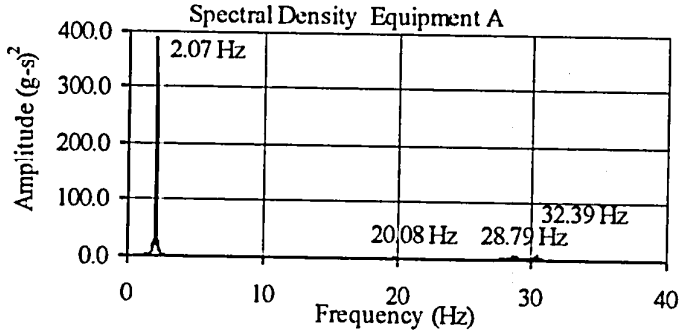

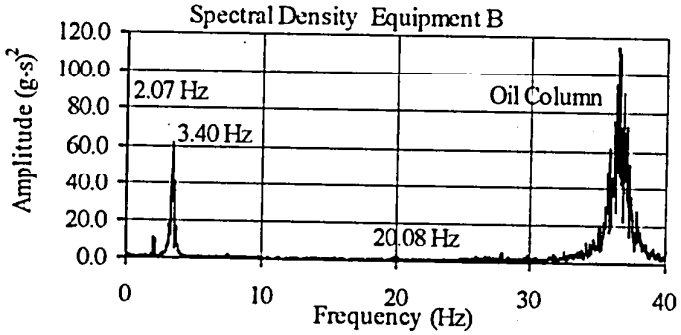

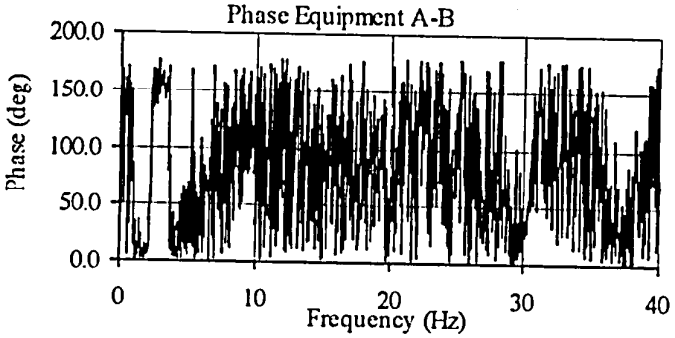

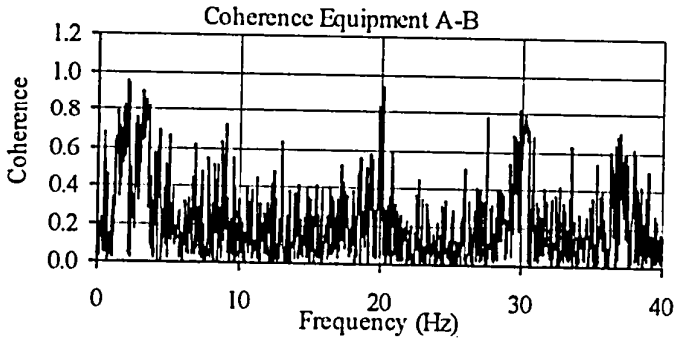

TEST RB-93
EQUIPMENT COMBINATION 2
INDIVIDUAL EQUIPMENT

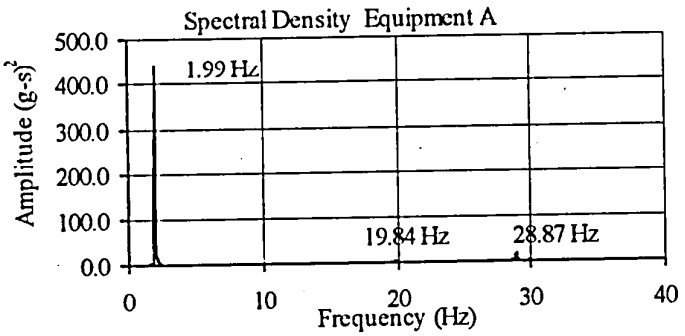

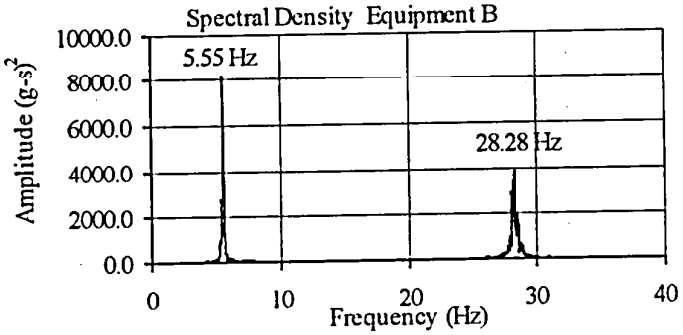

TEST RB-96
EQUIPMENT COMBINATION 2
SPRING 30-2022 CONNECTOR

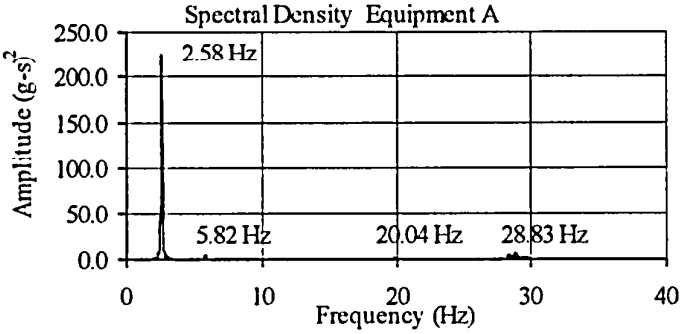

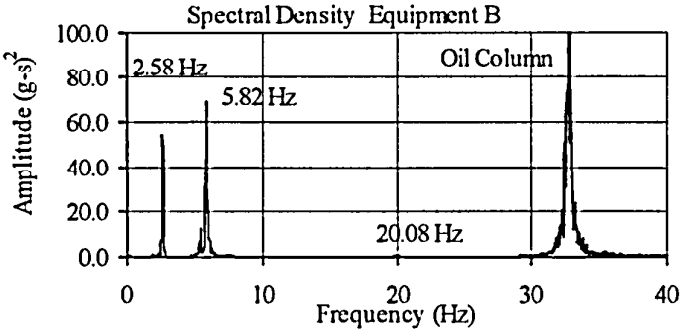

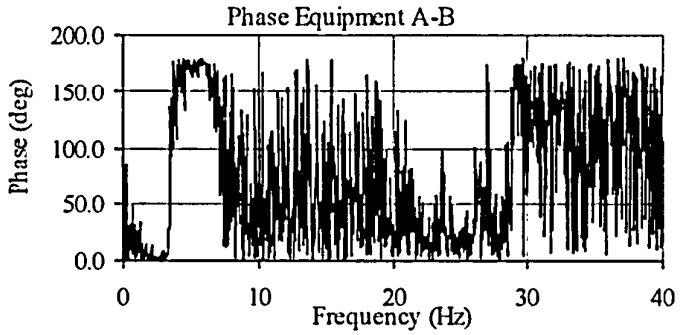

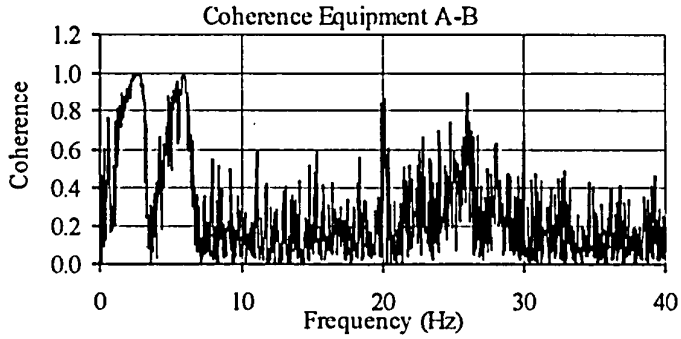

TEST RB-107
EQUIPMENT COMBINATION 2
BUS SLIDER CONNECTOR

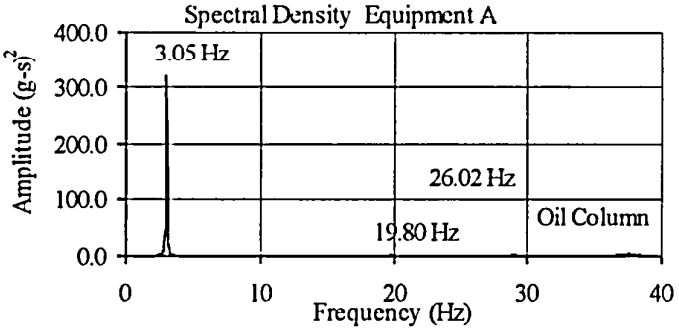

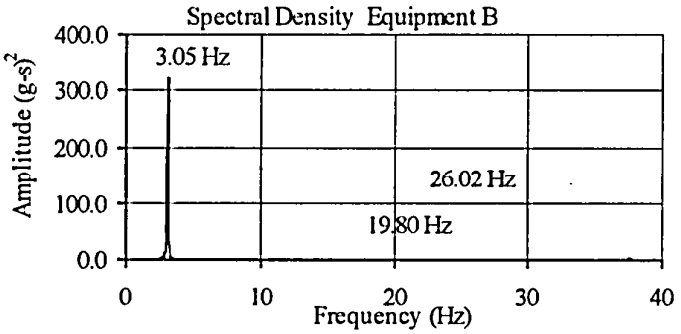

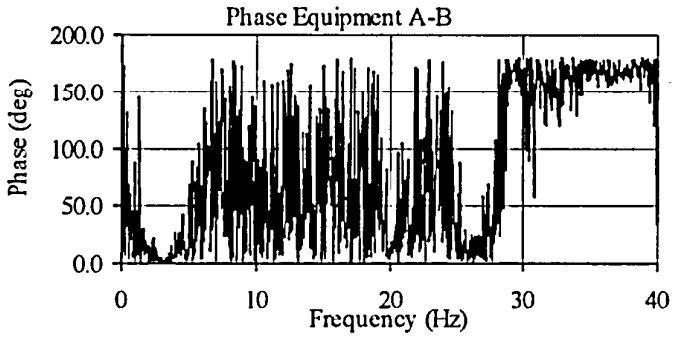

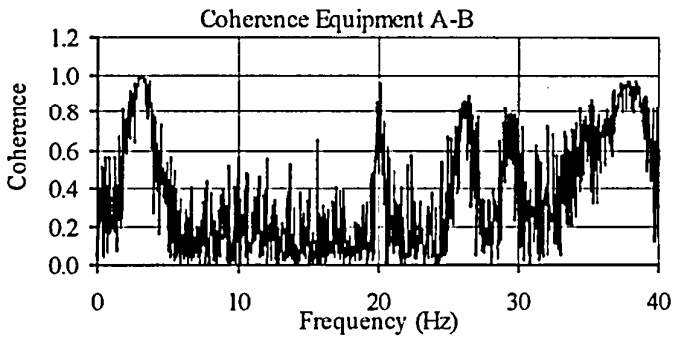

TEST RB-116
EQUIPMENT COMBINATION 2
BPA ISOLATOR CONNECTOR

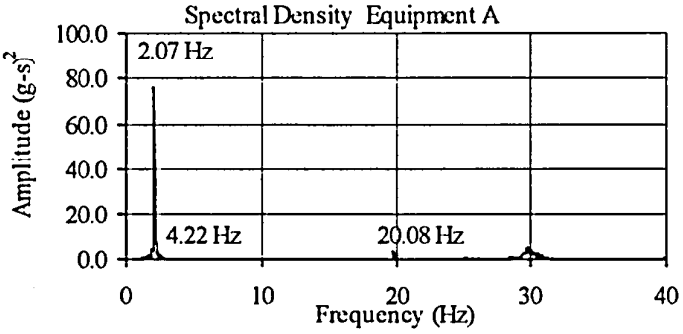

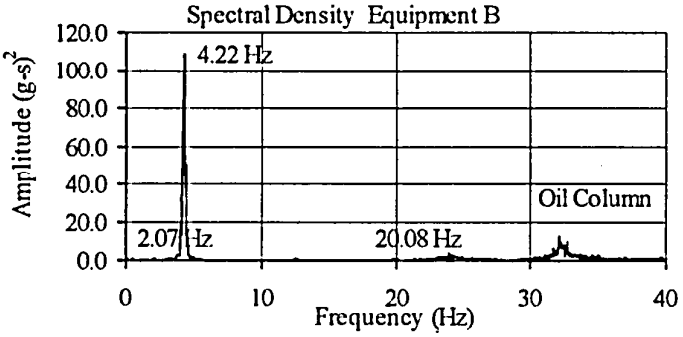

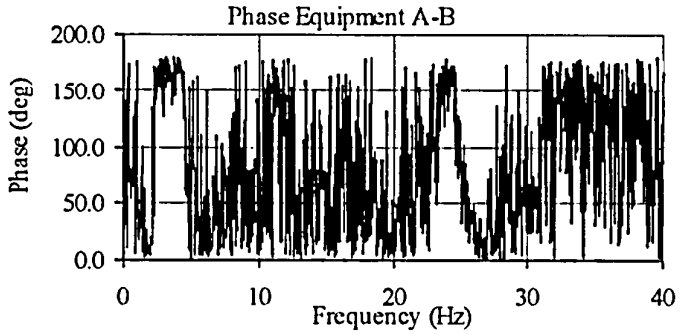

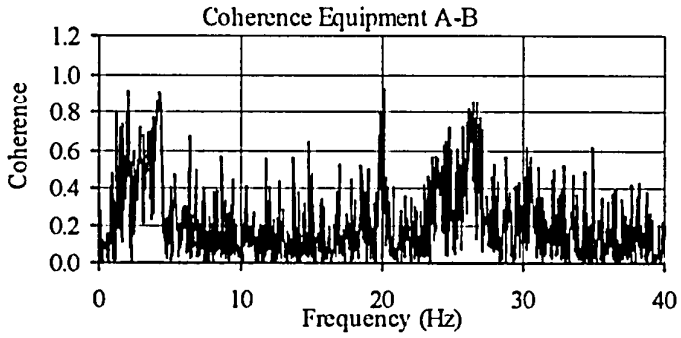

TEST RB-130
ADDITIONAL TESTS EQUIPMENT COMBINATION 5
INDIVIDUAL EQUIPMENT

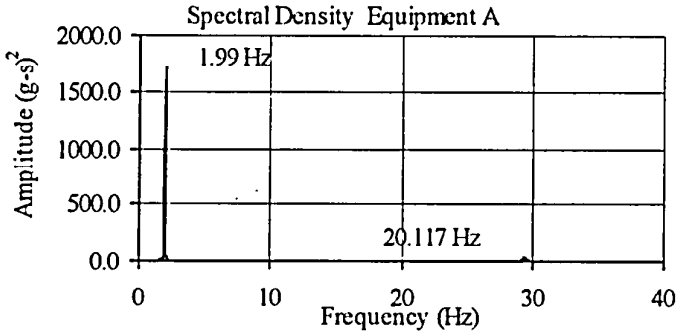

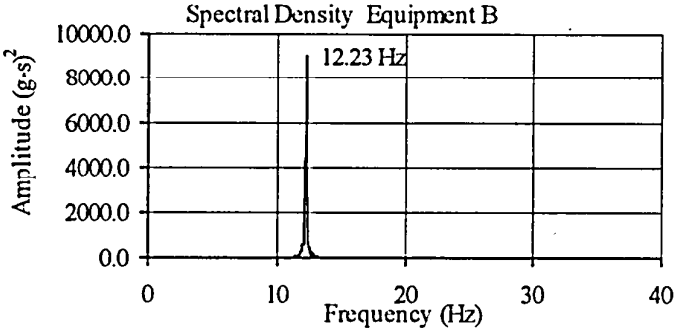

TEST RB-133
ADDITIONAL TESTS EQUIPMENT COMBINATION 5
SPRING 30-2022 CONNECTOR

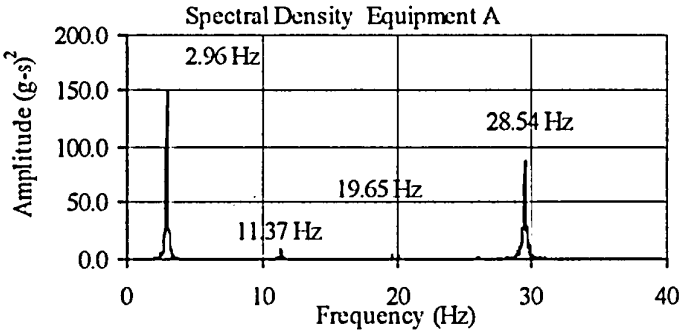

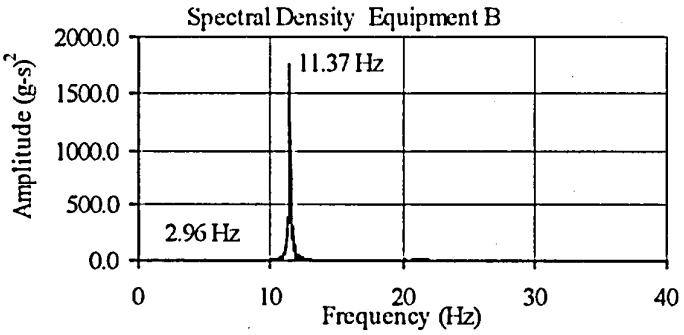

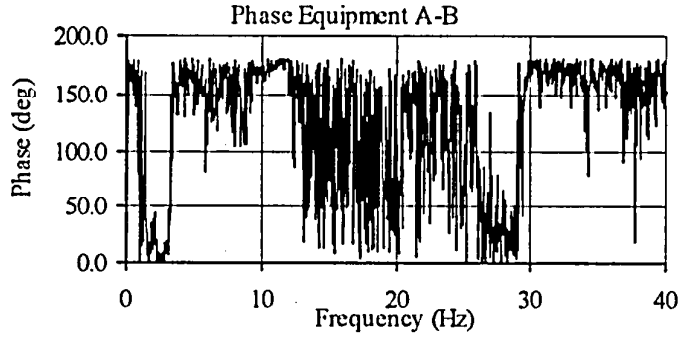

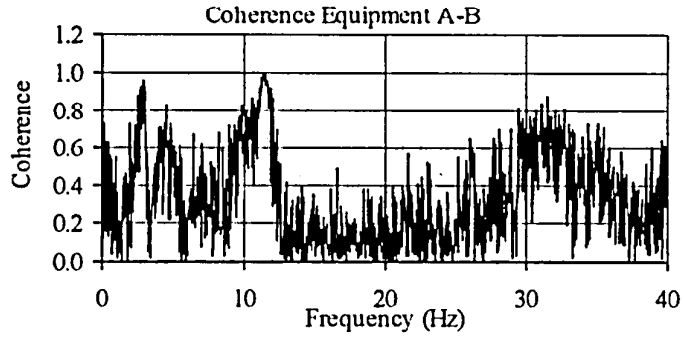

TEST RB-142
ADDITIONAL TESTS EQUIPMENT COMBINATION 5
BUS SLIDER CONNECTOR

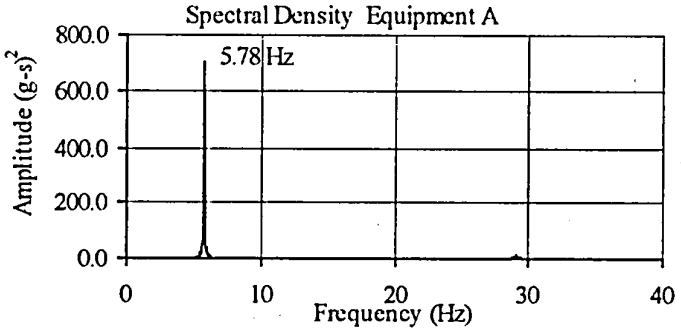

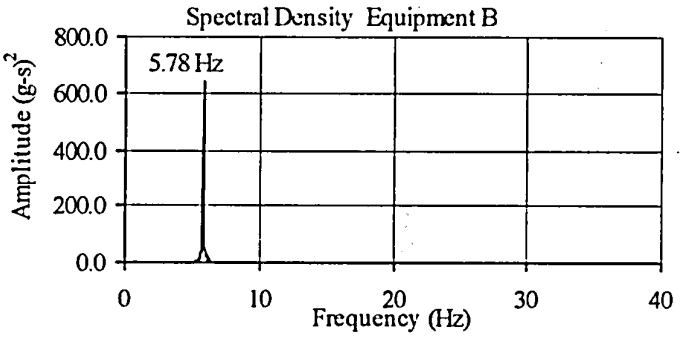

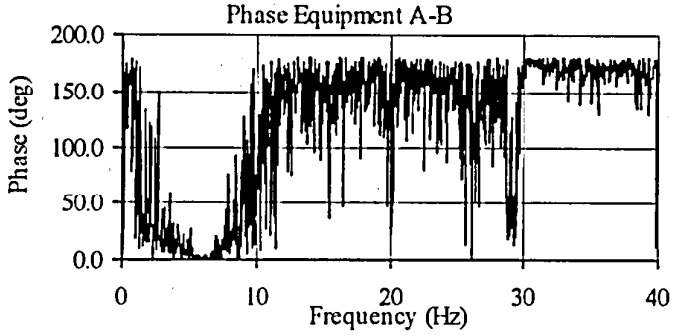

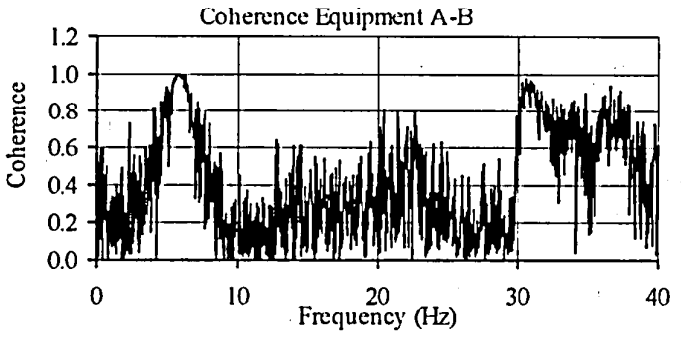

TEST RB-149
ADDITIONAL TESTS EQUIPMENT COMBINATION 5
BPA ISOLATOR CONNECTOR

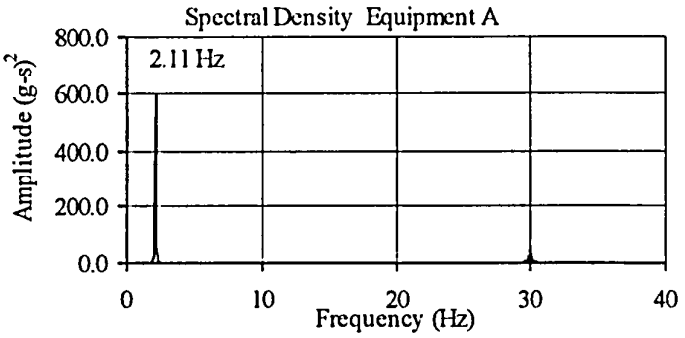

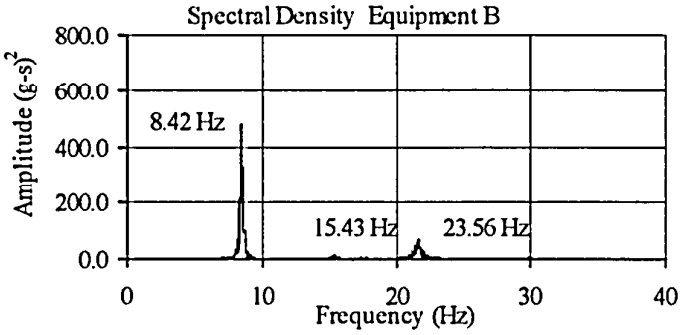

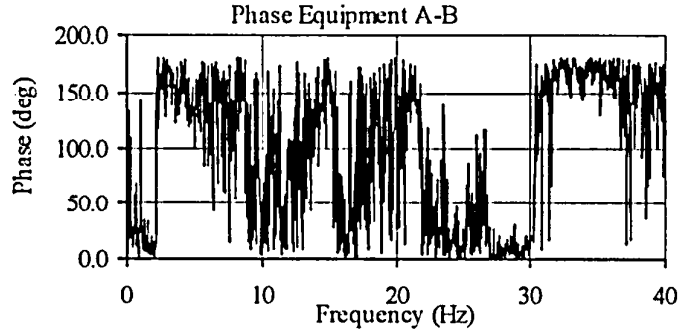

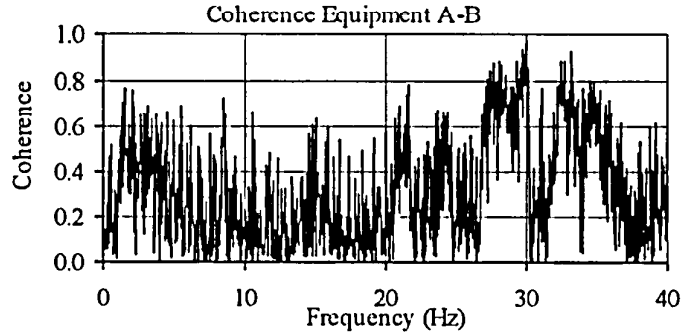

APPENDIX D

RESULTS OF DAMPING EVALUATION TESTS

TEST RB-2 AND TEST RB-3
EQUIPMENT COMBINATION 4
INDIVIDUAL EQUIPMENT

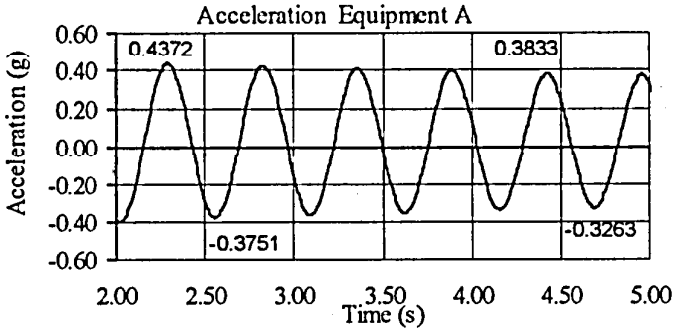

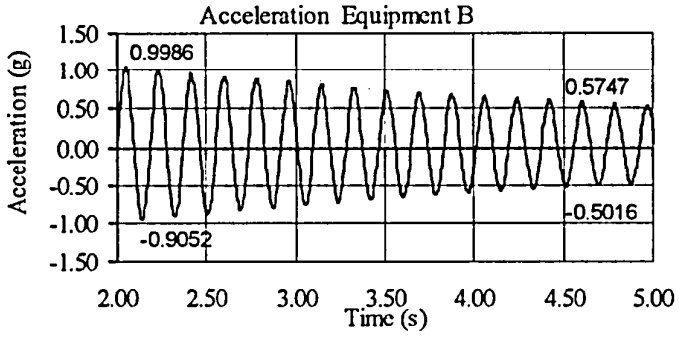

Equipment	First Double Amplitude A1 (g)	Second Double Amplitude A2 (g)	Number of intermediate cycles, p	Damping Ratio $\zeta = \frac{1}{2\pi p}\ln\left(\frac{A1}{A2}\right)$
A	0.8123	0.7096	4	0.0053
B	1.9038	1.0763	13	0.0070
Mean Damping Ratio				----

TEST RB-5 (FIRST MODE)
EQUIPMENT COMBINATION 4
SPRING 30-2022

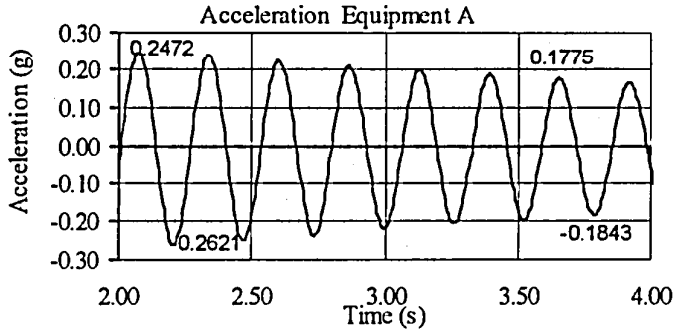

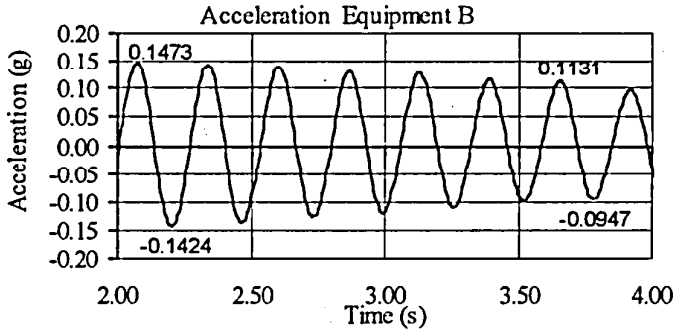

Equipment	First Double Amplitude A1 (g)	Second Double Amplitude A2 (g)	Number of intermediate cycles, p	Damping Ratio $\zeta = \frac{1}{2\pi p}\ln\left(\frac{A1}{A2}\right)$
A	0.5093	0.3618	6	0.0091
B	0.2897	0.2078	6	0.0088
Mean Damping Ratio				0.0090

TEST RB-5B (SECOND MODE)
EQUIPMENT COMBINATION 4
SPRING 30-2022

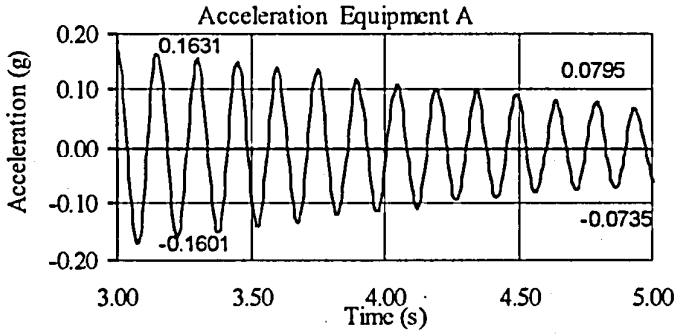

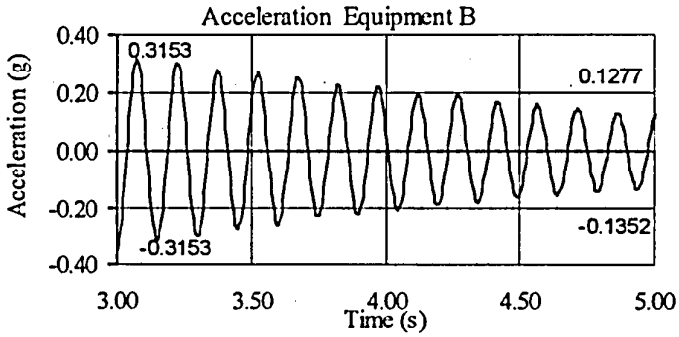

Equipment	First Double Amplitude A1 (g)	Second Double Amplitude A2 (g)	Number of intermediate cycles, p	Damping Ratio $\zeta = \frac{1}{2\pi p}\ln\left(\frac{A1}{A2}\right)$
A	0.3232	0.1530	11	0.0108
B	0.6306	0.2629	12	0.0116
Mean Damping Ratio				0.0112

TEST RB-11 AND TEST RB-12
EQUIPMENT COMBINATION 4
INDIVIDUAL EQUIPMENT

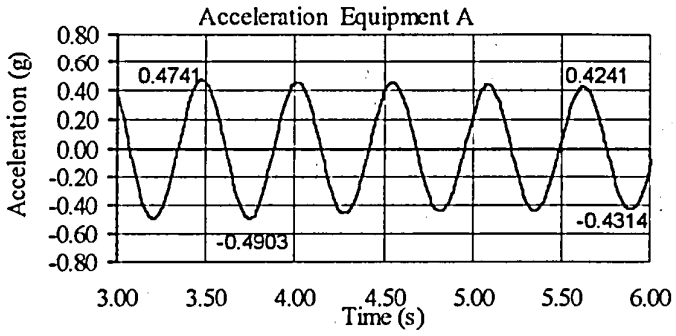

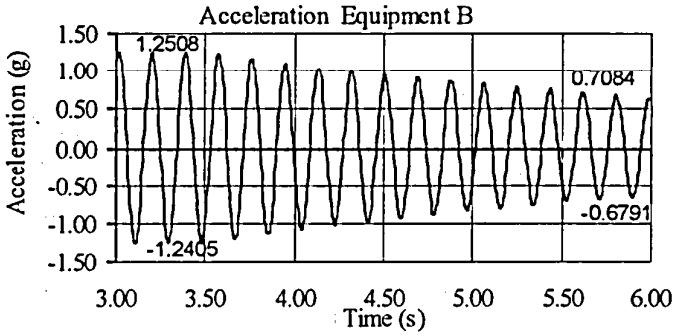

Equipment	First Double Amplitude A1 (g)	Second Double Amplitude A2 (g)	Number of intermediate cycles, p	Damping Ratio $\zeta = \frac{1}{2\pi p}\ln\left(\frac{A1}{A2}\right)$
A	0.9644	0.8555	4	0.0048
B	1.4913	1.3875	14	0.0008
Mean Damping Ratio				----

TEST RB-14
EQUIPMENT COMBINATION 4
BUS SLIDER

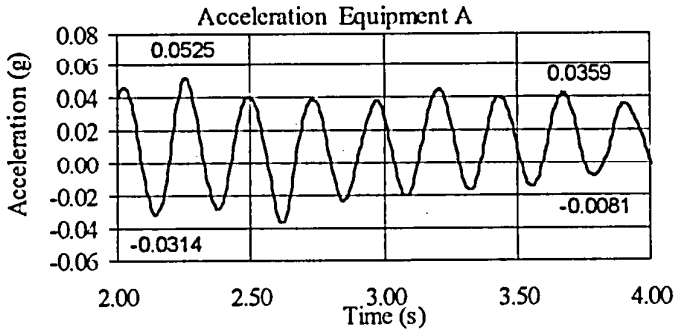

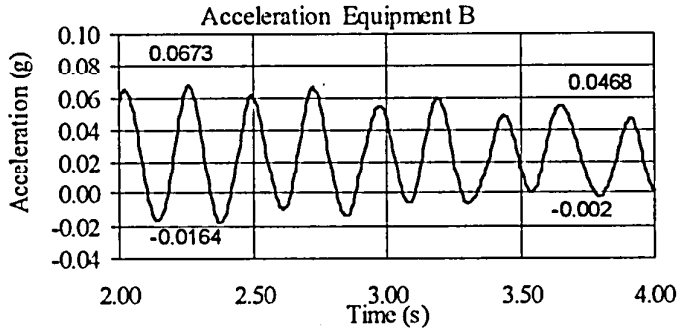

Equipment	First Double Amplitude A1 (g)	Second Double Amplitude A2 (g)	Number of intermediate cycles, p	Damping Ratio $\zeta = \frac{1}{2\pi p}\ln\left(\frac{A1}{A2}\right)$
A	0.0839	0.0440	6	0.0171
B	0.0837	0.0488	6	0.0143
Mean Damping Ratio				0.0157

TEST RB-23 (FIRST MODE)
EQUIPMENT COMBINATION 4
BPA ISOLATOR

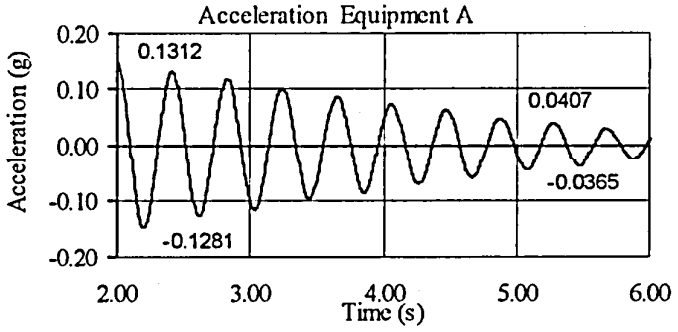

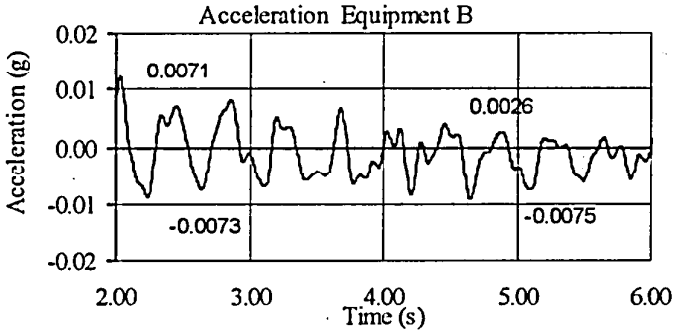

Equipment	First Double Amplitude A1 (g)	Second Double Amplitude A2 (g)	Number of intermediate cycles, p	Damping Ratio $\zeta = \frac{1}{2\pi p}\ln\left(\frac{A1}{A2}\right)$
A	0.2593	0.0772	7	0.0275
B	0.0144	0.0101	6	0.0094
Mean Damping Ratio				0.0185

TEST RB-23B (SECOND MODE)
EQUIPMENT COMBINATION 4
BPA ISOLATOR

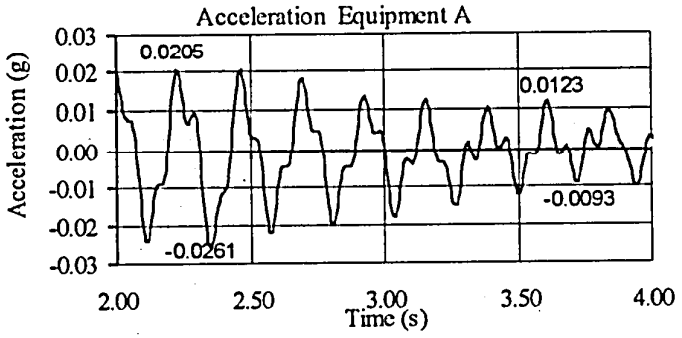

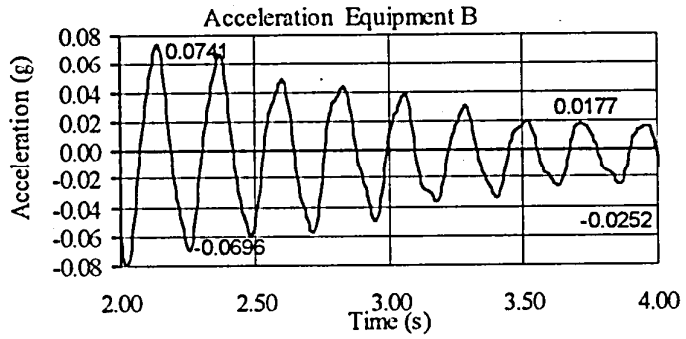

Equipment	First Double Amplitude A1 (g)	Second Double Amplitude A2 (g)	Number of intermediate cycles, p	Damping Ratio $\zeta = \frac{1}{2\pi p}\ln\left(\frac{A1}{A2}\right)$
A	0.0466	0.0216	6	0.0204
B	0.1437	0.0429	7	0.0275
Mean Damping Ratio				0.0240

TEST RB-34 AND TEST RB-35
EQUIPMENT COMBINATION 3
INDIVIDUAL EQUIPMENT

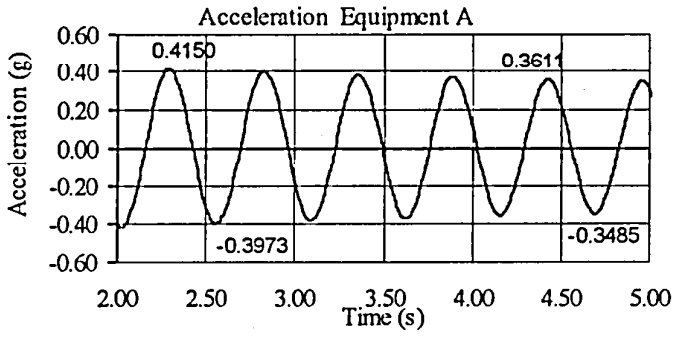

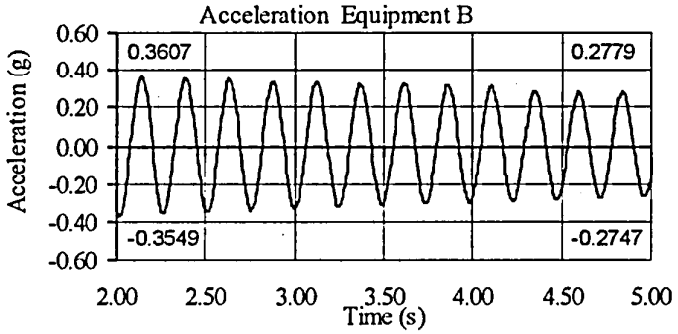

Equipment	First Double Amplitude A1 (g)	Second Double Amplitude A2 (g)	Number of intermediate cycles, p	Damping Ratio $\zeta = \frac{1}{2\pi p}\ln\left(\frac{A1}{A2}\right)$
A	0.8123	0.7096	4	0.0054
B	0.7156	0.5526	10	0.0041
Mean Damping Ratio				----

TEST RB-37 (FIRST MODE)
EQUIPMENT COMBINATION 3
SPRING 30-2022

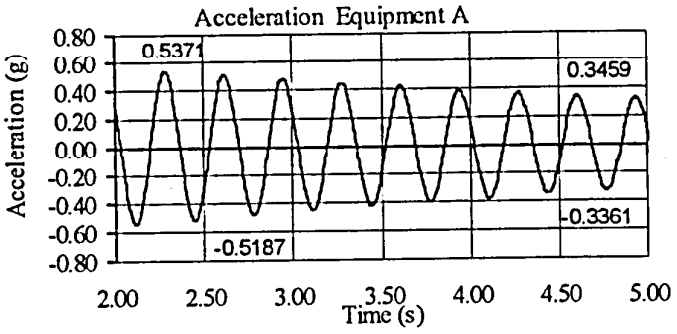

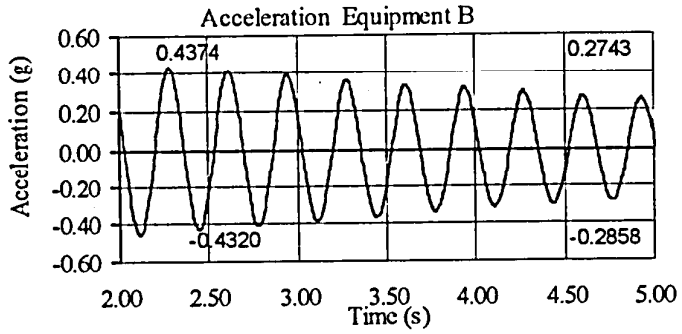

Equipment	First Double Amplitude A1 (g)	Second Double Amplitude A2 (g)	Number of intermediate cycles, p	Damping Ratio $\zeta = \frac{1}{2\pi p} \ln\left(\frac{A1}{A2}\right)$
A	1.0558	0.6820	7	0.0099
B	0.8694	0.5601	7	0.0100
Mean Damping Ratio				0.0100

TEST RB-37B (SECOND MODE)
EQUIPMENT COMBINATION 3
SPRING 30-2022

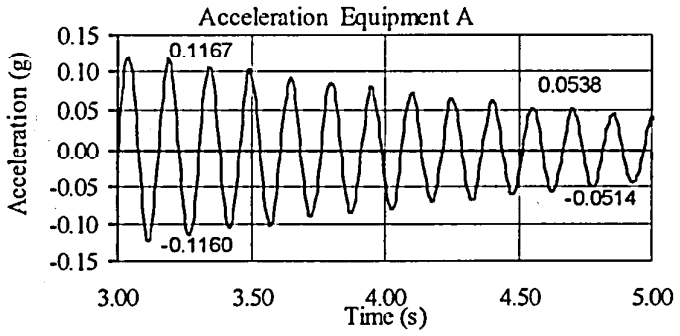

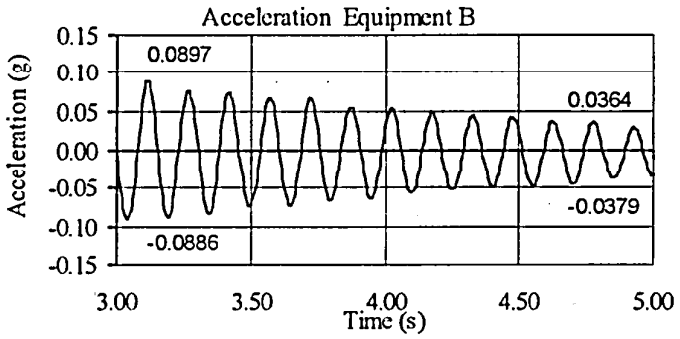

Equipment	First Double Amplitude A1 (g)	Second Double Amplitude A2 (g)	Number of intermediate cycles, p	Damping Ratio $\zeta = \frac{1}{2\pi p}\ln\left(\frac{A1}{A2}\right)$
A	0.2327	0.1052	10	0.0126
B	0.1783	0.0743	11	0.0127
Mean Damping Ratio				0.0127

TEST RB-46
EQUIPMENT COMBINATION 3
BUS SLIDER

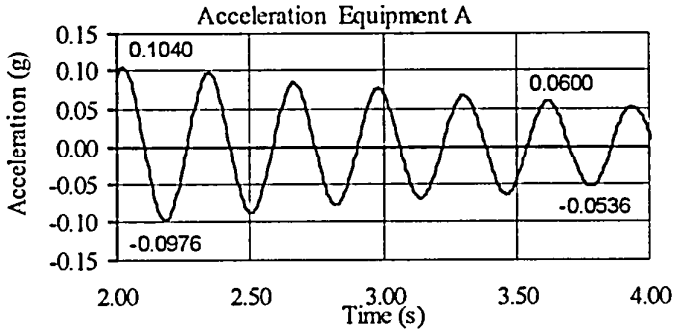

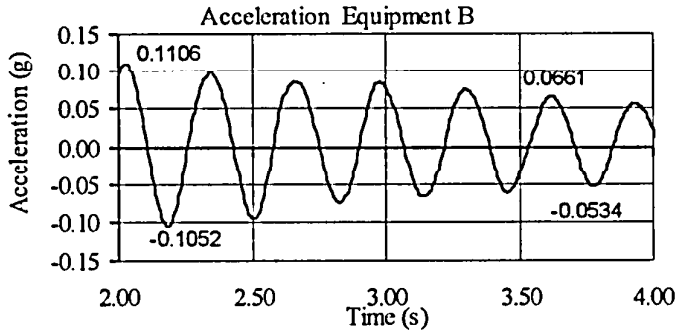

Equipment	First Double Amplitude A1 (g)	Second Double Amplitude A2 (g)	Number of intermediate cycles, p	Damping Ratio $\zeta = \frac{1}{2\pi p}\ln\left(\frac{A1}{A2}\right)$
A	0.2016	0.1136	5	0.0183
B	0.2158	0.1195	5	0.0188
Mean Damping Ratio				0.0186

TEST RB-55 (FIRST MODE)
EQUIPMENT COMBINATION 3
BPA ISOLATOR

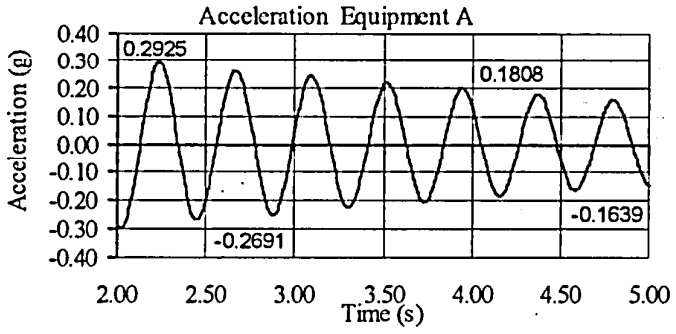

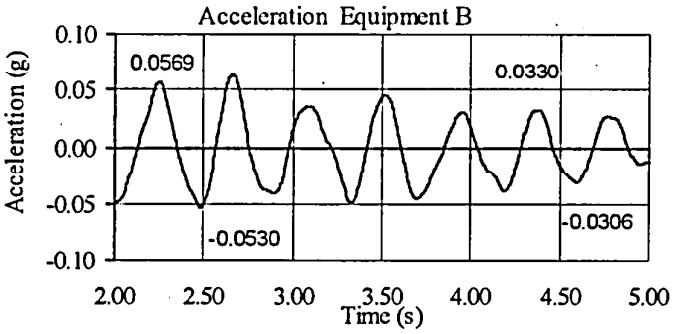

Equipment	First Double Amplitude A1 (g)	Second Double Amplitude A2 (g)	Number of intermediate cycles, p	Damping Ratio $\zeta = \frac{1}{2\pi p}\ln\left(\frac{A1}{A2}\right)$
A	0.5616	0.3447	5	0.0155
B	0.1099	0.0636	5	0.0174
Mean Damping Ratio				0.0165

TEST RB-55B (SECOND MODE)
EQUIPMENT COMBINATION 3
BPA ISOLATOR

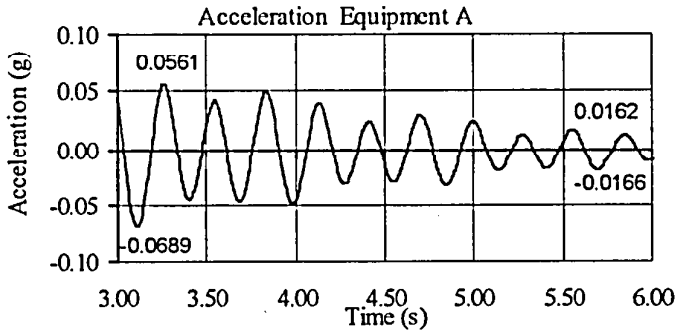

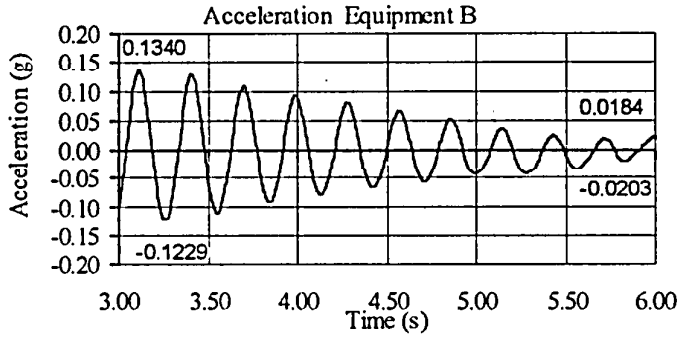

Equipment	First Double Amplitude A1 (g)	Second Double Amplitude A2 (g)	Number of intermediate cycles, p	Damping Ratio $\zeta = \frac{1}{2\pi p}\ln\left(\frac{A1}{A2}\right)$
A	0.125	0.0328	8	0.0266
B	0.2569	0.0387	9	0.0335
Mean Damping Ratio				0.0301

TEST RB-67 AND TEST RB-68
EQUIPMENT COMBINATION 1
INDIVIDUAL EQUIPMENT

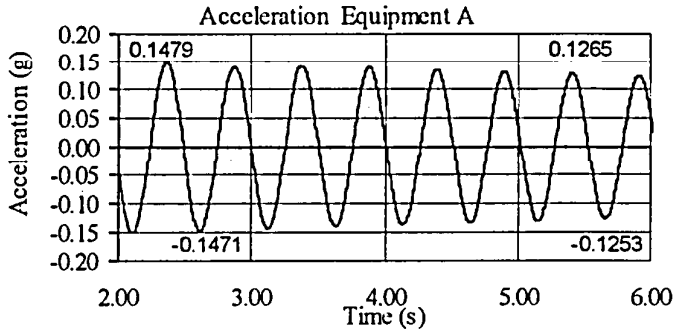

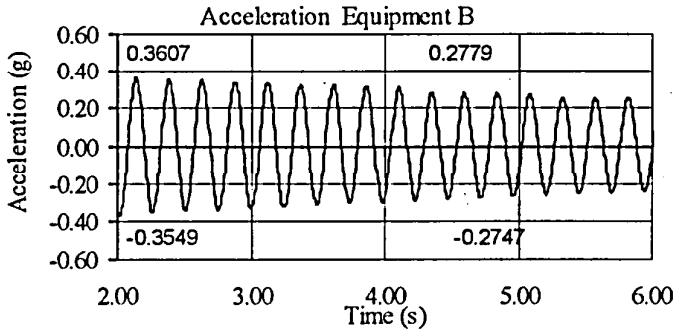

Equipment	First Double Amplitude A1 (g)	Second Double Amplitude A2 (g)	Number of intermediate cycles, p	Damping Ratio $\zeta = \frac{1}{2\pi p}\ln\left(\frac{A1}{A2}\right)$
A	0.2950	0.2518	6	0.0042
B	0.7156	0.5526	10	0.0041
Mean Damping Ratio				----

TEST RB-70 (FIRST MODE)
EQUIPMENT COMBINATION 1
SPRING 30-2022

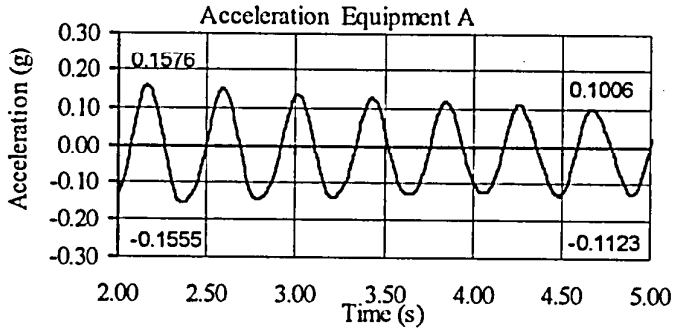

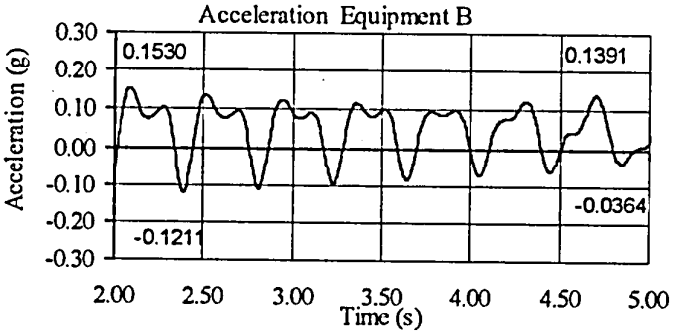

Equipment	First Double Amplitude A1 (g)	Second Double Amplitude A2 (g)	Number of intermediate cycles, p	Damping Ratio $\zeta = \frac{1}{2\pi p} \ln\left(\frac{A1}{A2}\right)$
A	0.3131	0.2129	6	0.0102
B	0.2741	0.1755	6	0.0118
Mean Damping Ratio				0.0110

TEST RB-70B (SECOND MODE)
EQUIPMENT COMBINATION 1
SPRING 30-2022

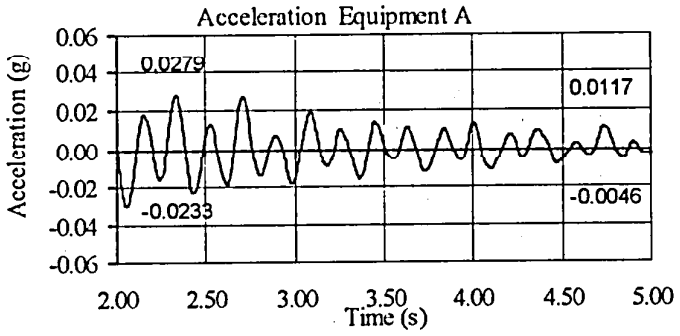

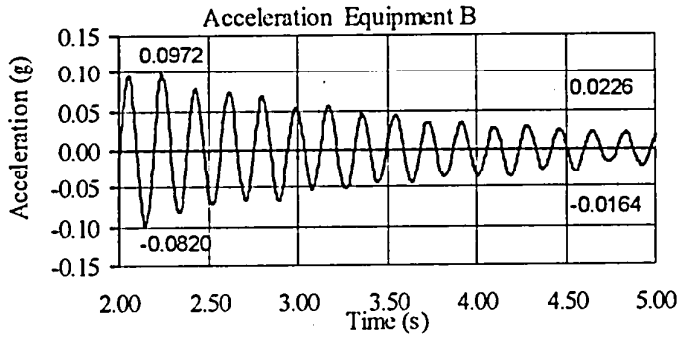

Equipment	First Double Amplitude A1 (g)	Second Double Amplitude A2 (g)	Number of intermediate cycles, p	Damping Ratio $\zeta = \frac{1}{2\pi p} \ln\left(\frac{A1}{A2}\right)$
A	0.0512	0.0163	13	0.0140
B	0.1792	0.0390	13	0.0187
Mean Damping Ratio				0.0164

TEST RB-77
EQUIPMENT COMBINATION 1
BUS SLIDER

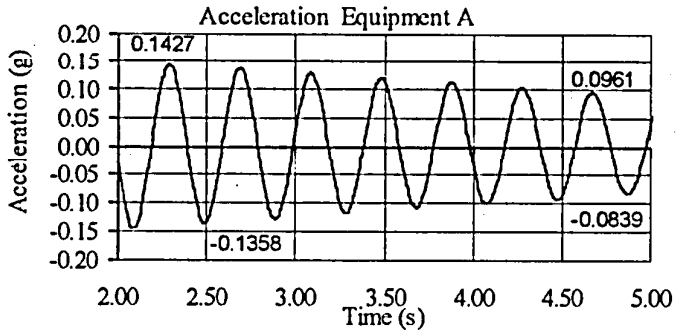

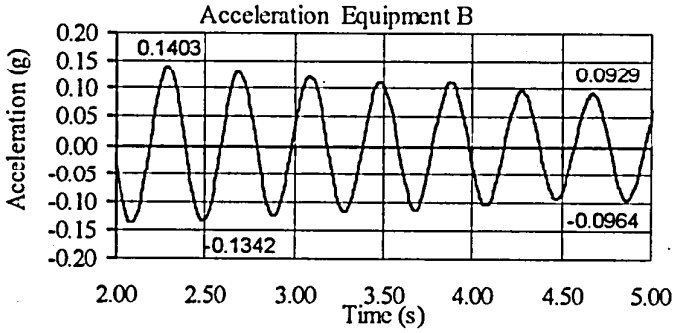

Equipment	First Double Amplitude A1 (g)	Second Double Amplitude A2 (g)	Number of intermediate cycles, p	Damping Ratio $\zeta = \frac{1}{2\pi p}\ln\left(\frac{A1}{A2}\right)$
A	0.2785	0.1800	6	0.0116
B	0.2745	0.1893	6	0.0099
Mean Damping Ratio				0.0108

TEST RB-84 (FIRST MODE)
EQUIPMENT COMBINATION 1
BPA ISOLATOR

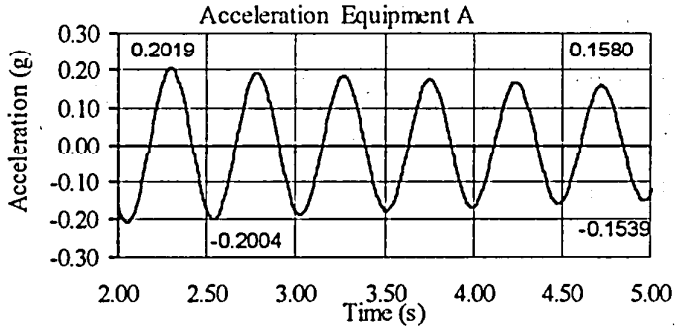

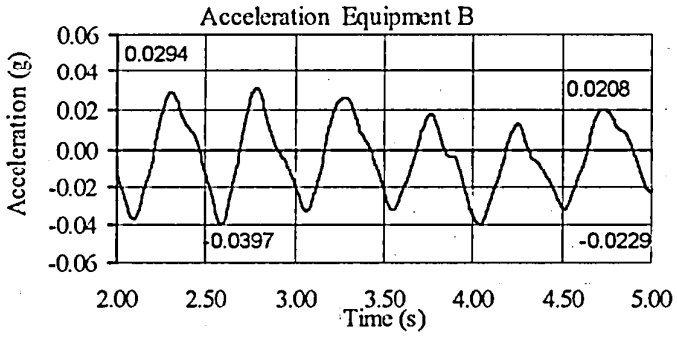

Equipment	First Double Amplitude A1 (g)	Second Double Amplitude A2 (g)	Number of intermediate cycles, p	Damping Ratio $\zeta = \frac{1}{2\pi p}\ln\left(\frac{A1}{A2}\right)$
A	0.4023	0.3119	5	0.0081
B	0.0691	0.0437	5	0.0146
Mean Damping Ratio				0.0114

TEST RB-84B (SECOND MODE)
EQUIPMENT COMBINATION 1
BPA ISOLATOR

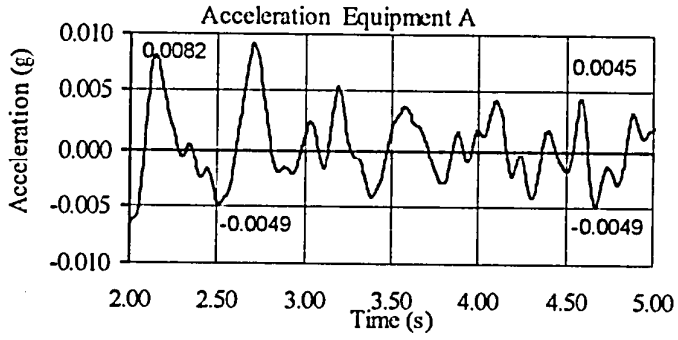

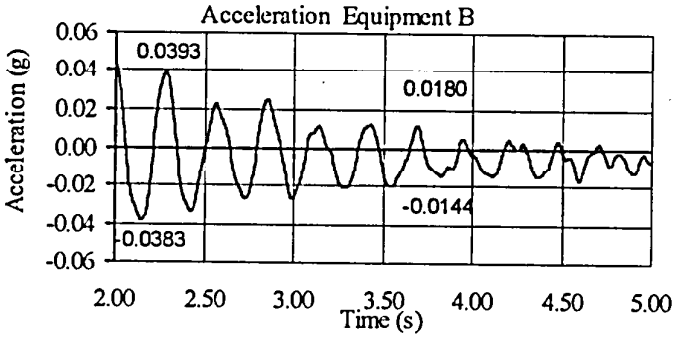

Equipment	First Double Amplitude A1 (g)	Second Double Amplitude A2 (g)	Number of intermediate cycles, p	Damping Ratio $\zeta = \frac{1}{2\pi p}\ln\left(\frac{A1}{A2}\right)$
A	0.0131	0.0094	5	0.0106
B	0.0776	0.0324	5	0.0278
Mean Damping Ratio				0.0192

TEST RB-97
EQUIPMENT COMBINATION 2
SPRING 30-2022

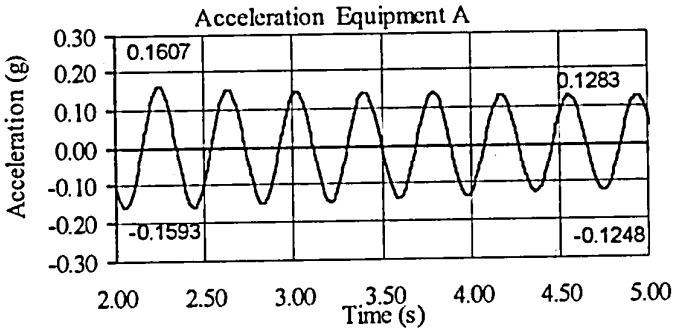

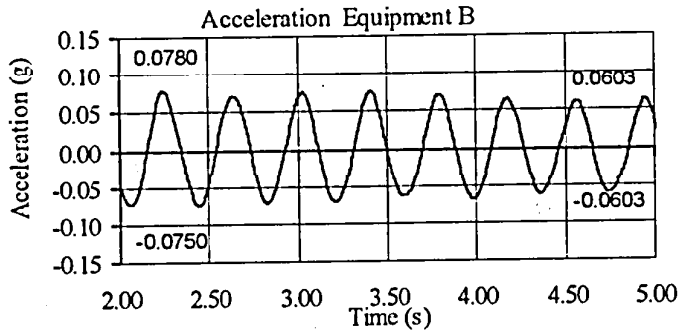

Equipment	First Double Amplitude A1 (g)	Second Double Amplitude A2 (g)	Number of intermediate cycles, p	Damping Ratio $\zeta = \frac{1}{2\pi p} \ln\left(\frac{A1}{A2}\right)$
A	0.3200	0.2531	6	0.0062
B	0.1530	0.1206	6	0.0063
Mean Damping Ratio				0.0063

TEST RB-108
EQUIPMENT COMBINATION 2
BUS SLIDER

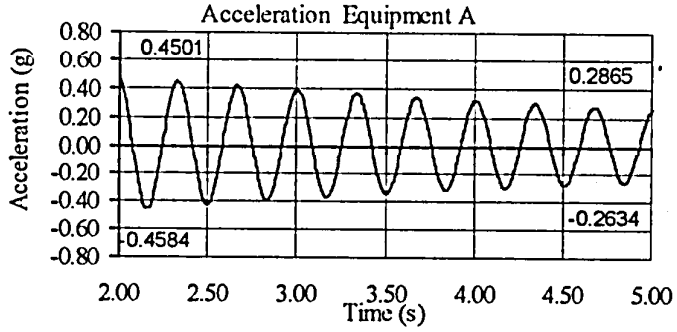

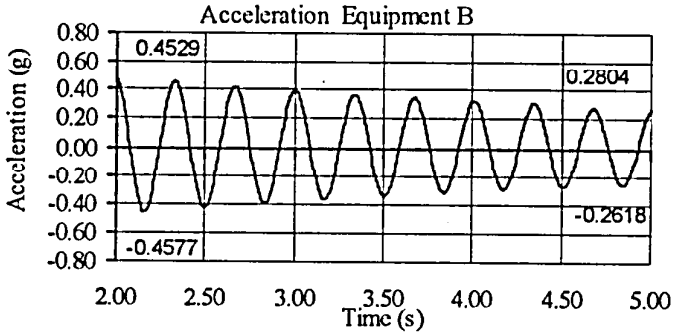

Equipment	First Double Amplitude A1 (g)	Second Double Amplitude A2 (g)	Number of intermediate cycles, p	Damping Ratio $\zeta = \frac{1}{2\pi p}\ln\left(\frac{A1}{A2}\right)$
A	0.9085	0.5499	7	0.0114
B	0.9106	0.5422	7	0.0118
Mean Damping Ratio				0.0116

TEST RB-117
EQUIPMENT COMBINATION 5
BPA ISOLATOR

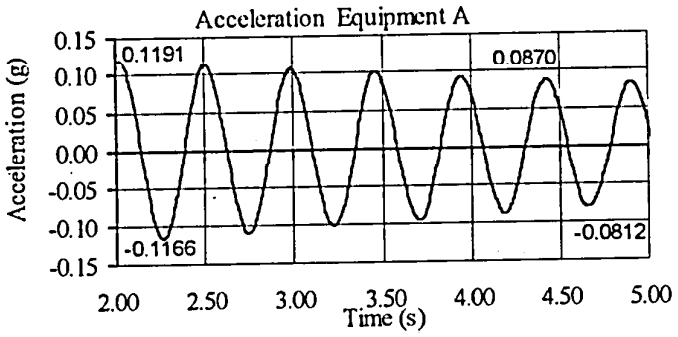

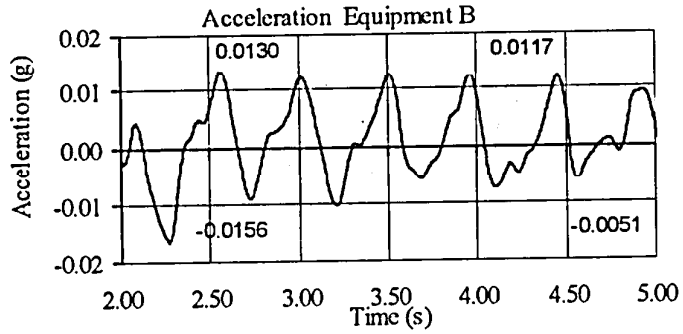

Equipment	First Double Amplitude A1 (g)	Second Double Amplitude A2 (g)	Number of intermediate cycles, p	Damping Ratio $\zeta = \frac{1}{2\pi p} \ln\left(\frac{A1}{A2}\right)$
A	0.2357	0.1682	5	0.0107
B	0.0286	0.0168	4	0.0212
Mean Damping Ratio				0.0160

TEST RB-131 AND TEST RB 132
ADDITIONAL TESTS EQUIPMENT COMBINATION 5
INDIVIDUAL EQUIPMENT

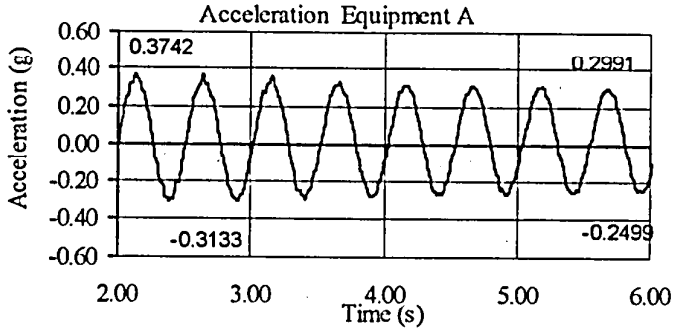

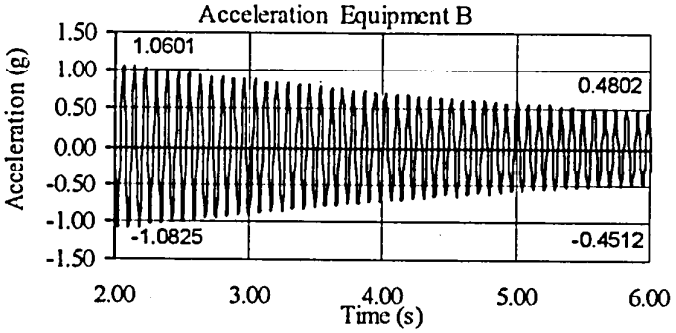

Equipment	First Double Amplitude A1 (g)	Second Double Amplitude A2 (g)	Number of intermediate cycles, p	Damping Ratio $\zeta = \frac{1}{2\pi p} \ln\left(\frac{A1}{A2}\right)$
A	0.6875	0.5490	7	0.0051
B	2.1426	0.9314	45	0.0029
Mean Damping Ratio				----

TEST RB-134 (FIRST MODE)
ADDITIONAL TESTS EQUIPMENT COMBINATION 5
SPRING 30-2022

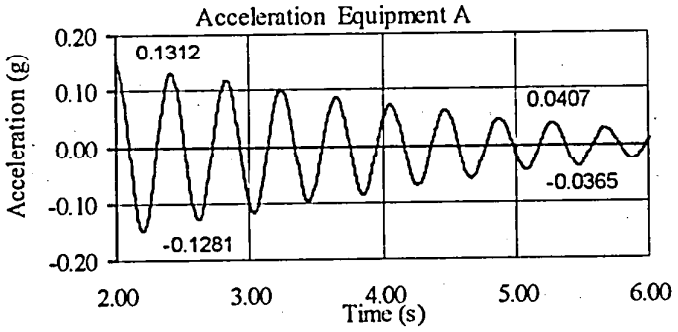

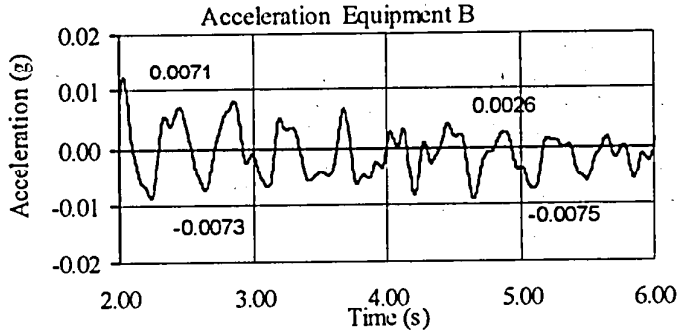

Equipment	First Double Amplitude A1 (g)	Second Double Amplitude A2 (g)	Number of intermediate cycles, p	Damping Ratio $\zeta = \frac{1}{2\pi p}\ln\left(\frac{A1}{A2}\right)$
A	0.2593	0.0772	7	0.0275
B	0.0144	0.0101	6	0.0094
Mean Damping Ratio				0.0185

TEST RB-135 (SECOND MODE)
ADDITIONAL TESTS EQUIPMENT COMBINATION 5
SPRING 30-2022

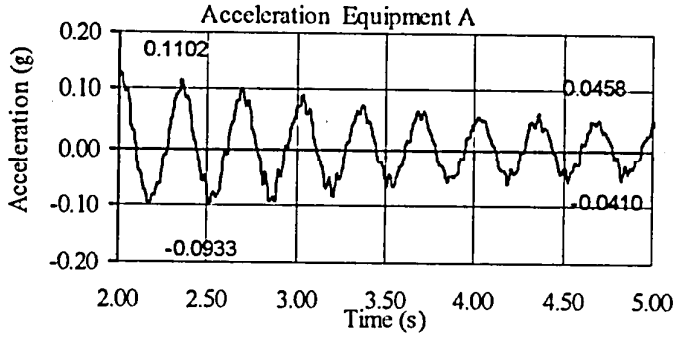

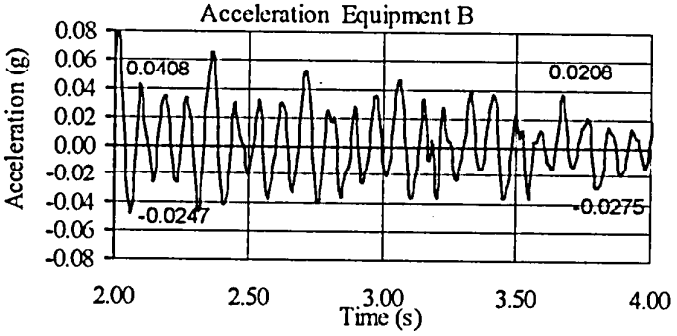

Equipment	First Double Amplitude A1 (g)	Second Double Amplitude A2 (g)	Number of intermediate cycles, p	Damping Ratio $\zeta = \frac{1}{2\pi p} \ln\left(\frac{A1}{A2}\right)$
A	0.2035	0.0868	7	0.0193
B	0.0655	0.0483	17	0.0285
Mean Damping Ratio				0.0239

TEST RB-143
ADDITIONAL TESTS EQUIPMENT COMBINATION 5
BUS SLIDER

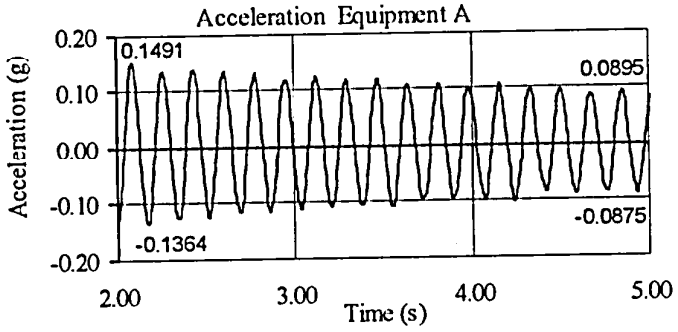

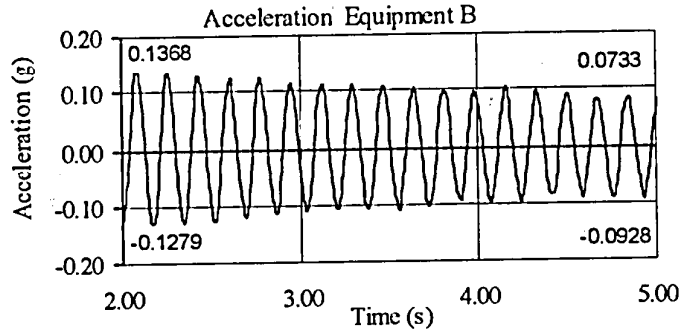

Equipment	First Double Amplitude A1 (g)	Second Double Amplitude A2 (g)	Number of intermediate cycles, p	Damping Ratio $\zeta = \frac{1}{2\pi p} \ln\left(\frac{A1}{A2}\right)$
A	0.2855	0.1770	16	0.0048
B	0.2647	0.1661	16	0.0046
Mean Damping Ratio				0.0047

TEST RB-150
ADDITIONAL TESTS EQUIPMENT COMBINATION 5
BPA ISOLATOR

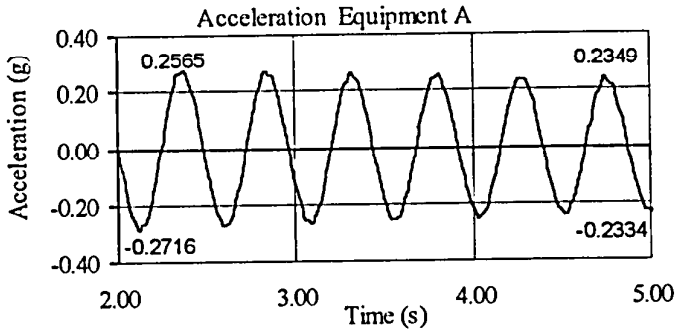

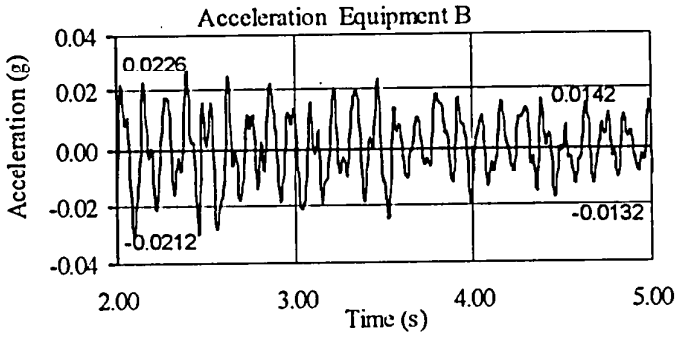

Equipment	First Double Amplitude A1 (g)	Second Double Amplitude A2 (g)	Number of intermediate cycles, p	Damping Ratio $\zeta = \frac{1}{2\pi p} \ln\left(\frac{A1}{A2}\right)$
A	0.5281	0.4683	5	0.0038
B	0.0438	0.0274	22	0.0034
Mean Damping Ratio				0.0036

APPENDIX E

RESULTS OF SEISMIC TESTS

TEST RB-6
EQUIPMENT COMBINATION 4, SPRING 30-2022
NEWHALL GROUND MOTION, 30% SPAN

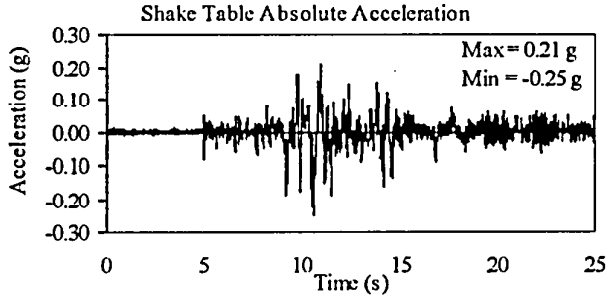

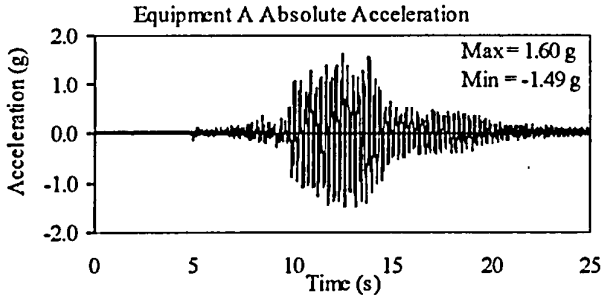

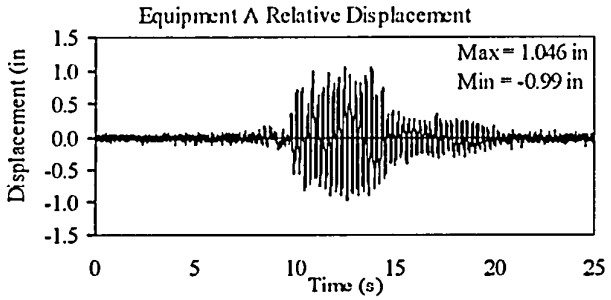

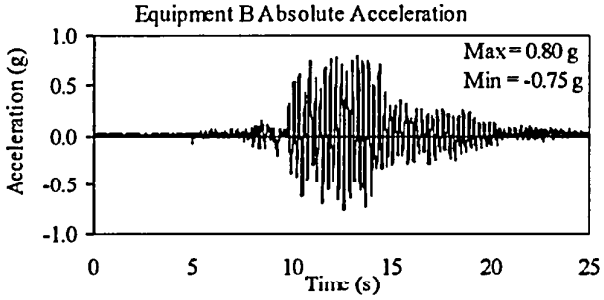

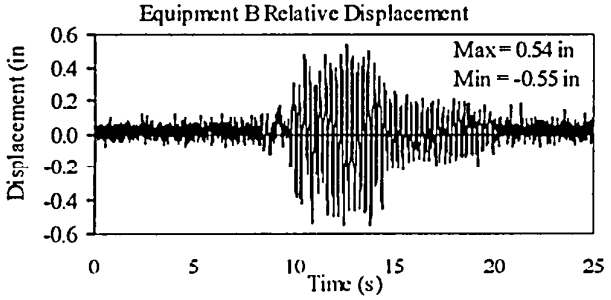

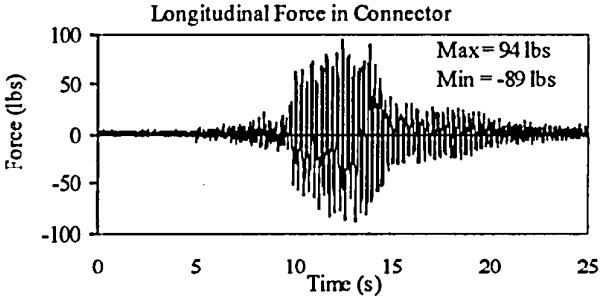

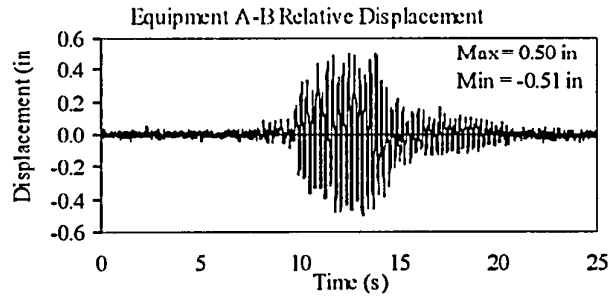

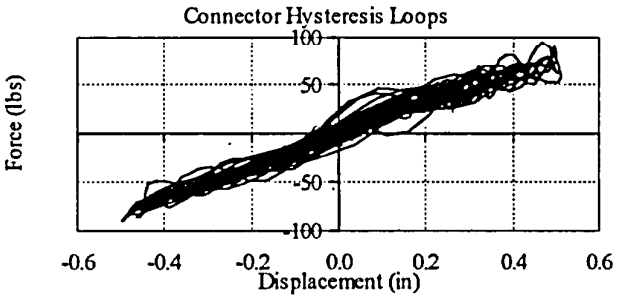

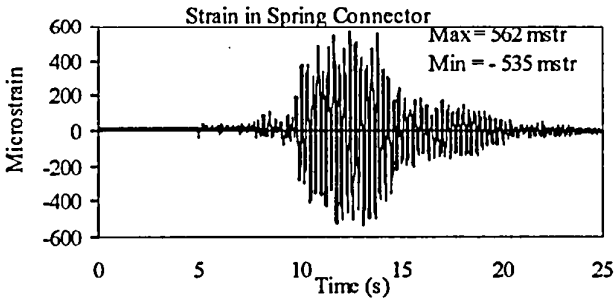

TEST RB-7
EQUIPMENT COMBINATION 4, SPRING 30-2022
NEWHALL GROUND MOTION, 100% SPAN

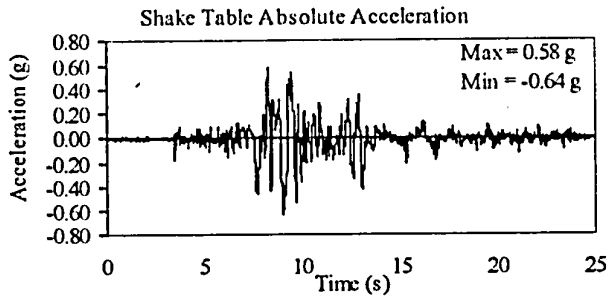

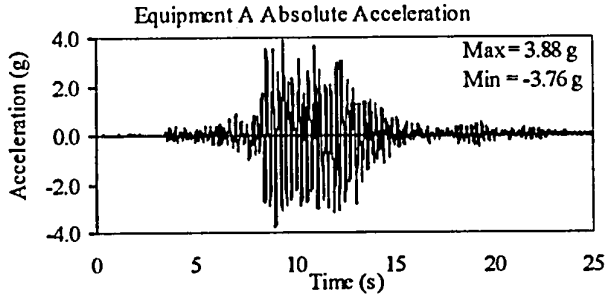

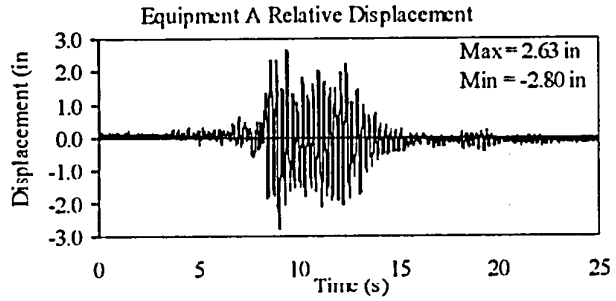

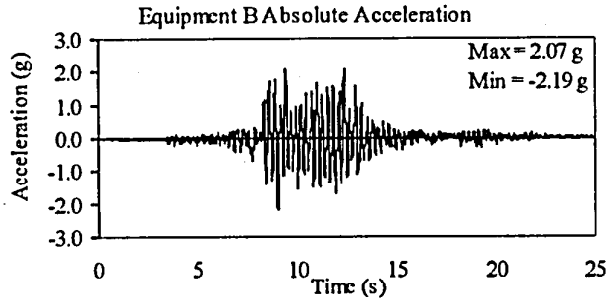

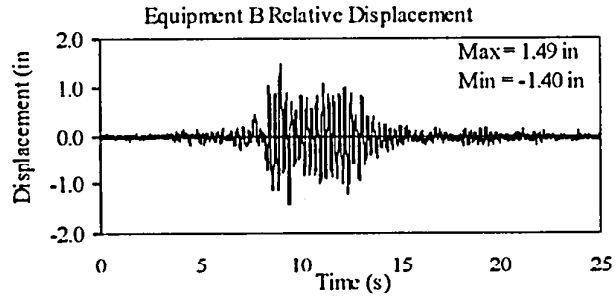

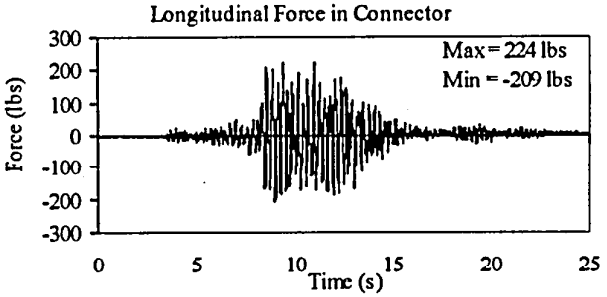

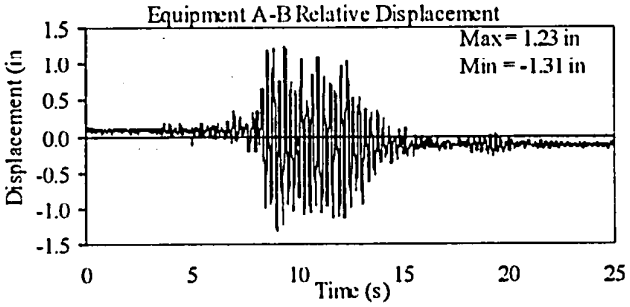

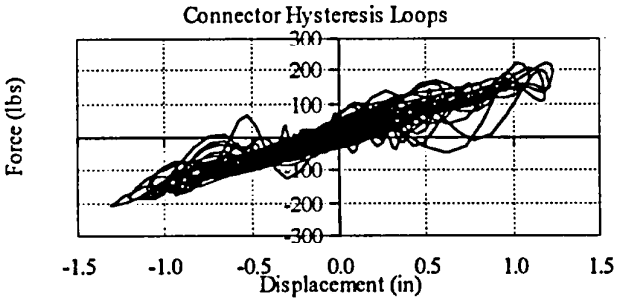

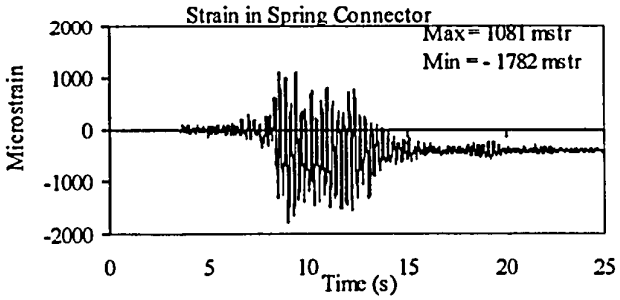

TEST RB-8
EQUIPMENT COMBINATION 4, SPRING 30-2022
TABAS GROUND MOTION, 25% SPAN

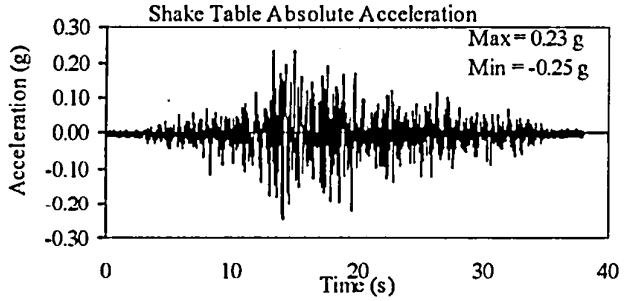

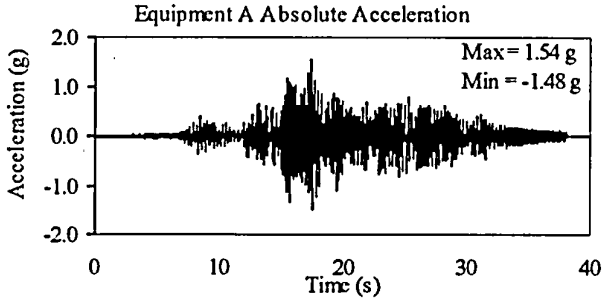

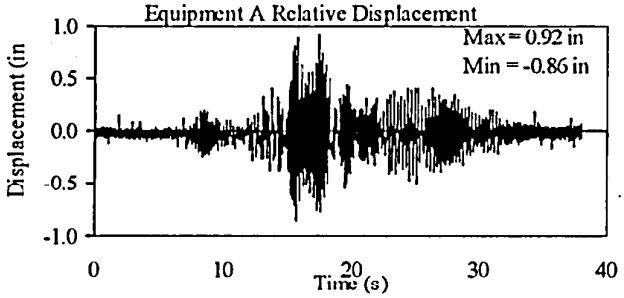

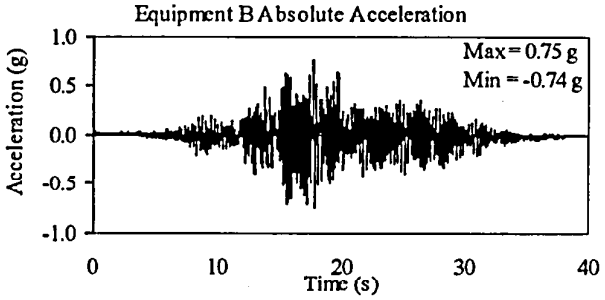

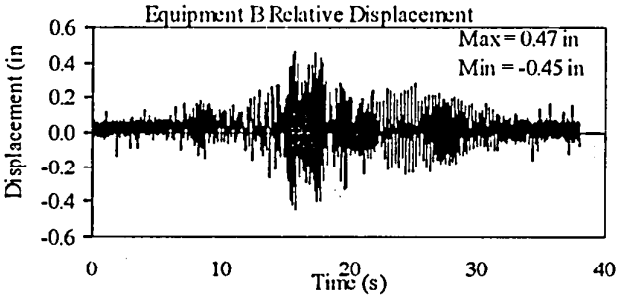

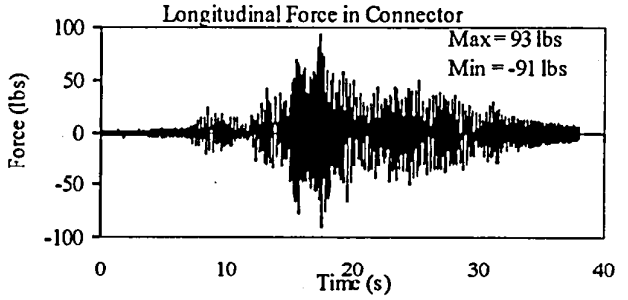

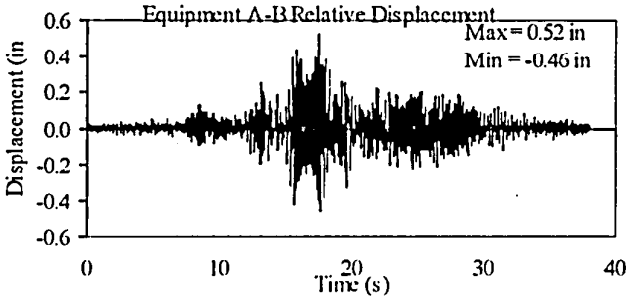

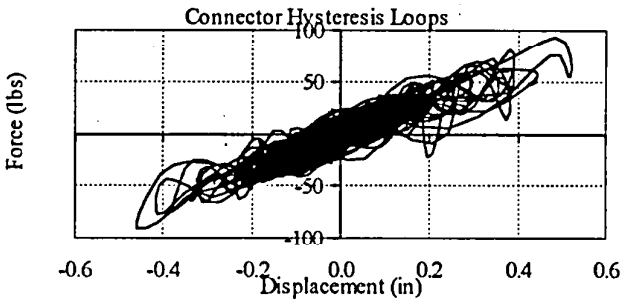

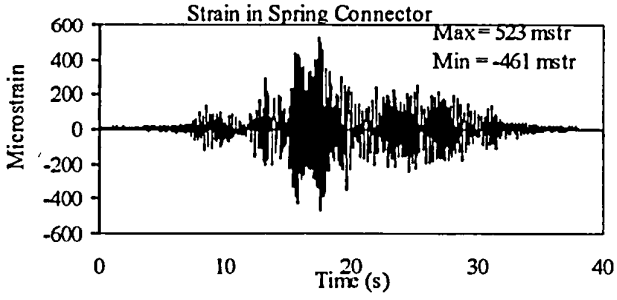

TEST RB-9
EQUIPMENT COMBINATION 4, SPRING 30-2022
TABAS GROUND MOTION, 50% SPAN

Shake Table Absolute Acceleration

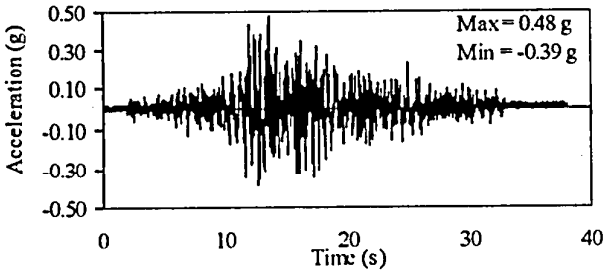

Equipment A Absolute Acceleration

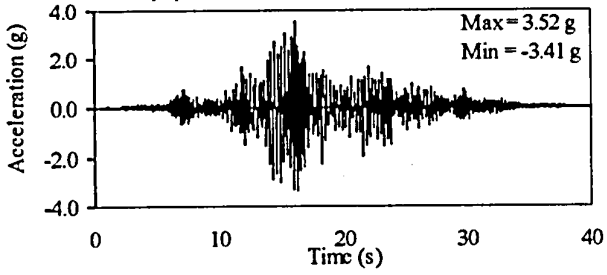

Equipment A Relative Displacement

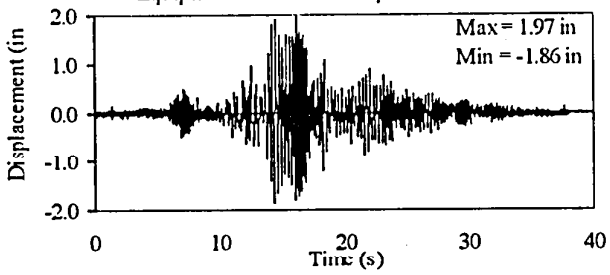

Equipment B Absolute Acceleration

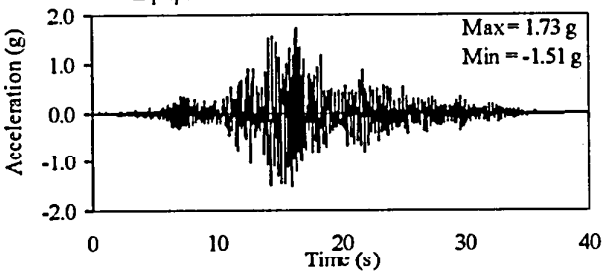

Equipment B Relative Displacement

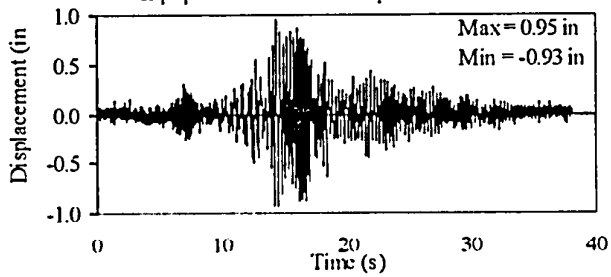

Longitudinal Force in Connector

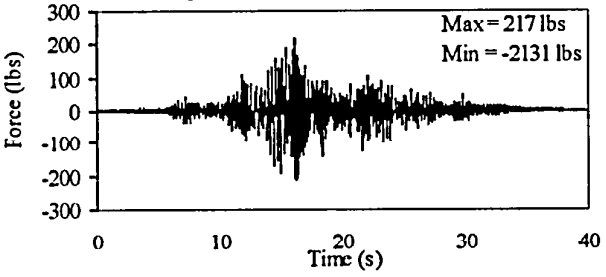

Equipment A-B Relative Displacement

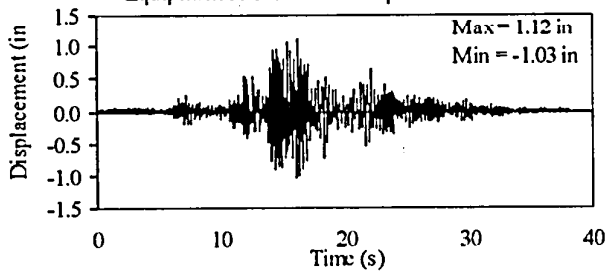

Connector Hysteresis Loops

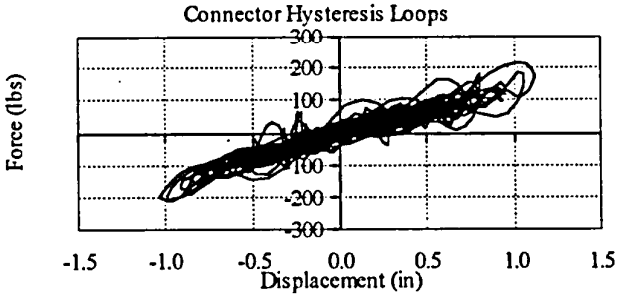

Strain in Spring Connector

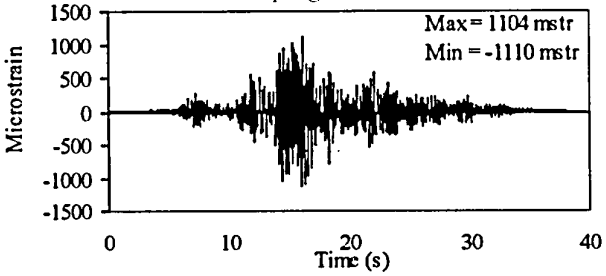

TEST RB-15
EQUIPMENT COMBINATION 4, BUS SLIDER
NEWHALL GROUND MOTION, 100% SPAN

Shake Table Absolute Acceleration

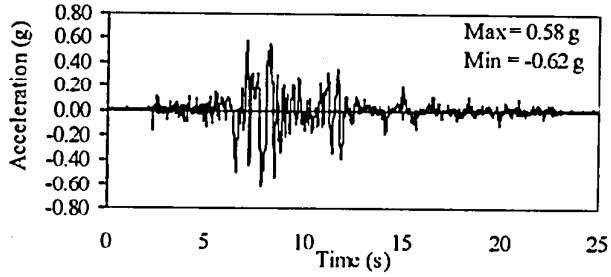

Equipment A Absolute Acceleration

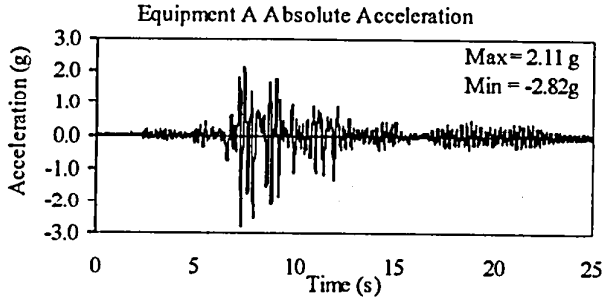

Equipment A Relative Displacement

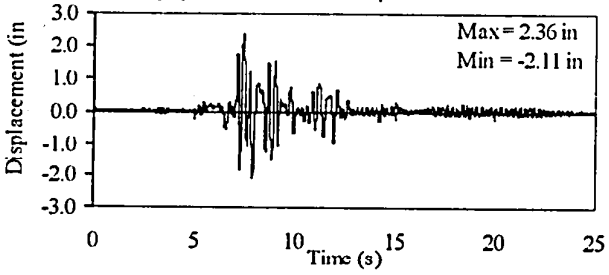

Equipment B Absolute Acceleration

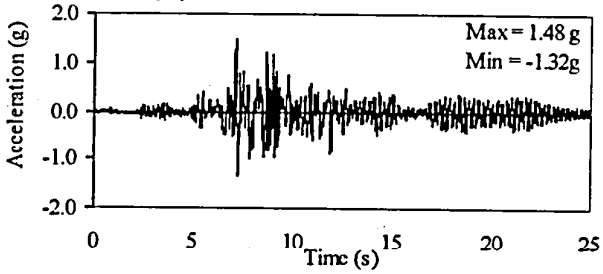

Equipment B Relative Displacement

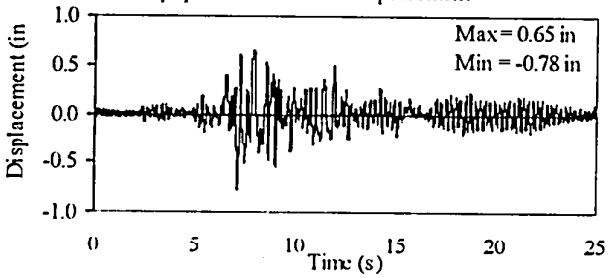

Longitudinal Force in Connector

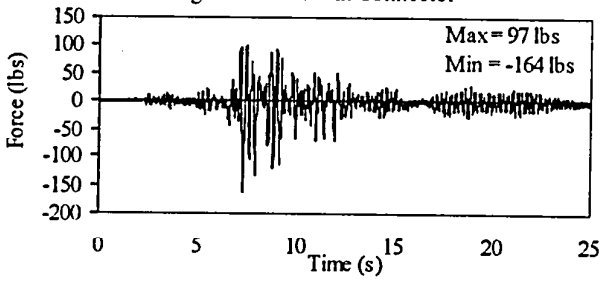

Equipment A-B Relative Displacement

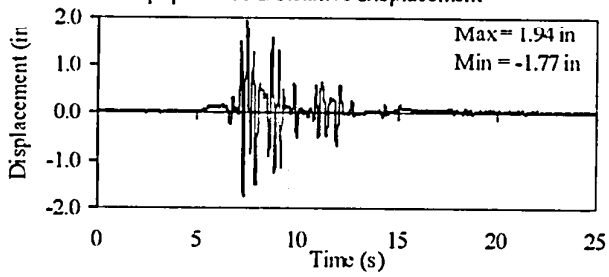

Connector Hysteresis Loops

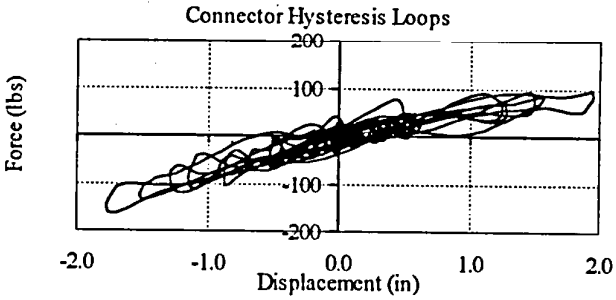

TEST RB-17
EQUIPMENT COMBINATION 4, BUS SLIDER
TABAS GROUND MOTION, 50% SPAN

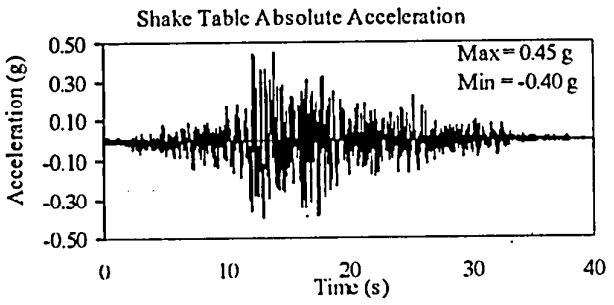

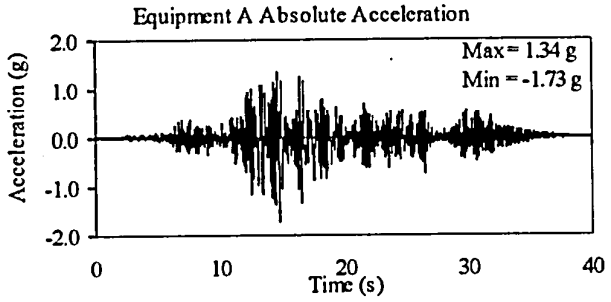

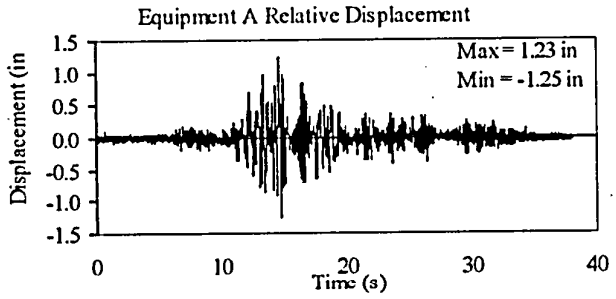

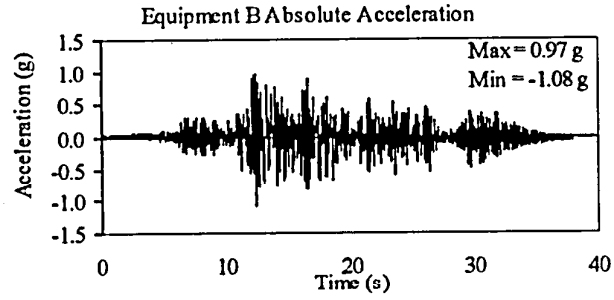

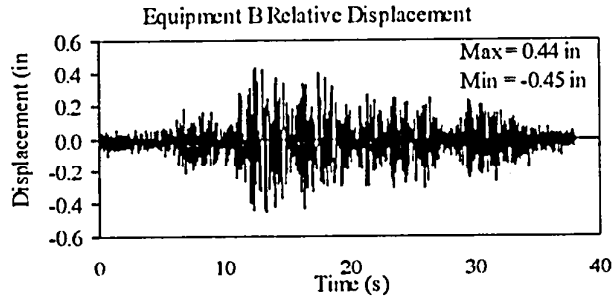

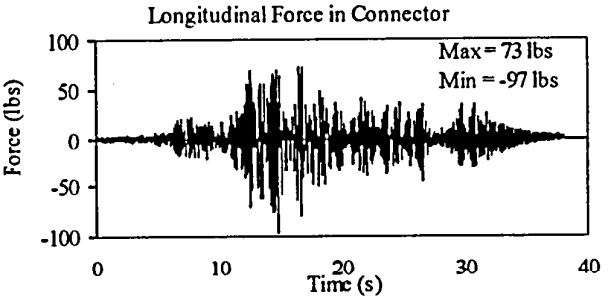

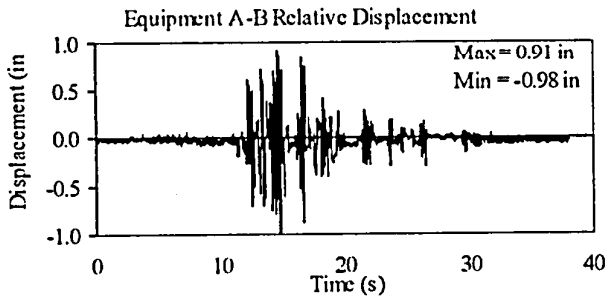

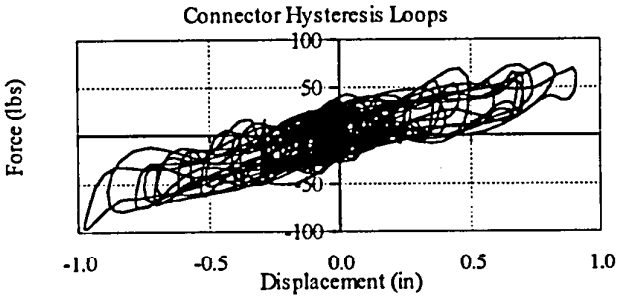

TEST RB-18
EQUIPMENT COMBINATION 4, BUS SLIDER
TABAS GROUND MOTION, 200% SPAN

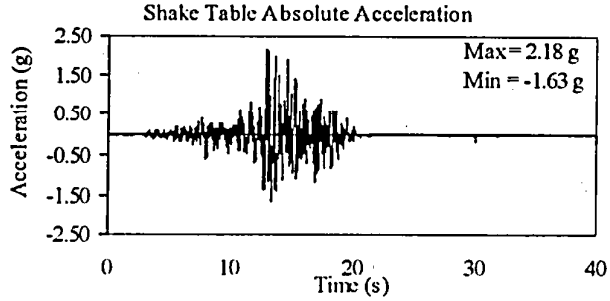

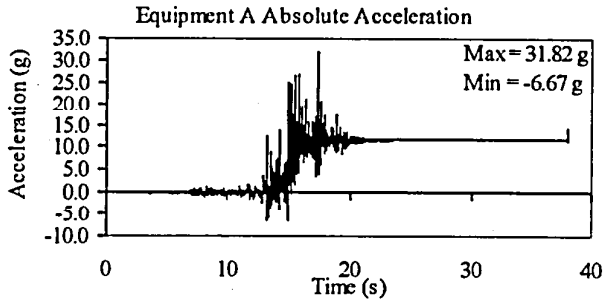

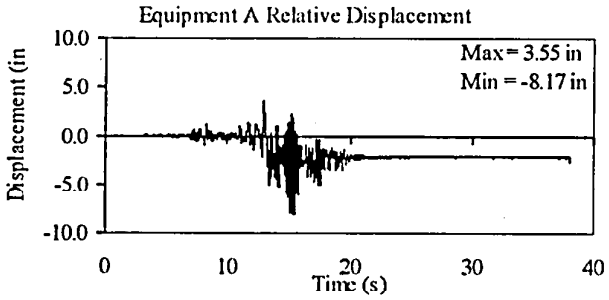

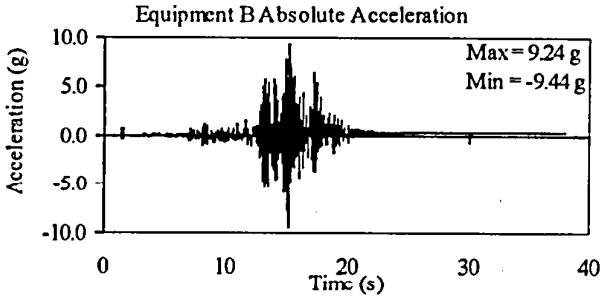

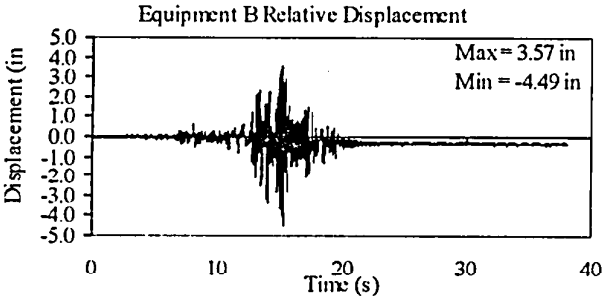

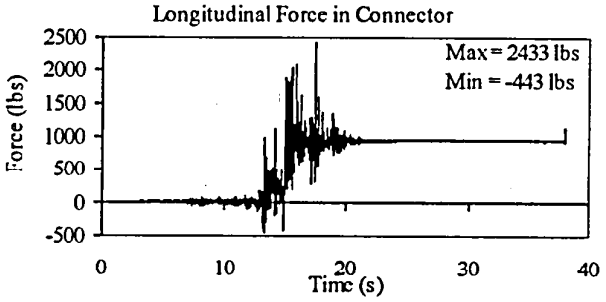

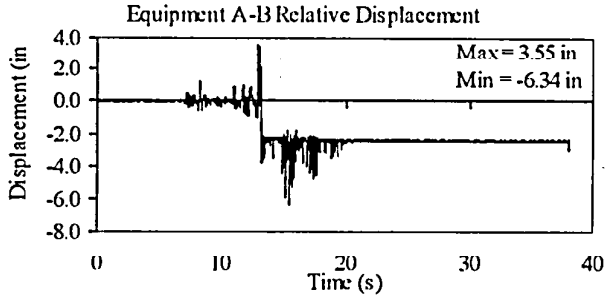

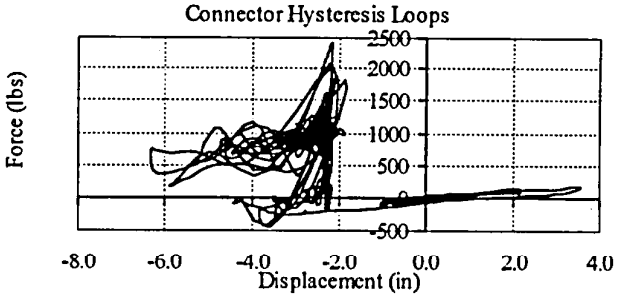

TEST RB-24
EQUIPMENT COMBINATION 4, BPA ISOLATOR
NEWHALL GROUND MOTION, 30% SPAN

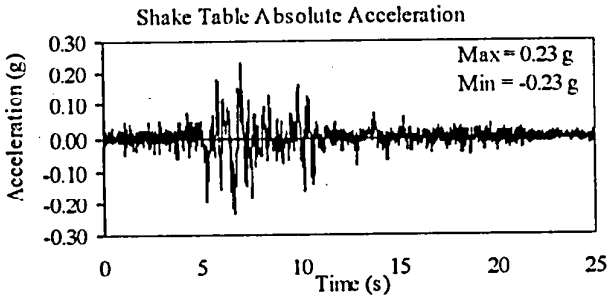

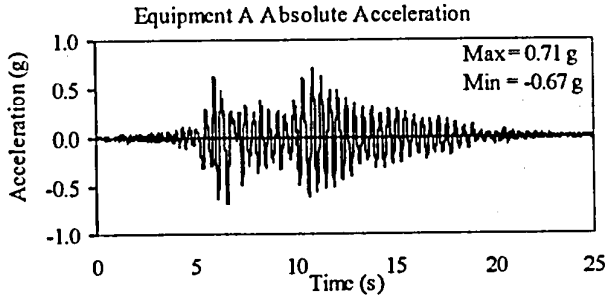

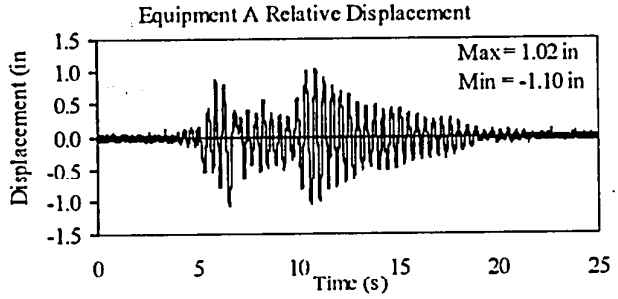

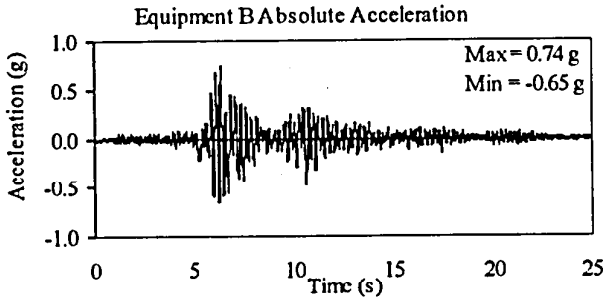

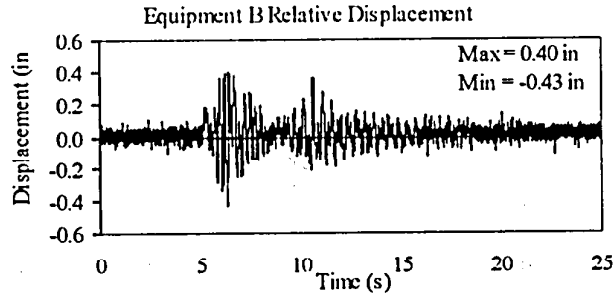

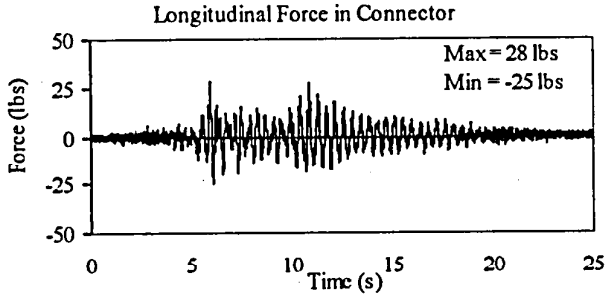

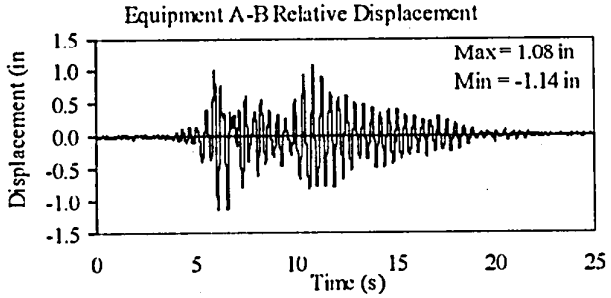

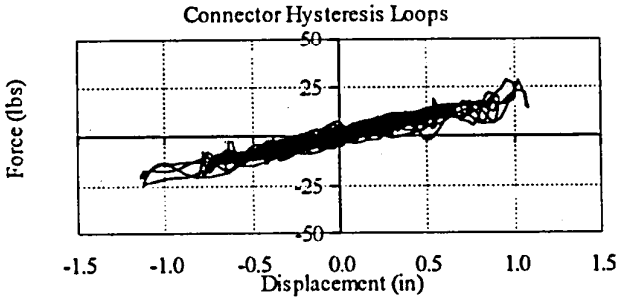

TEST RB-26
EQUIPMENT COMBINATION 4, BPA ISOLATOR
TABAS GROUND MOTION, 25% SPAN

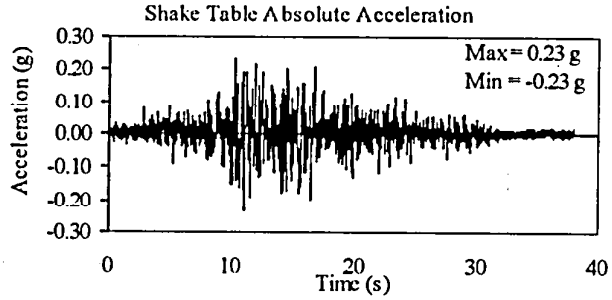

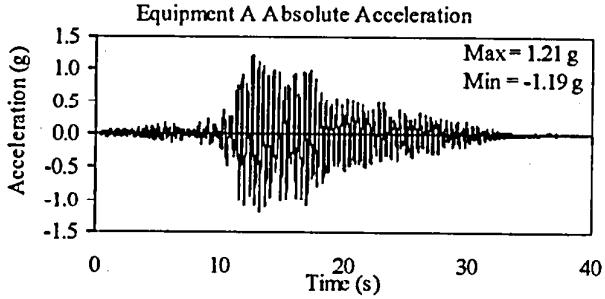

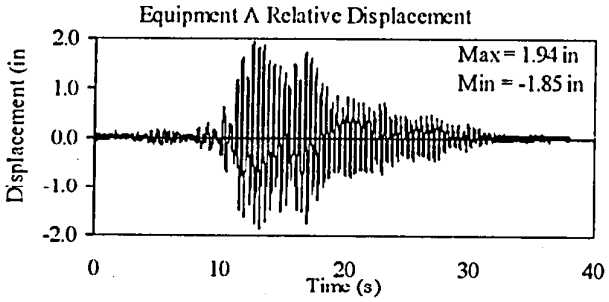

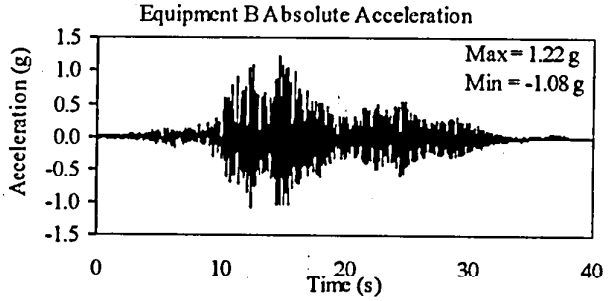

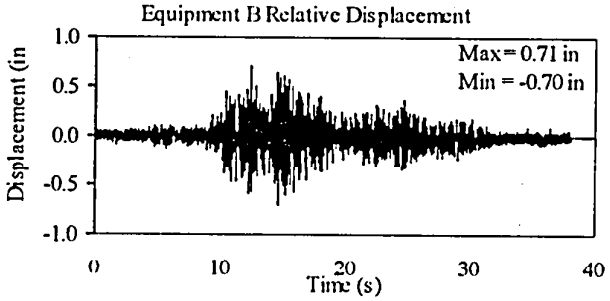

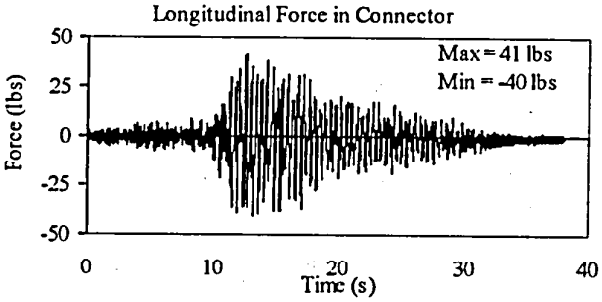

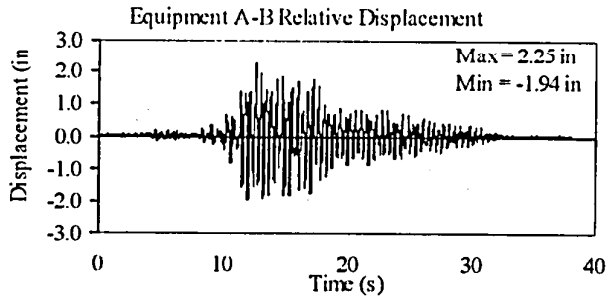

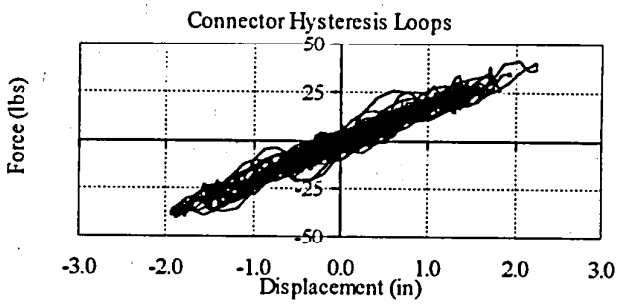

TEST RB-28
EQUIPMENT COMBINATION 4, INDIVIDUAL EQUIPMENT
NEWHALL GROUND MOTION, 30% SPAN

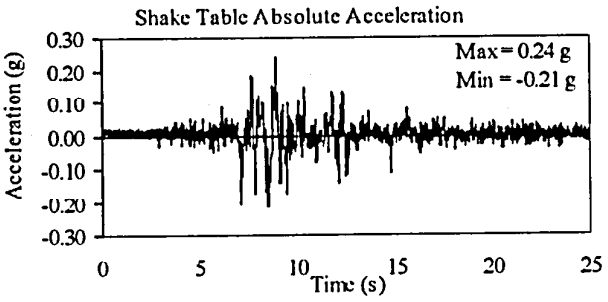

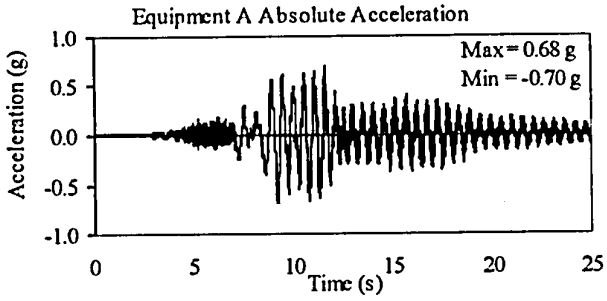

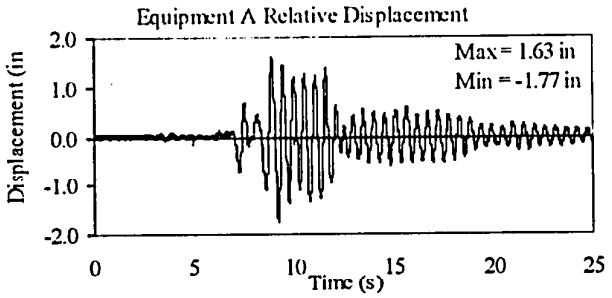

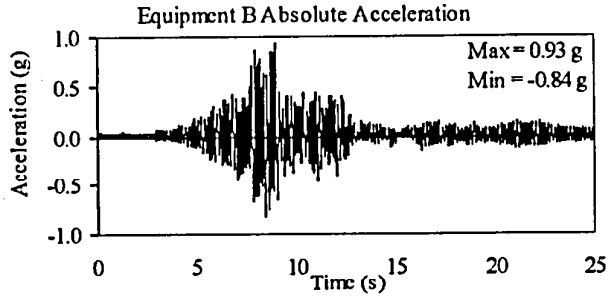

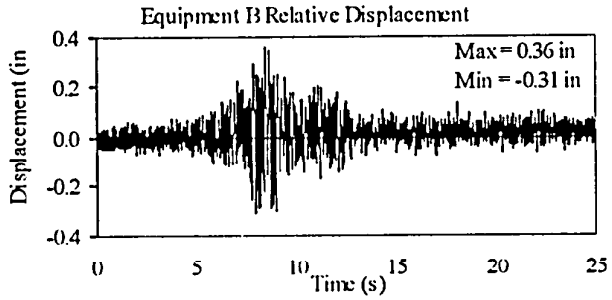

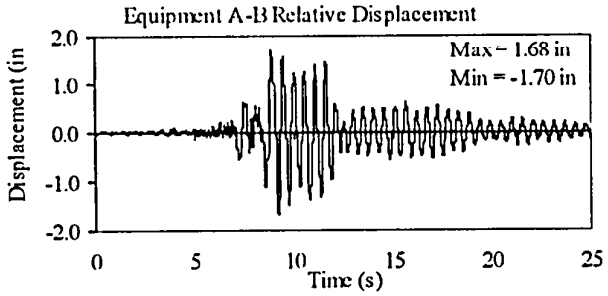

TEST RB-29
EQUIPMENT COMBINATION 4, INDIVIDUAL EQUIPMENT
NEWHALL GROUND MOTION, 100% SPAN

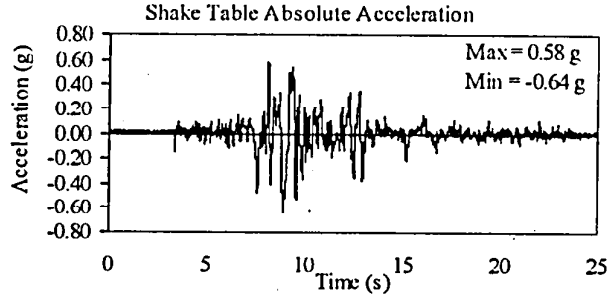

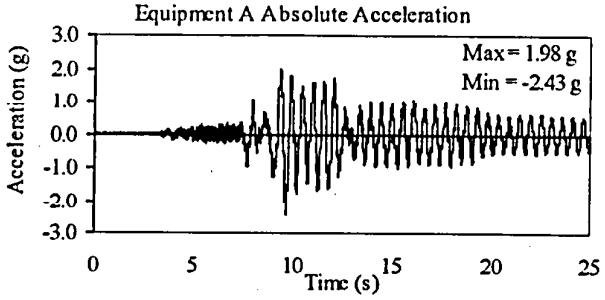

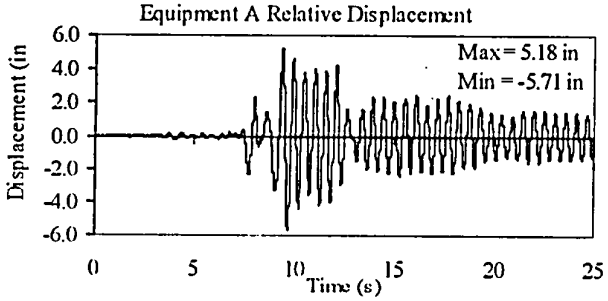

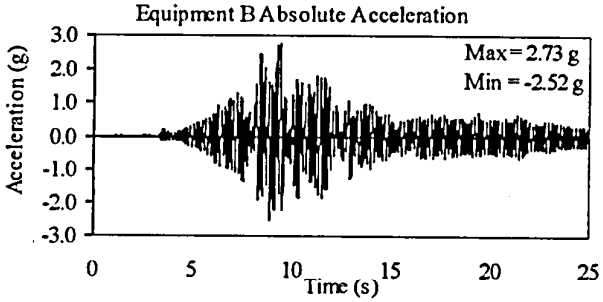

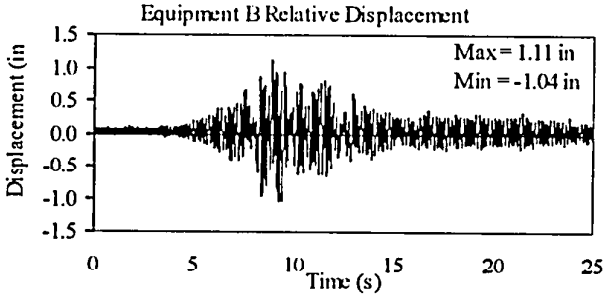

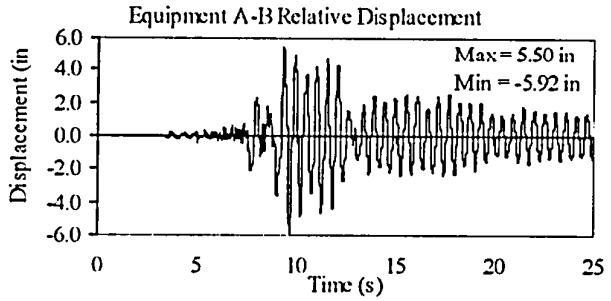

TEST RB-30
EQUIPMENT COMBINATION 4, INDIVIDUAL EQUIPMENT
TABAS GROUND MOTION, 25% SPAN

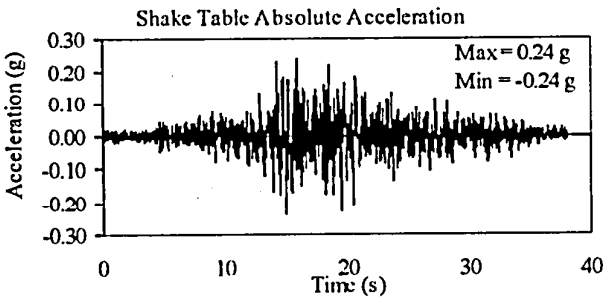

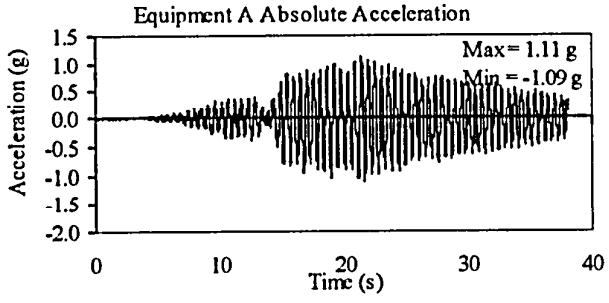

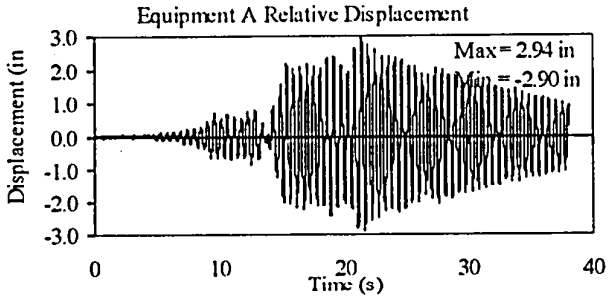

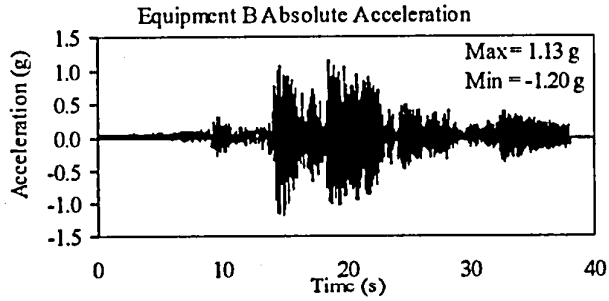

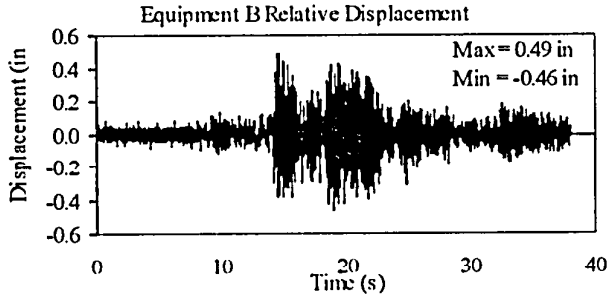

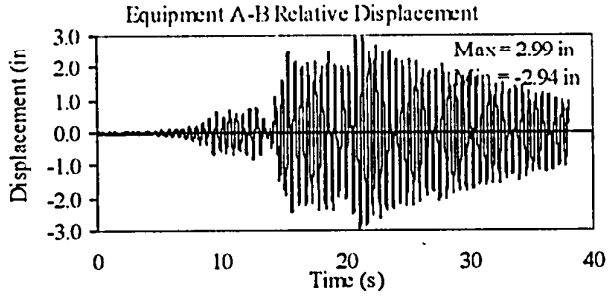

TEST RB-31
EQUIPMENT COMBINATION 4, INDIVIDUAL EQUIPMENT
TABAS GROUND MOTION, 50% SPAN

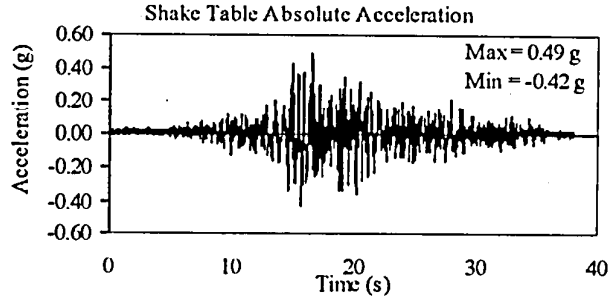

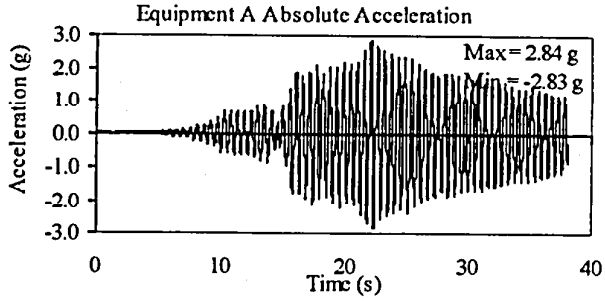

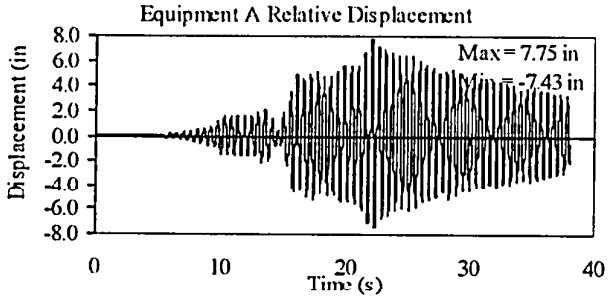

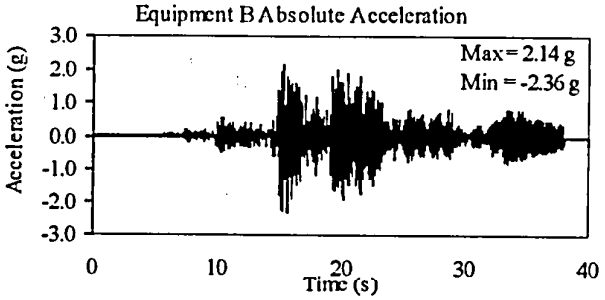

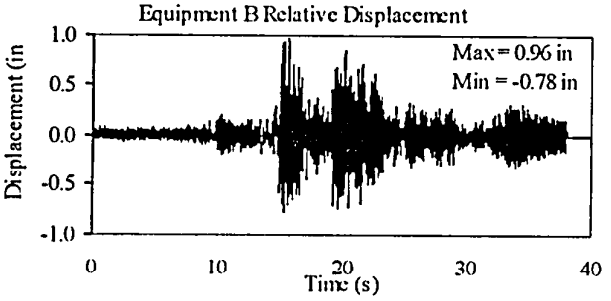

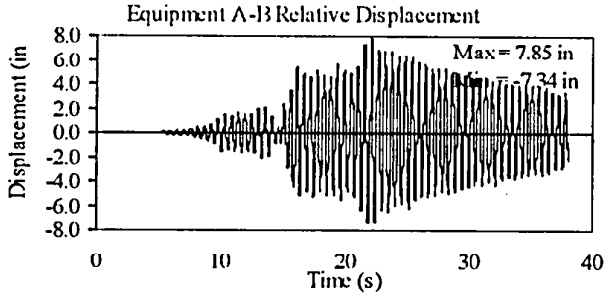

TEST RB-38
EQUIPMENT COMBINATION 3, SPRING 30-2022
NEWHALL GROUND MOTION, 30% SPAN

Shake Table Absolute Acceleration

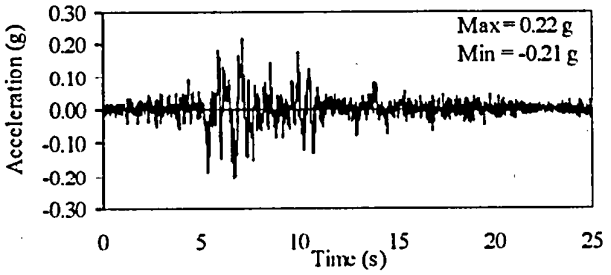

Equipment A Absolute Acceleration

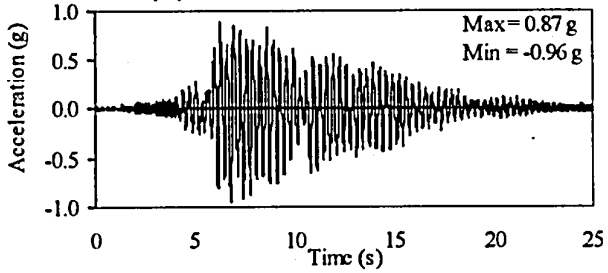

Equipment A Relative Displacement

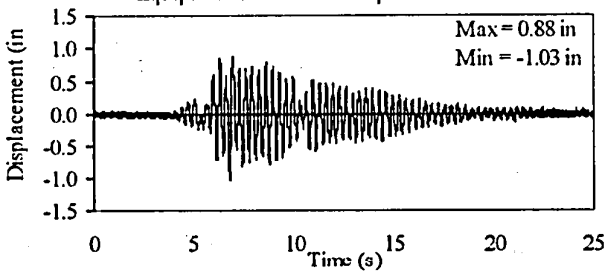

Equipment B Absolute Acceleration

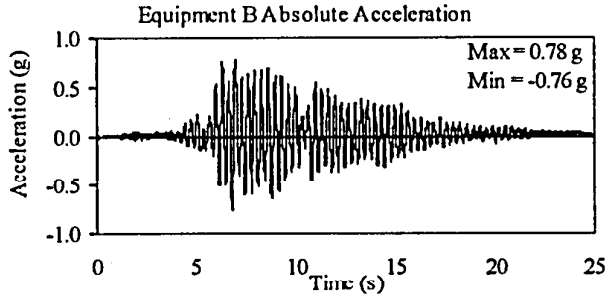

Equipment B Relative Displacement

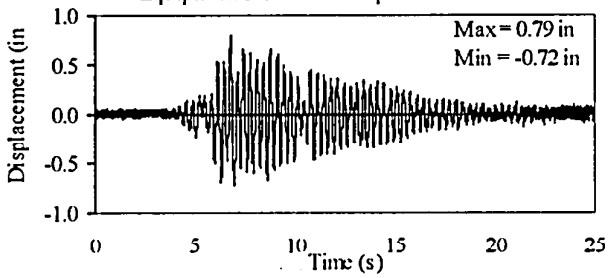

Longitudinal Force in Connector

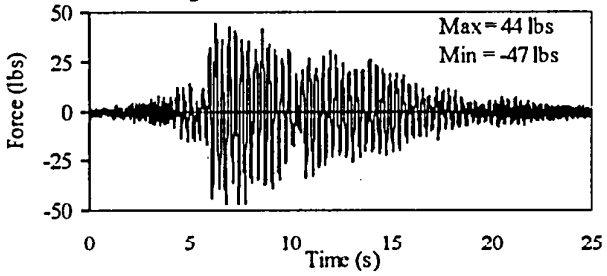

Equipment A-B Relative Displacement

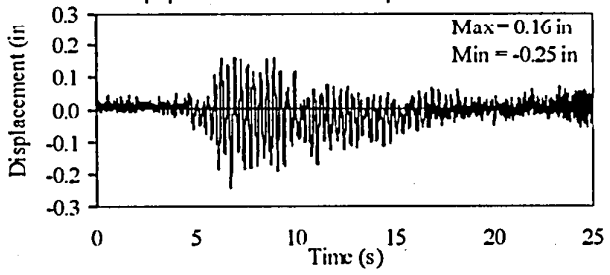

Connector Hysteresis Loops

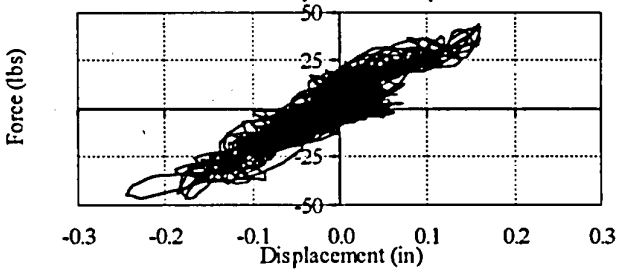

Strain in Spring Connector

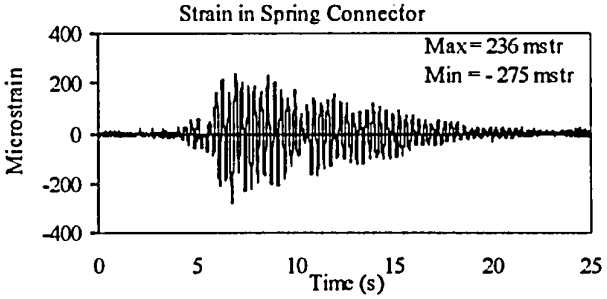

TEST RB-39
EQUIPMENT COMBINATION 3, SPRING 30-2022
NEWHALL GROUND MOTION, 100% SPAN

Shake Table Absolute Acceleration

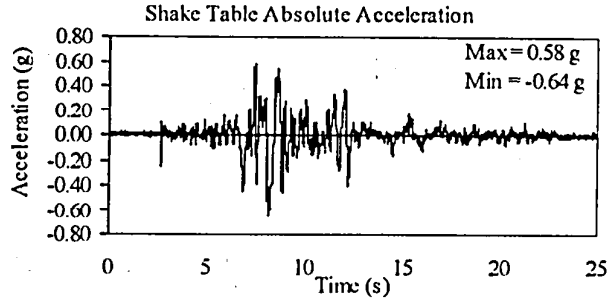

Equipment A Absolute Acceleration

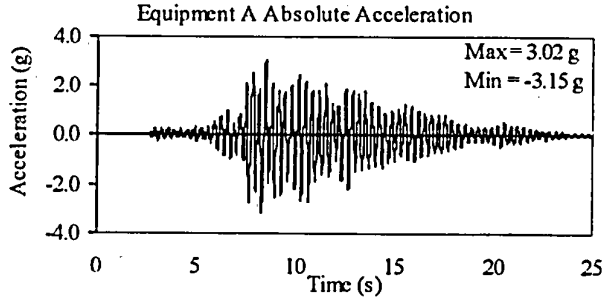

Equipment A Relative Displacement

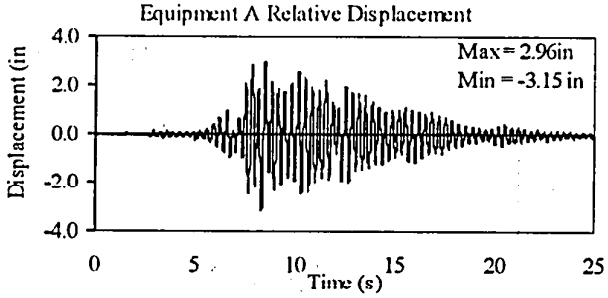

Equipment B Absolute Acceleration

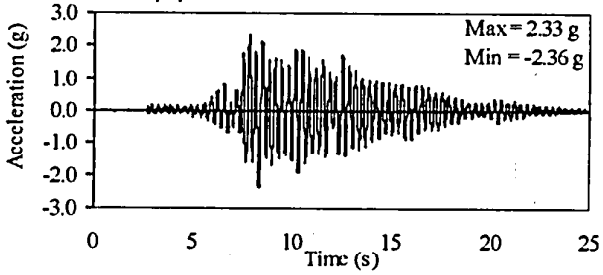

Equipment B Relative Displacement

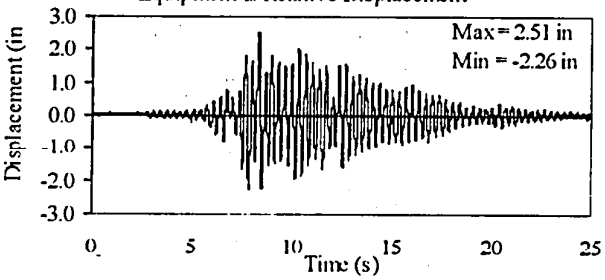

Longitudinal Force in Connector

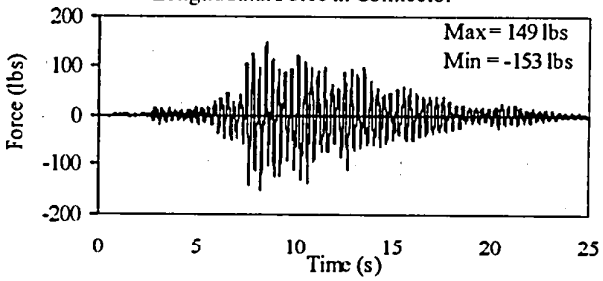

Equipment A-B Relative Displacement

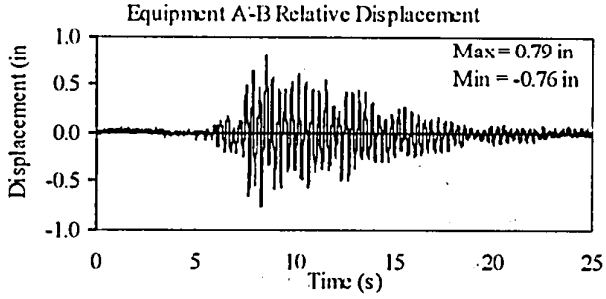

Connector Hysteresis Loops

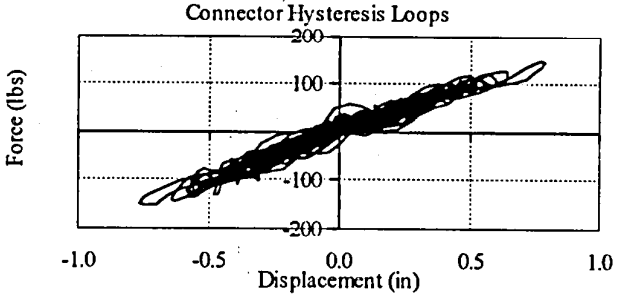

Strain in Spring Connector

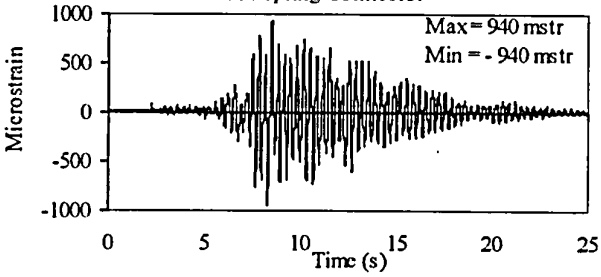

TEST RB-40
EQUIPMENT COMBINATION 3, SPRING 30-2022
TABAS GROUND MOTION, 25% SPAN

Shake Table Absolute Acceleration

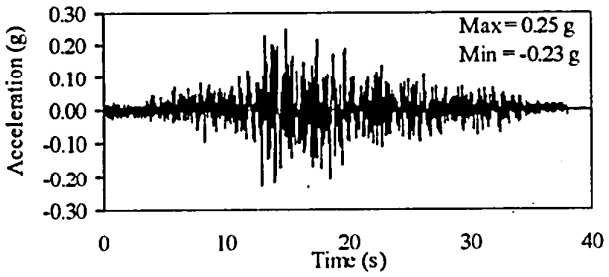

Equipment A Absolute Acceleration

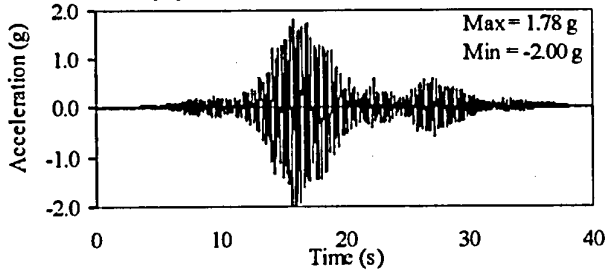

Equipment A Relative Displacement

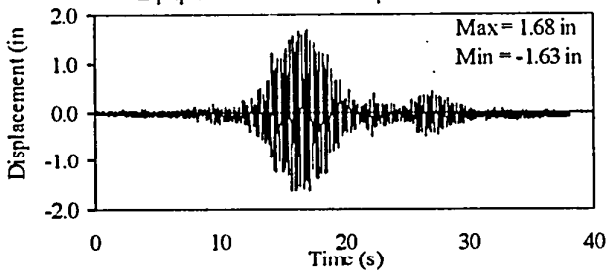

Equipment B Absolute Acceleration

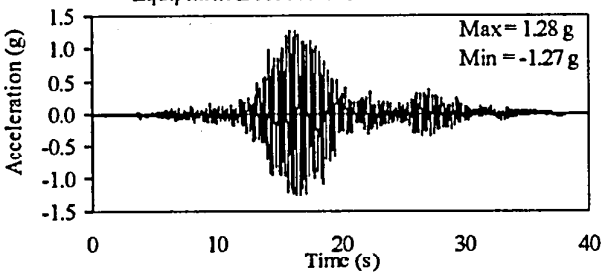

Equipment B Relative Displacement

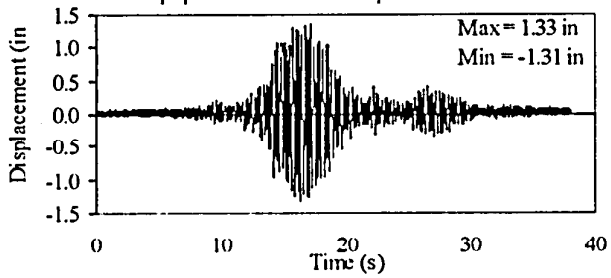

Longitudinal Force in Connector

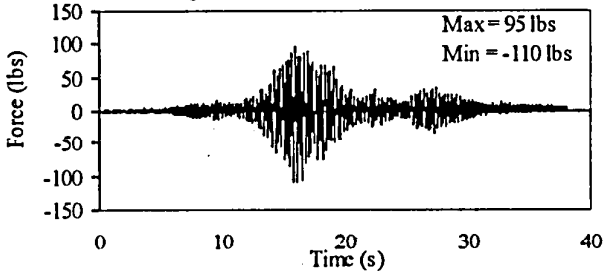

Equipment A-B Relative Displacement

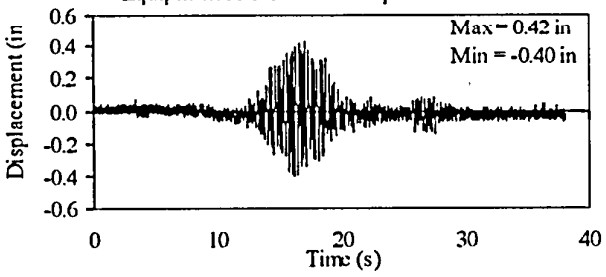

Connector Hysteresis Loops

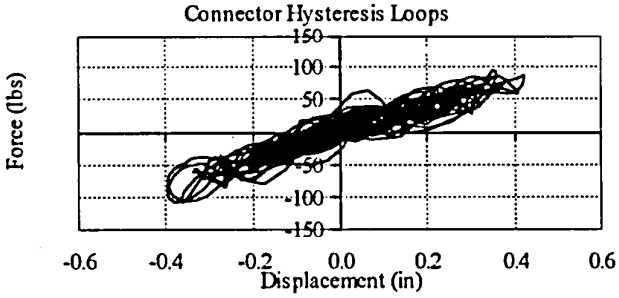

Strain in Spring Connector

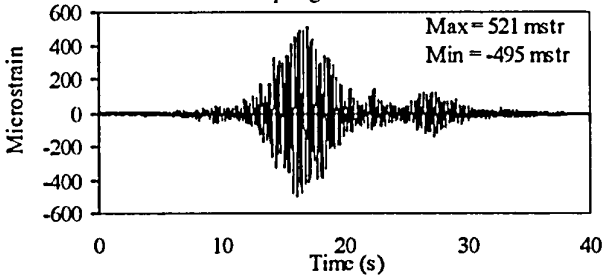

TEST RB-41
EQUIPMENT COMBINATION 3, SPRING 30-2022
TABAS GROUND MOTION, 50% SPAN

Shake Table Absolute Acceleration

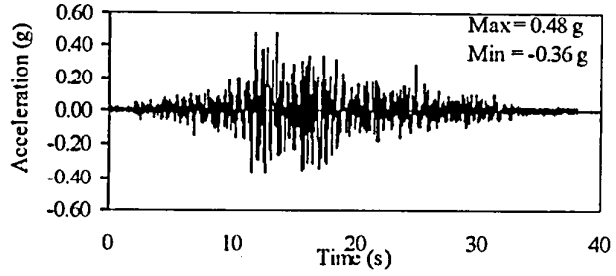

Equipment A Absolute Acceleration

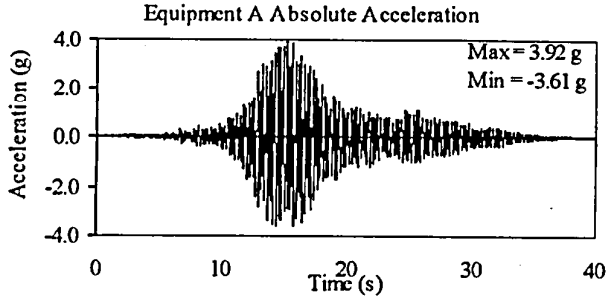

Equipment A Relative Displacement

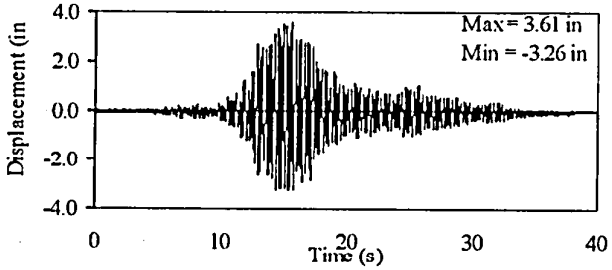

Equipment B Absolute Acceleration

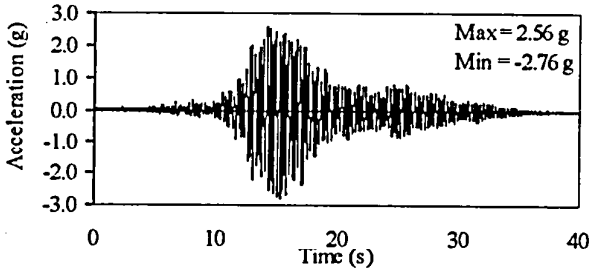

Equipment B Relative Displacement

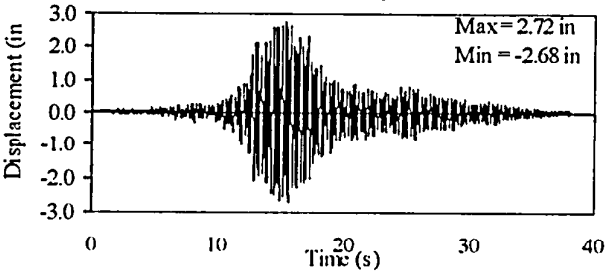

Longitudinal Force in Connector

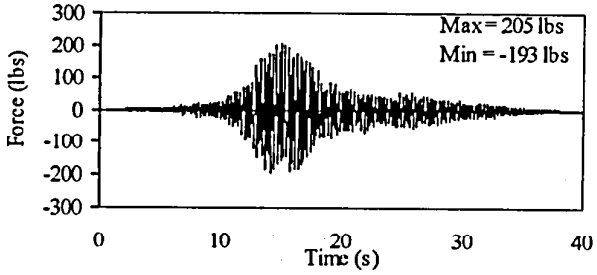

Equipment A-B Relative Displacement

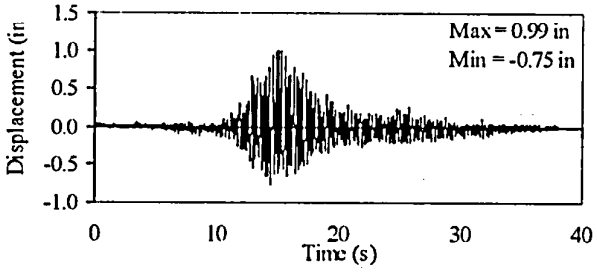

Connector Hysteresis Loops

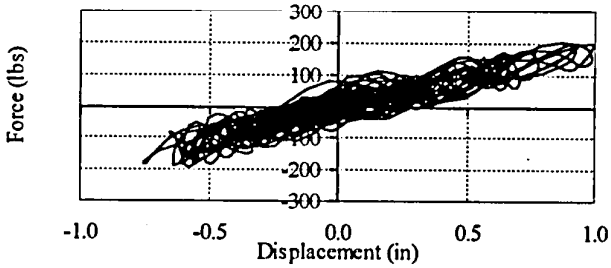

Strain in Spring Connector

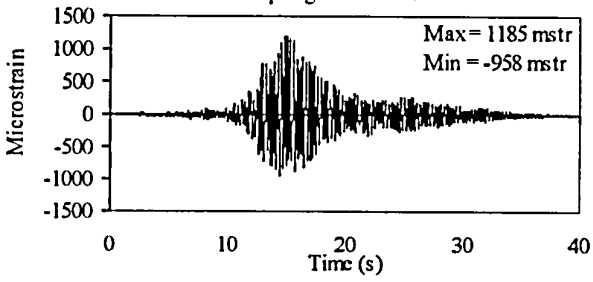

TEST RB-47
EQUIPMENT COMBINATION 3, BUS SLIDER
NEWHALL GROUND MOTION, 100% SPAN

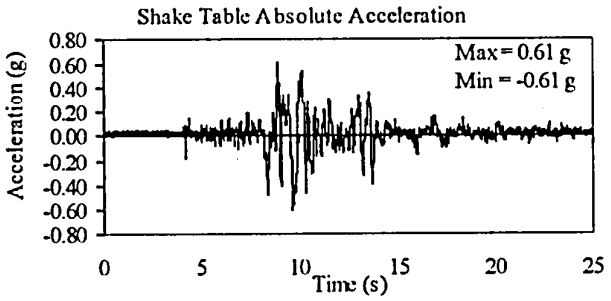

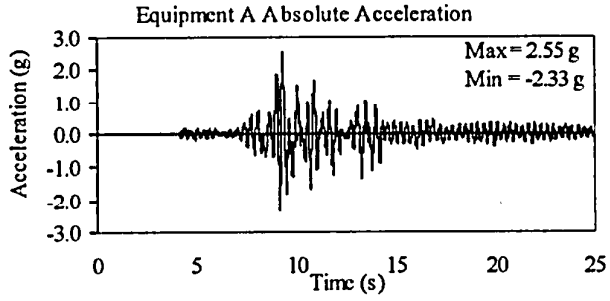

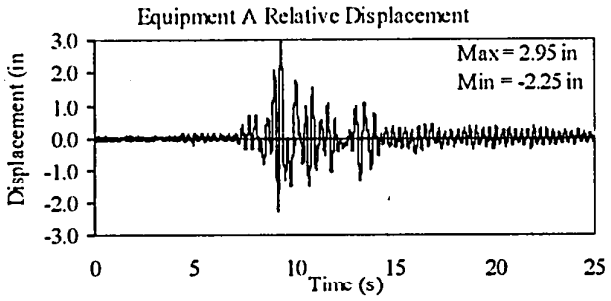

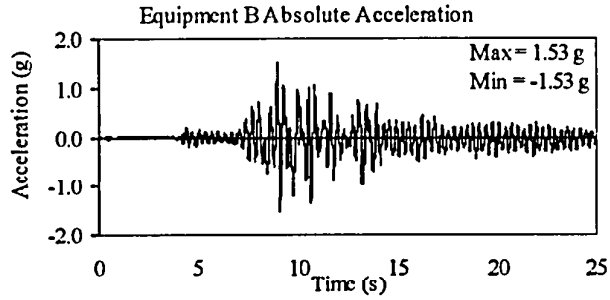

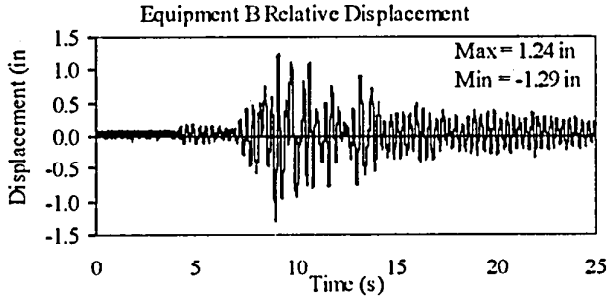

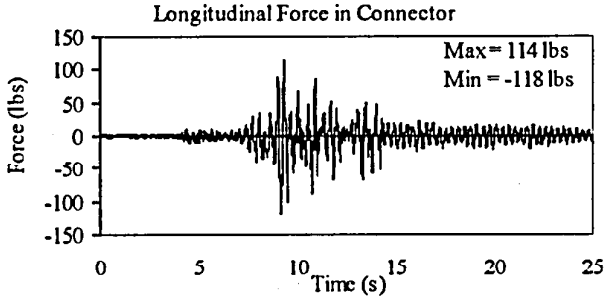

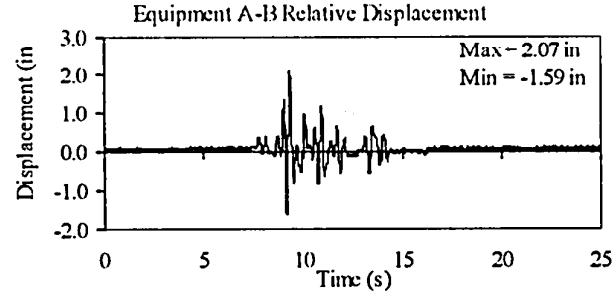

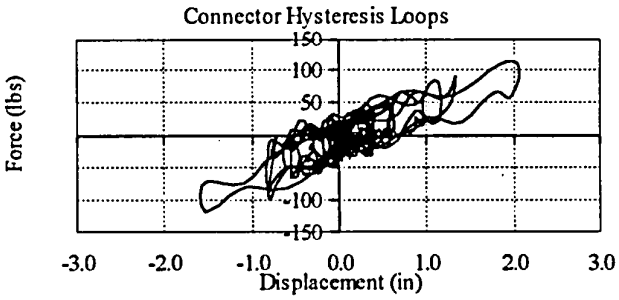

TEST RB-100
EQUIPMENT COMBINATION 2, SPRING 30-2022
TABAS GROUND MOTION, 50% SPAN

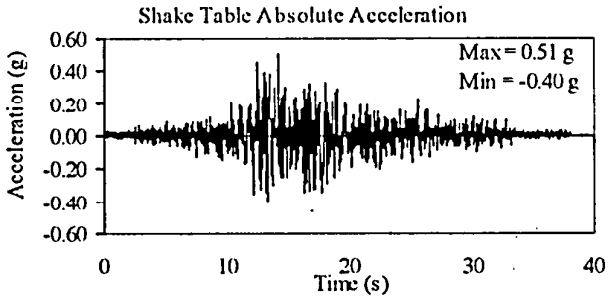

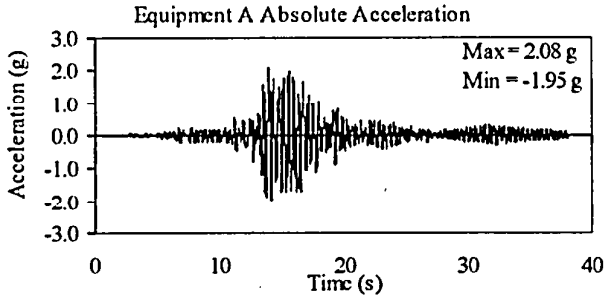

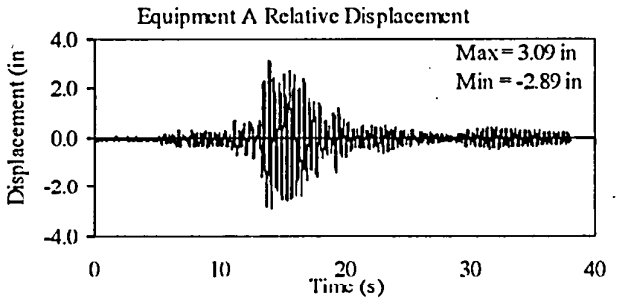

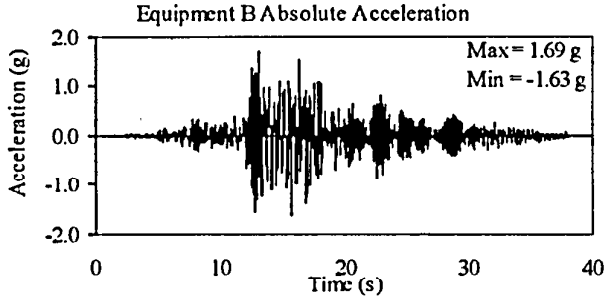

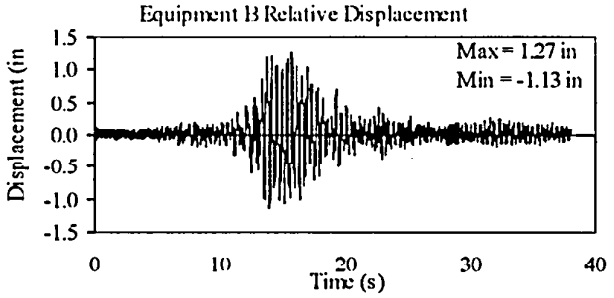

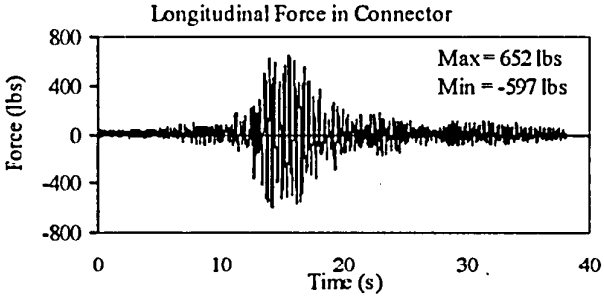

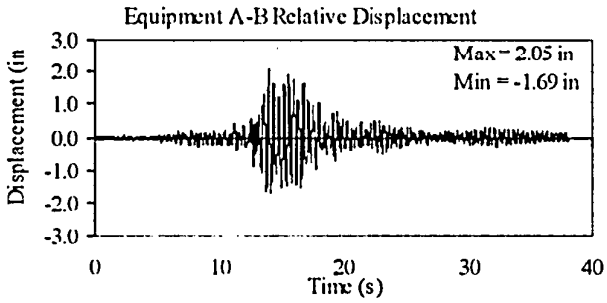

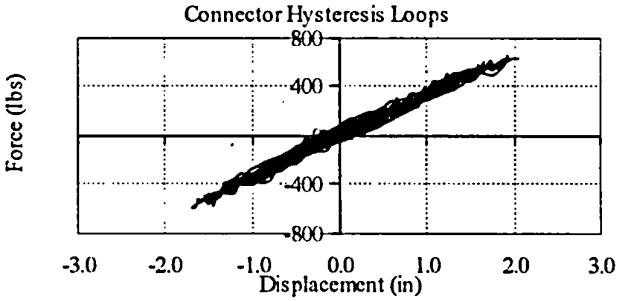

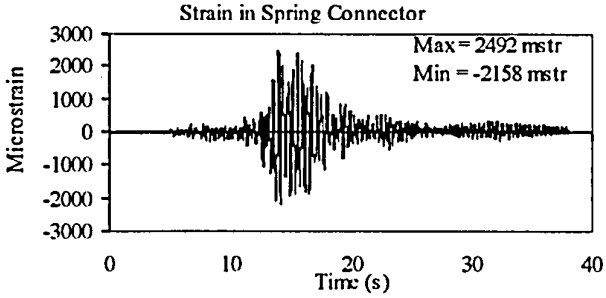

TEST RB-101
EQUIPMENT COMBINATION 2, SPRING 30-2022
NEWHALL GROUND MOTION, 100% SPAN

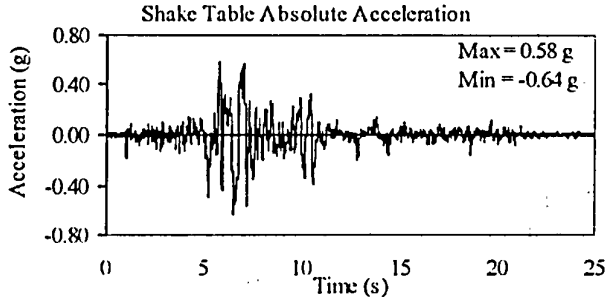

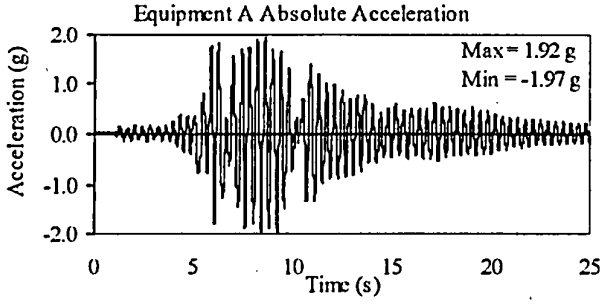

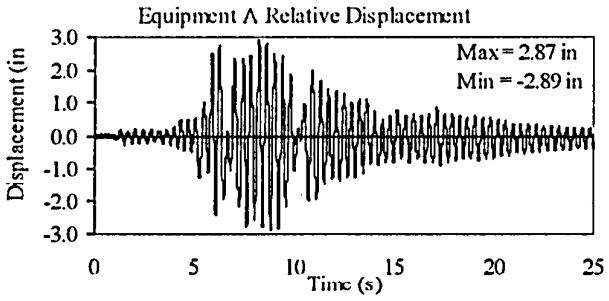

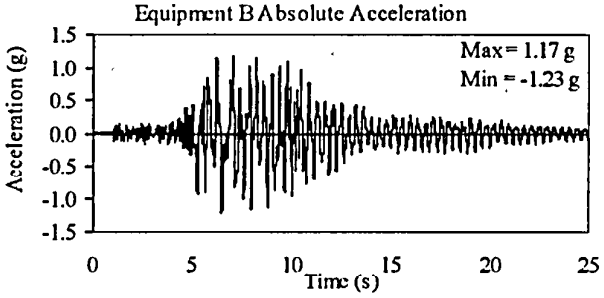

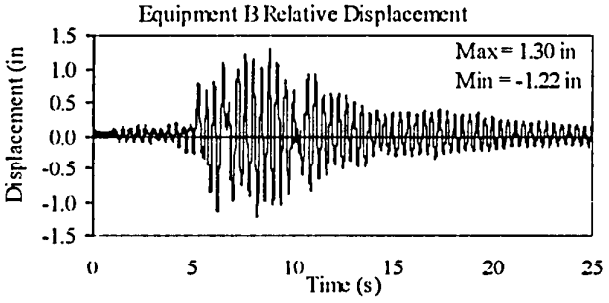

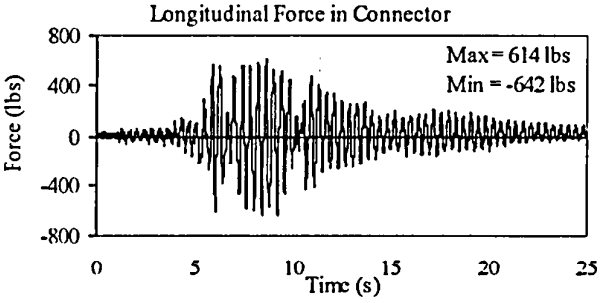

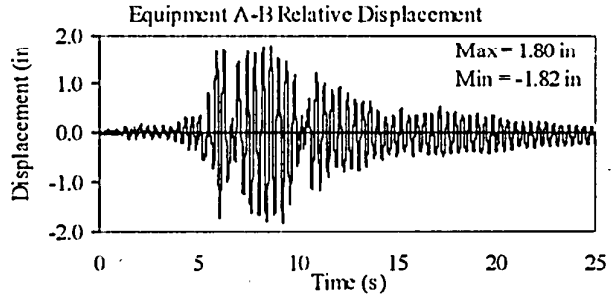

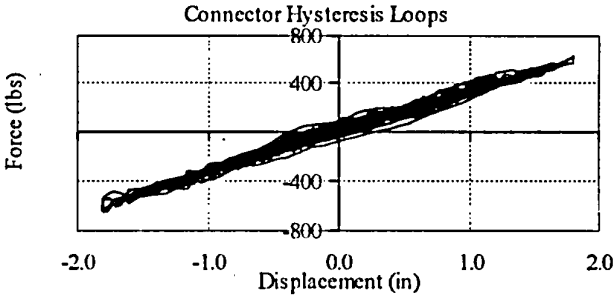

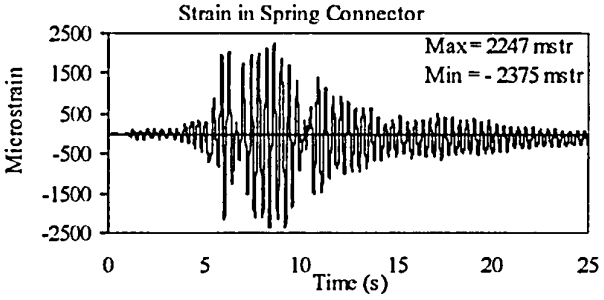

TEST RB-102
EQUIPMENT COMBINATION 2, SPRING 30-2022
TABAS GROUND MOTION, 100% SPAN

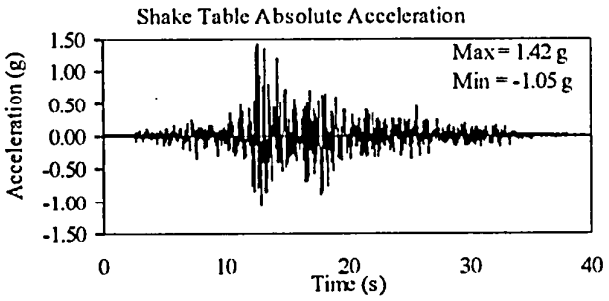

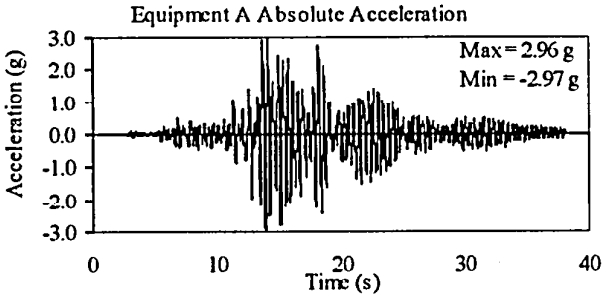

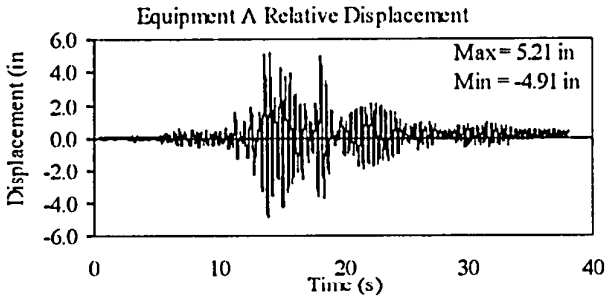

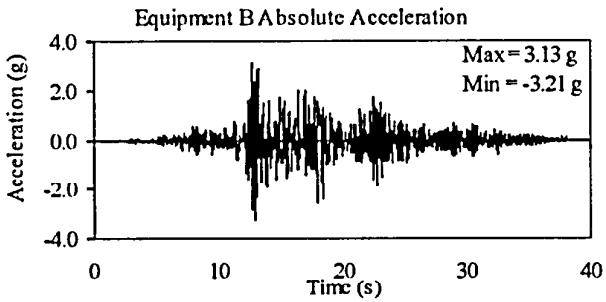

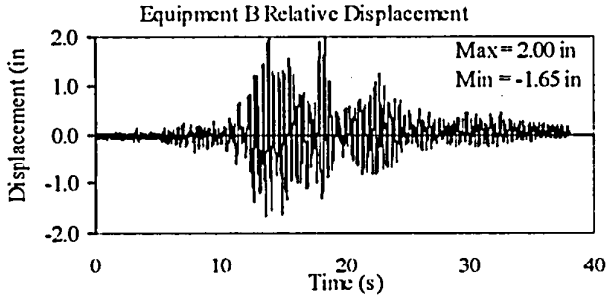

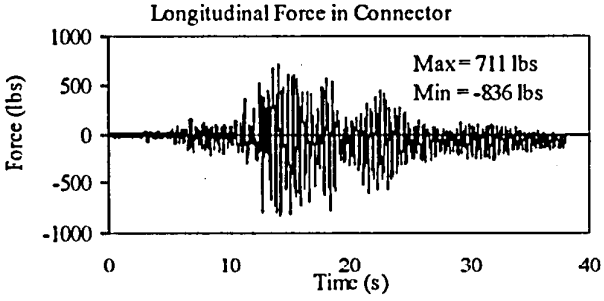

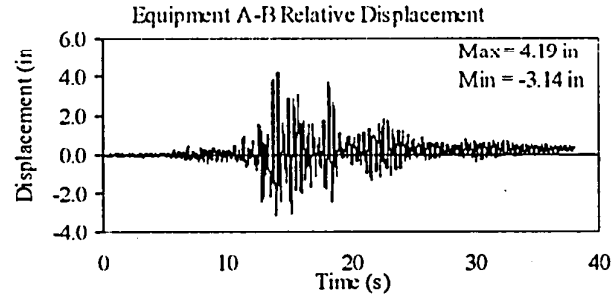

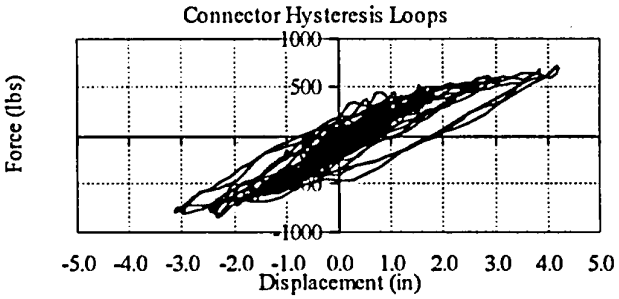

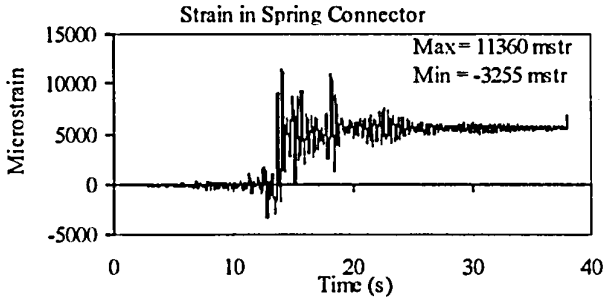

TEST RB-103
EQUIPMENT COMBINATION 2, SPRING 30-2022
TABAS GROUND MOTION, 150% SPAN

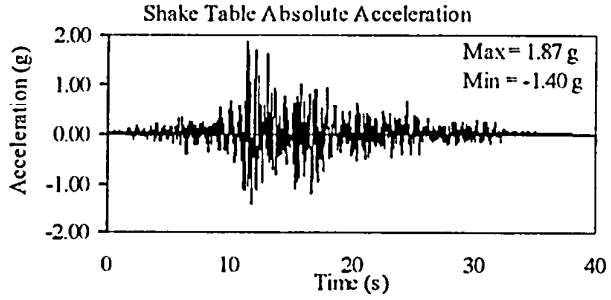

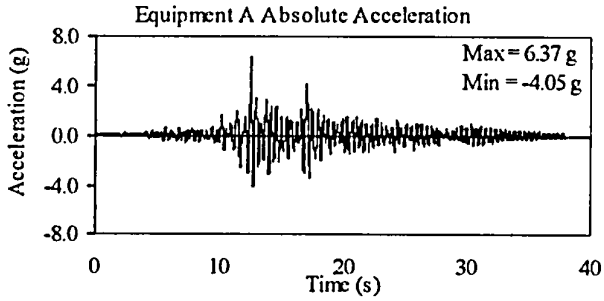

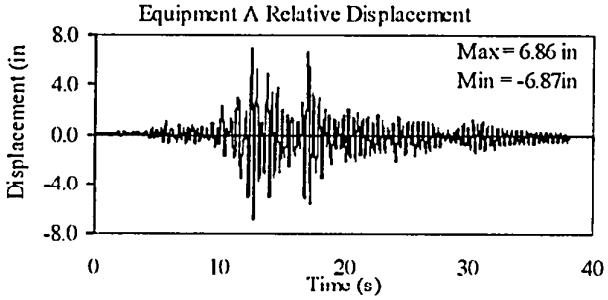

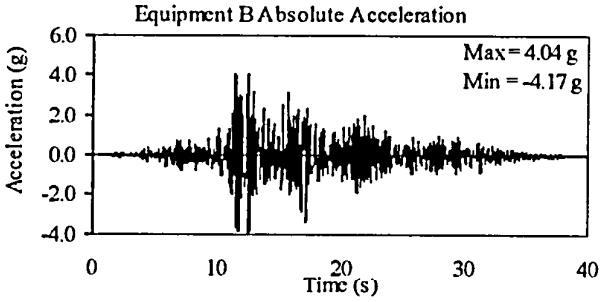

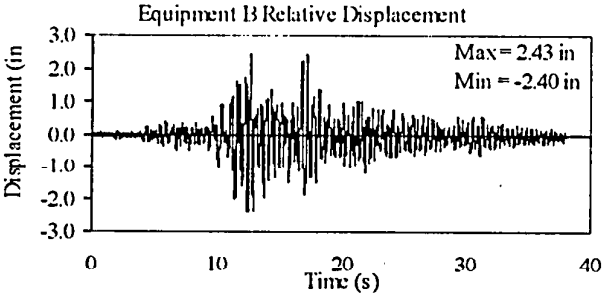

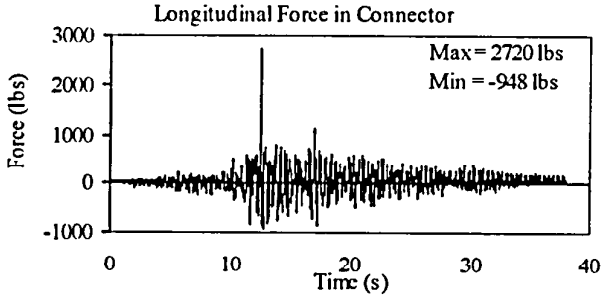

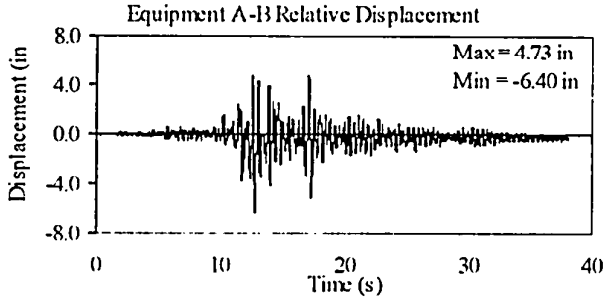

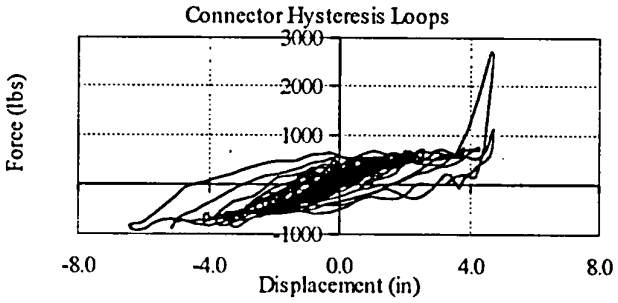

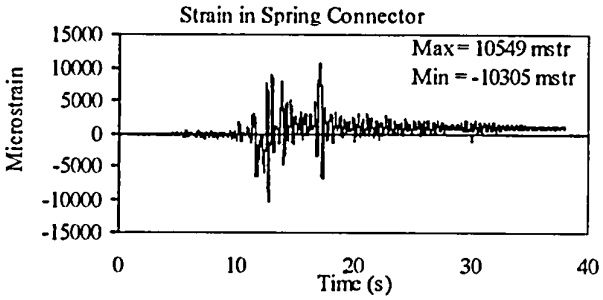

TEST RB-109
EQUIPMENT COMBINATION 2, BUS SLIDER
NEWHALL GROUND MOTION, 30% SPAN

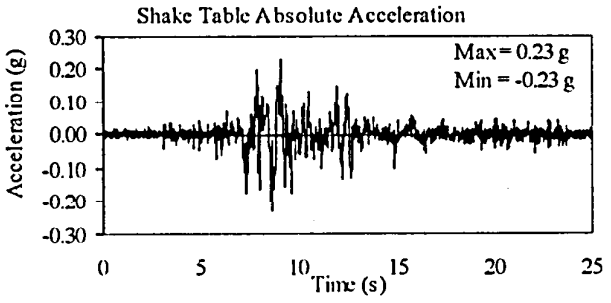

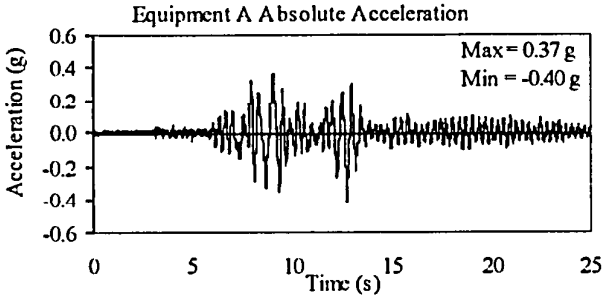

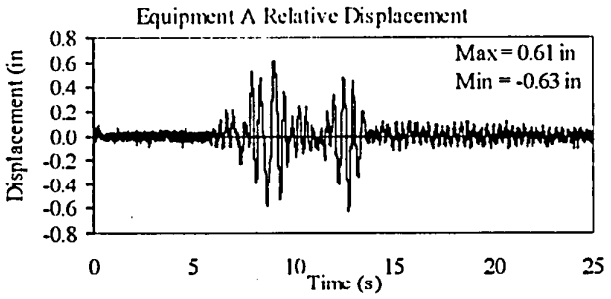

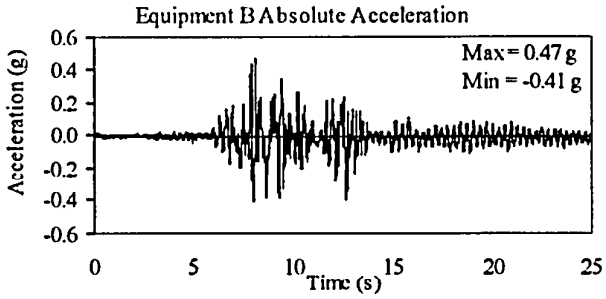

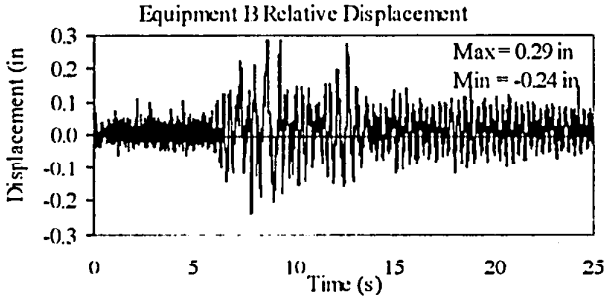

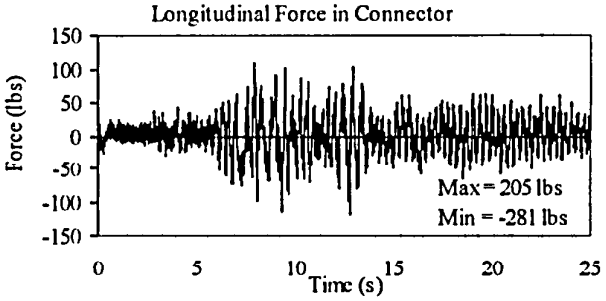

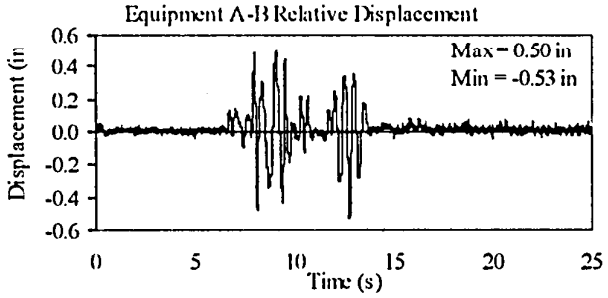

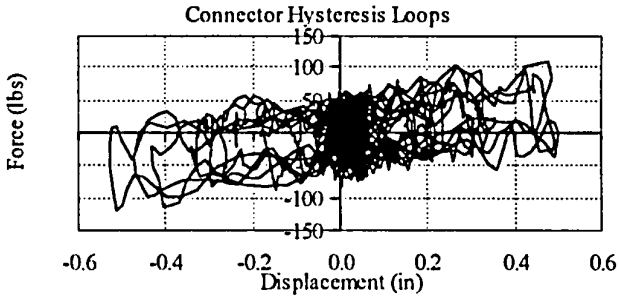

TEST RB-110
EQUIPMENT COMBINATION 2, BUS SLIDER
TABAS GROUND MOTION, 25% SPAN

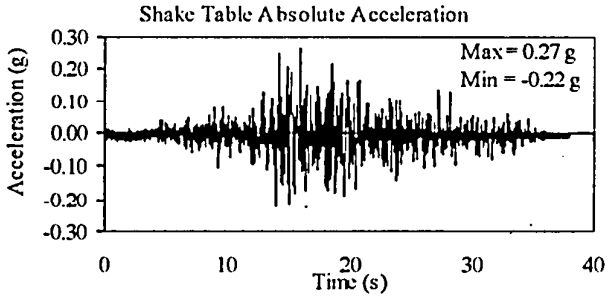

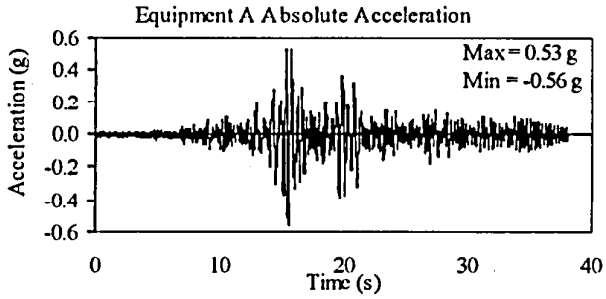

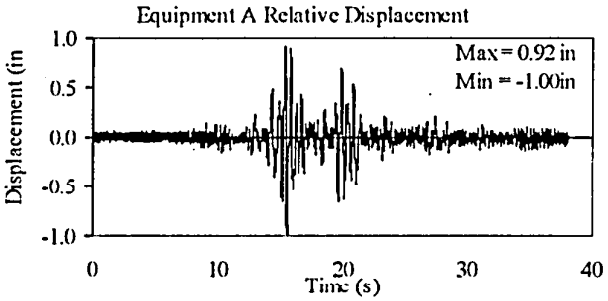

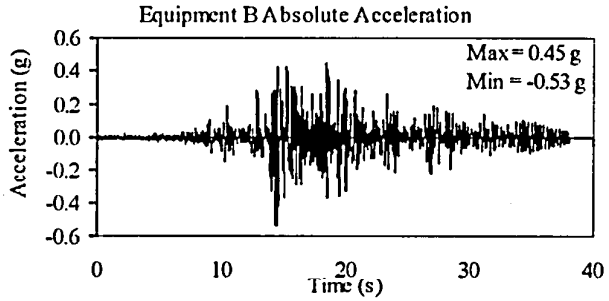

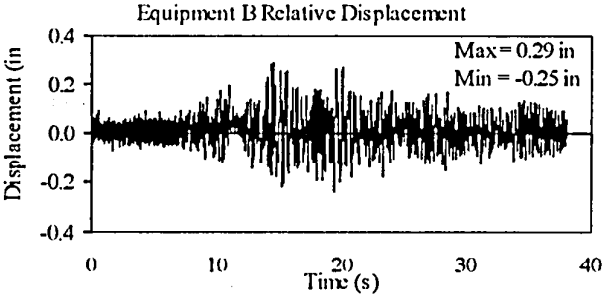

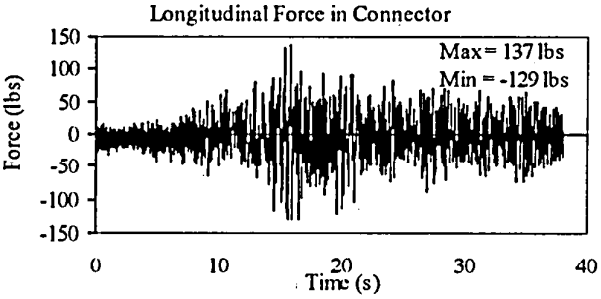

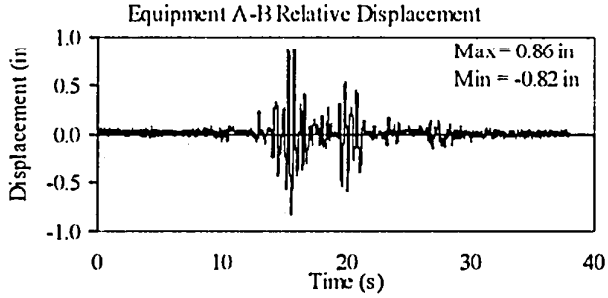

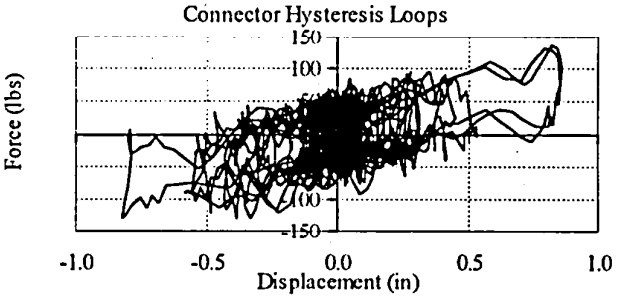

TEST RB-111
EQUIPMENT COMBINATION 2, BUS SLIDER
TABAS GROUND MOTION, 50% SPAN

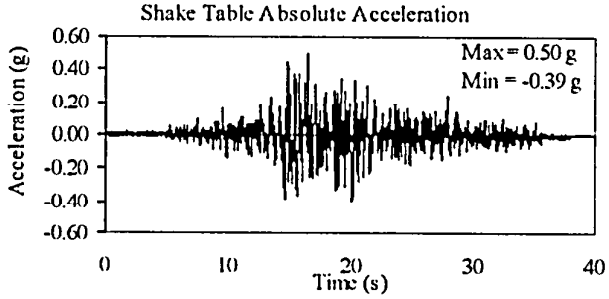

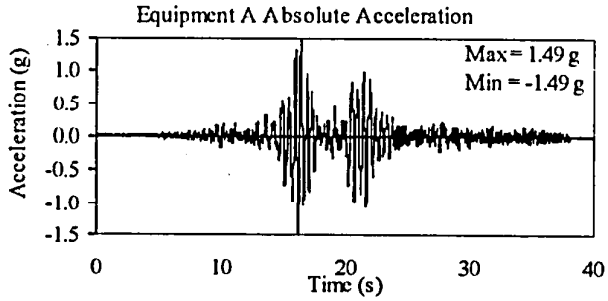

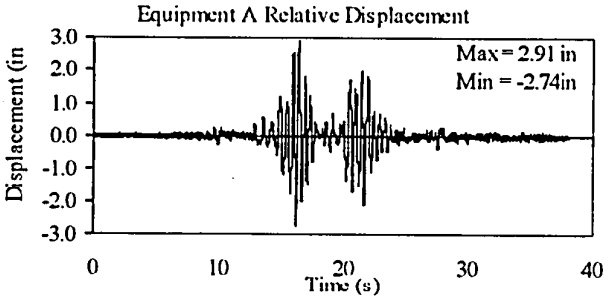

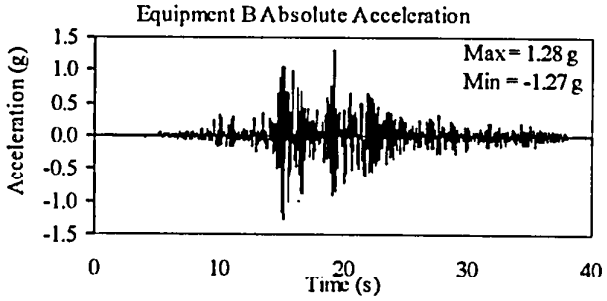

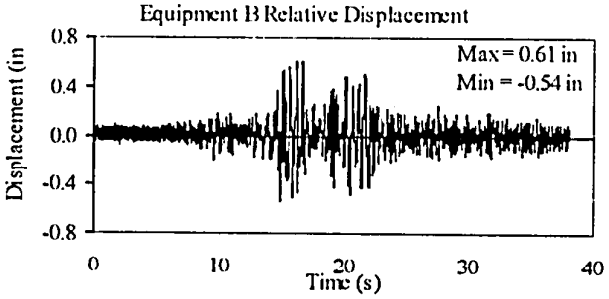

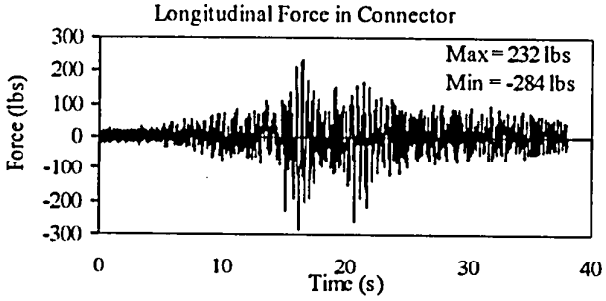

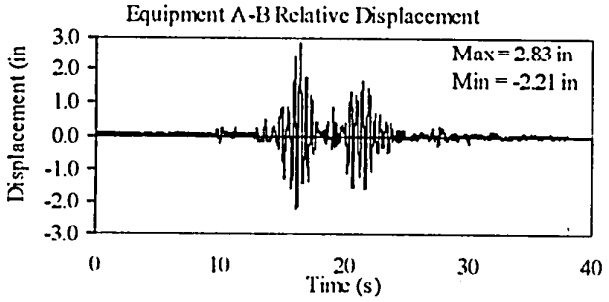

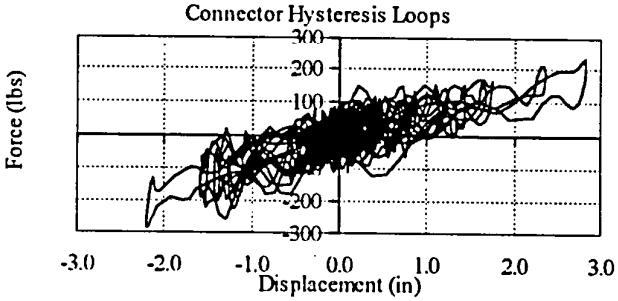

TEST RB-112
EQUIPMENT COMBINATION 2, BUS SLIDER
NEWHALL GROUND MOTION, 100% SPAN

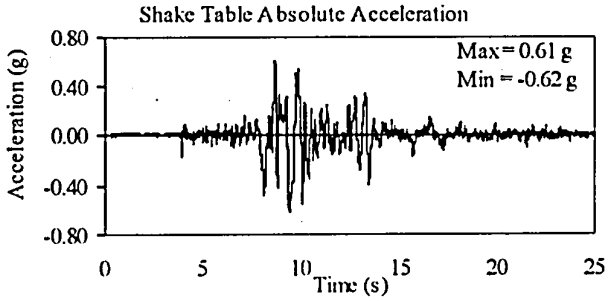

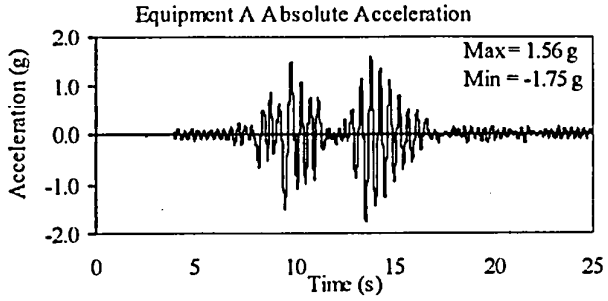

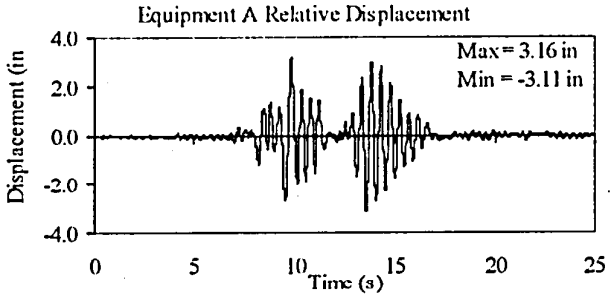

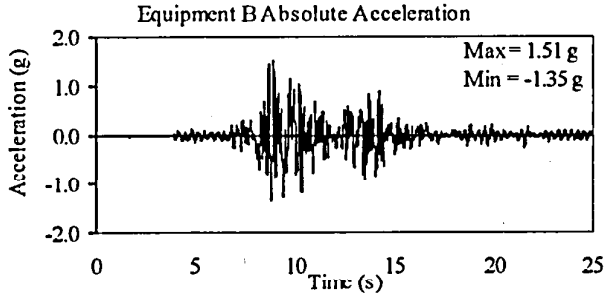

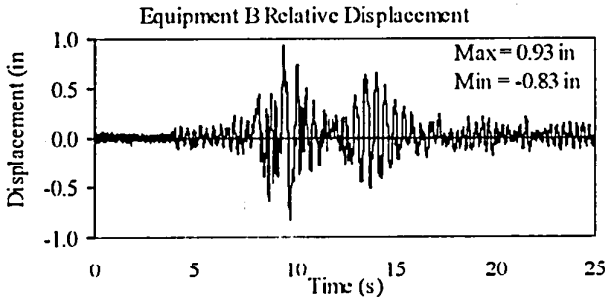

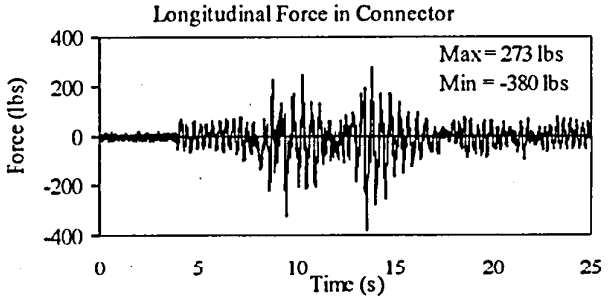

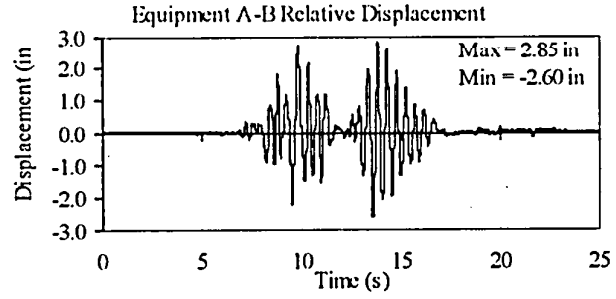

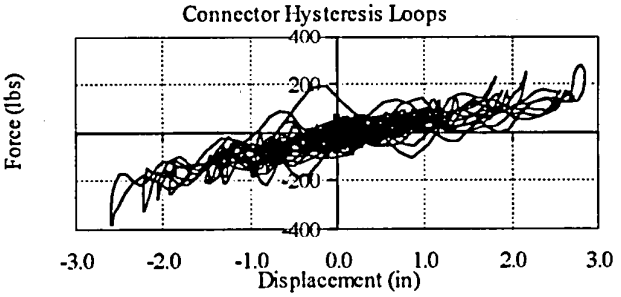

TEST RB-118
EQUIPMENT COMBINATION 2, BPA ISOLATOR
NEWHALL GROUND MOTION, 30% SPAN

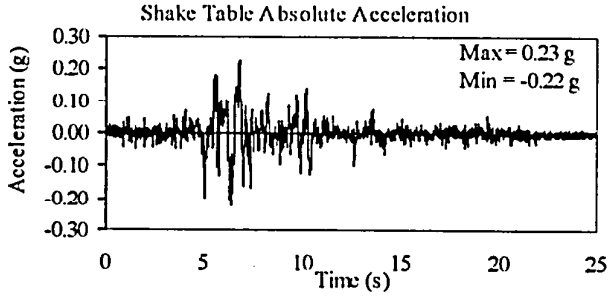

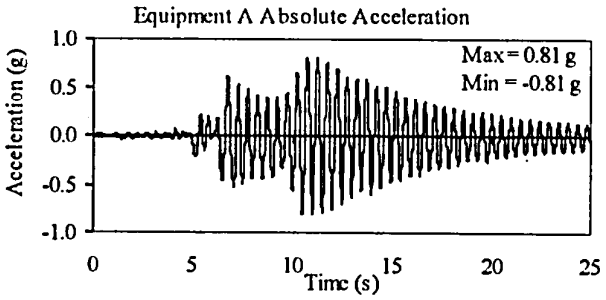

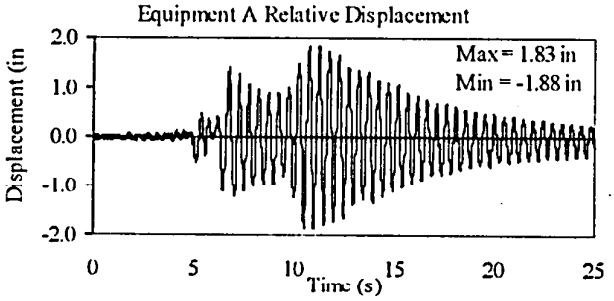

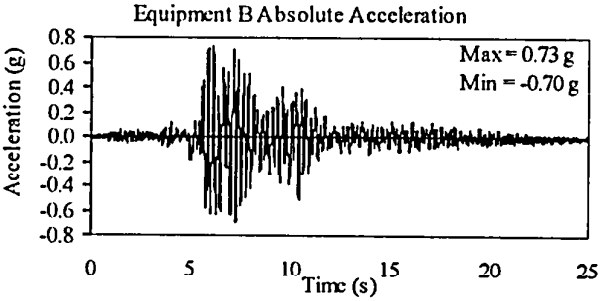

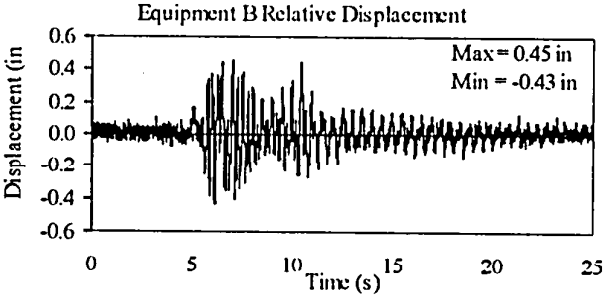

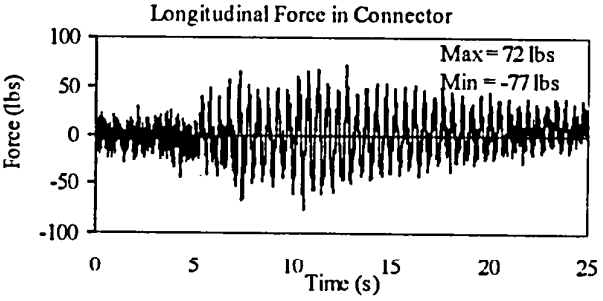

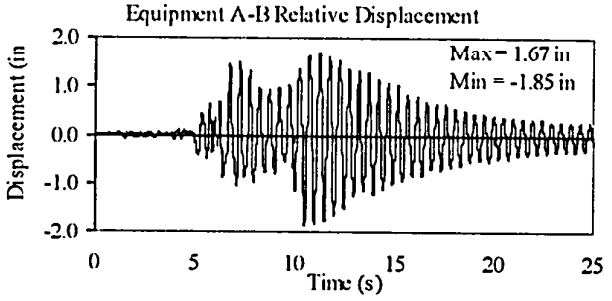

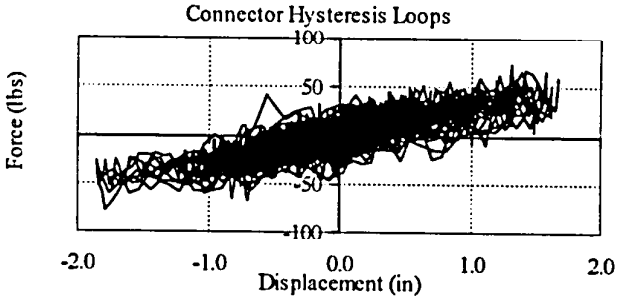

TEST RB-119
EQUIPMENT COMBINATION 2, BPA ISOLATOR
TABAS GROUND MOTION, 25% SPAN

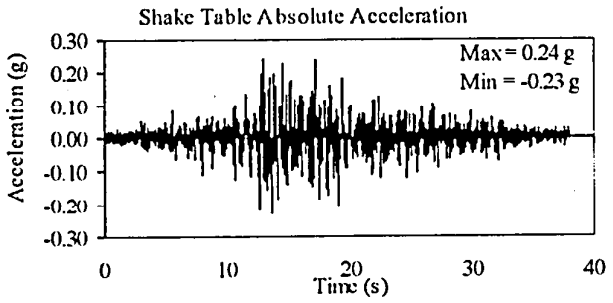

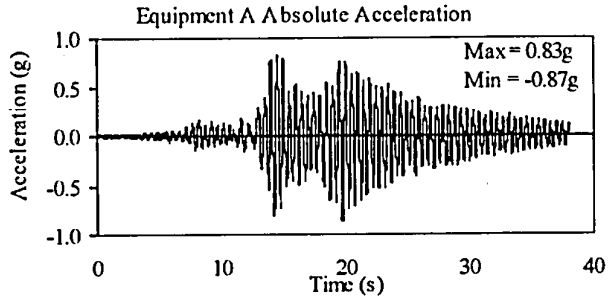

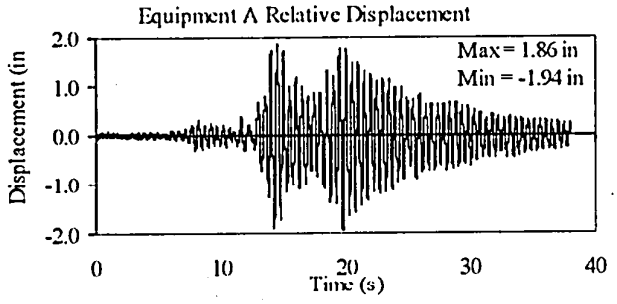

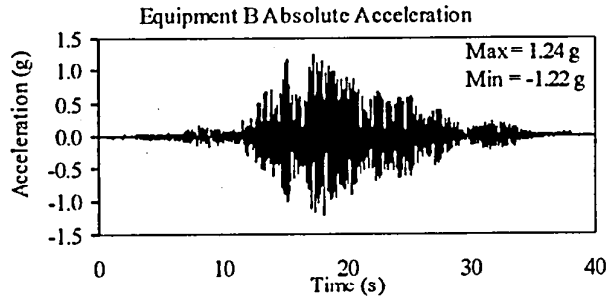

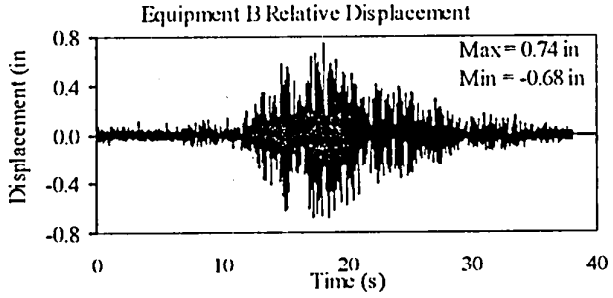

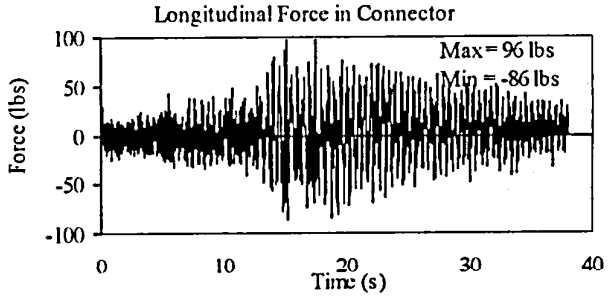

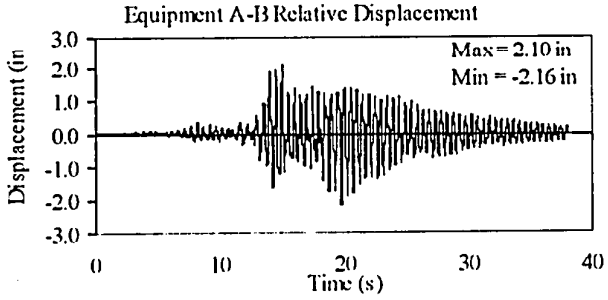

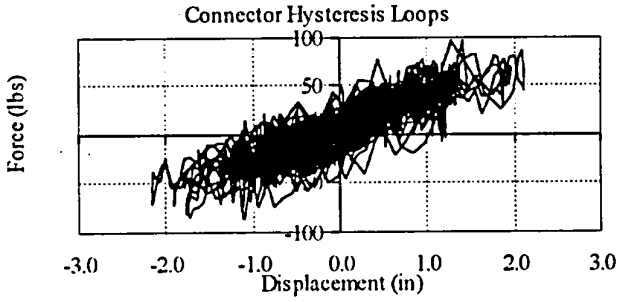

TEST RB-120
EQUIPMENT COMBINATION 2, BPA ISOLATOR
TABAS GROUND MOTION, 50% SPAN

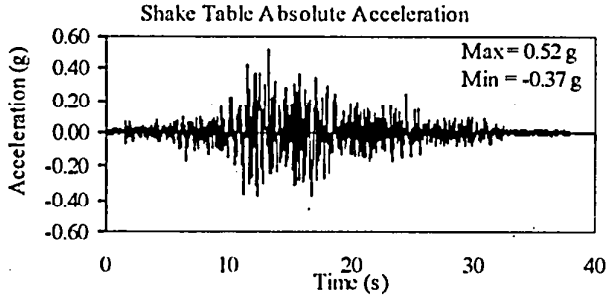

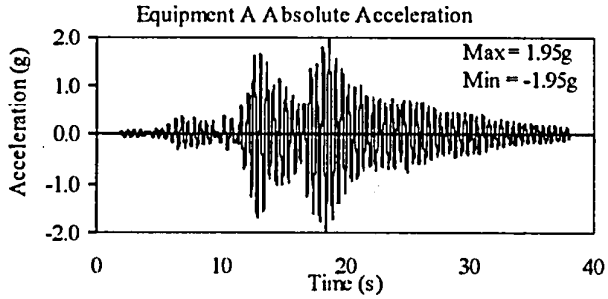

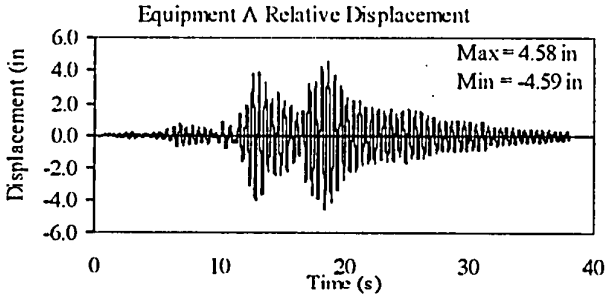

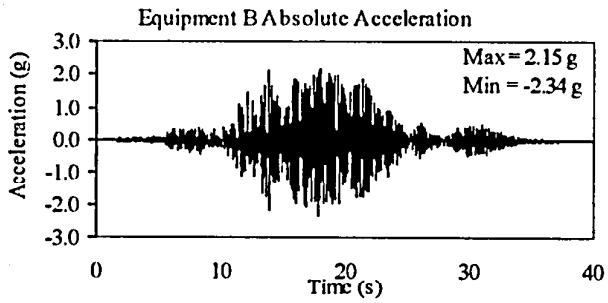

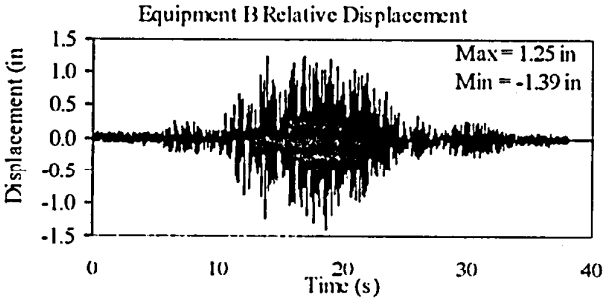

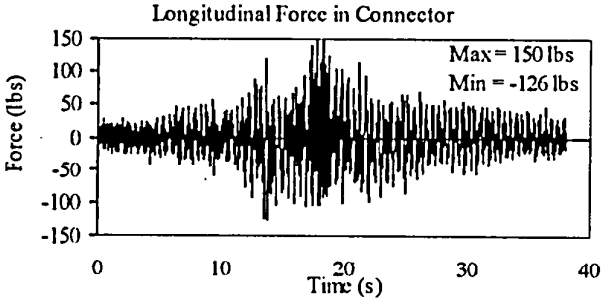

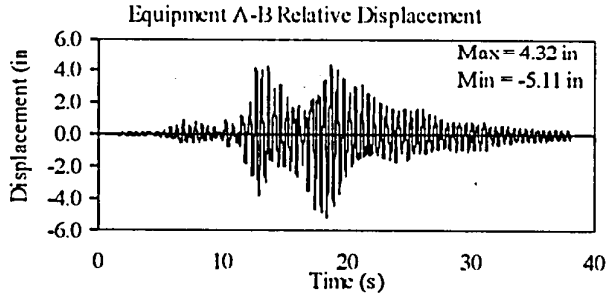

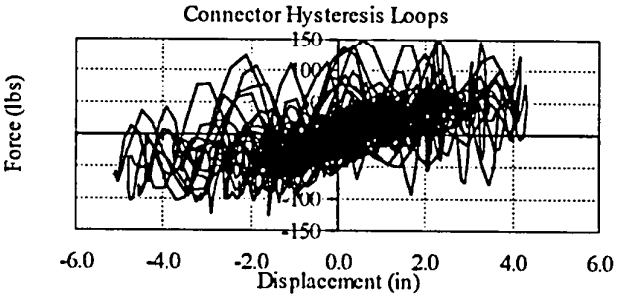

TEST RB-121
EQUIPMENT COMBINATION 2, BPA ISOLATOR
NEWHALL GROUND MOTION, 100% SPAN

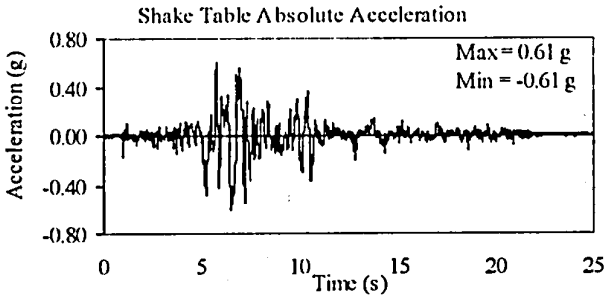

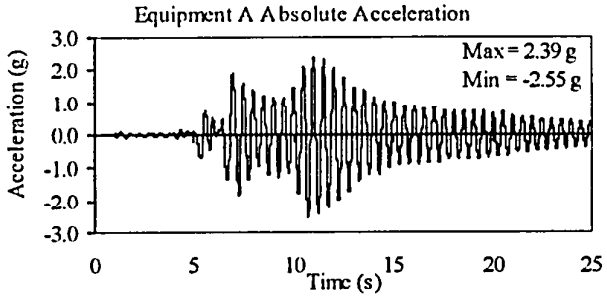

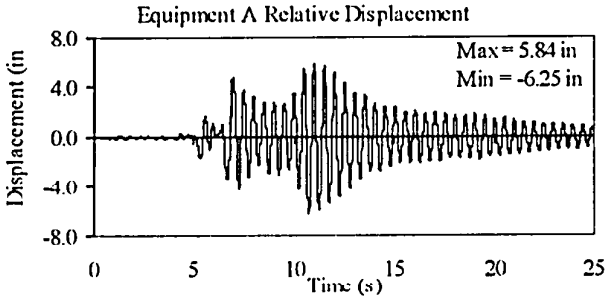

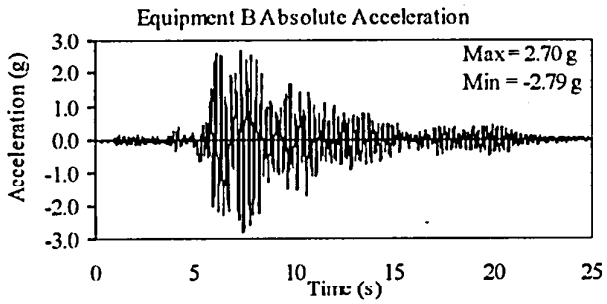

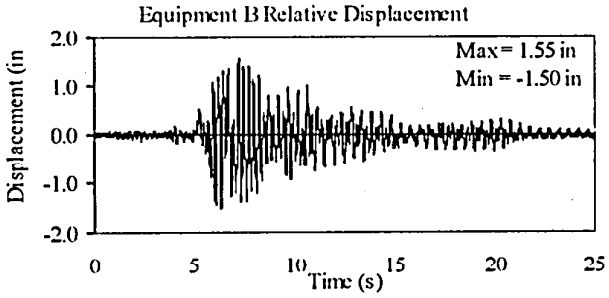

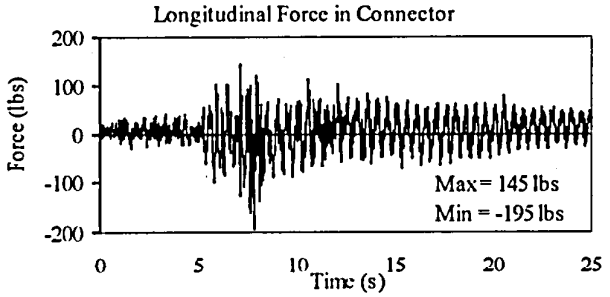

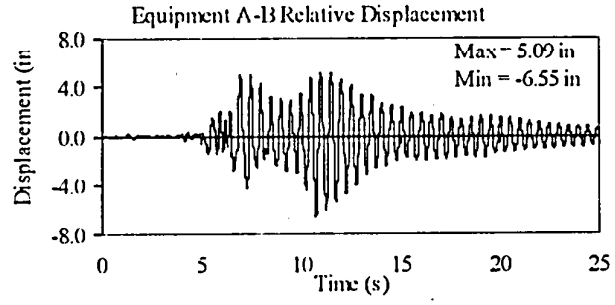

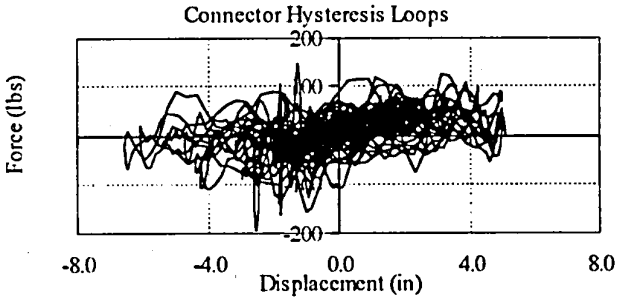

TEST RB-122
EQUIPMENT COMBINATION 2, BPA ISOLATOR
TABAS GROUND MOTION, 75% SPAN

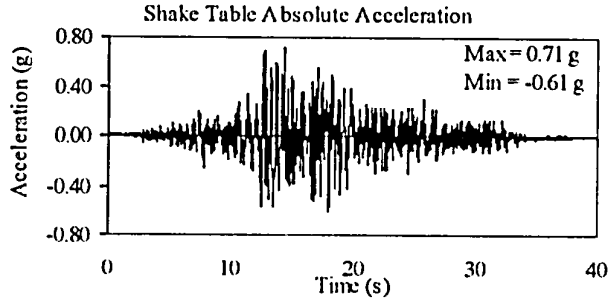

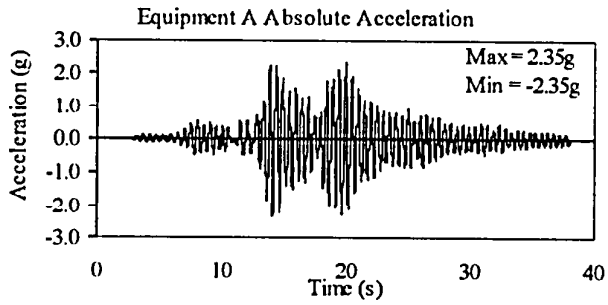

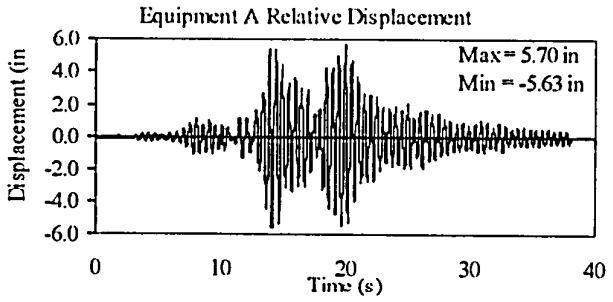

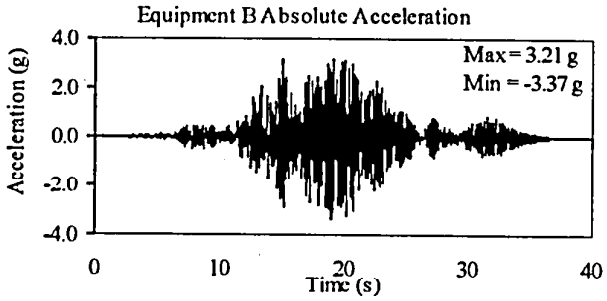

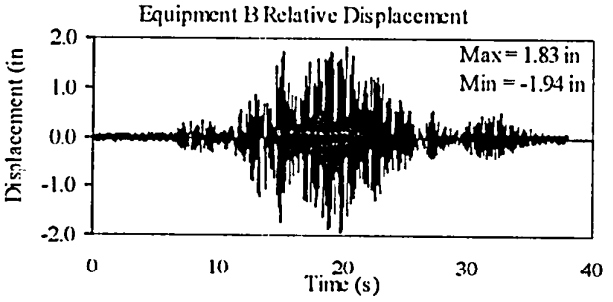

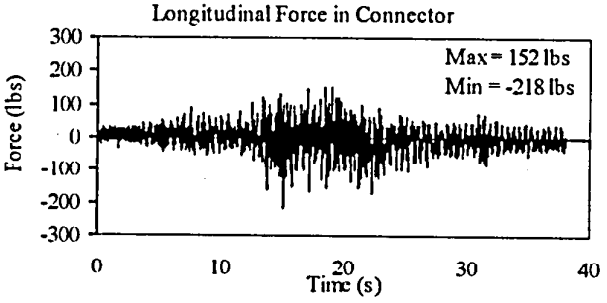

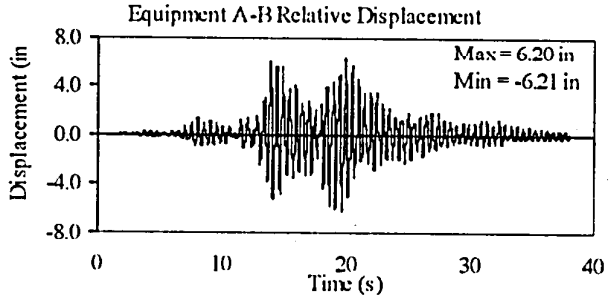

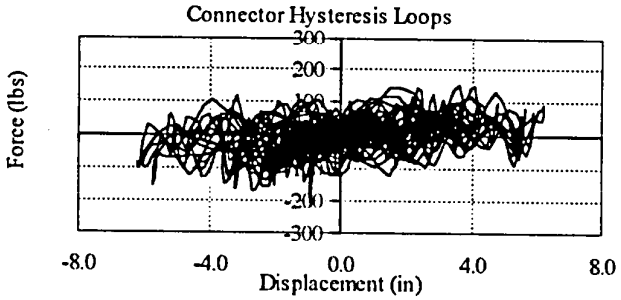

TEST RB-123
EQUIPMENT COMBINATION 2, BPA ISOLATOR
TABAS GROUND MOTION, 100% SPAN

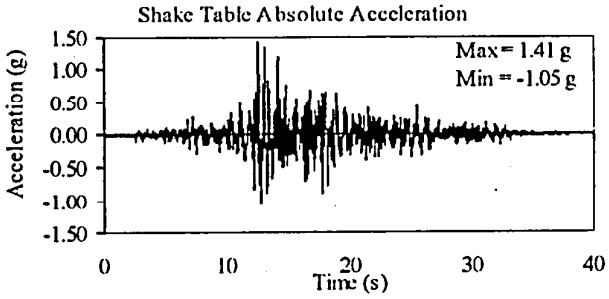

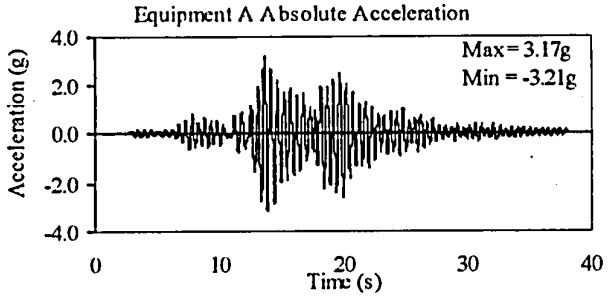

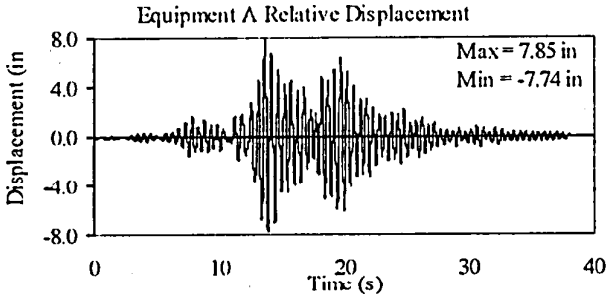

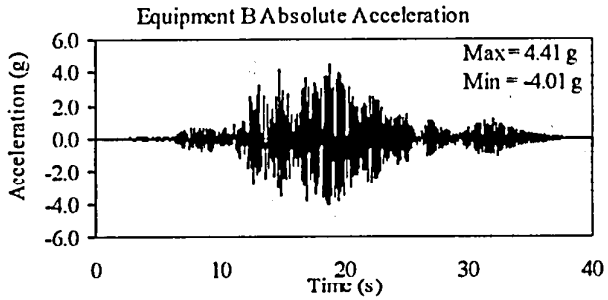

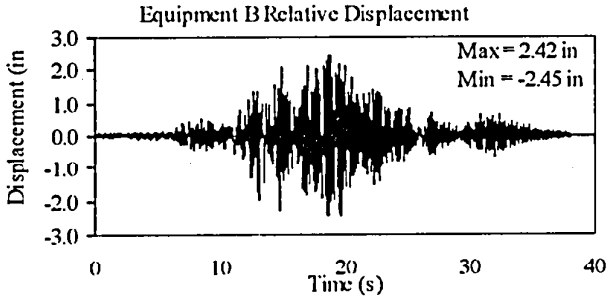

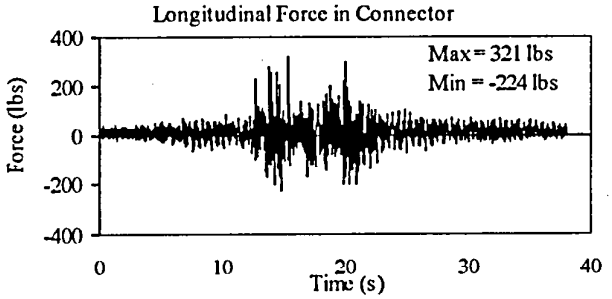

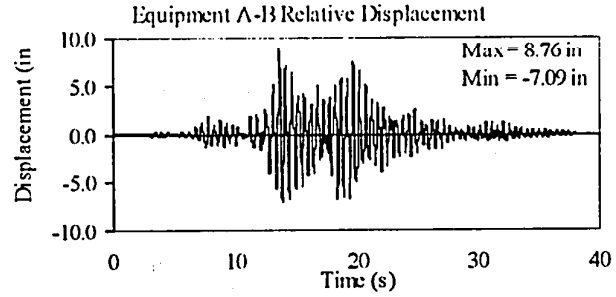

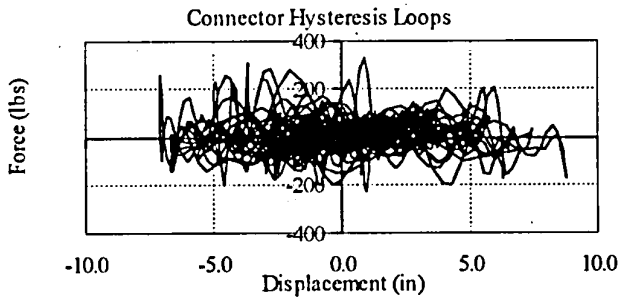

TEST RB-124
EQUIPMENT COMBINATION 2, INDIVIDUAL EQUIPMENT
NEWHALL GROUND MOTION, 30% SPAN

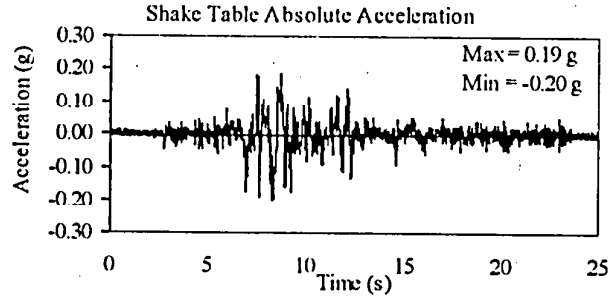

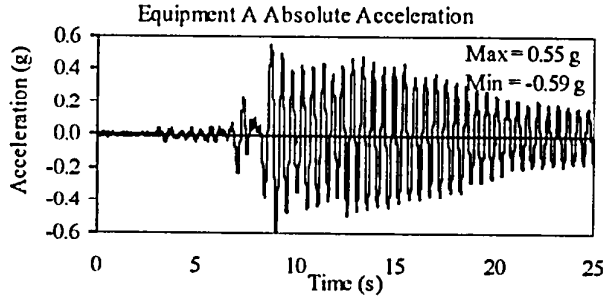

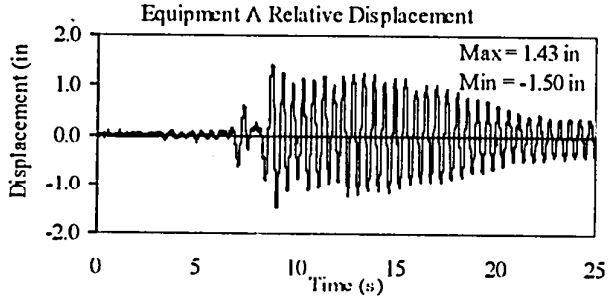

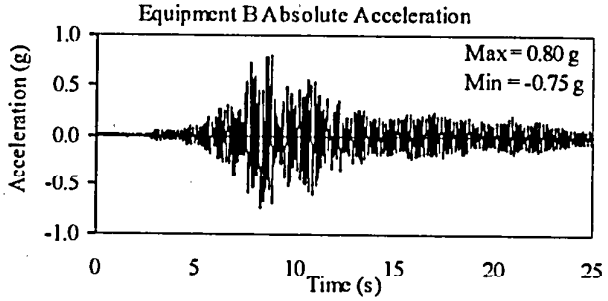

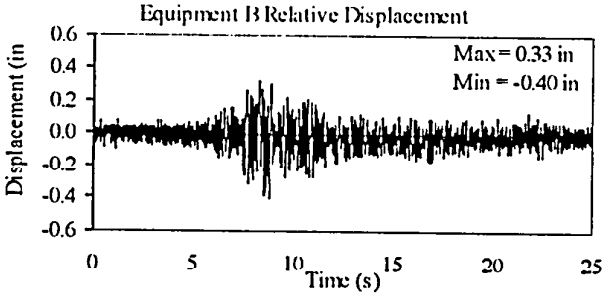

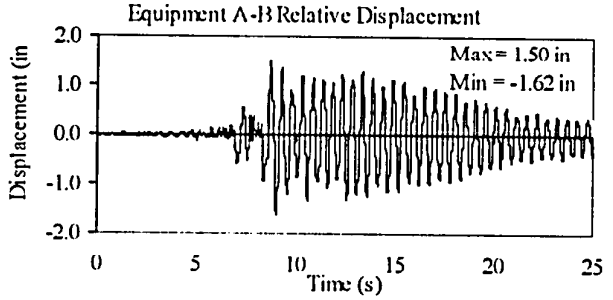

TEST RB-125
EQUIPMENT COMBINATION 2, INDIVIDUAL EQUIPMENT
TABAS GROUND MOTION, 25% SPAN

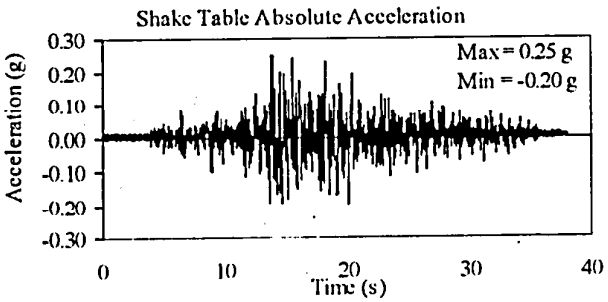

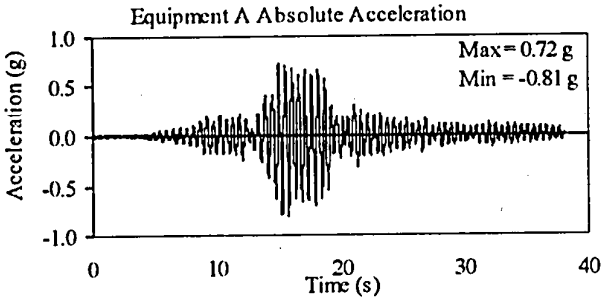

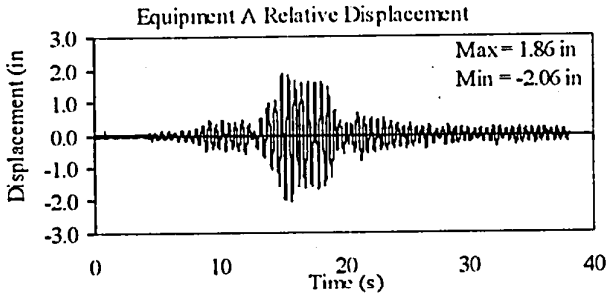

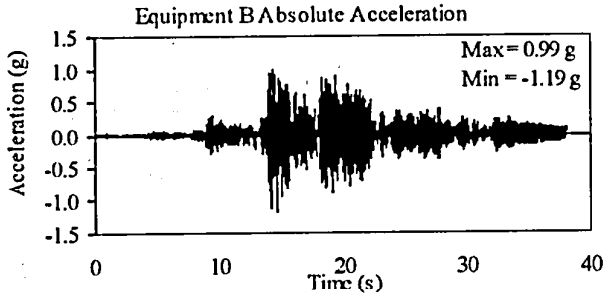

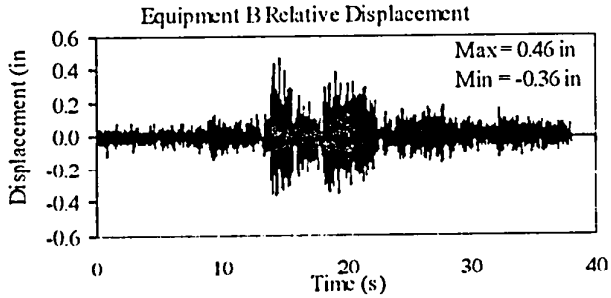

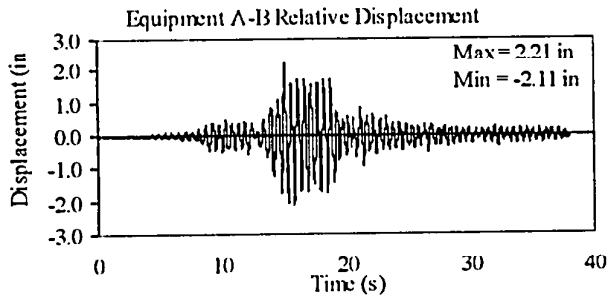

TEST RB-126
EQUIPMENT COMBINATION 2, INDIVIDUAL EQUIPMENT
TABAS GROUND MOTION, 50% SPAN

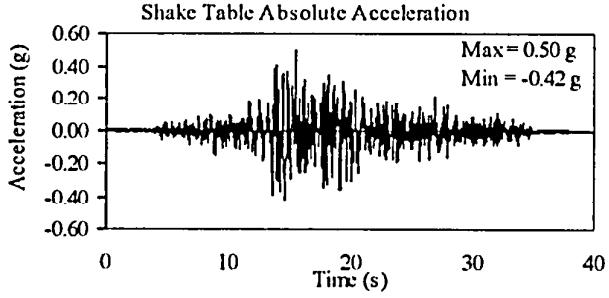

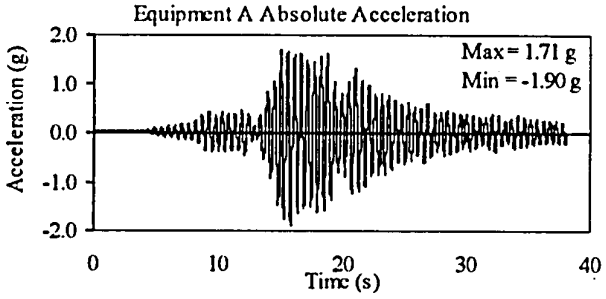

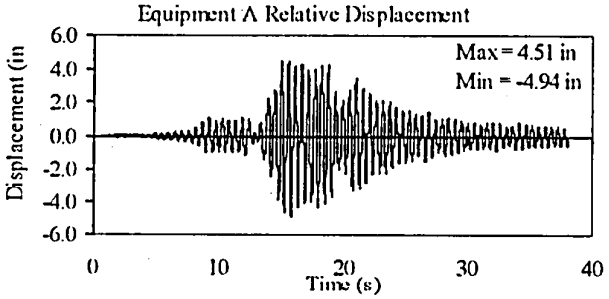

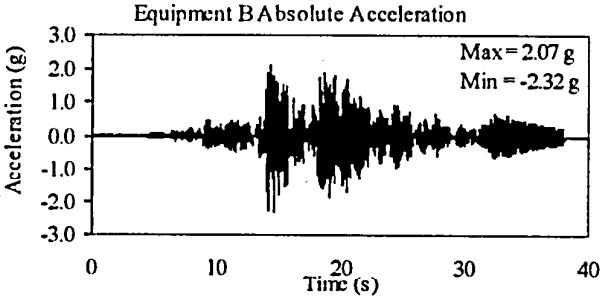

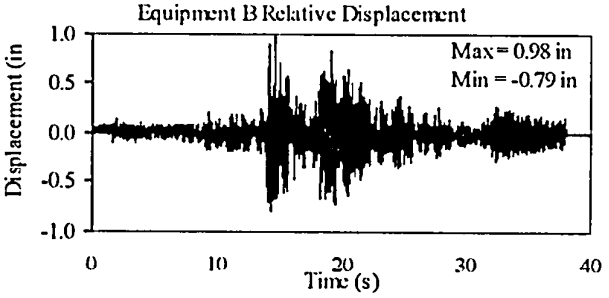

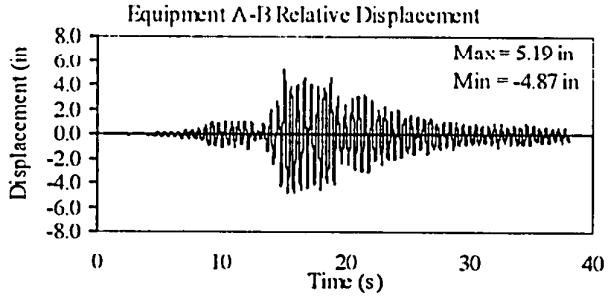

TEST RB-127
EQUIPMENT COMBINATION 2, INDIVIDUAL EQUIPMENT
NEWHALL GROUND MOTION, 100% SPAN

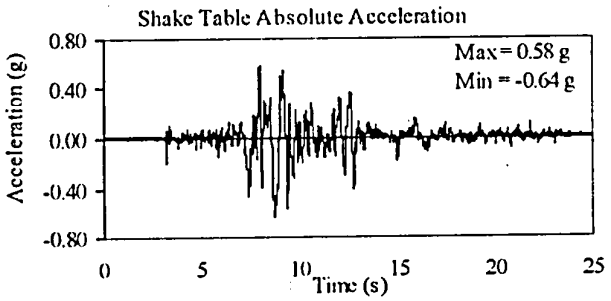

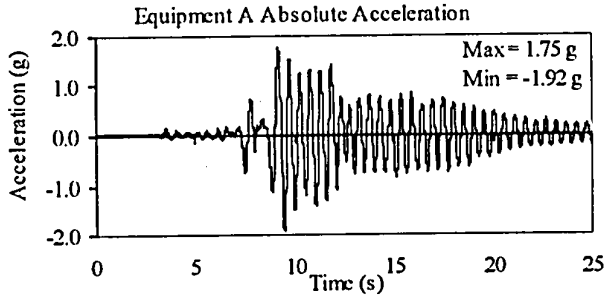

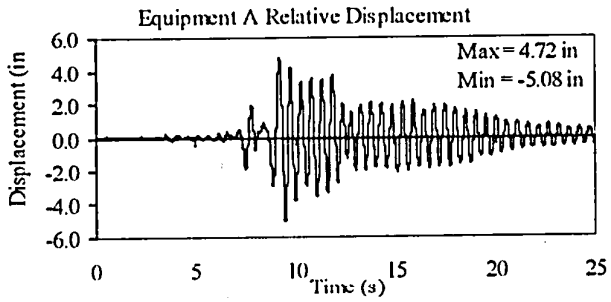

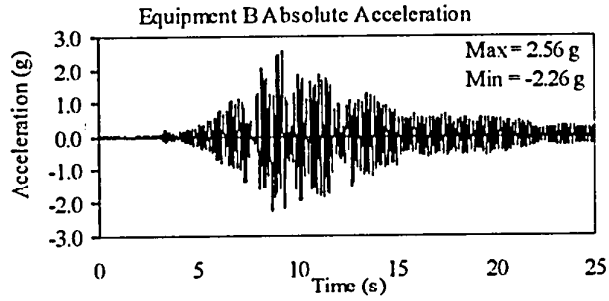

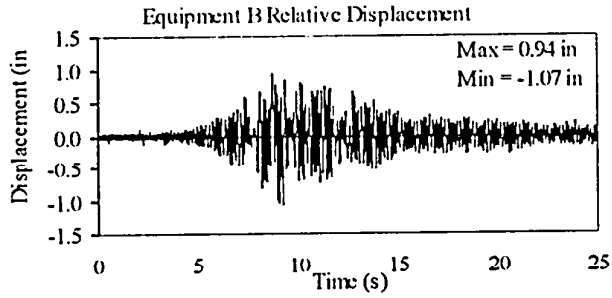

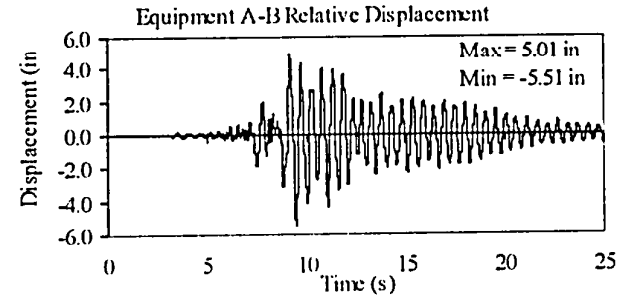

TEST RB-136
EQUIPMENT COMBINATION 5, SPRING 30-2022
NEWHALL GROUND MOTION, 30% SPAN

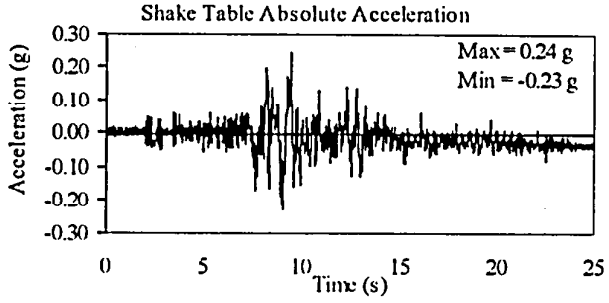

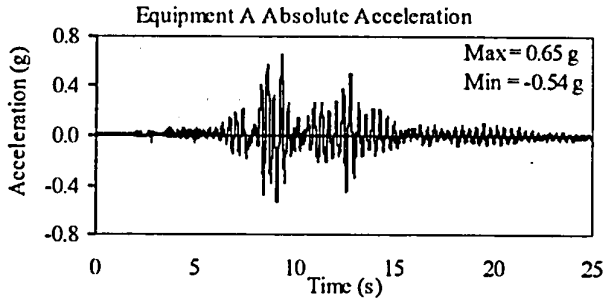

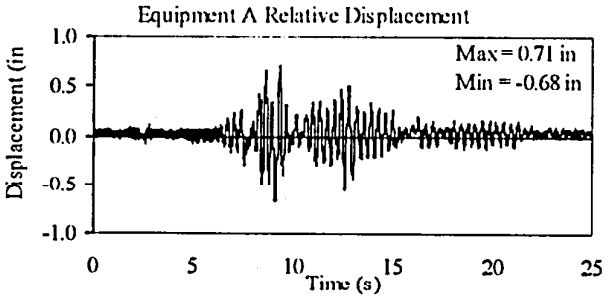

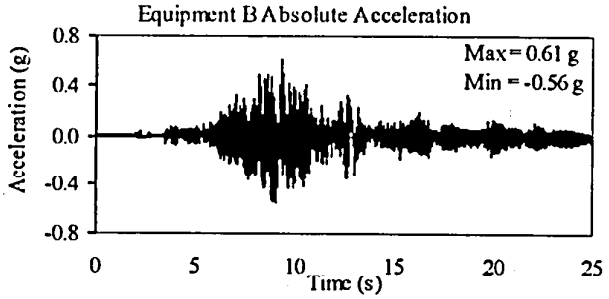

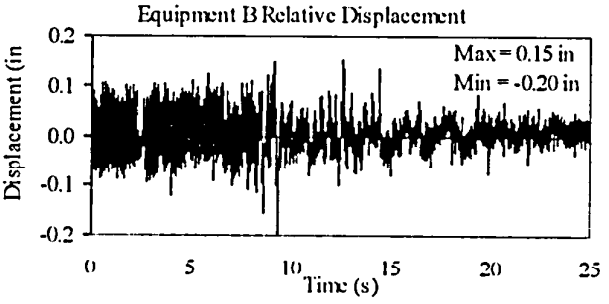

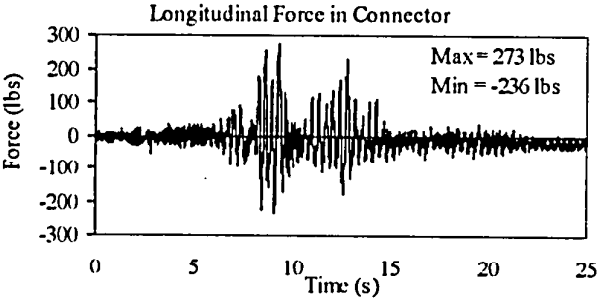

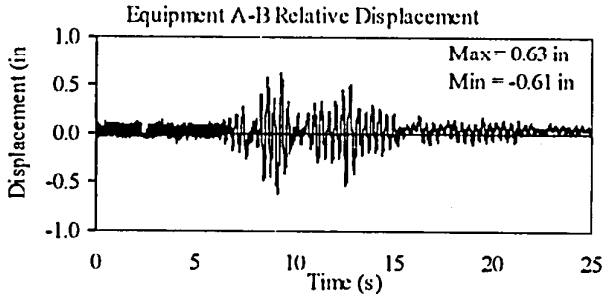

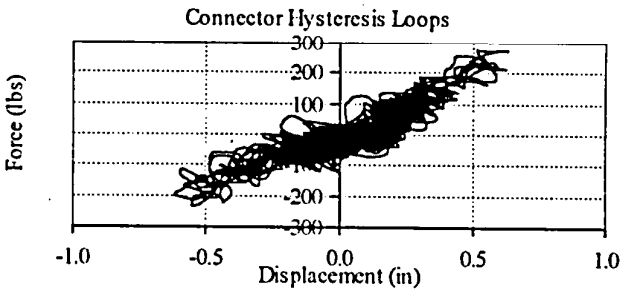

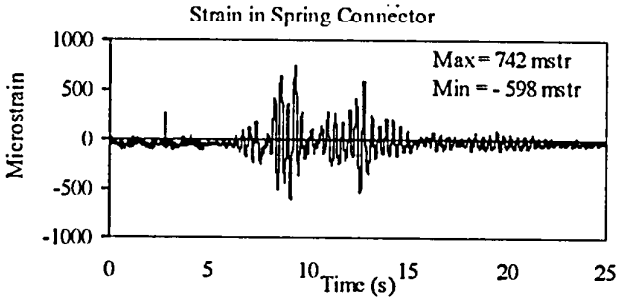

TEST RB-137
EQUIPMENT COMBINATION 5, SPRING 30-2022
TABAS GROUND MOTION, 25% SPAN

Shake Table Absolute Acceleration

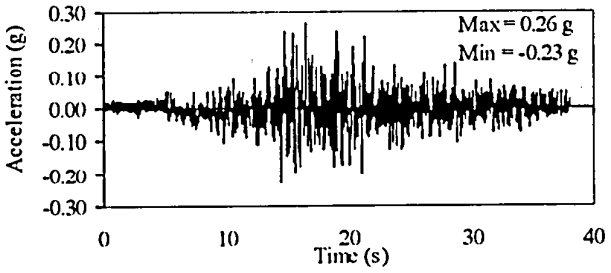

Equipment A Absolute Acceleration

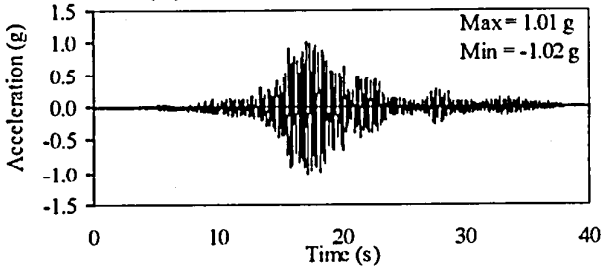

Equipment A Relative Displacement

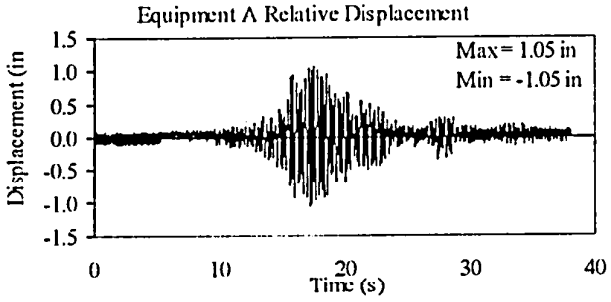

Equipment B Absolute Acceleration

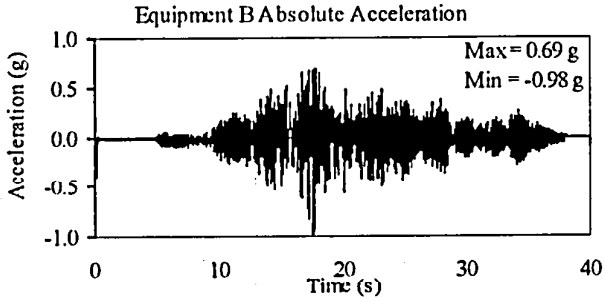

Equipment B Relative Displacement

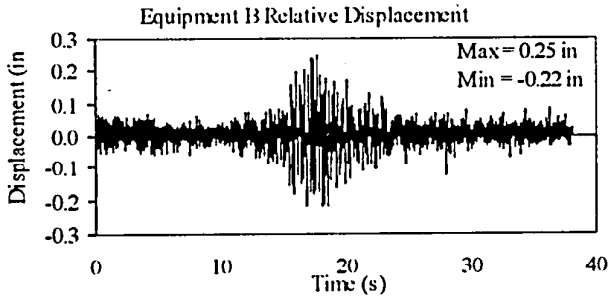

Longitudinal Force in Connector

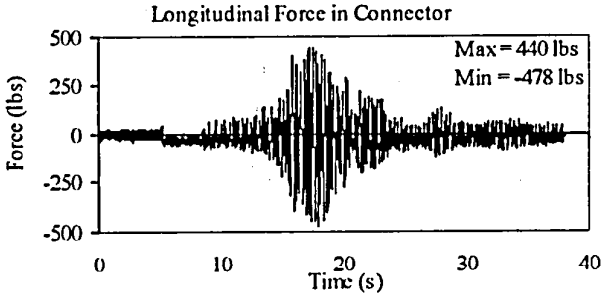

Equipment A-B Relative Displacement

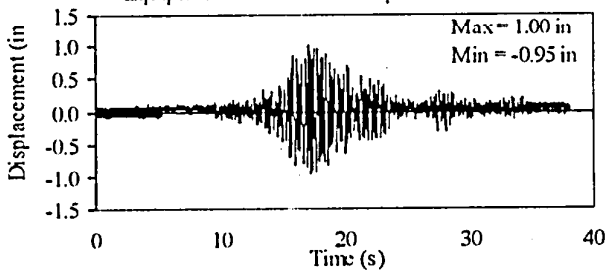

Connector Hysteresis Loops

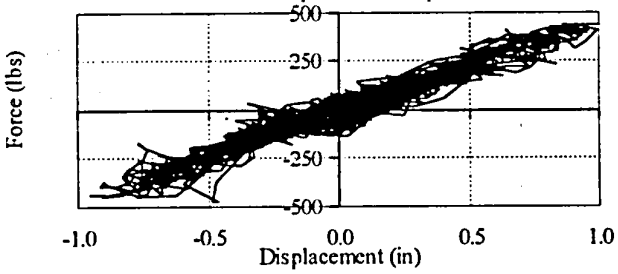

Strain in Spring Connector

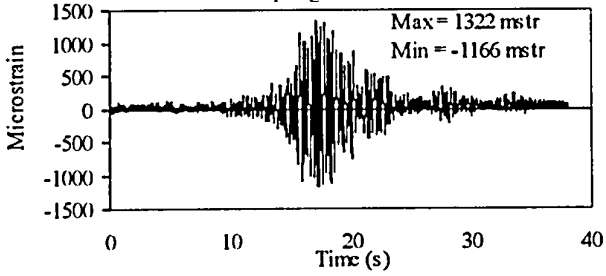

TEST RB-138
EQUIPMENT COMBINATION 5, SPRING 30-2022
TABAS GROUND MOTION, 50% SPAN

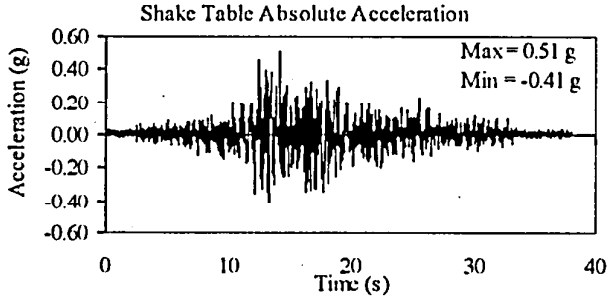

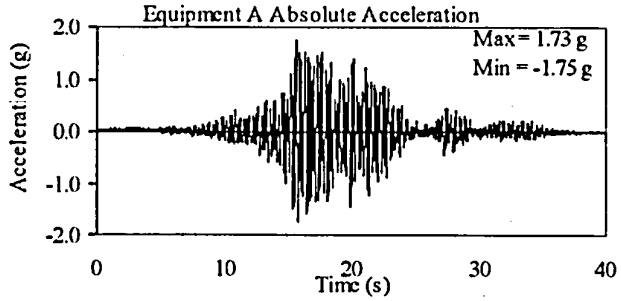

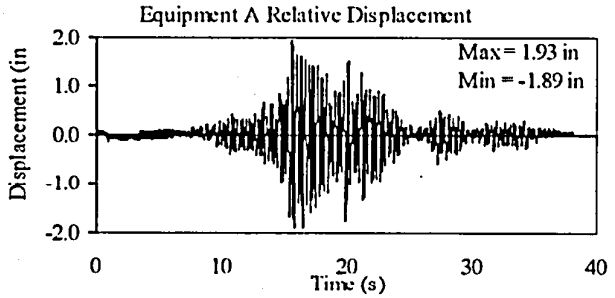

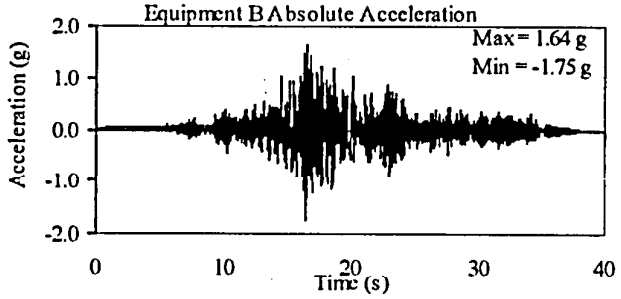

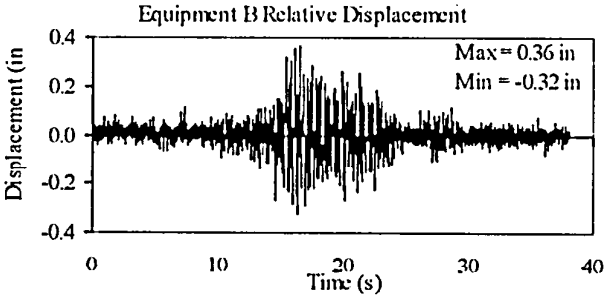

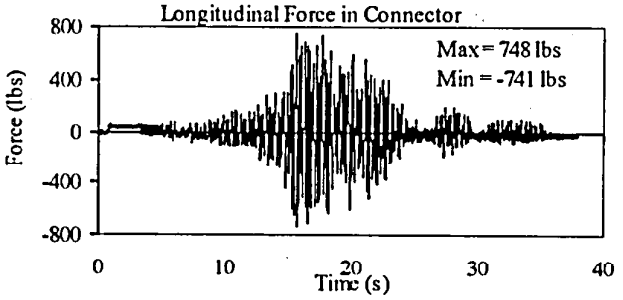

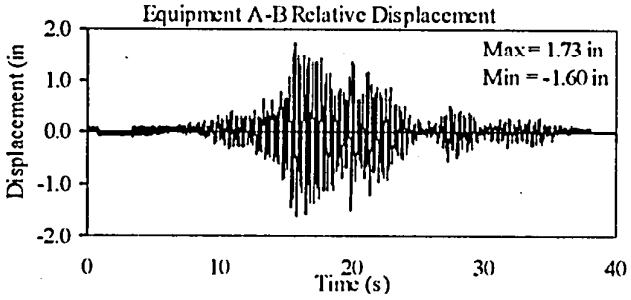

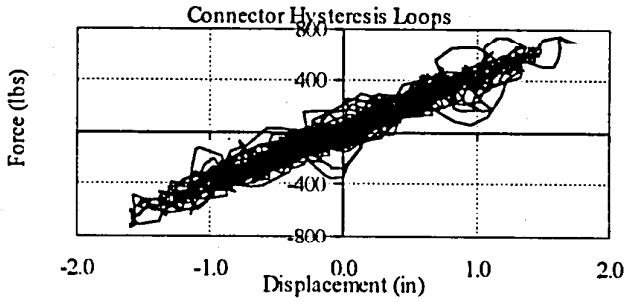

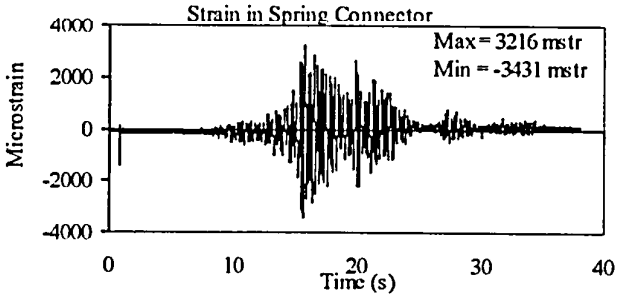

TEST RB-139
EQUIPMENT COMBINATION 5, SPRING 30-2022
NEWHALL GROUND MOTION, 100% SPAN

Shake Table Absolute Acceleration

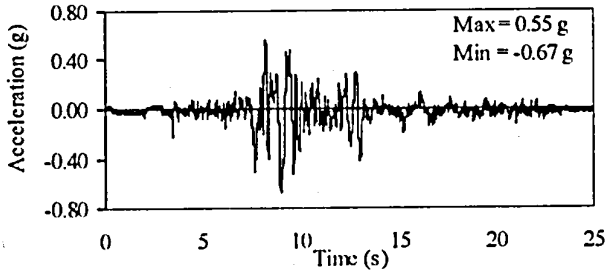

Equipment A Absolute Acceleration

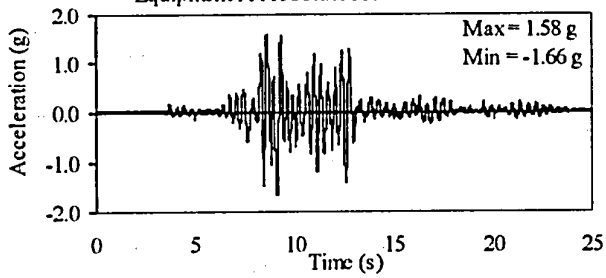

Equipment A Relative Displacement

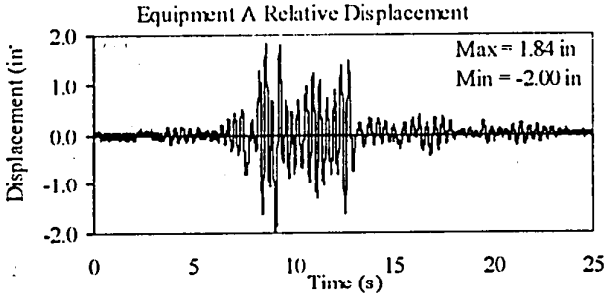

Equipment B Absolute Acceleration

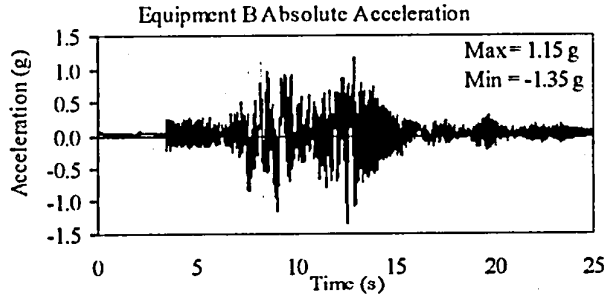

Equipment B Relative Displacement

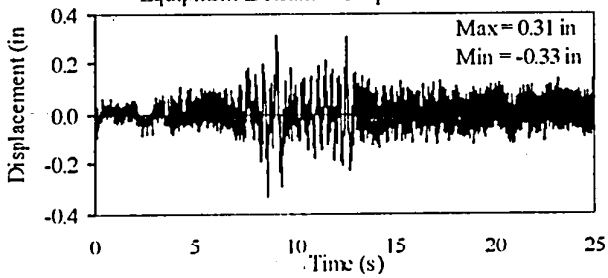

Longitudinal Force in Connector

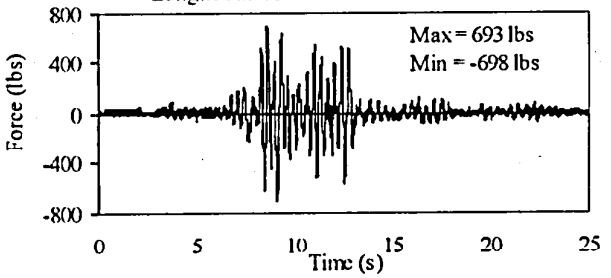

Equipment A-B Relative Displacement

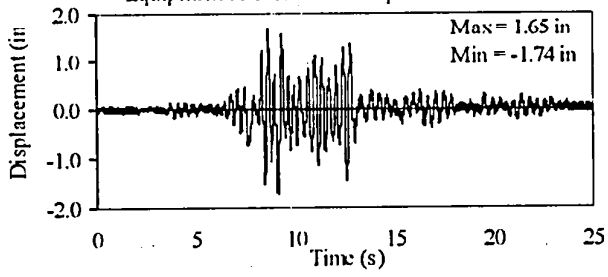

Connector Hysteresis Loops

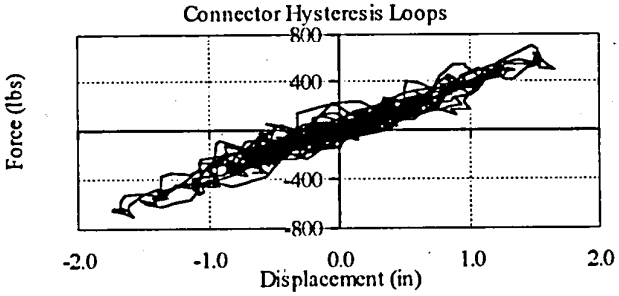

Strain in Spring Connector

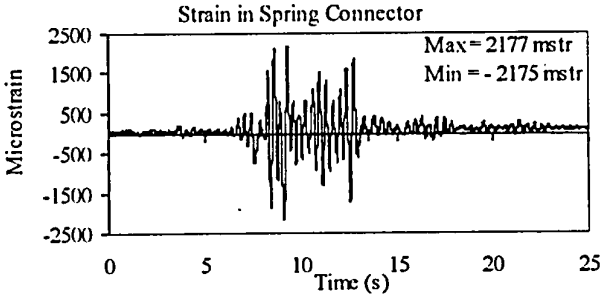

TEST RB-140
EQUIPMENT COMBINATION 5, SPRING 30-2022
TABAS GROUND MOTION, 100% SPAN

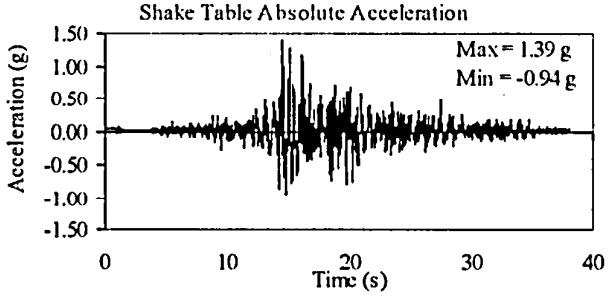

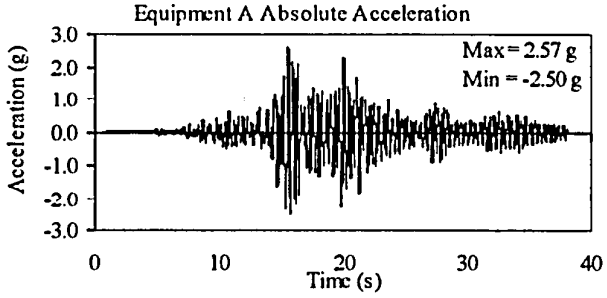

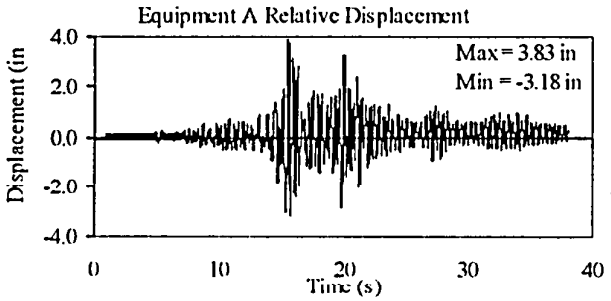

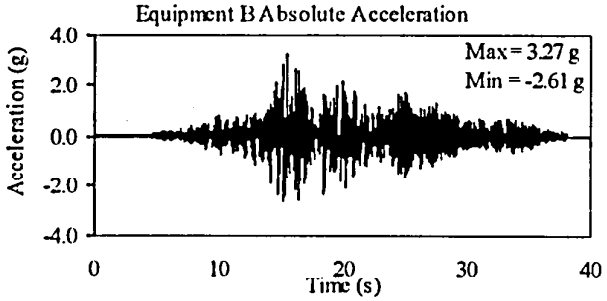

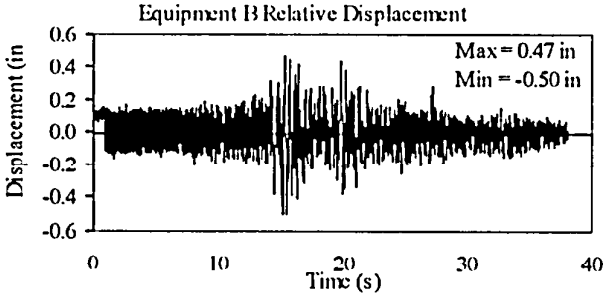

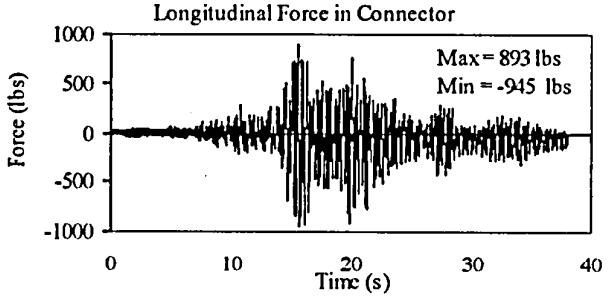

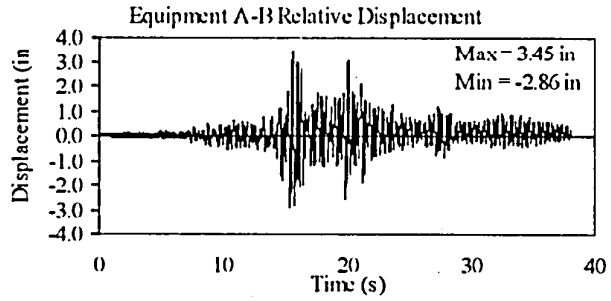

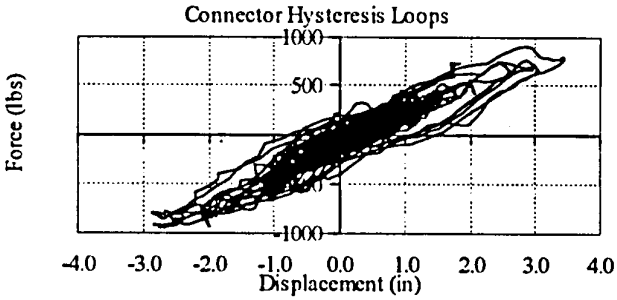

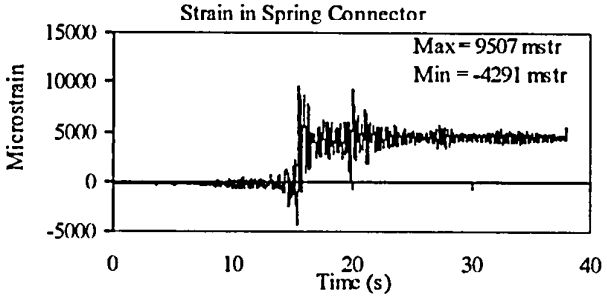

TEST RB-141
EQUIPMENT COMBINATION 5, SPRING 30-2022
TABAS GROUND MOTION, 150% SPAN

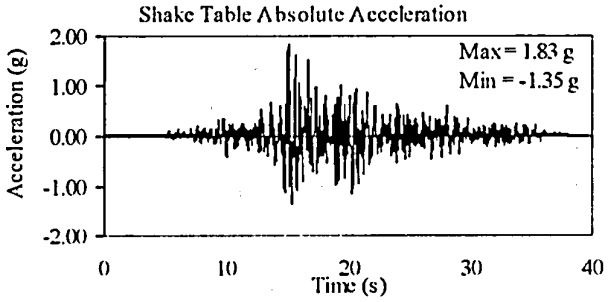

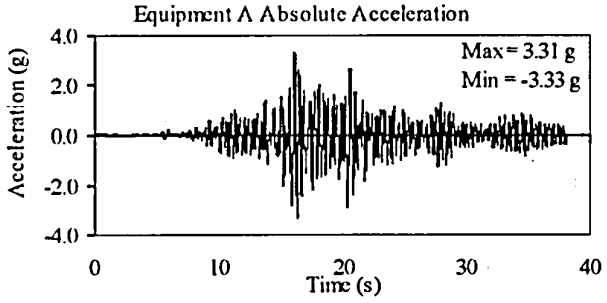

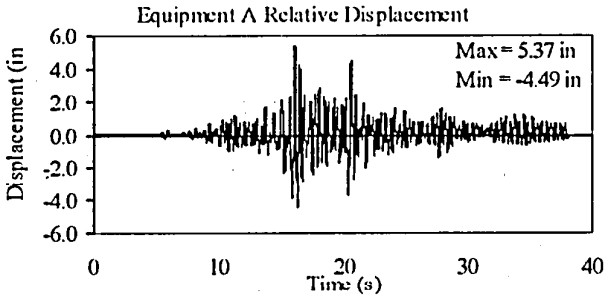

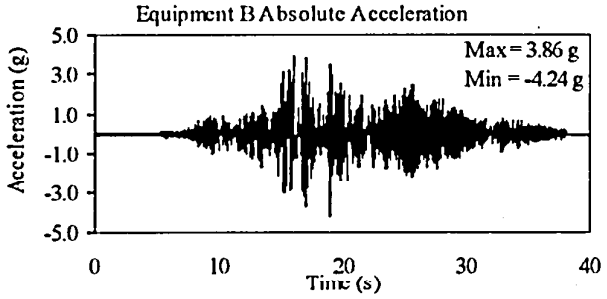

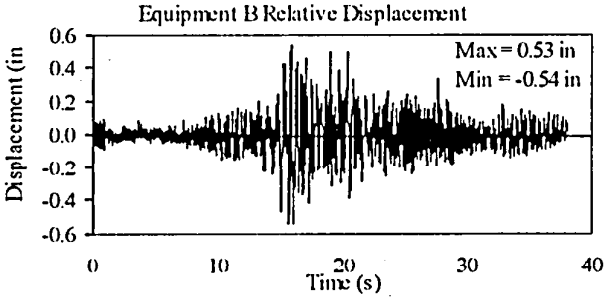

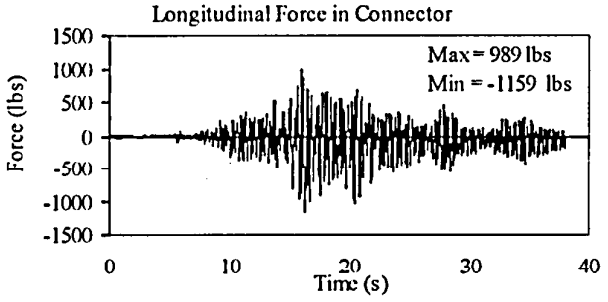

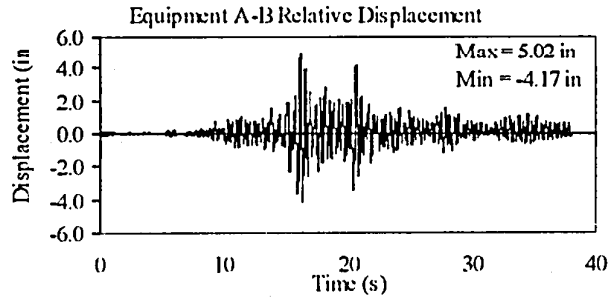

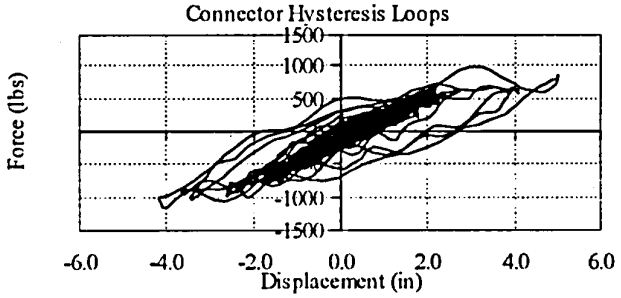

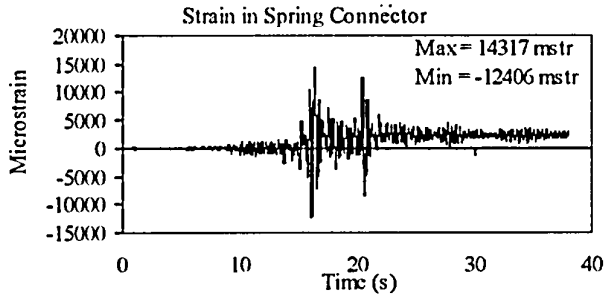

TEST RB-144
EQUIPMENT COMBINATION 5, BUS SLIDER
NEWHALL GROUND MOTION, 30% SPAN

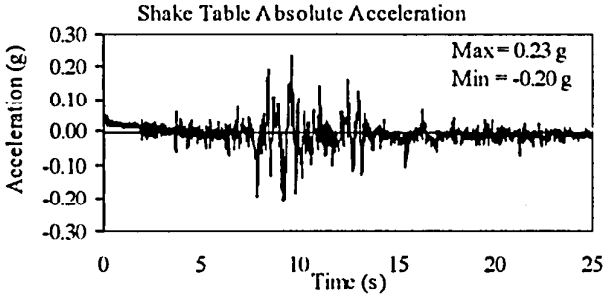

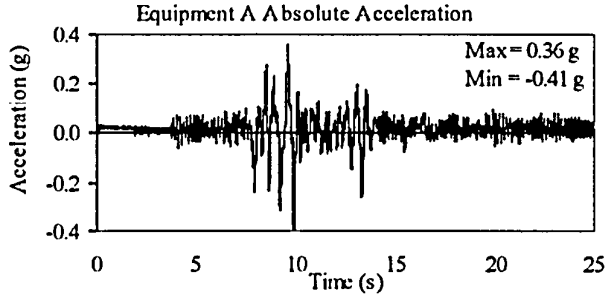

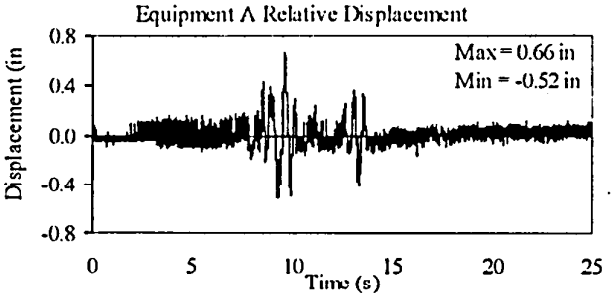

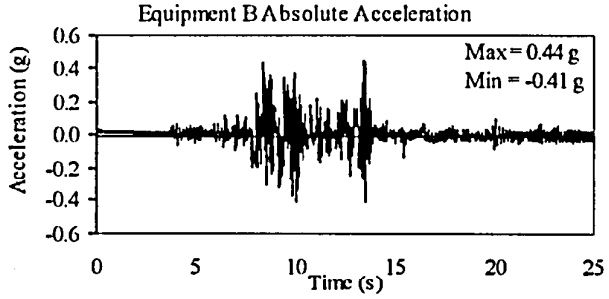

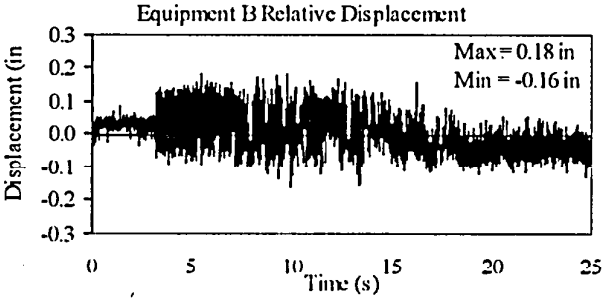

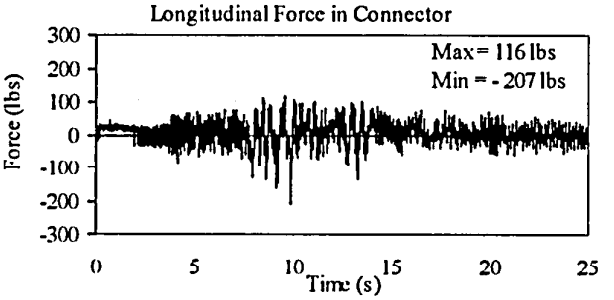

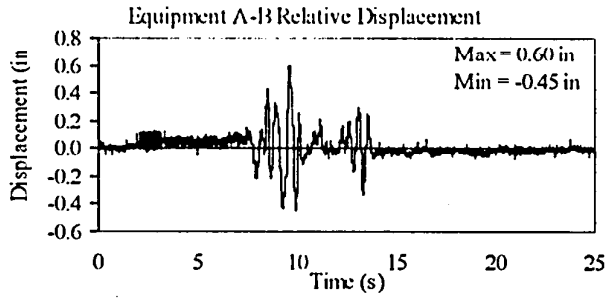

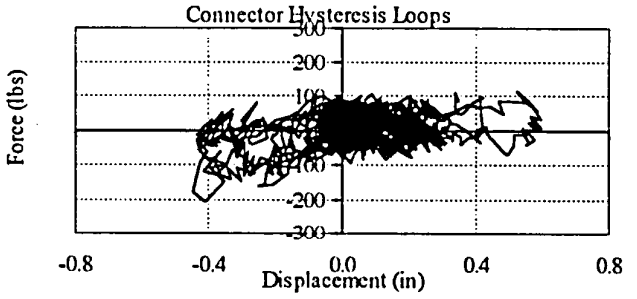

TEST RB-145
EQUIPMENT COMBINATION 5, BUS SLIDER
TABAS GROUND MOTION, 25% SPAN

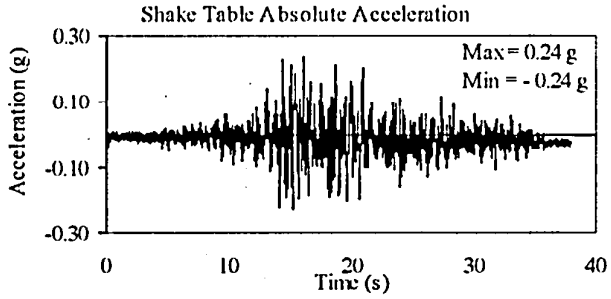

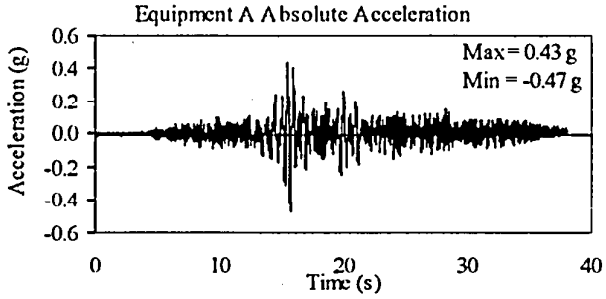

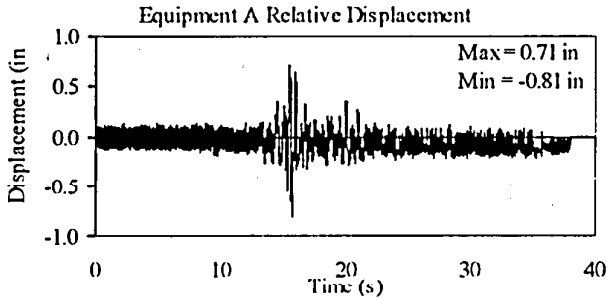

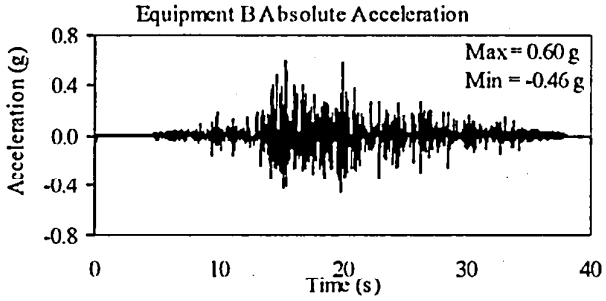

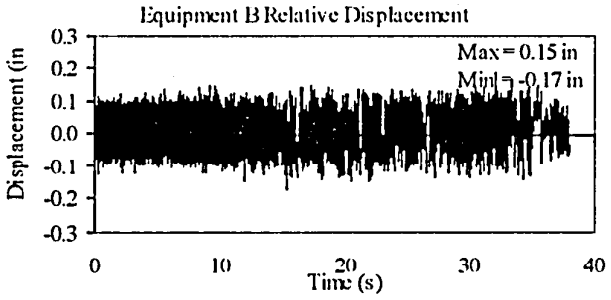

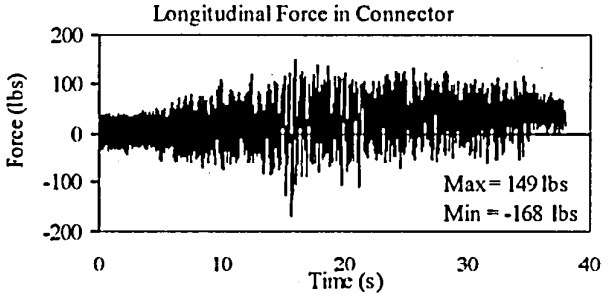

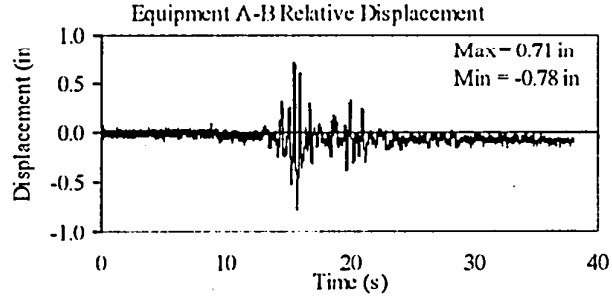

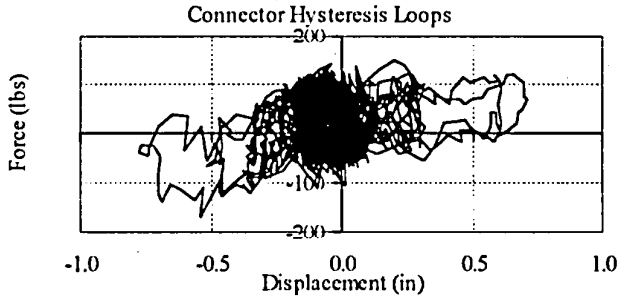

TEST RB-146
EQUIPMENT COMBINATION 5, BUS SLIDER
TABAS GROUND MOTION, 50% SPAN

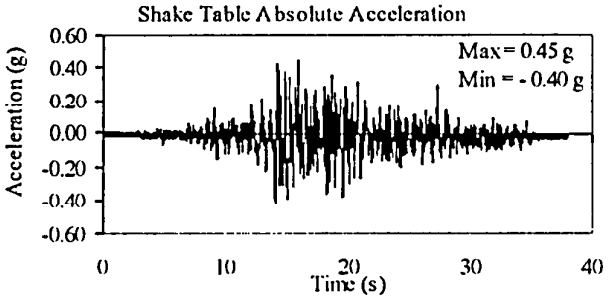

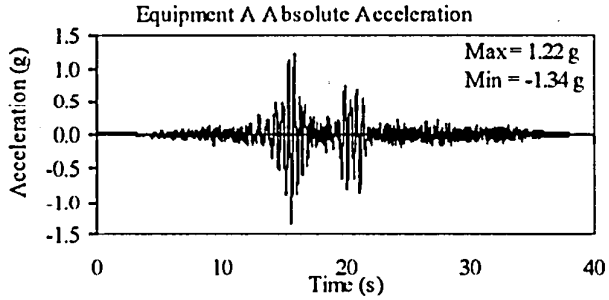

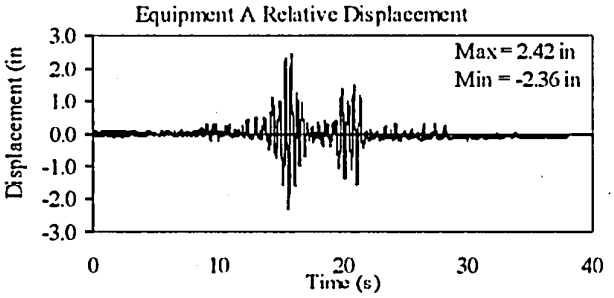

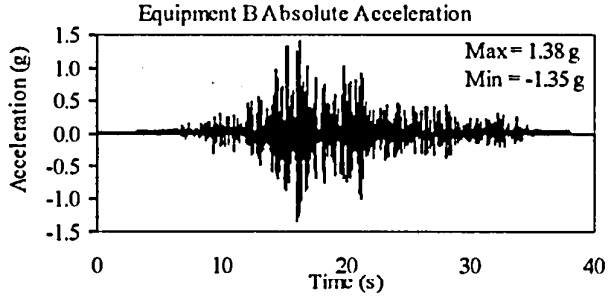

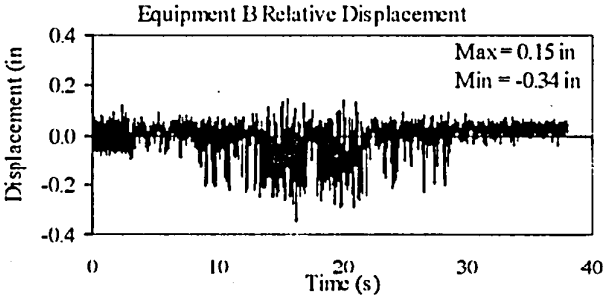

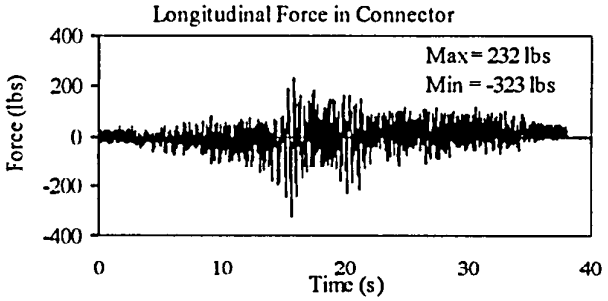

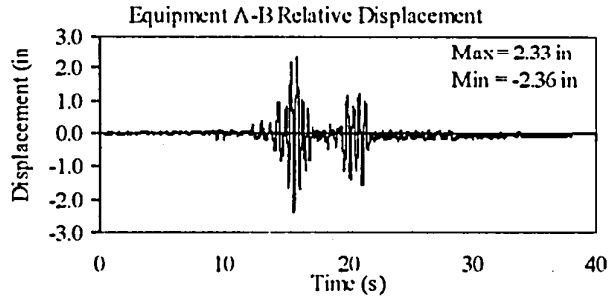

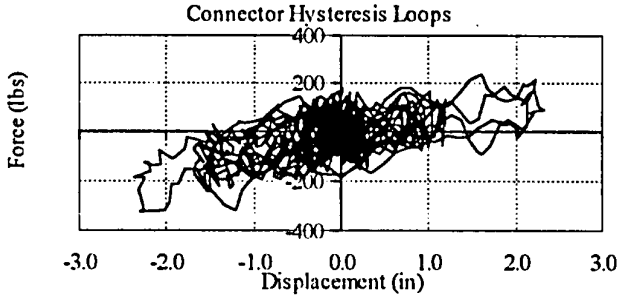

TEST RB-147
EQUIPMENT COMBINATION 5, BUS SLIDER
NEWHALL GROUND MOTION, 100% SPAN

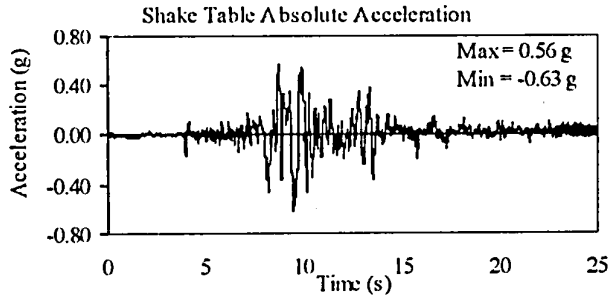

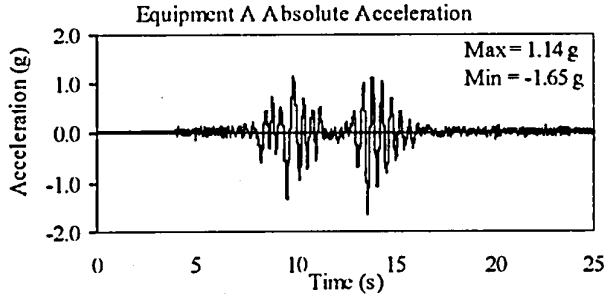

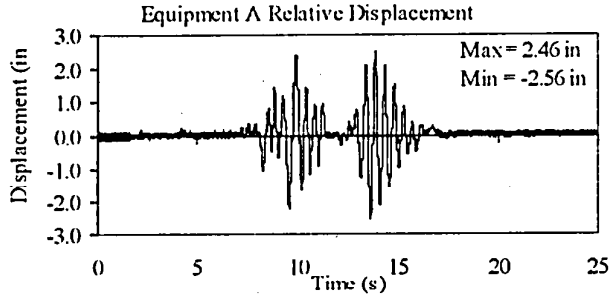

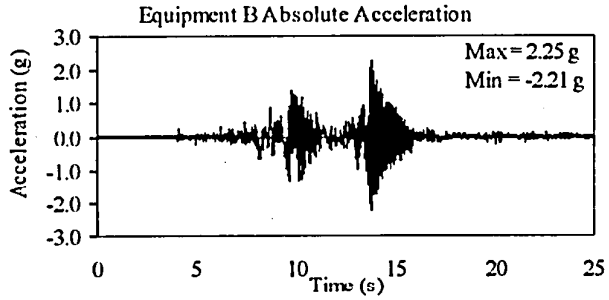

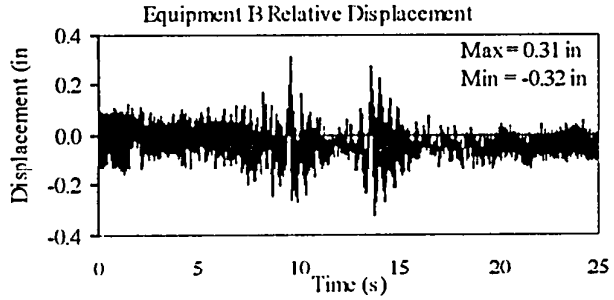

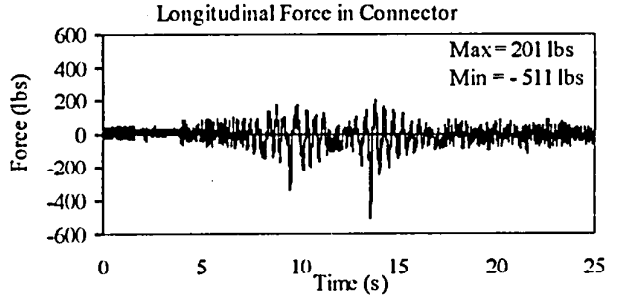

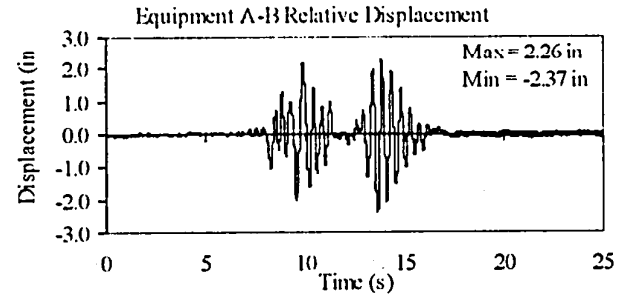

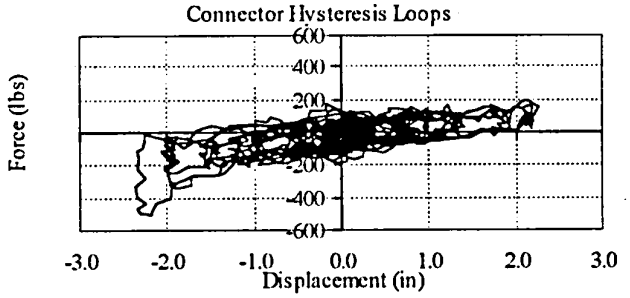

TEST RB-148
EQUIPMENT COMBINATION 5, BUS SLIDER
TABAS GROUND MOTION, 100% SPAN

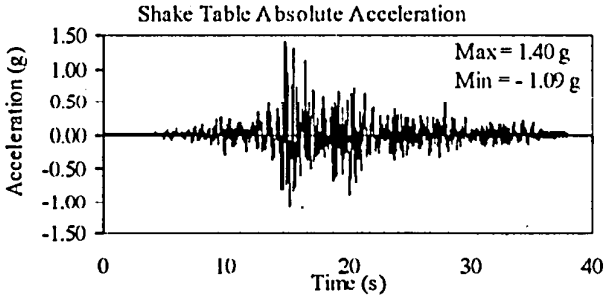

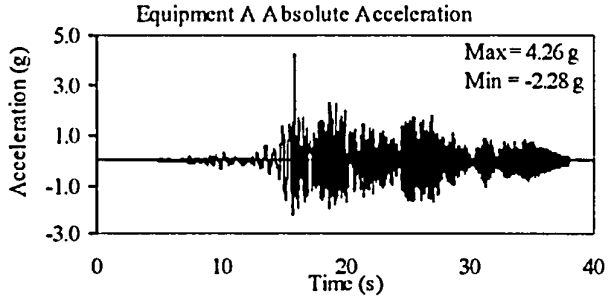

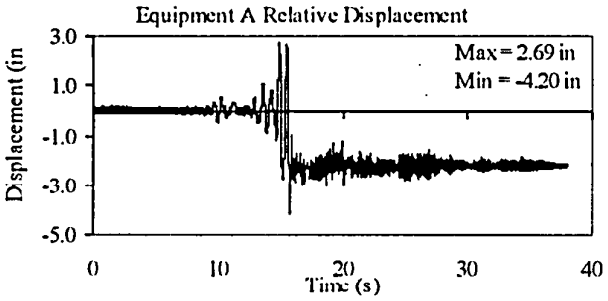

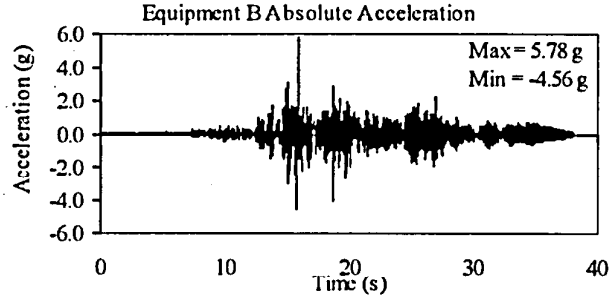

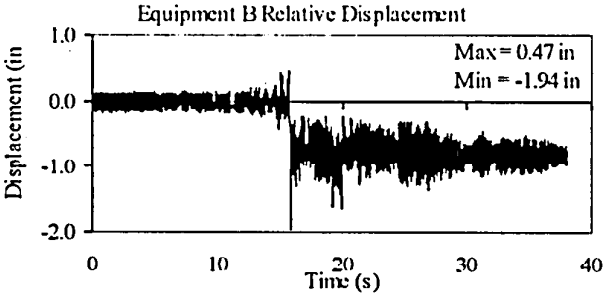

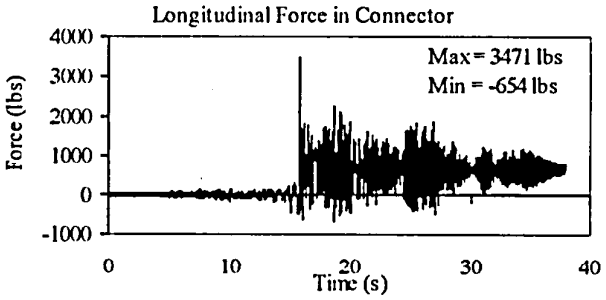

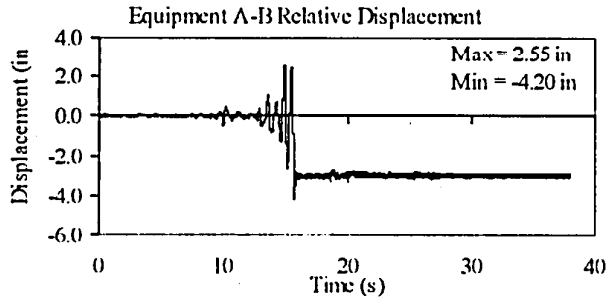

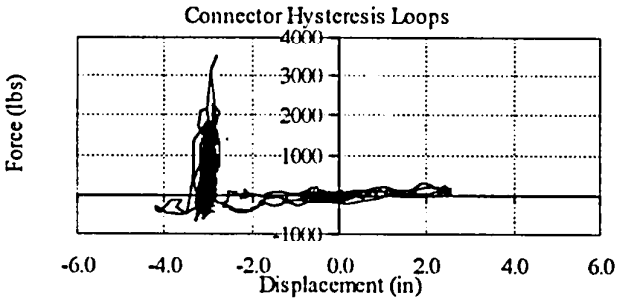

TEST RB-152
EQUIPMENT COMBINATION 5, BPA ISOLATOR
NEWHALL GROUND MOTION, 30% SPAN

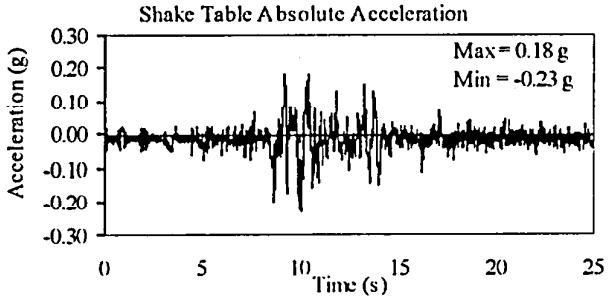

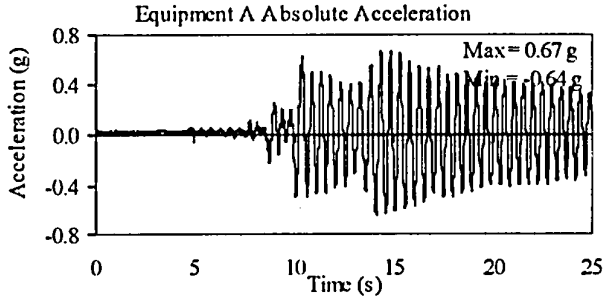

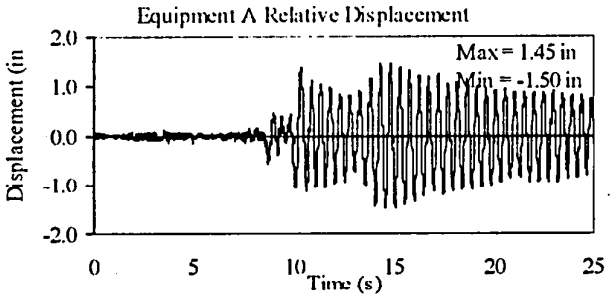

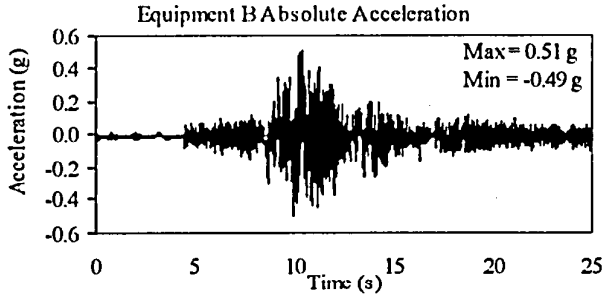

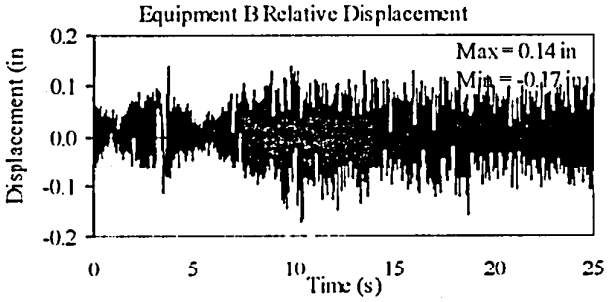

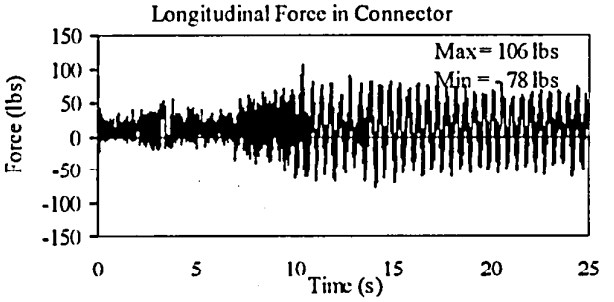

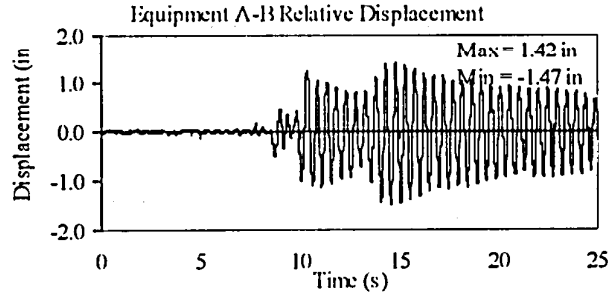

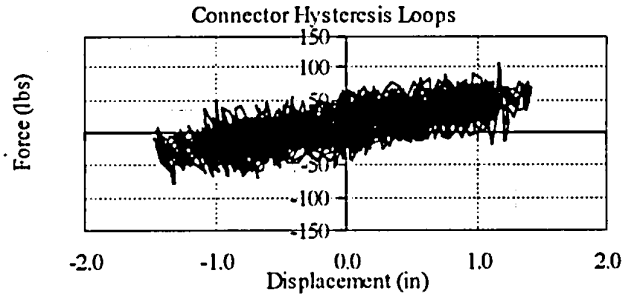

TEST RB-153
EQUIPMENT COMBINATION 5, BPA ISOLATOR
TABAS GROUND MOTION, 25% SPAN

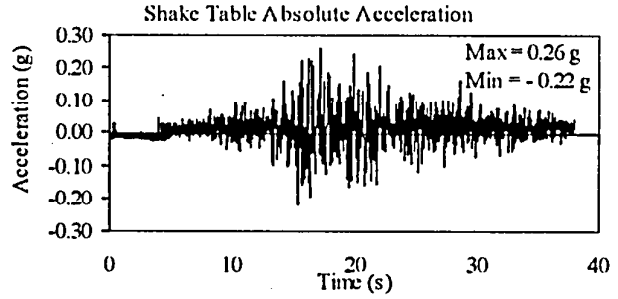

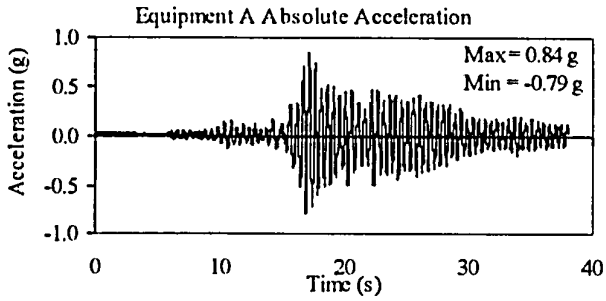

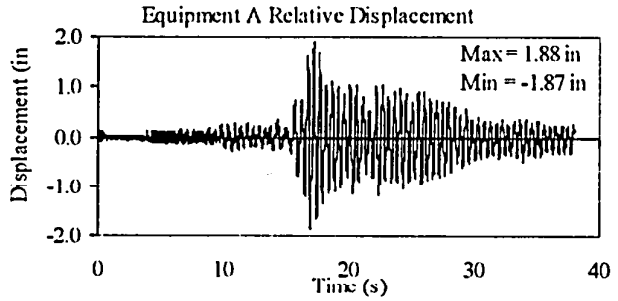

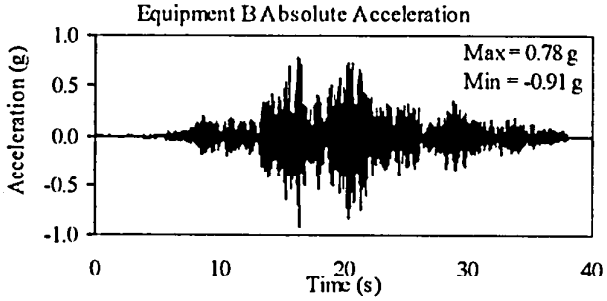

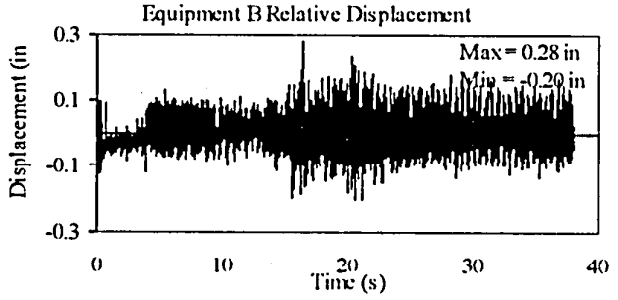

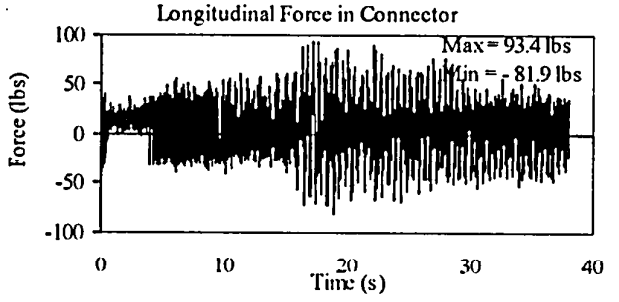

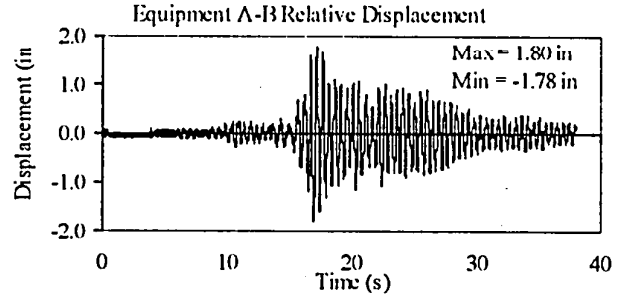

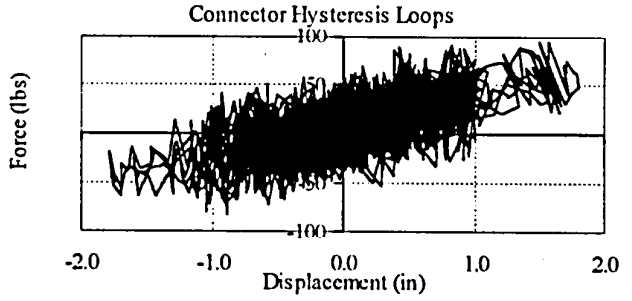

TEST RB-154
EQUIPMENT COMBINATION 5, BPA ISOLATOR
TABAS GROUND MOTION, 50% SPAN

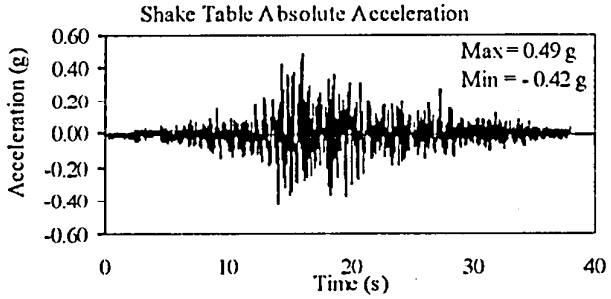

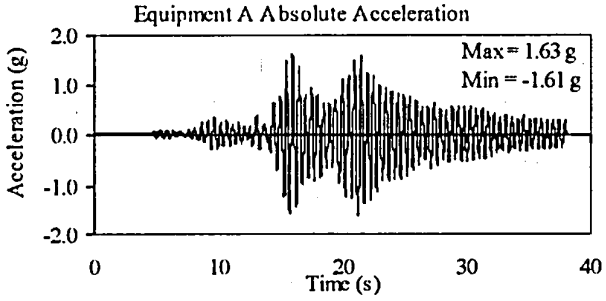

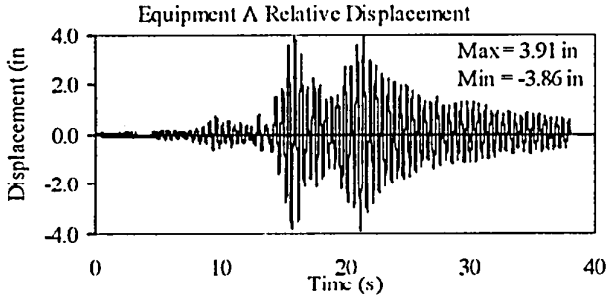

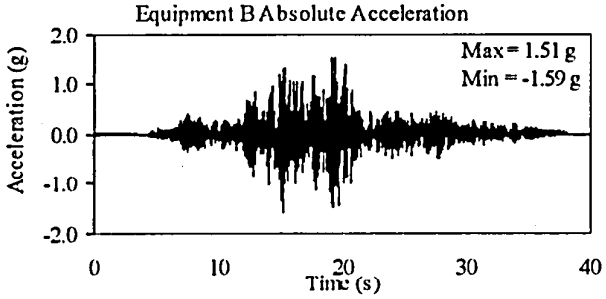

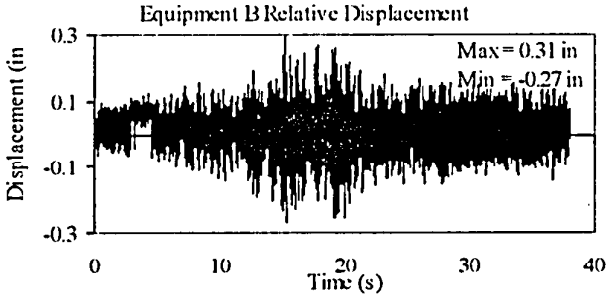

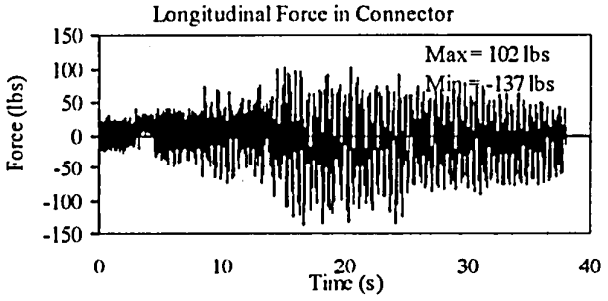

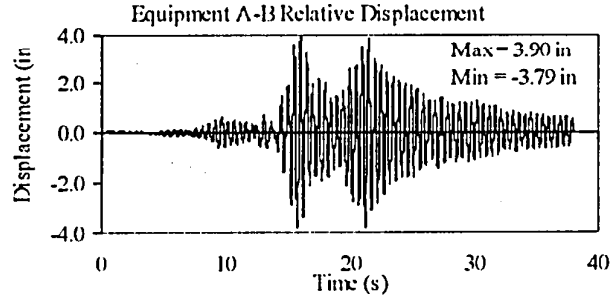

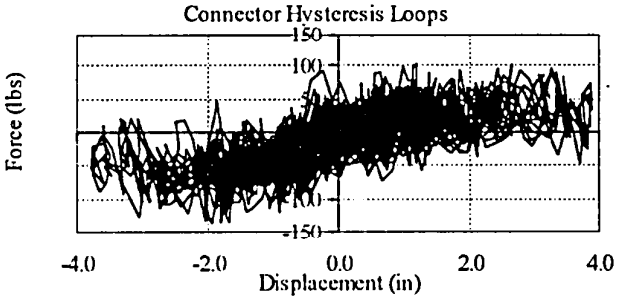

TEST RB-155
EQUIPMENT COMBINATION 5, BPA ISOLATOR
NEWHALL GROUND MOTION, 100% SPAN

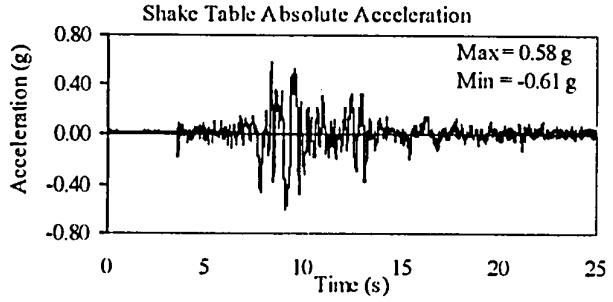

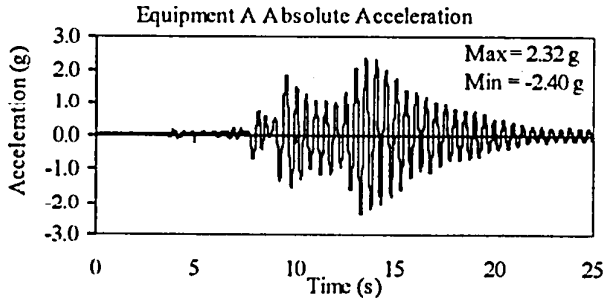

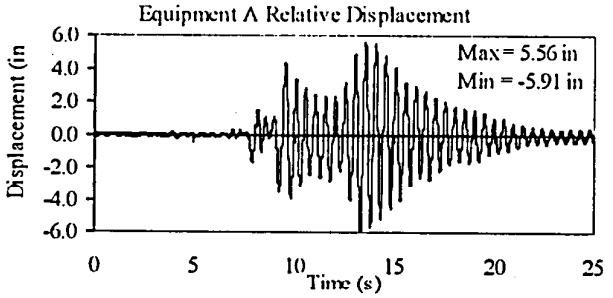

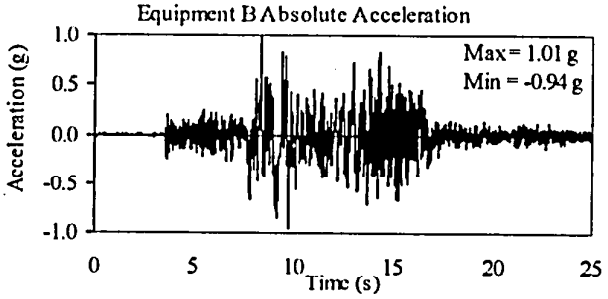

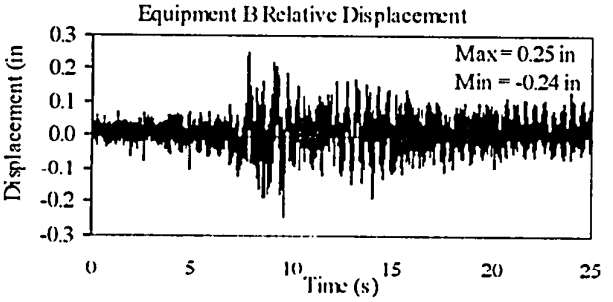

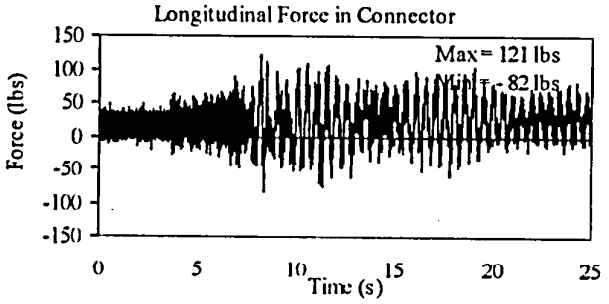

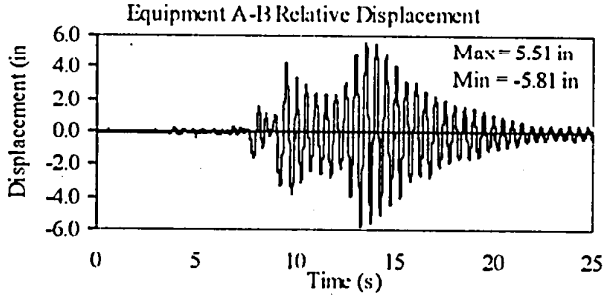

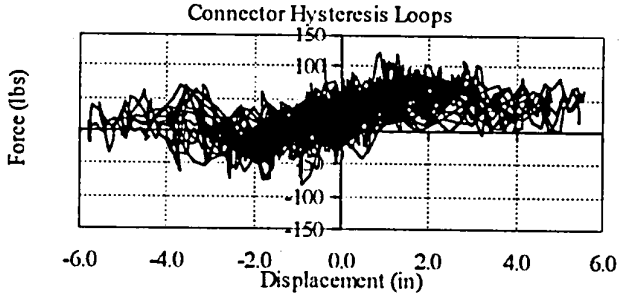

TEST RB-156
EQUIPMENT COMBINATION 5, BPA ISOLATOR
TABAS GROUND MOTION, 100% SPAN

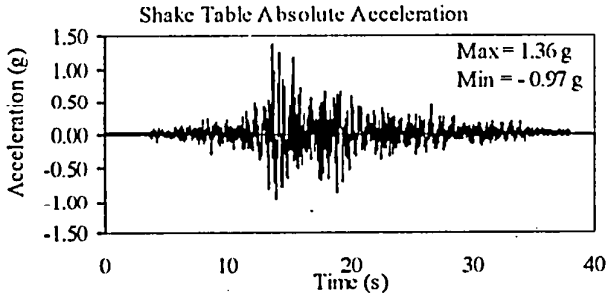

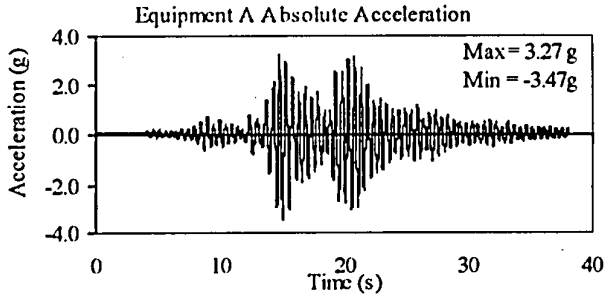

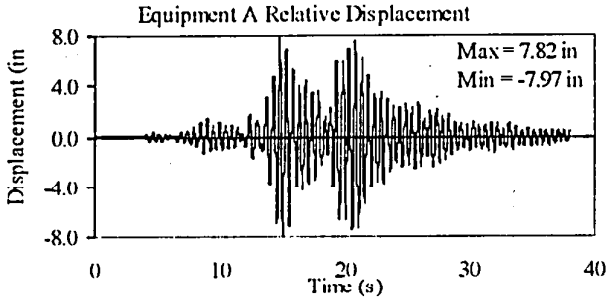

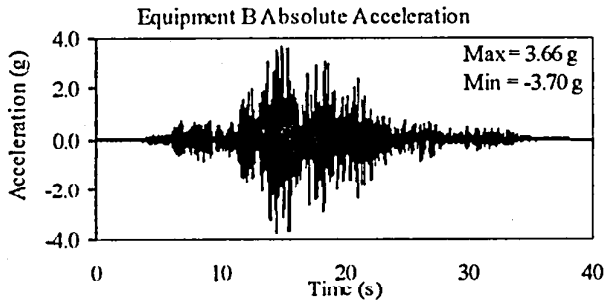

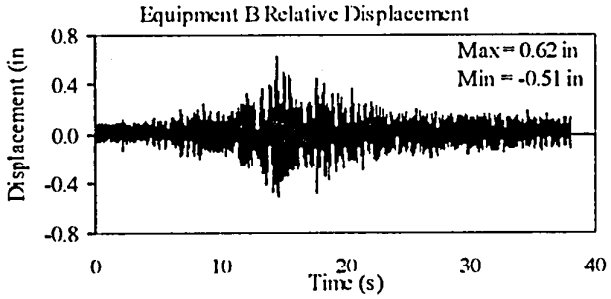

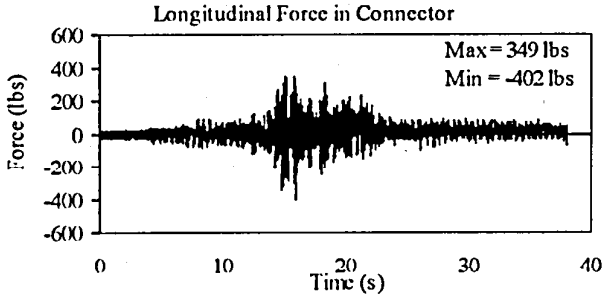

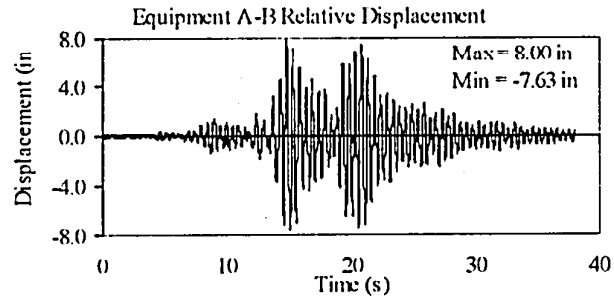

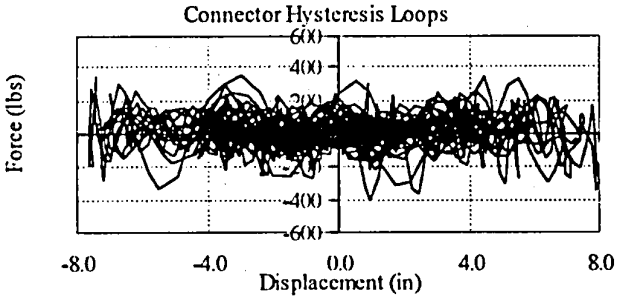

TEST RB-158
EQUIPMENT COMBINATION 5, INDIVIDUAL EQUIPMENT
NEWHALL GROUND MOTION, 30% SPAN

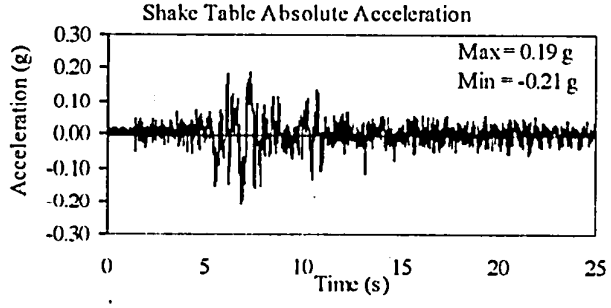

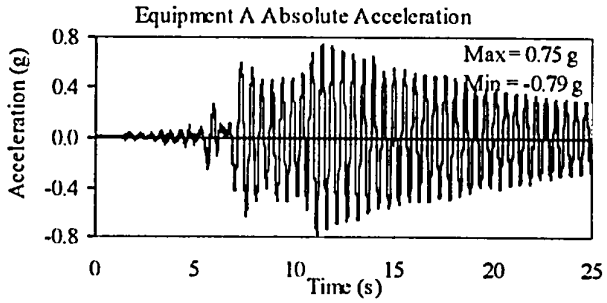

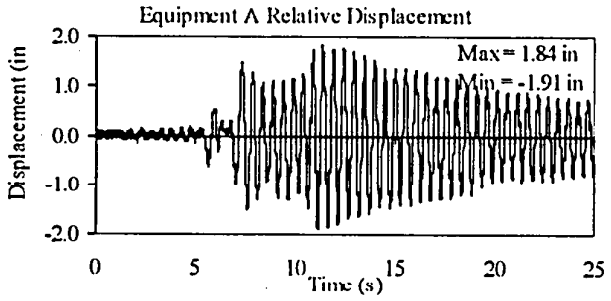

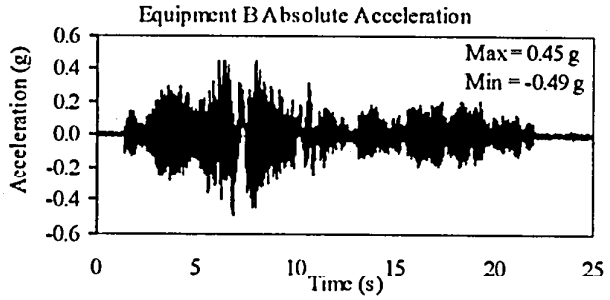

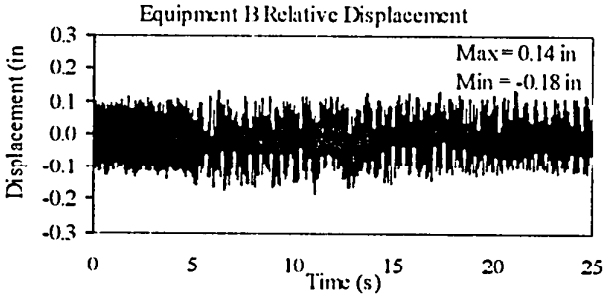

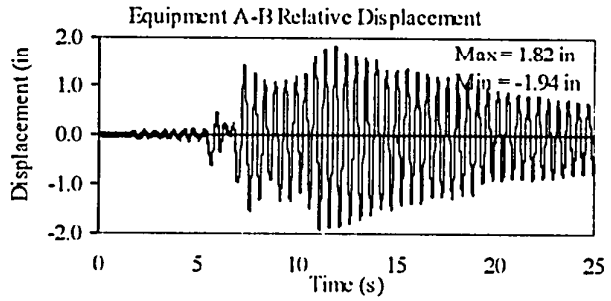

TEST RB-159
EQUIPMENT COMBINATION 5, INDIVIDUAL EQUIPMENT
TABAS GROUND MOTION, 25% SPAN

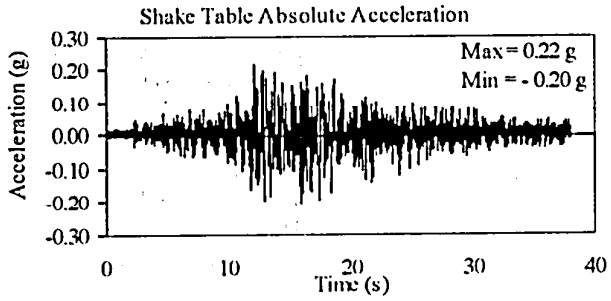

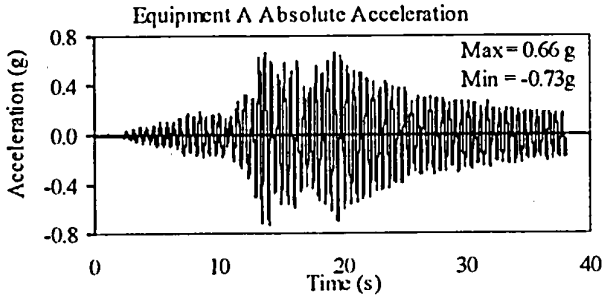

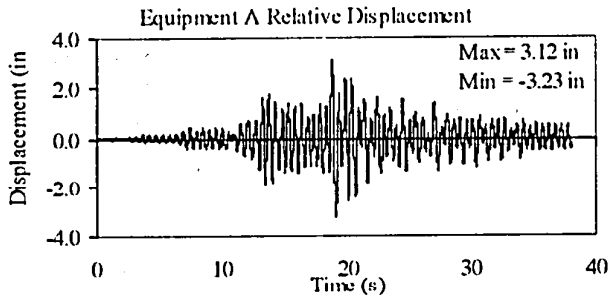

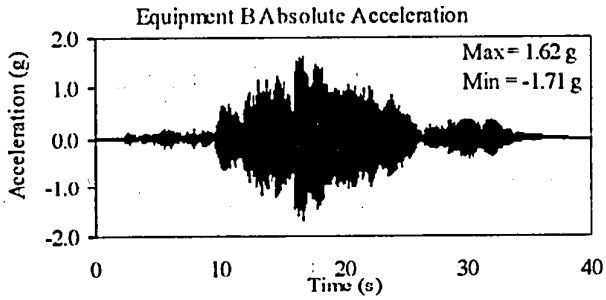

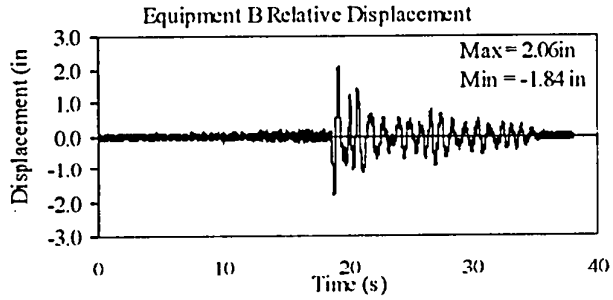

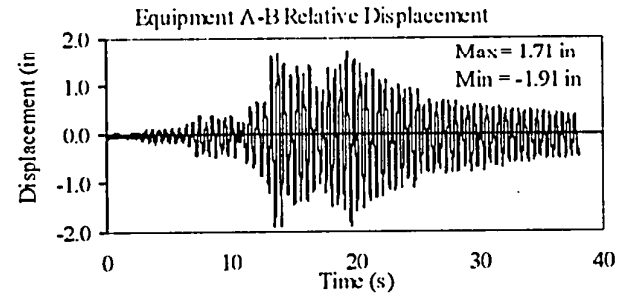

TEST RB-160
EQUIPMENT COMBINATION 5, INDIVIDUAL EQUIPMENT
TABAS GROUND MOTION, 50% SPAN

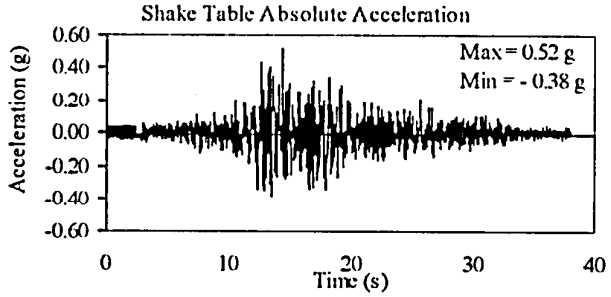

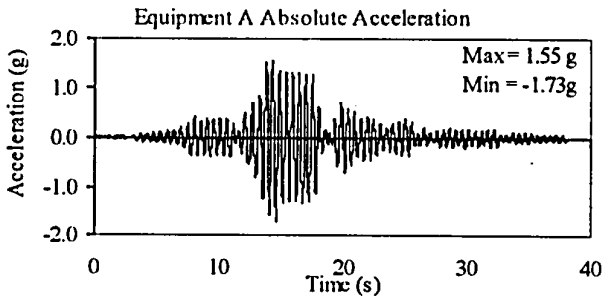

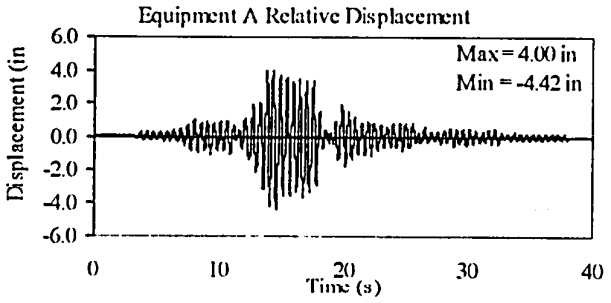

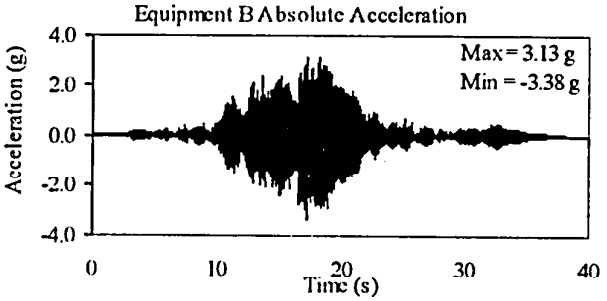

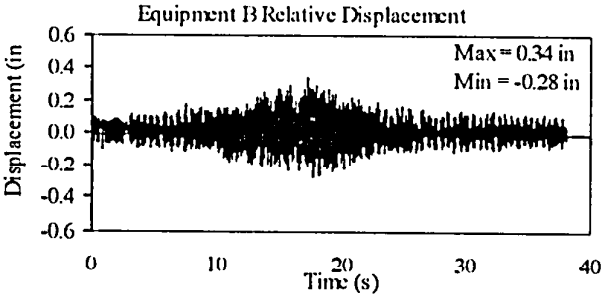

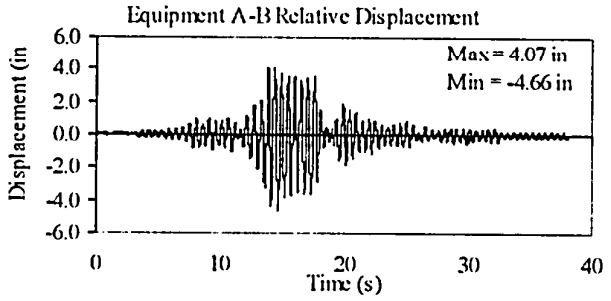

TEST RB-161
EQUIPMENT COMBINATION 5, INDIVIDUAL EQUIPMENT
NEWHALL GROUND MOTION, 100% SPAN